

広島大学学位請求論文

**Syntheses and Applications of
Sterically Hindered sp^3 Bases**

(立体障害のある sp^3 塩基の合成と応用)

2018 年

広島大学大学院理学研究科

化学専攻

森迫 祥吾

広島大学学位請求論文

**Syntheses and Applications of
Sterically Hindered sp^3 Bases**

(立体障害のある sp^3 塩基の合成と応用)

2018 年

広島大学大学院理学研究科

化学専攻

森迫 祥吾

目 次

1. 主論文

Syntheses and Applications of Sterically Hindered
 sp^3 Bases
(立体障害のある sp^3 塩基の合成と応用)
森迫 祥吾

2. 公表論文

- (1) Synthesis of a Sterically Demanding Dispiropiperidine and Its Application in Monoamidodialkyl Zincate Complexes
S. Morisako, R. Shang, Y. Yamamoto
Inorganic Chemistry, **2016**, *55*(20), 10767–10773.
- (2) Triaminotriborane(3): A Homocatenated Boron Chain Connected by B–B Multiple Bonds
S. Morisako, R. Shang, Y. Yamamoto, H. Matsui, M. Nakano
Angewandte Chemie International Edition, **2017**, *56*(48), 15234–15240;
Angewandte Chemie, **2017**, *129*(48), 15436–15442.

主論文

Syntheses and Applications of Sterically Hindered sp^3 Bases

Department of Chemistry,
Graduate School of Science
Hiroshima University

Shogo, MORISAKO

Abbreviations

Contents

Chapter 1. General Introduction

1-1. Bases	2
1-2. Sterically Hindered Secondary Amines	3
1-2-1. Amines as Bases	3
1-2-2. Amines as Amino-Substituents	5
References	7

Chapter 2. Designs and Syntheses of New Sterically Hindered Piperidines

2-1. Introduction	10
2-2. Attempt to Synthesize 2,2,6,6-Tetraethylpiperidine	11
2-3. New Sterically Hindered Dispiropiperidines Bearing Cyclohexyl Rings	12
2-4. New Sterically Hindered Piperidines Bearing Rigid Alkyl Group(s)	15
2-5. Conclusion and Outlook	17
Experimental Section	18
References	42

Chapter 3. Deprotonative-Metalation Reactions

3-1. Introduction	45
3-2. Synthesis of the Lithium Amide	46
3-3. Regioselective Enolization of Asymmetric Ketones	
3-4. Syntheses of Monoamidodialkyl Zincate Complexes	47
3-5. Regio- and Chemoselective (Aromatic)C–H Zincations of DiSubstituted Benzens	49
3-6. Conclusion and Outlook	51
Experimental Section	52
References	75

Chapter 5. Syntheses of Low Oxidation-State Boron Species and Their Reactivity

4-1. Introduction	80
4-2. Syntheses of Aminodichlorodiborenes	82

4-3. Attempts to Synthesize Ligand-Free Diaminodiborenes	83
4-4. Syntheses of Triaminotriboranes(3) and Naphthalene-Adducts	87
4-5. Facile Cleavage of a Carbon-Nitrogen Triple Bond in <i>tert</i> -Butyl Isocyanide Using a Triaminotriborane(3)	94
4-6. Reaction of Low-Coordinate Boron Species with Carbon Monoxide	99
4-7. Metal-Free Direct 1,2-Diborylation Reaction of Aldehydes Using a Triaminotriborane(3)	100
4-8. Reaction of a Triaminotriborane(3) with Other Multiple Bonds	102
4-9. Reaction of a Triaminotriborane(3) with Heteroatom Single Bonds	102
4-10. Reaction of a Triaminotriborane(3) with Other Nucleophiles	104
4-11. One-Electron Chemical Reductions of Coinage Metal Complexes Using a Triaminotriborane(3)	105
4-12. One-Electron Chemical Oxidations or Reductions of a Triaminotriborane(3)	107
4-13. Reaction of a Triaminotriborane(3) with Electrophiles	108
4-14. Syntheses of Cationic Bent Boron Chains Connected By Boron–Boron Multiple Bonds	109
4-15. Conclusion and Outlook	114
Experimental Section	115
References	159

List of Publication

Acknowledgement

Abbreviations

AcOEt	ethyl acetate
<i>n</i> BuLi	<i>n</i> -butyllithium
9-BBN	9-borabicyclononyl
cAAC	cyclic (alkyl)(amino)carbene
coe	cyclooctene
cy	cyclohexyl
DFT	density functional theory
DMAP	<i>N,N</i> -dimethylaminopyridine
DME	1,2-dimethoxyethane
DMSO	dimethyl sulfoxide
ESR	electron spin resonance
Et ₂ O	diethyl ether
GIAO	gauge-independent atomic orbital
HOMO	highest occupied molecular orbital
HR-MS	high resolution mass spectrometry
LiDA	lithium diisopropylamine
LiHMDS	lithium 1,1,1,3,3,3-hexamethyldisilazide (or lithium bis(trimethylsilyl)amide)
LiTMP	lithium 2,2,6,6-tetramethylpiperidide
LUMO	lowest occupied molecular orbital
MeOTf	methyl trifluoromethanesulfonate
MS	mass spectrometry
NBO	natural bond orbital
NHC	<i>N</i> -heterocyclic carbene
NMR	nuclear magnetic resonance
OTf	trifluoromethanesulfonate
PMHS	poly(methylhydrosiloxane)
PMP	1,2,2,6,6-pentamethylpiperidine
TBAC	tetra(<i>n</i> -butyl)ammonium chloride
<i>t</i> BuLi	<i>tert</i> -butyllithium
<i>t</i> BuNC	<i>tert</i> -butyl isocyanide
TD-DFT	time-dependent density functional theory
TEMPO	2,2,6,6-tetramethylpiperidine-1-oxyl
THF	tetrahydrofuran

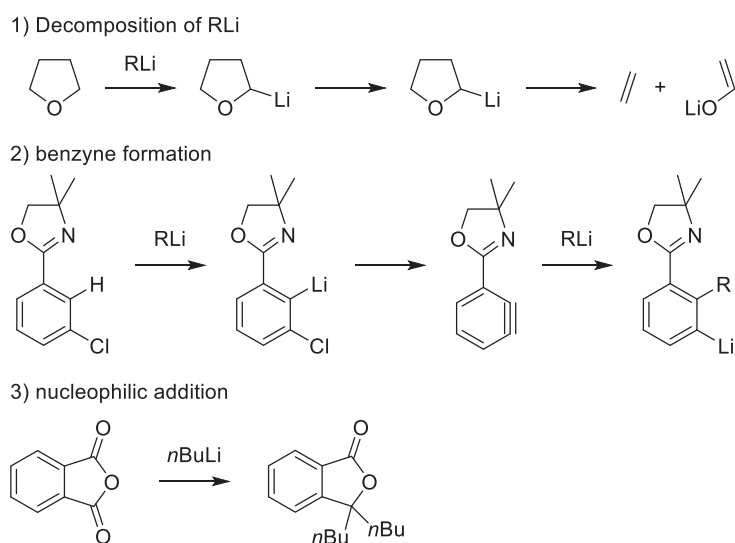
TMEDA	<i>N,N,N',N'</i> -tetramethylethylenediamine
TMP(H)	2,2,6,6-tetramethylpiperidine
TMSCl	trimethylsilyl chloride
WBI	Wiberg bond index

Chapter 1

General Introduction

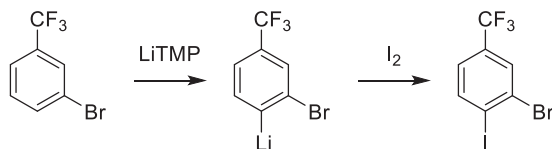
1-1. Bases

Organometallic bases (R–M) containing carbon–metal (C–M) bond(s), such as organolithium (RLi), organomagnesium (RMgX, R₂Mg) and organocuprate (LiCuR₂), are very important reagents in organic synthesis because they show strong basicity and nucleophilicity and also offer metal–halogen exchange reaction. However, due to their high reactivity originating in highly polarized C–M bonds, the life-time of organometallic bases (especially RLi) are generally short,^{1a} and decomposition and side-reactions can be proceeded (Scheme 1).^{1,2} Therefore, to use RLi, the strict temperature control (at the low temperature) is required and the poor functional group tolerance is a major hurdle.



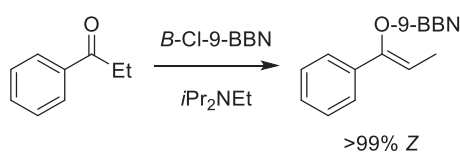
Scheme 1. Side-reactions of organolithium reagents.

In contrast, since lithium amides (LiNR₂) are relatively stable and prefer the deprotonative-metalation reactions to the lithium–halogen exchange reactions (Scheme 2),¹ LiNR₂ are also important bases in organic synthesis. In addition, it contributes to wide applications in various reactions that syntheses of LiNR₂ through the deprotonation reaction of secondary amines R₂N(H) by RLi are simple.



Scheme 2. Regio- and chemoselective deprotonation reaction.

On the other hand, in order to remove the proton and/or protic hydrogen, tertiary amines (NR_3) are widely used. For example, diisopropylethylamine ($i\text{Pr}_2\text{NEt}$) is often used as a base in the transition metal catalyzed reaction and selective enolate formation (Scheme 3),^{1c} because, in general, tertiary amines favor the deprotonation reaction than the nucleophilic attack. This is mainly due to the steric protection around the nitrogen atom by the three substituents at the nitrogen atom. Therefore, more sterically hindered NR_3 offer a high basicity and a poor nucleophilicity. In comparison to NR_3 , the nitrogen atoms of pyridines exploit weak basicity because of its sp^2 -hybridization. Then, highly nucleophilic DMAP is commonly used as a catalyst for acylation of alcohols and amines.^{1c}



Scheme 3. Selective enolate formation using diisopropylethylamine.

In certain case, typical organic solvents such as Et_2O and THF can act as a base. In 1992, Brookhart and co-workers reported the synthesis of the easily handled oxonium acid $[\text{H}(\text{OEt}_2)_2]^+[\text{B}(3,5\text{-(CF}_3)_2\text{C}_6\text{H}_3)_4]^-$ from the reaction of $\text{Na}[\text{B}(3,5\text{-(CF}_3)_2\text{C}_6\text{H}_3)_4]$ with HCl in OEt_2 .³ In this Brookhart's acid, OEt_2 behaved as a base and the resulting oxonium acid is a strong Brønsted acid which enable to protonate the ethylene coordinating to the transition metal. Similar oxonium acid $[\text{H}(\text{OEt}_2)_2]^+[\text{B}(\text{C}_6\text{F}_5)_4]^-$ was also reported by Jutzi and co-workers in 2000.⁴

1-2. Sterically Hindered Secondary Amines

1-2-1. Amines as Bases

As mentioned above, lithium amides and tertiary amines have been widely adopted in synthetic chemistry, and now are indispensable bases. To synthesize these bases, secondary amines are good candidates as follows: (i) the deprotonation reaction of $\text{R}_2\text{N(H)}$ by RLi or other organometallics is an easy and efficient method to form various metal amides (M-NR_2), (ii) the nucleophilic attack of $\text{R}_2\text{N(H)}$ or M-NR_2 to $\text{R}'\text{-X}$ ($\text{R}' = \text{alkyl, aryl; X} = \text{halide, sulfate, OTf etc.}$) provide the corresponding tertiary amines $\text{R}_2\text{NR}'$.

Metal-Amides: In synthetic chemistry, a regio-, chemo- and/or stereoselective synthesis is necessary to build up desired compounds. However, a number of reactive sites with R-M , M-NR_2 and NR_3 in organic molecules are large barriers to achieve the selective synthesis. In order to solve this problem, highly sterically hindered bases are often used. Especially among those bases, the large sterically hindered M-NR_2 and NR_3 can offer the remarkable regio- and chemoselectivity (in certain case, stereoselectivity) due to their high proton affinity and poor nucleophilicity and the large steric

hindrance between the base and the substituents in the substrate (Scheme 2, 3).¹ These useful sterically demanding bases are synthesized according to the aforementioned methods from sterically hindered secondary amines.

The three utility secondary amines to transform to $M-NR_2^5$ and/or NR_3 are shown in Figure 1, diisopropylamine (DA(H)),⁶ 1,1,1,3,3,3-hexamethyldisilazane (HMDS(H))⁷ and 2,2,6,6-tetramethylpiperidine (TMP(H)).⁸ DA(H) can be converted to LiDA and iPr_2NEt , HMDS(H) can be converted to MHMDS ($M = Li, Na, K$) and TMP(H) also can be converted to LiTMP, $TMPMgCl \cdot LiCl$ known as the Knochel-Hauser base,^{9,10} and other metal amides.^{1,5} A variety of versatile metal amides as deprotonation reagents have been still developed using these three amines. However, although it has passed a long time since these amines are firstly come into journals, no sterically hindered secondary amine, which takes the place of or is participated in the three amines, has not been reported. The requirements to expand the library of the bulky secondary amines are that an amine is (i) comparable to or more sterically demanding, (ii) easy and economic to access synthetically, and (iii) stable in the reaction with organometallics.

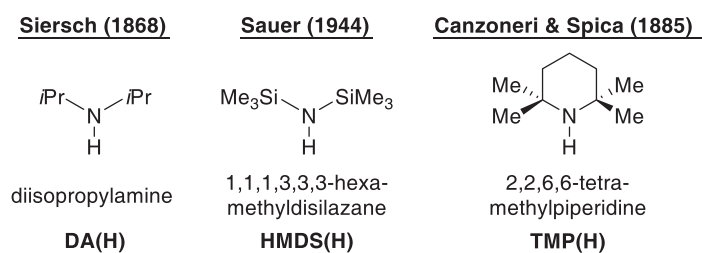


Figure 1. Commonly used sterically hindered secondary amines.

Therefore, this work aims to synthesize new sterically hindered secondary amine which meet aforementioned requirements, and apply the bulky amine as a base to the organic synthesis.

1-2-2. Amines as Amino-Substituents

The use of the sterically hindered $R_2N(H)$ is not limited to a base or transformation to $M-NR_2$ and R_2NR' . The NR_2 moiety of $R_2N(H)$ is also used as an amino-substituents. The amino-substituted atom/group (X) is subject to influence as follows: (i) the π -interaction with the nitrogen lone pair electron to decrease its electron-deficiency, (ii) the negative inductive effect to decrease its (σ -)electron density due to the high electronegativity of the nitrogen atom, and (iii) the steric protection to stabilize it kinetically (Figure 2).

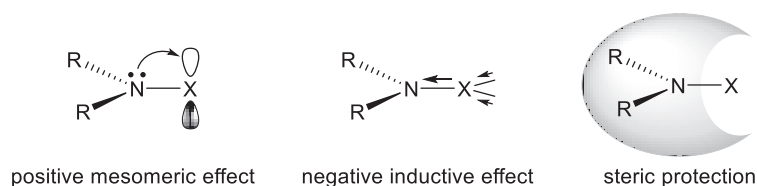


Figure 2. Influences of an amino-substituent to the adjacent atom/group.

Carbenes: By exploiting the influences of amino-substituents, labile chemical species have been isolated. For example, in 1991, Arduengo and co-workers firstly succeeded the isolation and structurally characterization of the singlet NHC.^{11,12} Subsequently, the sterically less demanding NHC,¹³ saturated-NHC,¹⁴ and acyclic diaminocarbene¹⁵ were isolated, which showed the possibility of the stabilization of labile chemical species using amino-substituents. Until now, a number of carbenes have been reported and widely utilized in organometallic and main-group chemistry,¹⁶ it may be considered that amino-substituents give those developments behind-the-scenes support. In the same way, the boryllithium, which was isoelectronic with NHCs, was also isolated by Yamashita and co-worker in 2006,¹⁷ and has also contributed to the advancement of organometallic and main-group chemistry. As mentioned above, sterically demanding secondary amines hold the promise to achieve the isolation of previously inaccessible chemical species and reveal their properties.

Nitroxyl Radicals: The secondary amines are also good precursors of nitroxyl radicals (nitroxides) with unpaired electron, which are widely adopted for alcohol oxidations,¹⁸ radical polymerization,¹⁹ radical batteries,²⁰ spin probes²¹ and antioxidants.²² In particular, TEMPO (Figure 3) is one of the most utilizing nitroxides because it is a chemically stable and small molecular weight oxygen free radical and a lower toxic reagent in comparison to heavy metals. This remarkable stability of TEMPO can be explained that (i) the four methyl groups at 2 and 6 positions sterically protect around the radical moiety and (ii) there is no hydrogen atom at α -positions adjacent to the nitrogen atom. The large steric hindrance of the less toxic TEMPO enables to oxidize primary alcohols selectively to provide corresponding carbonyl compounds, which have been establishing the position of TEMPO in organic synthesis as a rare applicable method for synthesis of pharmaceuticals.²³ The proposed reaction mechanism in basic solution is shown in Figure 3.^{23b,24} The

primary alcohol selectivity is originated from the difference in stability of complex of oxoammonium ion and alkoxide, in which the larger steric hindrance decrease the complex stability. In addition, it was reported that the sterically hindered alkoxyamine derived from the parent nitroxide can act as an efficient initiator/regulator for nitroxide-mediated radical polymerization of *n*-butyl acrylate.^{19d} Further investigations using sterically demanding nitroxides are desired.

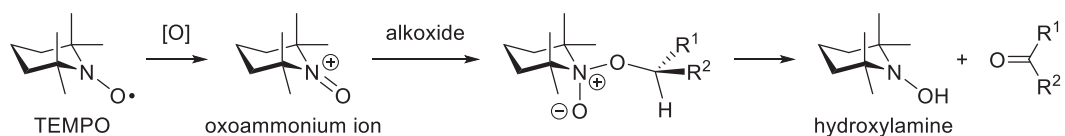


Figure 3. Proposed oxidation mechanism of alcohols using TEMPO in basic solution.

References

- [1]. (a) Clayden, J. In *Organolithiums: Selectivity for Synthesis*; Baldwin, J. E., Williams, R. M., Eds.; Tetrahedron Organic Chemistry Series 23; Elsevier Science Ltd., 2002; pp 1–375.
(b) Schlosser, M. Organoalkali Chemistry. In *Organometallics in Synthesis, Third Manual*; Schlosser, M., Ed.; John Wiley & Sons, Inc., 2013; pp 1–222.
Common utility alkyl lithium and lithium amide reagents (*n*-BuLi,*s*-BuLi,*t*-BuLi, LiDA, LiHMDS and LiTMP): (c) In *Handbook of reagents for organic synthesis: acidic and basic reagents*; Reich, H. J., Rigby, J. H., Eds.; Wiley, 1999; pp 66–74 (*n*-BuLi), 74–80 (*s*-BuLi), 81–87 (*t*-BuLi), 213–221 (LiDA), 221–224 (LiHMDS), 232–234 (LiTMP).
- [2]. Herberhold, M.; Biersack, M. *J. Organomet. Chem.* **1995**, *503*, 277–287.
- [3]. Brrokhart, M.; Grant, B.; Volpe, Jr. A. F. *Organometallics* **1992**, *11*, 3920–3922.
- [4]. Jutzi, P.; Müller, C.; Stammer, A.; Stammer, H.-g. **2000**, *19*, 1442–1444.
- [5]. Recent review about important alkalimetal amides, see: Mulvey, R. E.; Robertson, S. D. *Angew. Chem. Int. Ed.* **2013**, *52*, 11470–11487.
- [6]. Siersch, A. *Justus Liebigs Ann. Chem.* **1868**, *148*, 263–265.
- [7]. Sauer, R. O. *J. Am. Chem. Soc.* **1944**, *66*, 1707–1710.
- [8]. Canzoneri, F.; Spica, G. *Gazz. Chim. Ital.* **1885**, *15*, 1–4.
- [9]. Krasovskiy, A.; Krasovskaya, V.; Knochel, P. *Angew. Chem. Int. Ed.* **2006**, *45*, 2958–2961.
- [10]. The Knochel-Hauser base has higher functional tolerance and can be used as a deprotonation reagent without extremely low temperatures.
- [11]. Arduengo, III, A. J.; Harlow, R. L.; Kline, M. *J. Am. Chem. Soc.* **1991**, *113*, 361–363.
- [12]. Computational prediction about the π -donation and σ -withdrawing in the diaminocarbene (:C(NH₂)₂), see: Feller, D.; Borden, W. T.; Davidson, E. R. *Chem. Phys. Lett.* **1980**, *71*, 22–26.
- [13]. Arduengo, III, A. J.; Dias, H. V. R.; Harlow, R. L.; Kline, M. *J. Am. Chem. Soc.* **1992**, *114*, 5530–5534.
- [14]. Arduengo, III, A. J.; Goerlich, J. R.; Marshall, W. J. *J. Am. Chem. Soc.* **1995**, *117*, 11027–11028.
- [15]. Alder, R. W.; Allen, P. R.; Murray, M.; Orpen, A. G. *Angew. Chem. Int. Ed. Engl.* **1992**, *35*, 1121–1123.
- [16]. Recent reviews about carbene–main group chemistry, see: (a) Martin, C. D.; Soleilhavoup, M.; Bertrand, G. *Chem. Sci.* **2013**, *4*, 3020–3030.
(b) Wang, Y.; Robinson, G. H. *Inorg. Chem.* **2014**, *53*, 11815–11832.
- [17]. Segawa, Y.; Yamashita, Y.; Nozaki, K. *Science* **2006**, *314*, 113–115.
- [18]. Recent reviews, see: (a) Wertz, S.; Studer, A. *Green Chem.* **2013**, *15*, 3116–3134.
(b) Iwabuchi, Y. *Chem. Pharm. Bull.* **2013**, *61*, 1197–1213.
- [19]. (a) Miura, Y.; Nakamura, N.; Taniguchi, I. *Macromolecules* **2001**, *34*, 447–455.

- (b) Wetter, C.; Gierlich, J.; Knoop, C. A.; Müller, C.; Schulte, T.; Studer, A. *Chem. Eur. J.* **2004**, *10*, 1156–1166.
- (c) *Nitroxide Mediated Polymerization: From Fundamentals to Applications in Materials Science*; Gigmes, D., Ed.; Polymer Chemistry Series 19; Royal Chemistry Society, 2015; pp 1–500.
- (d) Jing, Y.; Tesch, M.; Wang, L.; Daniliuc, C. G.; Studer, A. *Tetrahedron* **2016**, *72*, 7665–7671.
- [20]. (a) Nakahara, K.; Iwasa, S.; Satoh, M.; Morioka, Y.; Iriyama, J.; Suguro, M.; Hasegawa, E. *Chem. Phys. Lett.* **2002**, *359*, 351.
- (b) Nakahara, K.; Iriyama, J.; Iwasa, S.; Suguro, M.; Satoh, M.; Cairns, E. J. *J. Power Sources* **2007**, *165*, 870.
- [21]. (a) Yordanov, A. T.; Yamada, K.; Krishna, M. C.; Mitchell, J. B.; Woller, E.; Cloninger, M.; Brechbiel, M. W. *Angew. Chem. Int. Ed.* **2001**, *40*, 2690–2692.
- (b) Utsumi, H.; Yamada, K.; Ichikawa, K.; Sakai, K.; Kinoshita, Y.; Matsumoto, S.; Nagai, M. *Proc. Natl. Acad. Sci. U.S.A.* **2006**, *103*, 1463–1468.
- [22]. (a) Krishna, M. C.; Russo, A.; Mitchell, J. B.; Goldstein, S.; Dafni, H.; Samuni, A. J. *Biol. Chem.* **1996**, *271*, 26026–26031.
- (b) Haidasz, E. A.; Meng, D.; Amorati, R.; Bascieri, A.; Ingold, K. U.; Valgimigli, L.; Pratt, D. *J. Am. Chem. Soc.* **2016**, *138*, 5290–5298.
- [23]. (a) Dugger, R. W.; Ragan, J. A.; Ripin, D. H. B. *Org. Process Res. Dev.* **2005**, *9*, 253–258.
- (b) Ciriminna, R.; Pagliaro, M. *Org. Process Res. Dev.* **2010**, *14*, 245–251.
- [24]. (a) Semmelhack, M. F.; Schmid, C. R.; Cortés, D. A. *Tetrahedron Lett.* **1986**, *27*, 1119–1122.
- (b) Bailey, W. F.; Bobbitt, J. M.; Wiberg, K. B. *J. Org. Chem.* **2007**, *72*, 4504–4509.

Chapter 2

Designs and Syntheses of New Sterically Hindered Piperidines

2-1. Introduction

As mentioned in chapter 1, the sterically hindered secondary amines which are currently widely used are DA(H), HMDS(H) and TMP(H) in organic synthesis chemistry and the field of labile chemical species. Among these amines, the TMP framework has unique merits: (i) higher stability as an amido because of no hydrogen atoms at α -positions adjacent to the nitrogen atom (Figure 1),^{1,2} (ii) larger steric hindrance (at least than DA),^{3,4} (iii) highest pKa value (DA, 35.7; HMDS, 29.7; TMP, 37.3).³

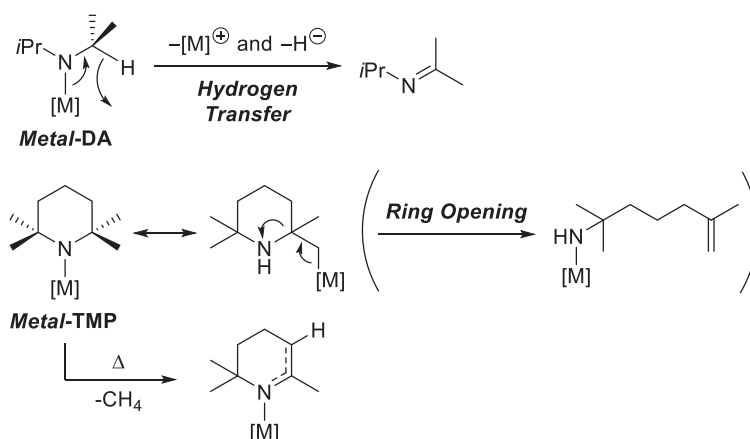


Figure 1. Decomposition reactions of metal-DA and metal-TMP.

Therefore, this work aims to synthesize new sterically demanding secondary amines possessing TMP backbone, which may offer comparable or additional steric bulk than that from TMP as alternatives for direct deprotonation reactions and an amino-substituent (Figure 2). We have chosen only alkyl groups (hydrocarbon systems) as the substituents at 2,6 positions in piperidine ring to suppress the decomposition and decrease the acidity of C-H bonds. In the research field of nitroxides, a number of 2,2,6,6-tetrasubstituted piperidin-4-one analogs have been developed,⁵ which allow us to come up that reduction of the C=O double bond to CH₂ provides desired amines.

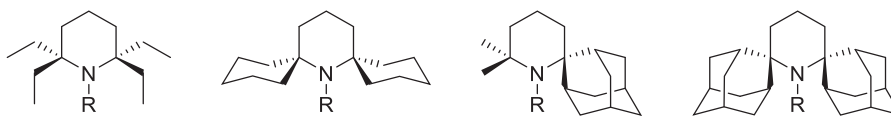
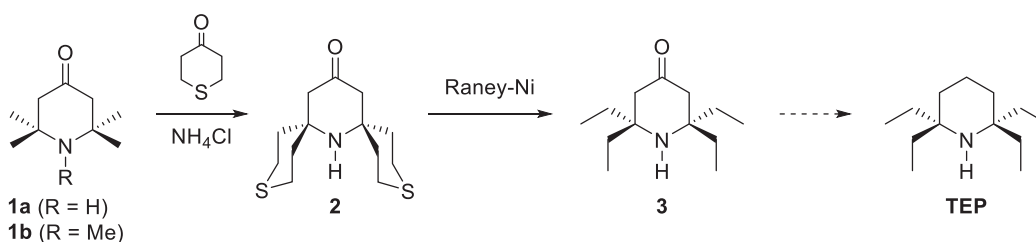


Figure 2. Target sterically hindered piperidine analogs. R = H, Me.

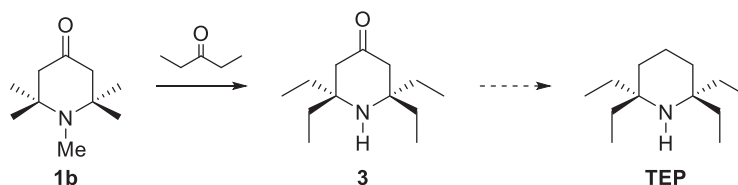
2-2. Attempt to Synthesize 2,2,6,6-Tetraethylpiperidine

Herein, the attempt to synthesize 2,2,6,6-tetraethylpiperidine (TEP) is reported. One of the starting material, 1,2,2,6,6-tetramethylpiperidin-4-one **1b**. Although it is commercially available, due to economic reasons, we prepared it from cheaper 2,2,6,6-tetramethylpiperidin-4-one **1a**.⁶ Then, according to the reported procedure,^{5c} we synthesized the previously reported ketone **2** through crossed aldol condensation of **1a** or **1b** and prepared tetrahydro-4*H*-thiopyran-4-one.⁷ In the case of using **1a** as a starting material, ketone **2** was obtained as a minor product. In contrast, in the case of using **1b**, ketone **2** was obtained in 34% yield.⁸ In this reaction, the undesired product **2'**,^{5d} in which only two methyl groups at the 6 position were replaced by one tetrahydro-2*H*-thiopyrane ring, was also obtained and detected by HR-MS. The desulfuration of **2** in EtOH at 60 °C using excess amount of Raney-Ni according the literature procedure^{5c} afforded the reported precursor **3**, which was detected by HR-MS (Scheme 1). Since the amount of obtained ketone **3**, the reduction reaction of **3** to TEP has not been attempted yet.



Scheme 1. Synthetic approach to 2,2,6,6-tetraethylpiperidine.

We also tried to synthesize **3** directly from **1b** by the crossed aldol condensation with 3-pentanone. Compound **3** and undesired **3'** (see Experimental Section) were detected by HR-MS of the resulting crude product. To provide **3** more cleanly, modification of reaction condition should be required.

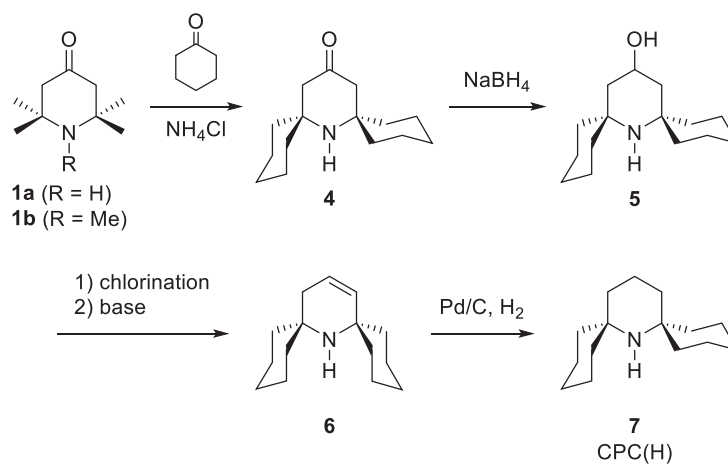


Scheme 2. Another synthetic approach to 2,2,6,6-tetraethylpiperidine.

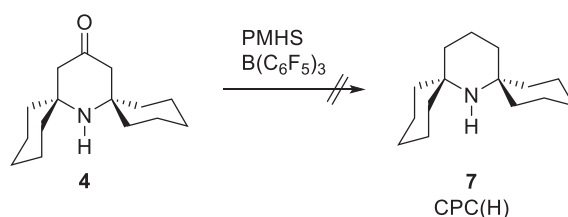
2-3. New Sterically Hindered Dispiropiperidines Bearing Cyclohexyl Rings

2-3-1. Designs and Syntheses

Herein, the synthesis of a new sterically hindered dispiropiperidines bearing cyclohexyl ring dispiro[cyclohexane-2,2'-piperidine-6',2''-cyclohexane] (CPC(H), **7**) and its *N*-methyl derivative is reported. Initial synthetic approach was shown in Scheme 3. In the beginning, to obtain the amine **7** bearing two cyclohexyl rings at 2,6 positions in piperidine ring, we attempted to synthesize previously reported 7-azadispiro[5.1.5.3]hexadecan-15-one **4**^{5a-c} as the precursor according to the modified reported procedure.⁹ As the literature said, the crossed aldol condensation of **1b** and cyclohexanone afforded ketone **4** in higher yield as compared to using **1a**. In the synthesis process of ketone **4**, 2,2-dimethyl-1-azadispiro[5.5]undecan-4-one (**4'**), in which only two methyl groups at the 6 position were replaced by one cyclohexyl ring, was also obtained as a major byproduct and detected by ¹H NMR. The proposed reaction mechanism from **1** to **4** was shown in Figure S11. The reduction of **4** with NaBH₄ in MeOH provided 7-azadispiro[5.1.5.3]hexadecan-15-ol **5** quantitatively. The chlorination of OH in **5** with SOCl₂ and TBAC and subsequent dehydrochlorination with NEt₃ afforded the corresponding 7-azadispiro[5.1.5.3]hexadec-14-ene **6**. Finally, desired CPC(H) **7** was obtained by the Pd/C catalyzed hydrogenation of **6**. However, because the reproducibility in the final step was poor, we had investigated other synthetic approaches.

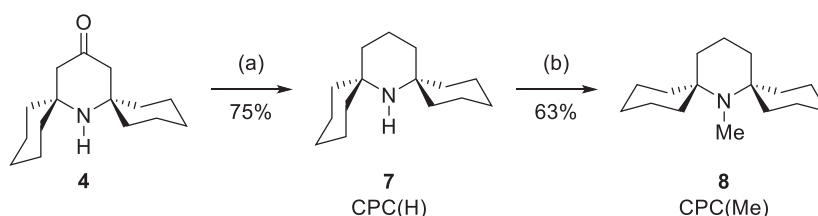
Scheme 3. Synthesis of CPC(H) **7**.

To simplify the synthesis of **7** and improve the yield, we tried to reduce **4** using hydride and strong Lewis acid (Scheme 4). We chose PMHS as a hydride and $B(C_6F_5)_3$ as a strong Lewis acid.¹⁰ The reaction mixture in CH_2Cl_2 was stirred at room temperature overnight. After changing the solvent to hexane following the filtration of the solution through silica gel short column, the resulting solution was dried under reduced pressure, then pale yellow oil was obtained as complex mixture. The catalytic amount of Lewis acid $B(C_6F_5)_3$ might be decomposed by contaminated water in commercially available PMHS.



Scheme 4. Reduction of **4** using PMHS and $B(C_6F_5)_3$.

Next, we attempted the one-step direct reduction from ketone **4** to the desired amine **7** using hydrazine. A Wolff–Kishner–Huang reduction¹¹ of ketone **4** afforded **7** in 75% yield (Scheme 5). The amine **7** can be methylated by treatment with paraformaldehyde and formic acid^{6a} to provide 1'-methyldispiro[3.3]heptan-2-amine (CPC(Me), **8**) in 63% yield. Compound **8** was also obtained from the reaction of *N*-lithio derivative (LiCPC, **9**) and MeOTf. Although the reaction of **9** with highly toxic MeOTf in Et_2O formed **8** quantitatively, the use of MeI formed **8** as a trace amount.



Scheme 5. Synthesis of dispiropiperidine analogs CPC(H) **7** and CPC(Me) **8**. Reagents and conditions: (a) $H_2NNH_2 \cdot H_2O$, DMSO, 60 °C, 1 h; then KOH, 130 °C, 2 h; then reflux, 8 h. (b) $HO(CH_2O)_nH$, HCO_2H , toluene, 130 °C, 12 h; then NaOH, r.t., 1 h. $HO(CH_2O)_nH$ = paraformaldehyde.

The 1H and $^{13}C\{^1H\}$ NMR spectra of **7** and **8** are unremarkable, with all signals lying within the expected range. Results from variable-temperature (VT) NMR experiments and preliminary DFT calculation on the energy gaps of possible conformational isomers of **7** and **8** suggested fluxional behaviors of **7** and nonfluxional behavior of **8** below room temperature (see Figure S15–18).

The structures of **7** and **8** were confirmed by X-ray crystal structure analyses. Their solid-state molecular structures are shown in Figure 2a and 2b. In both structures, all cyclohexyl groups assume the chair conformation. The parent amine **7** has an asymmetric structure, with one cyclohexyl ring equatorial and the other axial with respect to the C–N bond. The methyl derivative **8** has a symmetric structure in the solid state, with both cyclohexyl rings folded back, assuming equatorial positions. This might be due to the repulsions between the *N*-methyl and the cyclohexyl hydrogen atoms.

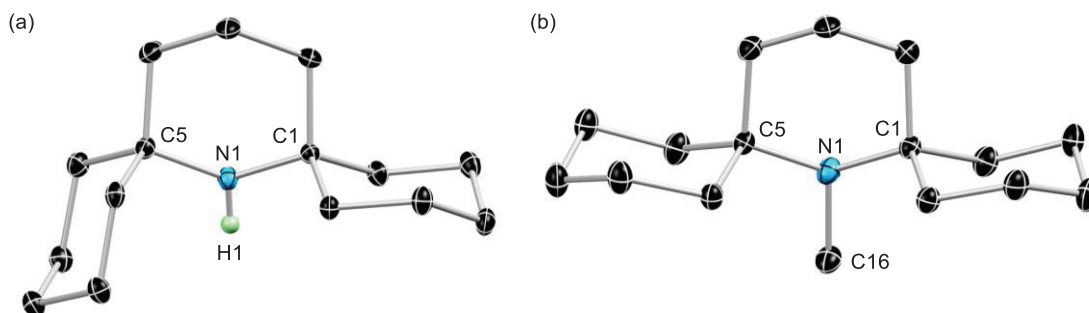
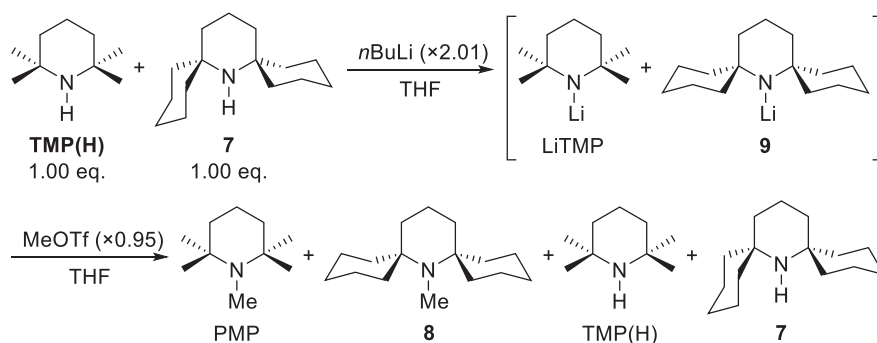


Figure 3. Molecular structures of (a) **7** and (b) **8** obtained from single-crystal X-ray diffraction analyses. Thermal ellipsoids are displayed at 30% probability. Hydrogen atoms except *N*–H are omitted for clarity. There are two independent molecules in the asymmetric unit of **8**, and one of these is shown. Selected bond angles (degrees) for CPC(H) (**7**): C1–N1–C5 121.5(2), C1–N1–H1 111(2), C5–N1–H1 118(3). Selected bond angles (degrees) for CPC(Me) (**8**): C1–N1–C5 120.0(2), C1–N1–C16 112.8(2), C5–N1–C16 113.5(2).

2-3-2. Competitive Methylation Reaction

In order to compare the steric effects of the methyl- and cyclohexyl-substituted derivatives, a competitive methylation reaction between TMP(H) and CPC(H) (**7**) was carried out (Scheme 6). A 1:1 mixture of both amines was lithiated completely at 0 °C with a slight excess of *n*BuLi (2.01 equiv). Then 0.95 equiv of MeOTf was added at 0 °C. The reaction mixture was stirred at the same temperature for 12 h before being quenched with *i*PrOH. The product mixture contained 56% 1,2,2,6,6-pentamethylpiperidine (PMP) and 44% **8** (results from repetition reactions are shown in Table S1). This suggested that LiCPC reacted only slightly more slowly than LiTMP, most likely due to the larger and more flexible cyclohexyl groups of **9**.

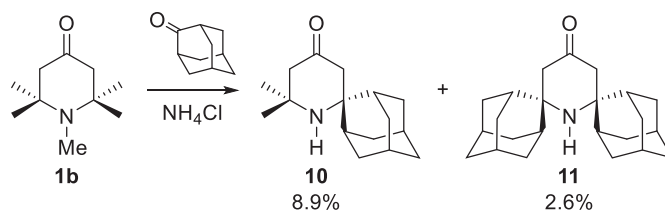


Scheme 6. Competitive methylation reaction. The product ratio of PMP to **8** was determined from the ^1H NMR spectrum of the crude product mixture. The product ratio of TMP(H) to **7** could not be determined by ^1H NMR of the crude product mixture because of the overlapping of the signals corresponding to both compounds. Reagents and conditions: (lithiation) $n\text{BuLi} \times 2.01$ equiv of THF, 0°C , 1 h; (methylation) $\text{MeOTf} \times 0.95$ equiv of THF, 0°C , 12 h; then $i\text{PrOH}$.

2-5. Designs and Syntheses of New Sterically Hindered Piperidines Bearing Rigid Alkyl Group(s)

As shown in section 2-4, the result of competitive methylation reaction between TMP(H) and CPC(H) **7** indicated that the steric hindrance around the nitrogen atom in **7** was slightly increased in comparison to that in TMP(H). The reason why this difference is slightly is most likely due to the flexibility of cyclohexyl rings as observed by VT- ^1H NMR and preliminary calculation for **7**. Then, we assumed that sterically hindered and “rigid” alkyl group(s) increases the steric hindrance around the nitrogen atom dramatically. Herein, attempts to synthesize new sterically hindered piperidines bearing rigid alkyl group(s) are reported.

Under the similar reaction condition and method to synthesize **7** (see section 2-3), a crossed aldol condensation reaction of **1b** and 2-adamantanone afforded the precursor (1*R*,3*S*,5*r*,7*r*)-6',6'-dimethylspiro[adamantane-2,2'-piperidin]-4'-one (**10**) and (1*R*,1''*R*,3*S*,3''*S*,5*R*,5''*R*,7*R*,7''*R*)-dispiro[adamantane-2,2'-piperidine-6',2''-adamantan]-4'-one (**11**) in 8.9 % and 2.6% yields, respectively (Scheme 7) accompanying with the generation of 1,3-di((1*R*,3*R*,5*R*,7*S*)-adamantan-2-ylidene)propan-2-one (**12**, Figure S2). This undesired product **12** may be able to be converted to **11** using NH_3 as the similar method to synthesize **1a** from 2,6-dimethyl-2,5-heptadien-4-one and NH_3 .^{11,12} To improve the isolated yields of **10** and **11**, modification of reaction condition and Triton B (benzyltrimethylammonium hydroxide) should be required.^{5c}



Scheme 7. Synthesis of 2,2,6,6-tetrasubstituted piperidine precursors **10** and **11**.

The ^1H NMR and ^{13}C NMR spectra of **10** and **11** are unremarkable. Their structures were confirmed by X-ray crystal structure analyses. Their solid-state molecular structures are shown in Figure 4a and 4b. In both structures, adamantyl groups cover the nitrogen lone pair electrons. In the molecular structure of **11**, the piperidine ring was distorted from stable chair form, mostly due to the large steric repulsion between adamantyl groups at the 2,6 positions.

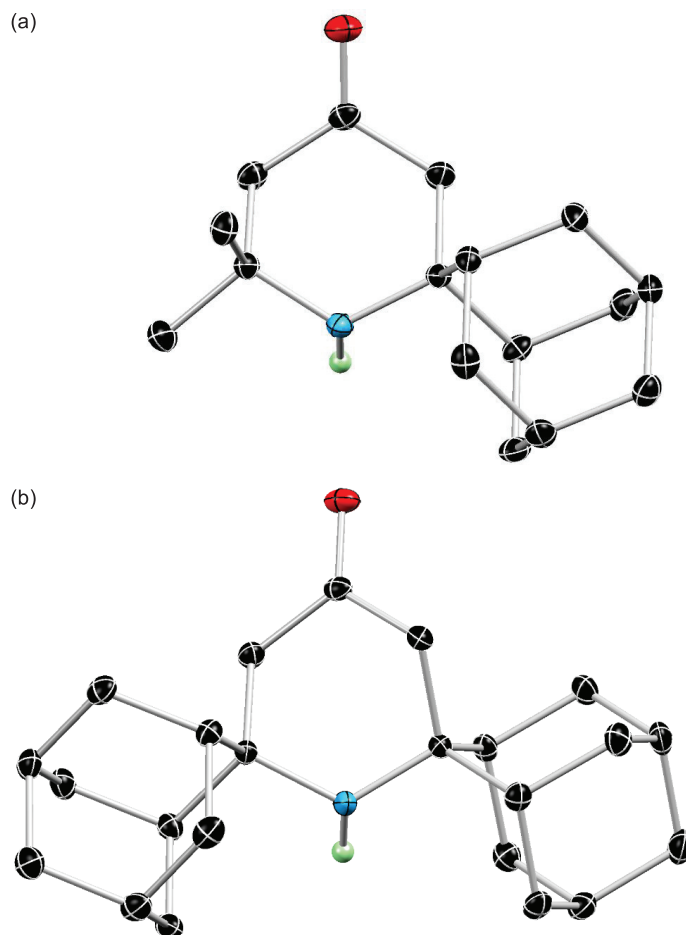
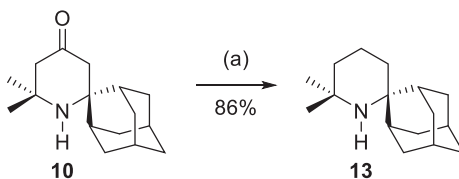


Figure 4. Molecular structures of (a) **10** and (b) **11** obtained from single-crystal X-ray diffraction analyses. Thermal ellipsoids are displayed at 30% probability. Hydrogen atoms except N–H are omitted for clarity.

A Wolff–Kishner–Huang reduction¹¹ of ketone **10** afforded (1*R*,3*S*,5*r*,7*r*)-6',6'-dimethylspiro[adamantane-2,2'-piperidine] **13** in 86% yield (Scheme 8). Compound **13** was characterized by ¹H and ¹³C NMR measurements and elemental analysis. The molecular structure was confirmed by single-crystal X-ray diffraction analysis (Figure 5). The piperidine ring has a chair conformation. As expected, the adamantyl group effectively covers the nitrogen lone pair electrons, which indicates that the steric hindrance around nitrogen atom in **13** may be larger than those of TMP(H) and CPC(H).



Scheme 8. Synthesis of 2,2,6,6-tetrasubstituted piperidine **13**.

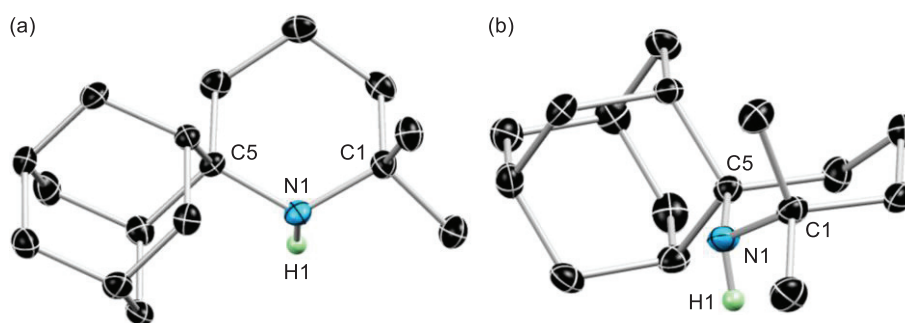


Figure 5. Molecular structure of **13** obtained from single-crystal X-ray diffraction analysis. (a) Top view and (b) side view. Thermal ellipsoids are displayed at 30% probability. Hydrogen atoms except *N*-H are omitted for clarity. Selected bond distances (Angstroms) and angles (degrees) for **13**: N1–C1 1.482(2), N1–C5 1.489(2), N1–H1 0.85(2); C1–N1–C5 120.5(2), C1–N1–H1 106.3(14), C5–N1–H1 106.2(14).

2-6. Conclusion and Outlook

In conclusion, we developed a convenient synthetic procedure for a series of new 2,2,6,6-tetrasubstituted piperidines from commercially available starting materials. A competitive methylation reaction between TMP(H) and CPC(H) (**7**) revealed that the steric hindrance around the nitrogen atom in **7** was only slightly larger than that of TMP(H), most likely due to the flexibility of cyclohexyl rings. In contrast, piperidine analog **13** bearing a more rigid alkyl group indicates the increase of the steric hindrance in comparison to those of TMP(H) and **7**. The large scale synthesis of **13** and modification of reaction conditions to synthesize ketone **10** and **11** are future subjects.

Experimental Section

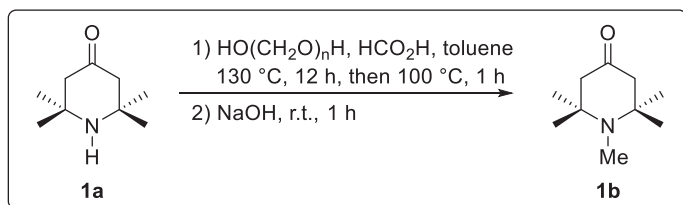
General Considerations

All syntheses were carried out under inert atmosphere with standard Schlenk unless otherwise stated. Tetrahydrofuran (THF) and toluene were freshly distilled from Na/benzophenone prior to use. Dimethyl sulfoxide (DMSO) and 2,2,6,6-tetramethylpiperidine (TMP(H)) were distilled from CaH₂ and stored over 4 Å molecular sieves. MeOTf was freshly distilled prior to use. CH₂Cl₂ was distilled from CaH₂ prior to use. CDCl₃ was distilled from CaH₂ or passed through aluminum short column prior to use. Other chemicals were used as supplied. Column chromatography was carried out using Kanto silica gel 60N (spherical, neutral) or Merck KGaA aluminum oxide 90 acc. to Brockmann (activity II–III).

General Measurements

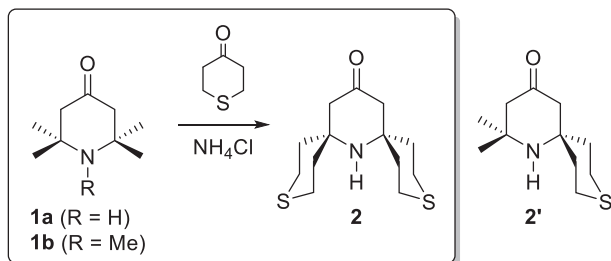
¹H NMR (400 MHz) and ¹³C NMR (100 MHz) spectra were recorded using a JEOL EX-400 or AL-400 NMR spectrometer. The ¹H and ¹³C NMR chemical shifts (δ scale) are determined by residual protons of the solvent (¹H, CDCl₃, δ = 7.26 ppm) or the solvent itself (¹³C, CDCl₃). Melting points were measured with a Yanagimoto micromelting point apparatus and are uncorrected. The elemental analyses were performed using a PerkinElmer 2400CHNS elemental analyzer. Mass spectra were measured with a Thermo Fisher Scientific model LTQ Orbitrap XL by using the ESI-TOF in the positive ion mode with solution samples.

Synthesis of **1b**



The desired product is commercially available. However, we prepared from 2,2,6,6-tetramethylpiperidin-4-one according to the literature method.^{6a} Formic acid (15.1 mL, 400 mmol) was added to a heated toluene solution (90 °C) of 2,2,6,6-tetramethylpiperidin-4-one (62.1 g, 400 mmol) and paraformaldehyde (18.2 g, 603 mmol). Fitted with a Dean-Stark apparatus, the reaction mixture was then refluxed for 11 h to remove the water azeotropically at 130 °C. The reaction mixture was kept at 100 °C for another hour before allowed to cool to room temperature, to which NaOH (8.11g, 203 mmol) was added. After 1 hours of stirring, the NaOH was filtered and the filtrate was freed of solvent under reduced pressure. The crude product was purified by distillation under reduced pressure (70–72 °C/2.0 mmHg) to provide analytically pure desired product (58.6 g, 346 mmol, 87%) as a yellow oil. ¹H NMR (CDCl₃, 400 MHz): δ = 2.37 (4H, s), 2.32 (3H, s), 1.13 ppm (12H, s).

Synthesis of **2**

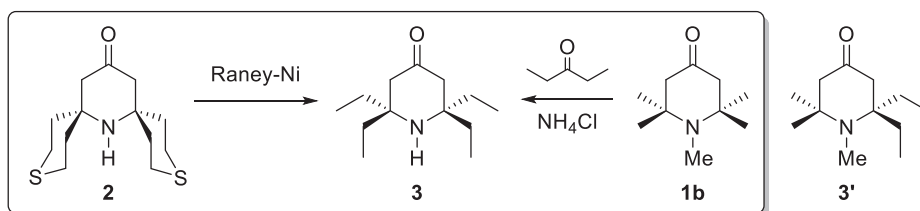


Preparation of **2** was carried out according to the literature method.^{5c}

2. ^1H NMR (CDCl_3 , 400 MHz): δ = 2.94 (4H, m), 2.49 (4H, m), 2.29 (4H, s), 1.85 (8H, m), 0.82 ppm (1H, br s); HR-MS (ESI positive): Calcd for $\text{C}_{13}\text{H}_{22}\text{ONS}_2$ 272.1140 found 272.1137 for $[\text{M}+\text{H}]^+$.

2'. HR-MS (ESI positive): Calcd for $\text{C}_{11}\text{H}_{20}\text{ONS}$ 214.1261 found 214.1260 for $[\text{M}+\text{H}]^+$.

Synthesis of **3**

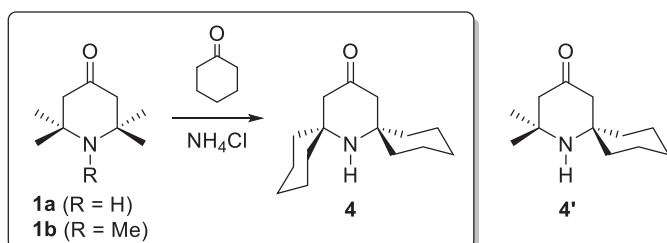


Preparations of **3** through the desulfuration of **2** or closed aldol condensation of **1b** and 3-pentanone were carried out according to the literature method.^{5c} Fresh Raney-Ni (slurry in water, Tokyo Chemical Industry) was used.

3. HR-MS (ESI positive): Calcd for $\text{C}_{13}\text{H}_{26}\text{ON}$ 212.2008 found 212.2009 for $[\text{M}+\text{H}]^+$.

3'. HR-MS (ESI positive): Calcd for $\text{C}_{11}\text{H}_{22}\text{ON}$ 184.1695 found 184.1696 for $[\text{M}+\text{H}]^+$.

Synthesis of **4**

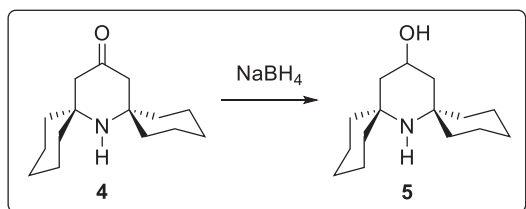


Compound **4** was prepared from 1,2,2,6,6-pentamethylpiperidin-4-one **1b** according to the previously reported procedure.^{5c} To a flask charged with NH_4Cl (19.3 g, 361 mmol), a DMSO (90 mL) solution of 1,2,2,6,6-Pentamethylpiperidin-4-one (10.1 g, 59.4 mmol) and cyclohexanone (18.7 mL, 180 mmol) were added in sequence at room temperature. The reaction mixture solution was

warmed to 60 °C and stirred for 5 h in a sealed reaction vessel before being cooled to the room temperature, to which water (400 mL) was added. After stirring for 1 h, the reaction solution was treated with aqueous HCl (7%, 120 mL) and stirred for 13 h.* The reaction mixture solution was washed with ether (×3) to remove byproducts. The aqueous phase was adjusted to pH 9 using aqueous K₂CO₃ (10%) and extracted with AcOEt (×4). The combined organic layer (AcOEt) was washed with saturated aqueous NaCl solution, dried over Na₂SO₄ and freed of volatiles under reduced pressure. The residual solid was purified by column chromatography (silica gel) with hexane/AcOEt (1:1) as the eluent to give 7-azadispiro[5.1.5.3]hexadecan-15-one (**4**) (9.23 g, 39.2 mmol, 66%) as a pale yellow solid (*R*_f = 0.54). ¹H NMR (CDCl₃, 400 MHz): δ = 2.31 (4H, s), 1.7–1.3 ppm (20H, m); ¹³C NMR (100 MHz, CDCl₃): δ = 211.55 (C), 56.85 (CH₂), 52.28 (C), 40.75 (CH₂), 25.67 (CH₂), 22.34 ppm (CH₂).

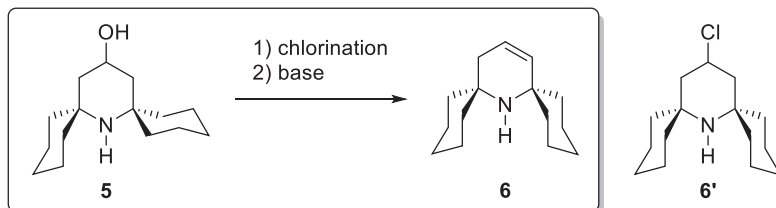
*: In large scale reactions, precipitates are often generated. In these cases, the reaction mixture was filtered. The filtrate was treated as described above. The filtered solid was mainly the ammonium salt of **1**. The water slurry of this ammonium salt was treated with aqueous K₂CO₃ (10%) to pH 9 and extracted with AcOEt (×4). The combined organic layer (AcOEt) was washed with saturated aqueous NaCl solution, dried over Na₂SO₄ and freed of volatiles under reduced pressure to give an additional batch of product.

Synthesis of **5**



MeOH (453 mL) without drying was added slowly to a flask charged with sodium borohydride (36.2 g, 957 mmol) and **4** (22.6 g, 96.0 mmol) at room temperature. After the stirring for 3 hours, water (500 mL) was added to the reaction mixture. The solution was extracted with CH₂Cl₂ (×4). The combined organic layer was washed with saturated aqueous NaCl solution and dried over MgSO₄. After the removal of solvents under reduced pressure, compound **5** was obtained as a brown gum (quant.). ¹H NMR (CDCl₃, 400 MHz): δ = 3.98 (1H, tt, ³*J* = 12 and 4.4 Hz), 2.16 (2H, dd, ²*J* = 12 Hz, ³*J* = 3.5 Hz), 1.67–1.36 (20H, m), 0.89 ppm (2H, dd, ²*J* = 12 Hz, ³*J* = 12 Hz).

Synthesis of **6**

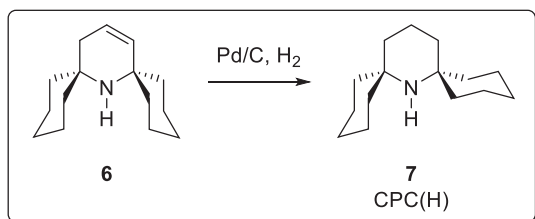


Toluene (164 mL) solution of **5** (26.8 g, 113 mmol) was added dropwise to toluene (100 mL) solution of TBAC (15.8 g, 56.7 mmol) and SOCl_2 (30 mL, 235 mmol) at 85 °C. After the heating at 85 °C for 2 hours, the reaction mixture was cooled to room temperature following drying. Dry NEt_3 as purchased from SAJ (100 mL, 717 mmol) was added dropwise to the resulting product. The mixture was stirred at room temperature for 3 hours, acidified with aqueous HCl solution (10%, pH 1–2). The insoluble precipitate was dissolved with CH_2Cl_2 . The solution was washed with ether. The aqueous phase was adjusted to pH 9 using an aqueous K_2CO_3 solution and then extracted with ether ($\times 4$). The combined organic layer was washed with saturated aqueous NaCl solution and dried over Na_2SO_4 . The desired compound **6** was obtained as a major product in the brown crude oil. Sometimes, the chlorinated compound **6'** was also included as a minor product.

6. ^1H NMR (CDCl_3 , 400 MHz): δ = 5.72 (1H, d, 3J = 10 Hz), 5.64 (1H, td, 3J = 4.1, 10 Hz), 1.90 (2H, dd, 3J = 4.9, 4J = 1.7 Hz), 1.70–1.29 ppm (20H, m); HR-MS (ESI positive): Calcd for $\text{C}_{15}\text{H}_{26}\text{N}$ 220.2060 found 220.2060 for $[\text{M}+\text{H}]^+$.

6'. HR-MS (ESI positive): Calcd for $\text{C}_{15}\text{H}_{27}\text{NCl}$ 256.1831 found 256.1827 for $[\text{M}+\text{H}]^+$.

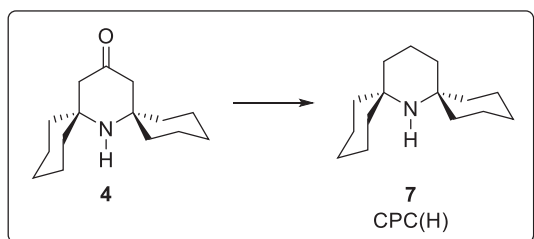
Synthesis of **7** from **6**



EtOH (2 mL) was added to a flask charged with **5** (39.0 mg, 0.178 mmol) and Pd/C (15.2 mg, 14.3 mmol) under H_2 atmosphere (balloon). The reaction mixture was stirred at room temperature for 1 day and filtered passed through Celite. The desired compound **7** was obtained as a pale orange oil (35.6 mg, 0.161 mmol, 90%).

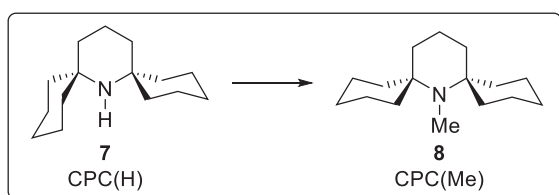
*: In large scale reactions, it was required to concentrate the reaction mixture to obtain **7**.

Synthesis of 7 from 4



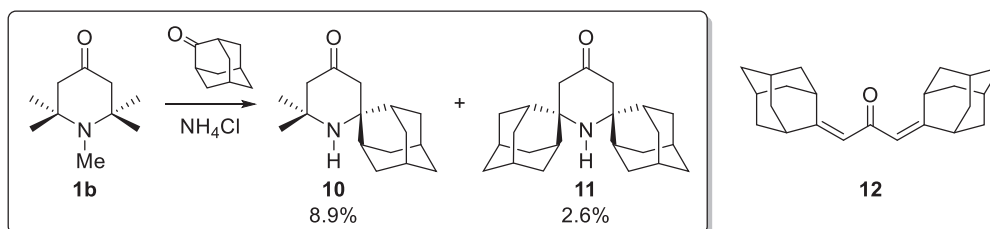
The DMSO used in this step was not dried. Hydrazine monohydrate (95 mL, 1.96 mol) was added to a solution of 7-azadispiro[5.1.5.3]hexadecan-15-one (**1**) (64.1 g, 0.272 mol) in DMSO (180 mL) at 60 °C. The solution was stirred at 80 °C for 1 h before KOH (50.4 g, 0.900 mol) was added at the same temperature. The resulting mixture was heated to 130 °C for 6 h before being heated to 190 °C to remove water azeotropically (over 12 h). The resulting solution was cooled to ambient temperature before water (120 mL) and toluene (75 mL) were added. The mixture was stirred at room temperature for 1 h and acidified with aqueous HCl solution (10%, pH 1–2). The precipitate was filtered and washed with ether. The filtrate was adjusted to pH 9 using an aqueous K₂CO₃ solution and then extracted with AcOEt (4 × 400 mL). The combined organic layer was washed with saturated aqueous NaCl solution and dried over Na₂SO₄. The filtered precipitate was added to water (ca. 1 L), and the suspension was also adjusted to pH 9 using aqueous K₂CO₃ solution and then extracted with AcOEt (4 × 400 mL). The combined organic layer was washed with saturated aqueous NaCl solution and dried over Na₂SO₄. All AcOEt extracts were combined and concentrated under reduced pressure. The residual brown oil was preliminarily purified by column chromatography (aluminum) with AcOEt as the eluent. The resultant orange oil was further purified by distillation under reduced pressure (ca. 62 °C/ 0.2 mmHg) to give CPC(H) (**7**) (44.9 g, 203 mmol, 75%) as a colorless oil. After this oil was cooled at –30 °C, the oil solidified into a white solid. Recrystallization of this solid from CH₂Cl₂ at –30 °C afforded crystals suitable for X-ray crystallographic analysis. Mp 34–35 °C. ¹H NMR (CDCl₃, 400 MHz): δ = 1.13–2.00 ppm (26H, m). ¹³C NMR (CDCl₃, 100 MHz): δ = 51.24 (C), 40.30 (CH₂), 36.08 (CH₂), 26.28 (CH₂), 22.52 (CH₂), 17.03 ppm (CH₂). Anal. Calcd for C₁₅H₂₇N: C, 81.38; H, 12.29; N, 6.33. Found: C, 81.77; H, 12.22; N, 6.61.

Synthesis of **8**



Formic acid (0.190 mL, 5.00 mmol) was added dropwise to a toluene (20 mL) solution of **7** (1.00 g, 4.52 mmol) and paraformaldehyde (190 mg, 6.34 mmol) at 90 °C. The reaction mixture was heated to 130 °C for 18 h with stirring followed by another hour at 100 °C before being cooled to ambient temperature, to which NaOH (108 mg, 2.70 mmol) was added as a solid. The mixture was stirred for 1 h, and the sodium hydroxide was filtered off. The solvent was concentrated, and the residual solid was purified by column chromatography (silica gel) with AcOEt as the eluent to give CPC(Me) (**8**) (155 mg, 0.698 mmol, 70%) as a white solid ($R_f = 0.07$). Recrystallization from CH₃CN at ambient temperature gave crystals suitable for X-ray crystallographic analysis. Mp 58–59 °C. ¹H NMR (CDCl₃, 400 MHz): $\delta = 2.33$ (3H, s), 1.80–1.18 (24H, m), 1.10–0.91 ppm (2H, m). ¹³C NMR (CDCl₃, 100 MHz): $\delta = 56.95$ (C), 33.81 (CH₂), 33.28 (CH₂), 27.10 (CH₃), 25.95 (CH₂), 23.23 (CH₂), 16.28 ppm (CH₂). Anal. Calcd for C₁₆H₂₉N: C, 81.63; H, 12.42; N, 5.95. Found: C, 81.81; H, 12.80; N, 6.03.

Synthesis of **10** and **11**



The DMSO used in this step was not dried. To a flask charged with NH₄Cl (9.63 g, 180 mmol), 1,2,2,6,6-Pentamethylpiperidin-4-one (10.16 g, 60.0 mmol), DMSO (150 mL) and 2-adamantanone (13.52 g, 90.0 mmol) were added in sequence at room temperature. The reaction mixture solution was warmed to 60 °C and stirred for 6 h in a sealed reaction vessel before being cooled to the room temperature, to which water was added. After stirring for 1 h, the reaction solution was acidified with aqueous HCl (10%, pH 1–2) and stirred for 12 h. The reaction mixture solution was washed with ether (×3) to remove 2-adamantanone and **12**, which were separated by column chromatography (silica gel) with hexane/AcOEt (1:1) as the eluent. The aqueous phase was adjusted to pH 9 using aqueous K₂CO₃ (10%) and extracted with AcOEt (×4). The combined organic layer (AcOEt) was washed with saturated aqueous NaCl solution, dried over Na₂SO₄ and freed of volatiles under reduced pressure. The residual solid was purified by column chromatography (silica

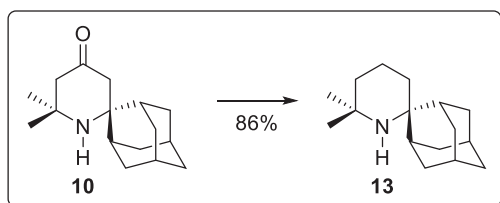
gel) with hexane/AcOEt (7:1) as the eluent to give the ketone **10** (1.32 g, 5.32 mmol, 8.9%) as a brown solid. The other fractions including **11** were purified by column chromatography (silica gel) with hexane/AcOEt (10:1) as the eluent and recrystallization to give the ketone **11** (0.537 g, 1.58 mmol, 2.6%) as a colorless solid.

10. **Mp** °C: $^1\text{H NMR}$ (CDCl_3 , 400 MHz): δ = 2.53 (2H, s), 2.38–2.20 (4H, m), 2.00–1.45 (12H, m), 1.22 ppm (7H, s); $^{13}\text{C NMR}$ (100 MHz, CDCl_3): δ = 211.97 (C), 77.21 (C), 61.66 (CH_2), 54.89 (C), 54.51 (CH_2), 50.13 (CH_2), 38.61 (CH), 33.62 (CH_3), 33.08 (CH_2), 32.16 (CH_2), 27.29 (CH), 27.13 ppm (CH); Anal. Calcd for $\text{C}_{16}\text{H}_{25}\text{NO}$: C, 77.68; H, 10.19; N, 5.66. Found: C, 77.97; H, 10.07; N, 5.52.

11. **Mp** °C: $^1\text{H NMR}$ (CDCl_3 , 400 MHz): δ = 2.60 (4H, s), 2.46–2.22 (4H, m), 2.02–1.45 (24H, m), 1.24 ppm (1H, br); $^{13}\text{C NMR}$ (100 MHz, CDCl_3): δ = 212.48 (C), 58.46 (C), 48.58 (CH_2), 39.72 (CH_2), 38.59 (CH), 33.80 (CH_2), 33.19 (CH_2), 27.13 (CH), 27.01 ppm (CH); Anal. Calcd for $\text{C}_{23}\text{H}_{33}\text{NO}$: C, 81.37; H, 9.80; N, 4.13. Found: C, 81.44; H, 9.99; N, 4.08.

12. **Mp** °C: $^1\text{H NMR}$ (CDCl_3 , 400 MHz): δ = 5.96 (2H, s), 4.15 (2H, br), 2.37 (2H, br), 2.07–1.76 ppm (24H, m); $^{13}\text{C NMR}$ (100 MHz, CDCl_3): δ = 193.28 (C), 170.32 (C), 119.58 (CH_2), 41.69 (CH), 40.47 (CH_2), 39.38 (CH_2), 37.02 (CH_2), 32.93 (CH), 28.07 ppm (CH); Anal. Calcd for $\text{C}_{23}\text{H}_{30}\text{N}$: C, 85.66; H, 9.38. Found: C, 85.82; H, 9.70.

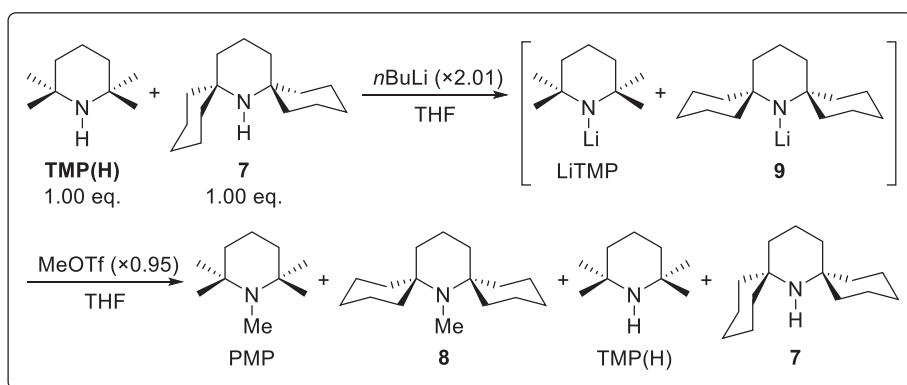
Synthesis of **13**



Hydrazine monohydrate (1.45 mL, 29.9 mmol) was added to a solution of ketone **10** (0.990 g, 4.00 mmol) in DMSO (15 mL) at 60 °C. The solution was stirred at 60 °C for 1 h before KOH (0.768 g, 13.7 mmol) was added at the same temperature. The resulting mixture was heated to 130 °C for 2 h before being heated to 190 °C to remove water azeotropically (over 8 h). The resulting solution was cooled to ambient temperature before water (1.5 mL) and toluene (1.0 mL) were added. The mixture was stirred at room temperature for 1 h and acidified with aqueous HCl solution (10%, pH 1–2). The solution was washed with ether. The aqueous phase was adjusted to pH 9 using an aqueous K_2CO_3 solution and then extracted with AcOEt ($\times 4$). The combined organic layer was washed with saturated aqueous NaCl solution and dried over Na_2SO_4 and freed of volatiles under reduced pressure. The residue was purified by column chromatography (aluminum) with AcOEt as the eluent to give **13** (0.801 g, 3.43 mmol, 86%) as a pale orange oil. After this oil was cooled at -30 °C, the oil solidified into a pale orange solid. Recrystallization of this solid from

AcOEt at $-30\text{ }^{\circ}\text{C}$ afforded crystals suitable for X-ray crystallographic analysis. **Mp $^{\circ}\text{C}$.** ^1H NMR (CDCl_3 , 400 MHz): $\delta = 2.29\text{--}2.12$ (2H, m), $2.02\text{--}1.89$ (2H, m), $1.84\text{--}1.41$ (14H, m), $1.38\text{--}1.27$ (2H, m), 1.12 ppm (6H, s). ^{13}C NMR (CDCl_3 , 100 MHz): $\delta = 55.19$ (C), 50.05 (C), 39.03 (CH_2), 38.89 (CH_2), 37.64 (CH_2), 34.00 (CH_2), 33.84 (CH_2), 32.66 (CH_2), 31.88 (CH_3), 27.91 (CH), 27.56 (CH), 17.55 ppm (CH_2). Anal. Calcd for $\text{C}_{16}\text{H}_{27}\text{N}$: C, 82.34; H, 11.66; N, 6.00. Found: C, 82.42; H, 11.70; N, 5.93.

Competitive Methylation Reaction



n -Butyl lithium (1.60 M in hexane, 3.50 mL, 5.60 mmol) was added to a THF solution of TMP(H) (393 mg, 2.78 mmol) and 7 (616 mg, 2.78 mmol) dropwise at $-78\text{ }^{\circ}\text{C}$. After addition, the reaction mixture was slowly warmed to $0\text{ }^{\circ}\text{C}$ and stirred at $0\text{ }^{\circ}\text{C}$ for 1 h. MeOTf (0.300 mL, 2.65 mmol) was added to the resulting suspension and the reaction mixture was stirred at $0\text{ }^{\circ}\text{C}$ or $-30\text{ }^{\circ}\text{C}$ for 12 h. The residual lithium amides were quenched by addition of $i\text{PrOH}$ at $0\text{ }^{\circ}\text{C}$. Afterwards, the solution was adjusted to pH 10 with aqueous HCl solution (10%) before extracted with CH_2Cl_2 (4×40 mL). The combined organic layer was washed with saturated aqueous NaCl solution, dried over Na_2SO_4 and concentrated under reduced pressure. The product ratio was determined by ^1H NMR of this crude product mixture and is summarized in Table S1.

Table S1. The observed product ratio

Entry	THF	Reaction temp. ($^{\circ}\text{C}$)	Ratio PMP : 8
1	12.4 mL	0	1.26 : 1.00
2	28.0 mL	0	1.26 : 1.00
3	28.0 mL	0	1.26 : 1.00
4	28.0 mL	-30	1.16 : 1.00
5	28.0 mL	-30	1.16 : 1.00

The reproducibility was observed. The product ratio of PMP to **8** was lower at $-30\text{ }^{\circ}\text{C}$ (entries 4 and 5) than that observed at $0\text{ }^{\circ}\text{C}$ (entries 1–3), most likely due to the more suppressed ring flipping of cyclohexyl rings at lower temperature.

Crystal Structure Determination

Crystals suitable for X-ray structural determination were mounted on a *Bruker SMART APEXII* CCD diffractometer. Samples were irradiated with graphite monochromated Mo-K α radiation ($\lambda=0.71073$ Å) at 173 K for data collection. The data were processed using the *APEX* program suite. All structures were solved by the *SHELXT* program (ver: 2014/5). Refinement on F^2 was carried out by full-matrix least-squares using the *SHELXL* in the *SHELX* software package (ver: 2014/7)¹³ and expanded using Fourier techniques. All non-hydrogen atoms were refined using anisotropic thermal parameters. The hydrogen atoms except for N–H (in **7**) were assigned to idealized geometric positions and included in the refinement with isotropic thermal parameters. The *SHELXL* was interfaced with *ShelXle* GUI (ver: 742) for most of the refinement steps.¹⁴ The pictures of molecules were prepared using *Pov-Ray* 3.7.0.¹⁵ The crystallographic data are summarized in Table S2 and S3.

Molecular Structure

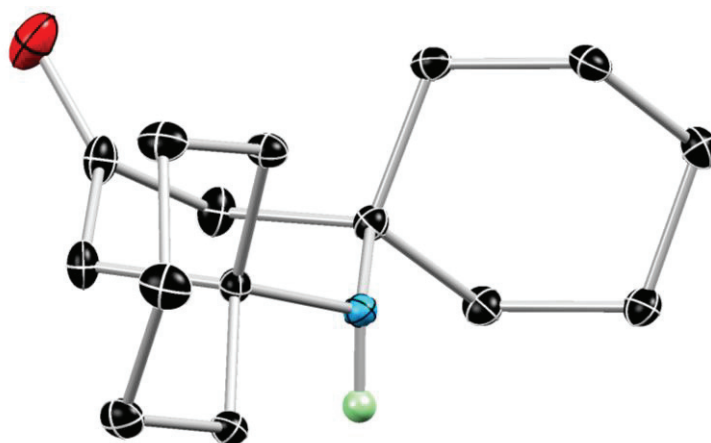


Figure S1. Molecular structure of **4** obtained from single-crystal X-ray diffraction analysis. Thermal ellipsoids are displayed at 30% probability. Hydrogen atoms except N–H are omitted for clarity.

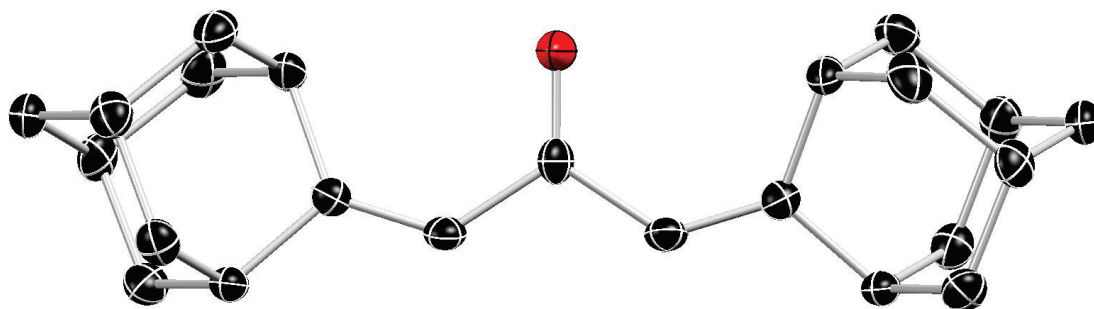


Figure S2. Molecular structure of **12** obtained from single-crystal X-ray diffraction analysis. Thermal ellipsoids are displayed at 30% probability. Hydrogen atoms except N–H are omitted for clarity.

Table S2. Crystallographic data.

	4	7	8
Formula	C ₁₅ H ₂₅ NO	C ₁₅ H ₂₇ N	C ₁₆ H ₂₉ N
Mol wt	235.36	221.37	235.40
Crystal system	Monoclinic	orthorhombic	monoclinic
Space group	<i>P2₁/n</i>	<i>P2₁2₁2₁</i>	<i>P2₁/n</i>
Color	colorless	colorless	colorless
Habit	block	block	needle
Cryst dimens, mm	0.333 × 0.259 × 0.189	0.11 × 0.10 × 0.10	0.08 × 0.04 × 0.02
<i>a</i> , Å	6.0130(5)	6.0545(7)	8.3640(11)
<i>b</i> , Å	25.431(2)	11.8787(15)	31.759(4)
<i>c</i> , Å	8.9724(8)	18.202(2)	10.5541(14)
<i>α</i> , deg	90	90	90
<i>β</i> , deg	107.4250(10)	90	92.253(2)
<i>γ</i> , deg	90	90	90
<i>V</i> , Å ³	1309.0(2)	1309.1(3)	2801.4(6)
<i>Z</i>	4	4	8
<i>D</i> _{calc} , g cm ⁻³	1.194	1.123	1.116
Abs coeff, mm ⁻¹	0.073	0.064	0.063
<i>F</i> (000)	520	496	1056
Temp, K	173(2)	173(2)	173(2)
Reflections	7543	7952	16980
Independent	3104	3067	7014
<i>R</i> _{int}	0.0141	0.0179	0.0362
Parameters	158	149	309
<i>R</i> ₁ [<i>I</i> > 2σ(<i>I</i>)]	0.0404	0.0358	0.0580
<i>wR</i> ₂ (all data)	0.1055	0.0968	0.1518
Goodness of fit	1.028	1.043	1.019
solv for crystallization	CH ₃ CN	CH ₂ Cl ₂ , -30 °C	CH ₃ CN

CCDC-1491871 (**7**) and 1491872 (**8**) contain the supplementary crystallographic data. These data can be obtained free of charge from the Cambridge Crystallographic Data Centre via www.ccdc.cam.ac.uk/data_request/cif

Table S3. Crystallographic data.

	10	11
Formula	C ₁₆ H ₂₅ NO	C ₂₃ H ₃₃ NO
Mol wt	247.37	339.50
Crystal system	Monoclinic	Triclinic
Space group	<i>P</i> 2 ₁ / <i>c</i>	<i>P</i> -1
Color	colorless	colorless
Habit	plate	block
Cryst dimens, mm	0.310 × 0.080 × 0.040	0.282 × 0.233 × 0.146
<i>a</i> , Å	8.7820(8)	6.8234(6)
<i>b</i> , Å	11.9846(11)	11.0008(9)
<i>c</i> , Å	12.9802(12)	12.4696(11)
<i>α</i> , deg	90	85.1360(10)
<i>β</i> , deg	100.2730(10)	80.6460(10)
<i>γ</i> , deg	90	76.1900(10)
<i>V</i> , Å ³	1344.2(2)	895.83(13)
<i>Z</i>	4	2
<i>D</i> _{calc} , g cm ⁻³	1.222	1.259
Abs coeff, mm ⁻¹	0.075	0.075
<i>F</i> (000)	544	372
Temp, K	173(2)	173(2)
Reflections	3160	4645
Independent	3160	3435
<i>R</i> _{int}	?	0.0123
Parameters	170	230
<i>R</i> ₁ [<i>I</i> > 2σ(<i>I</i>)]	0.0417	0.0417
<i>wR</i> ₂ (all data)	0.1560	0.0qq73
Goodness of fit	1.038	1.074
solv for crystallization	CH ₂ Cl ₂	hexane, boiling to r.t.

Table S4. Crystallographic data.

	12	13
Formula	C ₂₃ H ₃₀ O	C ₁₆ H ₂₇ N
Mol wt	322.47	233.38
Crystal system	monoclinic	monoclinic
Space group	<i>C2/c</i>	<i>P2₁/c</i>
Color	colorless	colorless
Habit	plate	plate
Cryst dimens, mm	0.120 × 0.080 × 0.030	0.156 × 0.126 × 0.018
<i>a</i> , Å	6.611(3)	8.8309(19)
<i>b</i> , Å	11.216(5)	11.962(3)
<i>c</i> , Å	23.639(11)	12.873(3)
<i>α</i> , deg	90	90
<i>β</i> , deg	97.196(7)	97.788(3)
<i>γ</i> , deg	90	90
<i>V</i> , Å ³	1739.1(14)	1347.4(5)
<i>Z</i>	4	4
<i>D</i> _{calc} , g cm ⁻³	1.232	1.150
Abs coeff, mm ⁻¹	0.073	0.065
<i>F</i> (000)	704	520
Temp, K	173(2)	173(2)
Reflections	4207	6321
Independent	1674	2471
<i>R</i> _{int}	0.0257	0.0212
Parameters	110	160
<i>R</i> ₁ [<i>I</i> > 2σ(<i>I</i>)]	0.0942	0.0526
<i>wR</i> ₂ (all data)	0.2783	0.1388
Goodness of fit	1.174	1.086
solv for crystallization	CH ₂ Cl ₂	Ethyl acetate, -30 °C

NMR Spectra

NMR Spectra of CPC(H) (7)

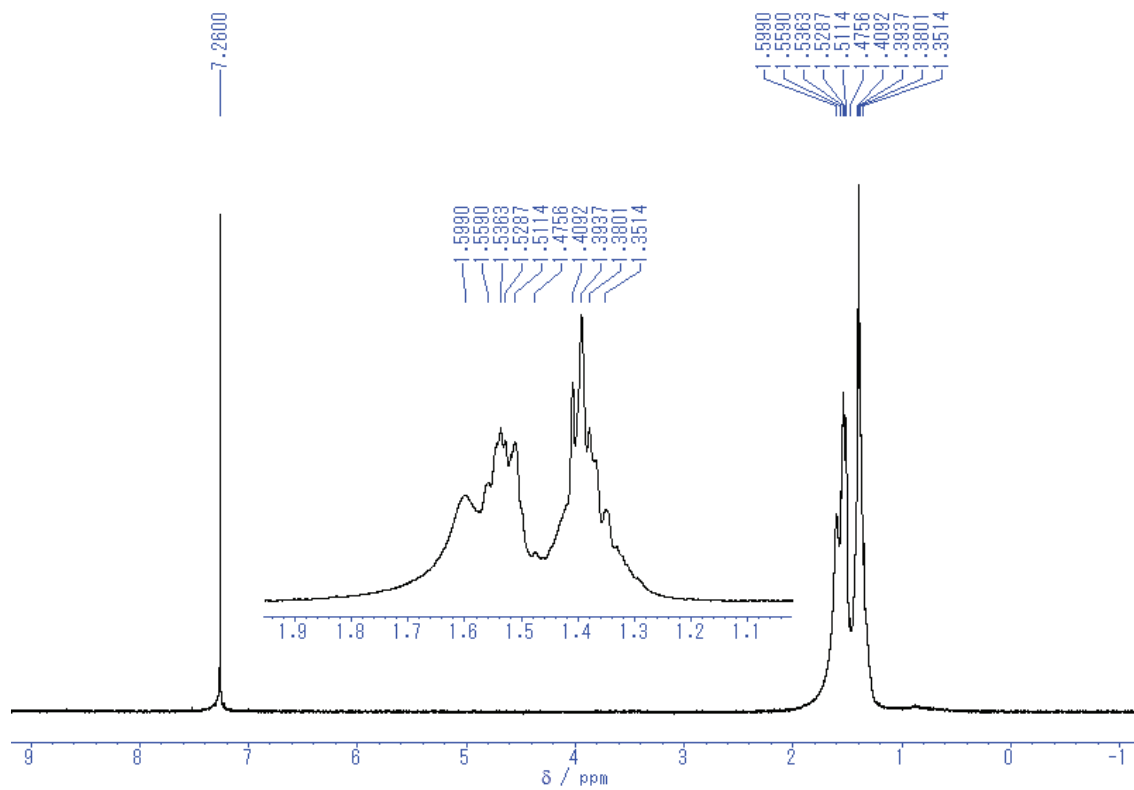


Figure S3. ^1H NMR spectrum (400 MHz) of **7** in CDCl_3 .

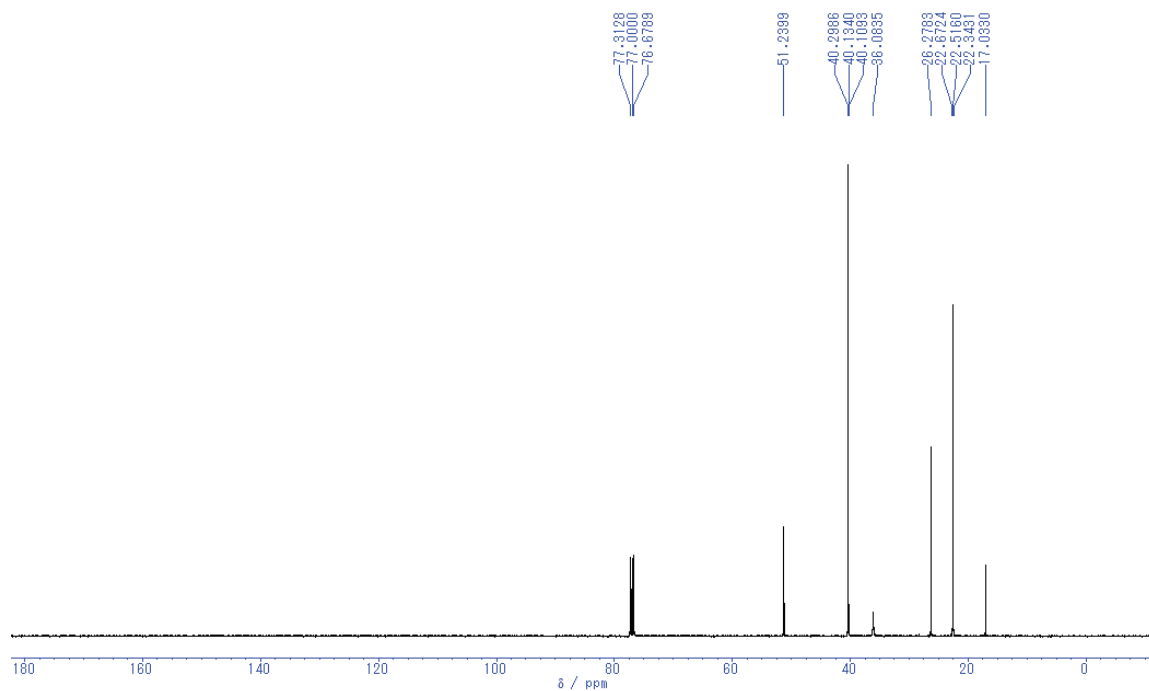


Figure S4. $^{13}\text{C}\{^1\text{H}\}$ NMR spectrum (100 MHz) of **7** in CDCl_3 .

NMR Spectra of CPC(Me) (**8**)

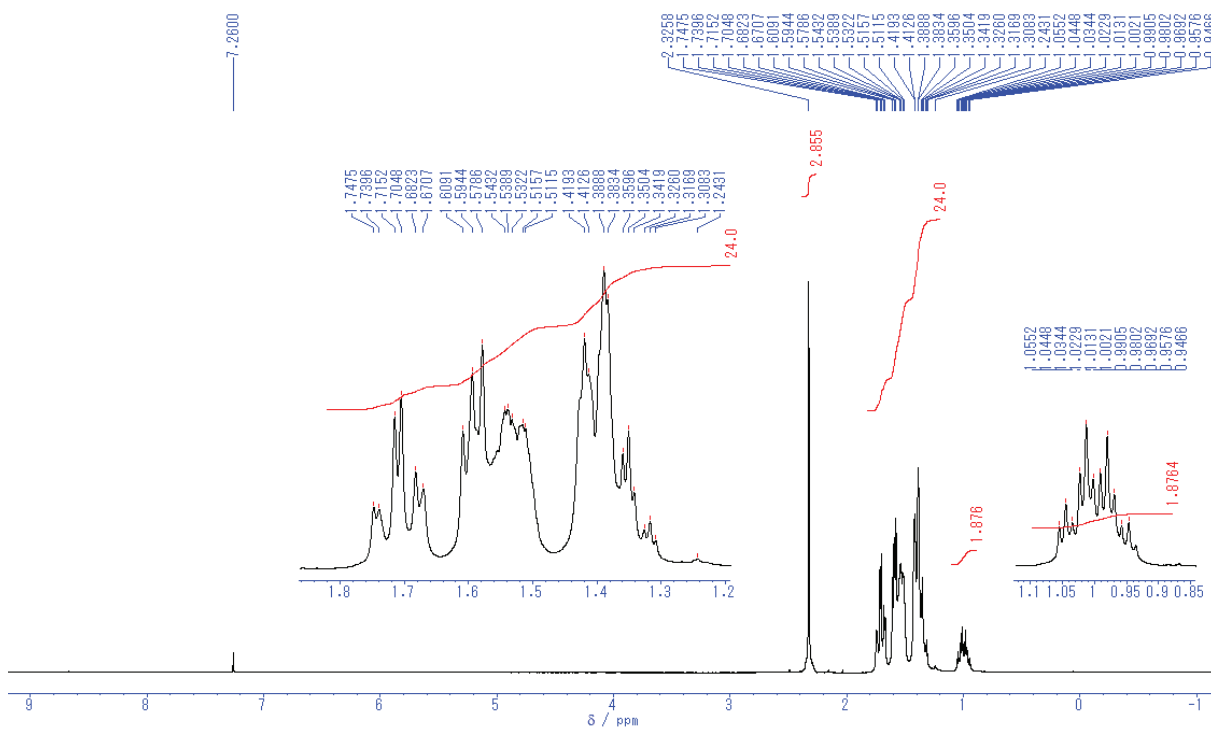


Figure S5. ^1H NMR spectrum (400 MHz) of **8** in CDCl_3 .

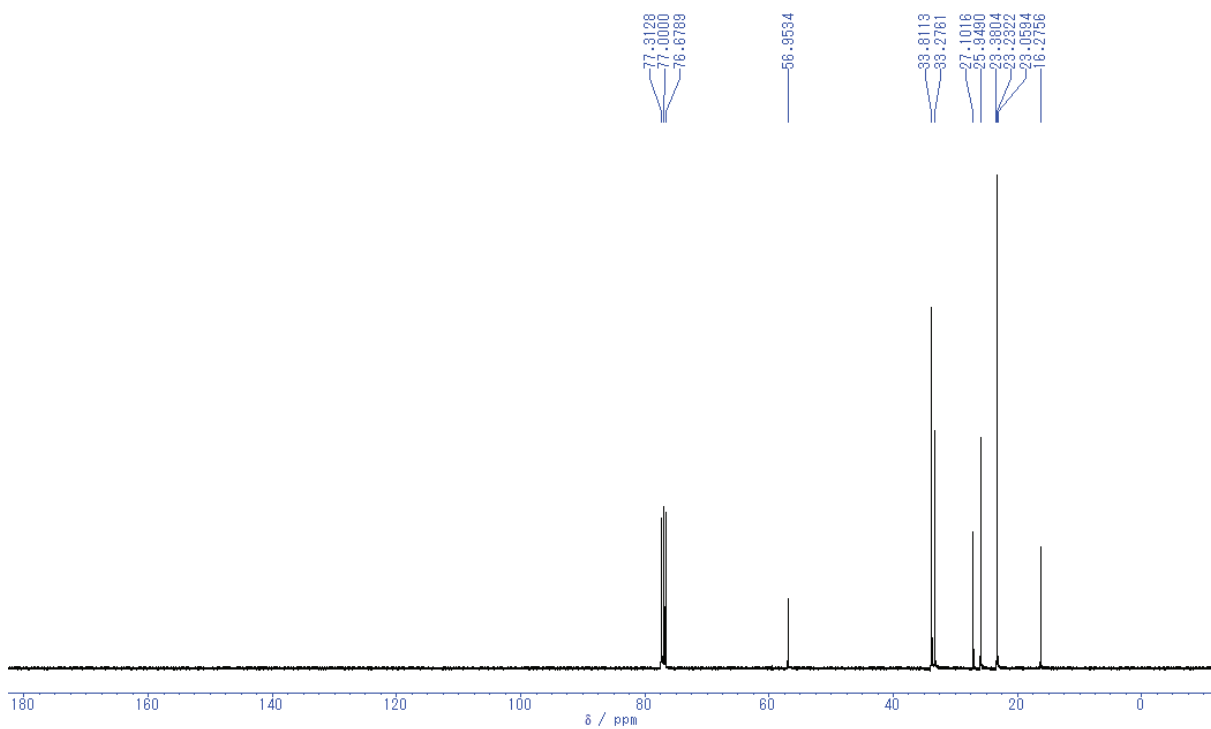


Figure S6. $^{13}\text{C}\{^1\text{H}\}$ NMR spectrum (100 MHz) of **8** in CDCl_3 .

NMR Spectra of **10**

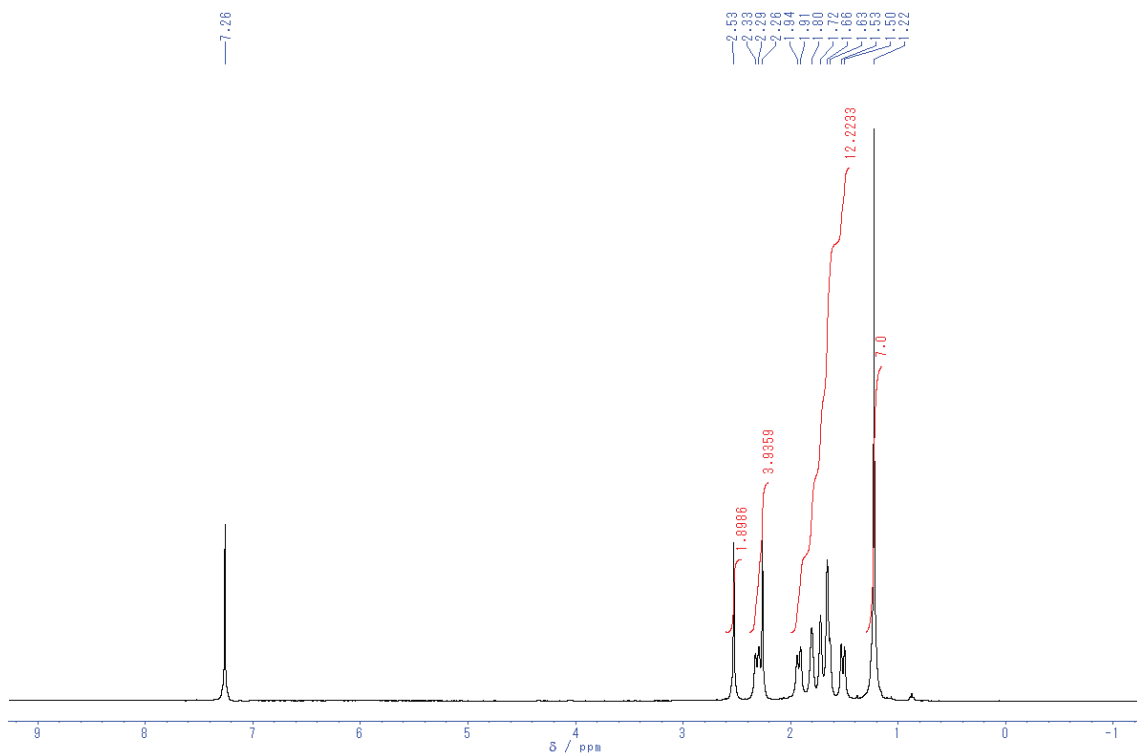


Figure S7. ¹H NMR spectrum (400 MHz) of **10** in CDCl₃.

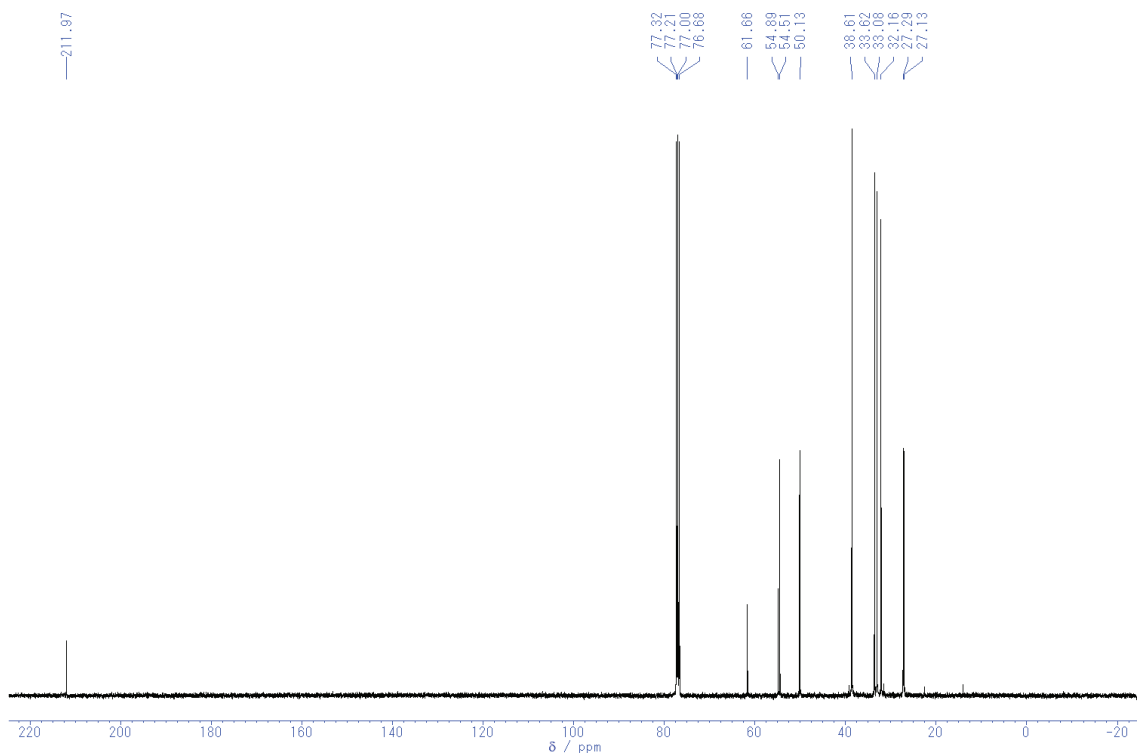


Figure S8. ¹³C NMR spectrum (400 MHz) of **10** in CDCl₃.

NMR Spectra of **11**

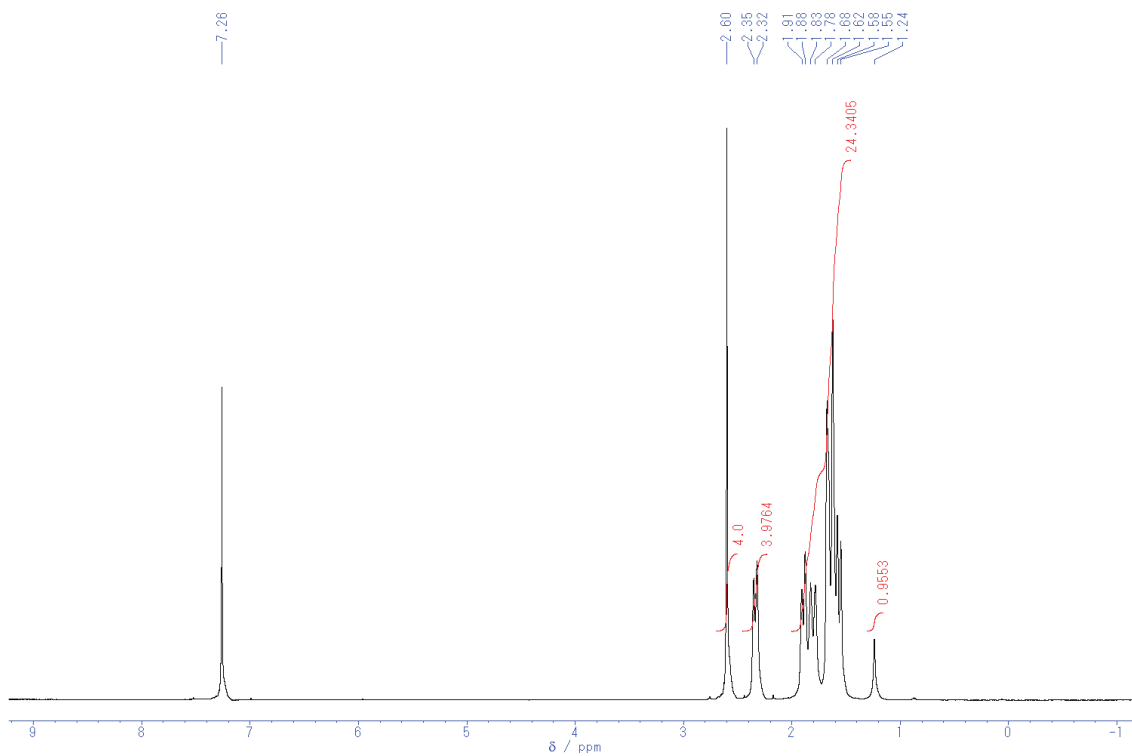


Figure S9. ^1H NMR spectrum (400 MHz) of **11** in CDCl_3 .

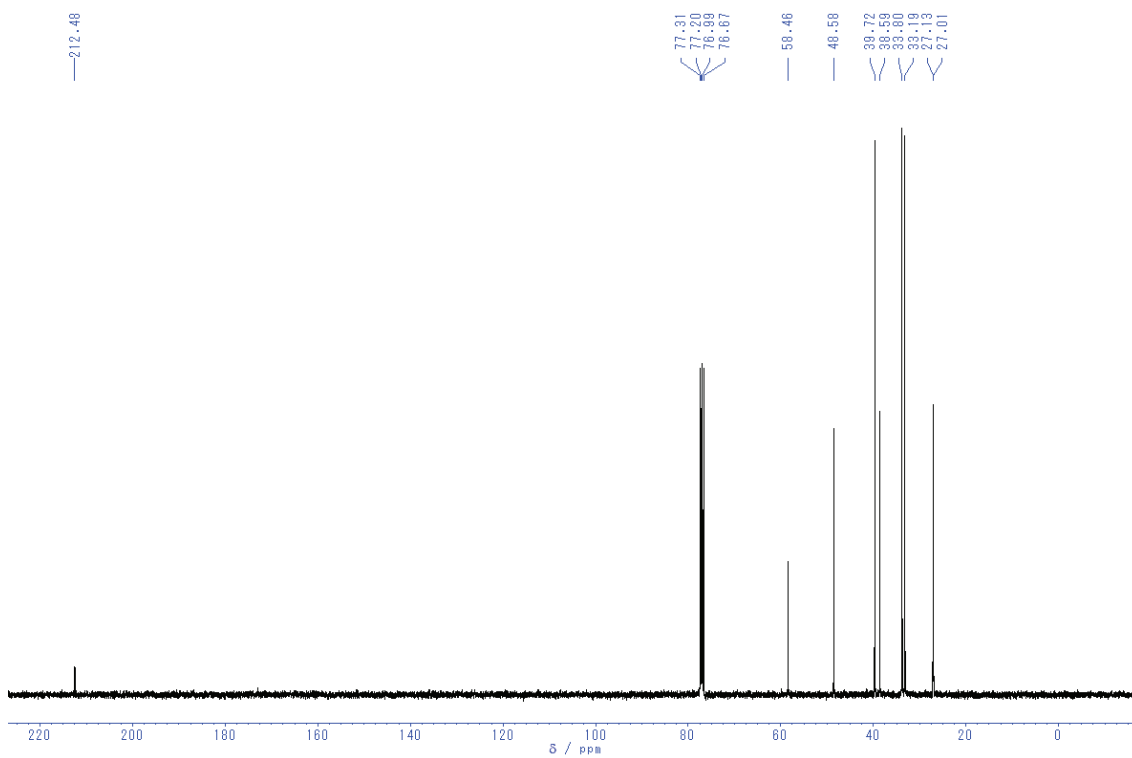


Figure S10. ^{13}C NMR spectrum (400 MHz) of **11** in CDCl_3 .

NMR Spectra of **12**

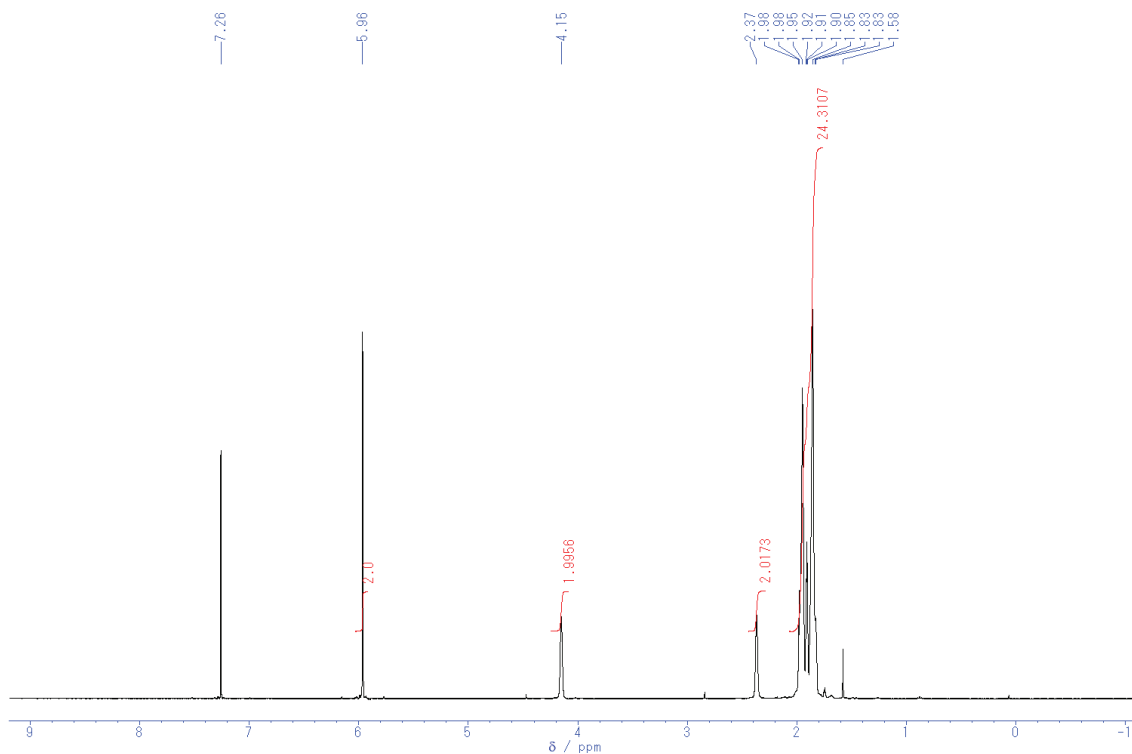


Figure S11. ¹H NMR spectrum (400 MHz) of **12** in CDCl₃.

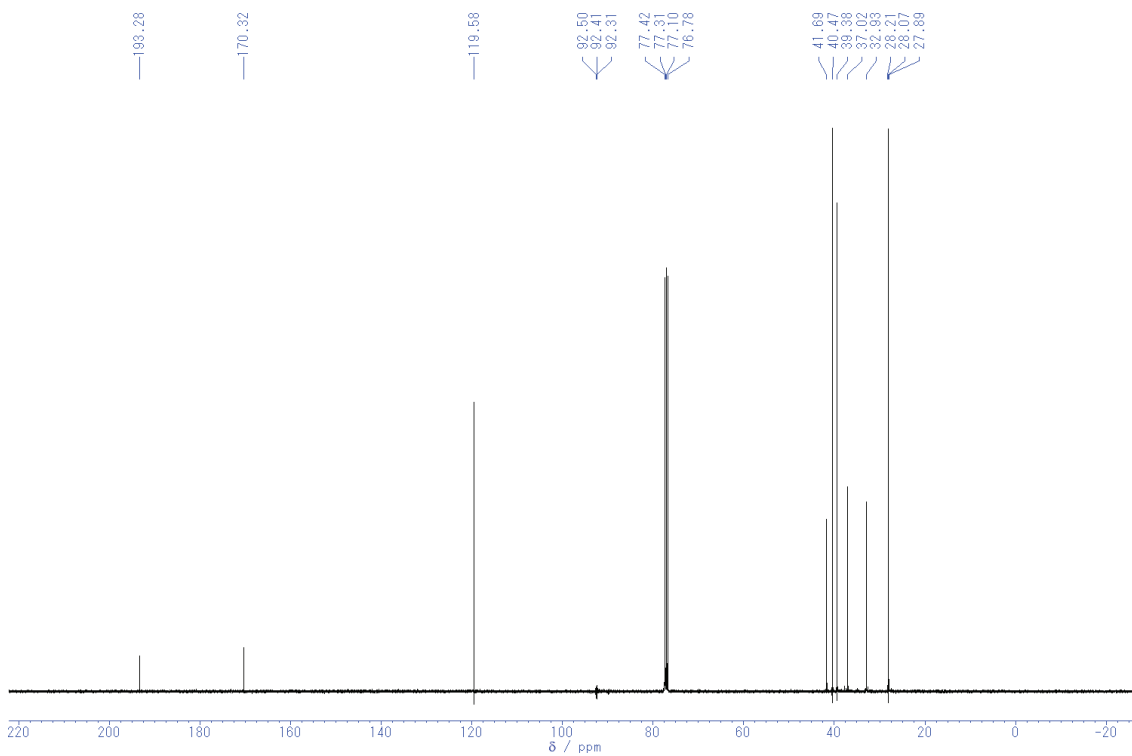


Figure S12. ¹³C NMR spectrum (400 MHz) of **12** in CDCl₃.

NMR Spectra of **13**

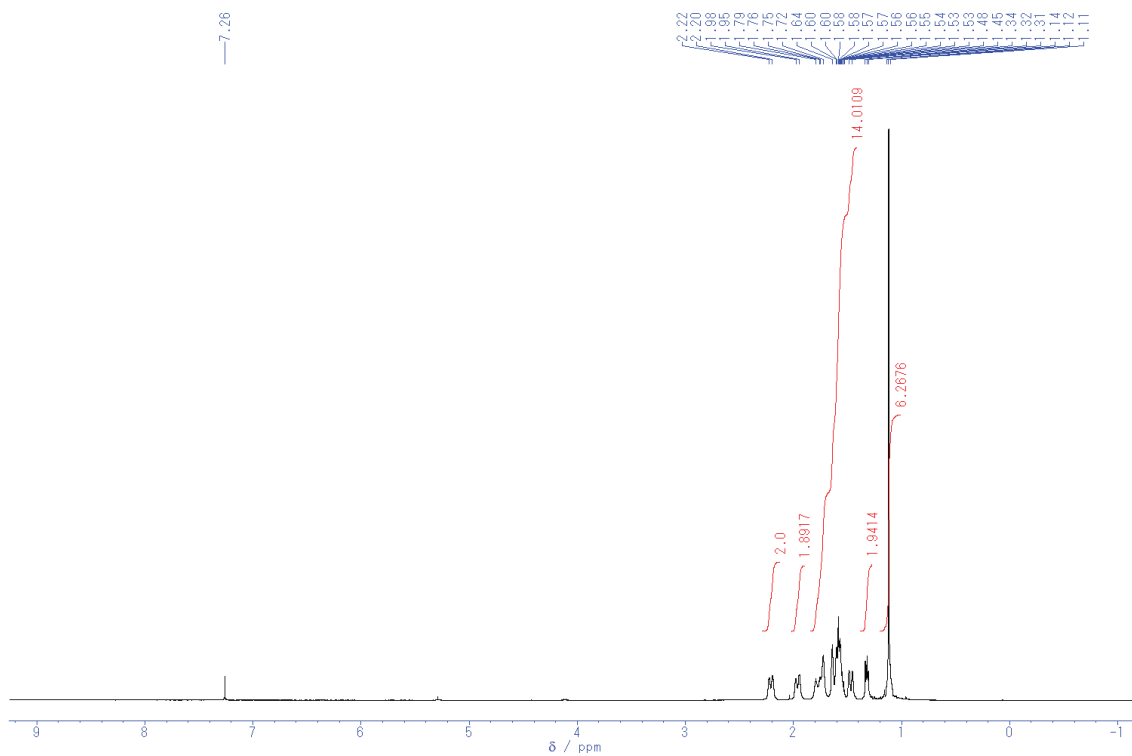


Figure S13. ¹H NMR spectrum (400 MHz) of **13** in CDCl₃.

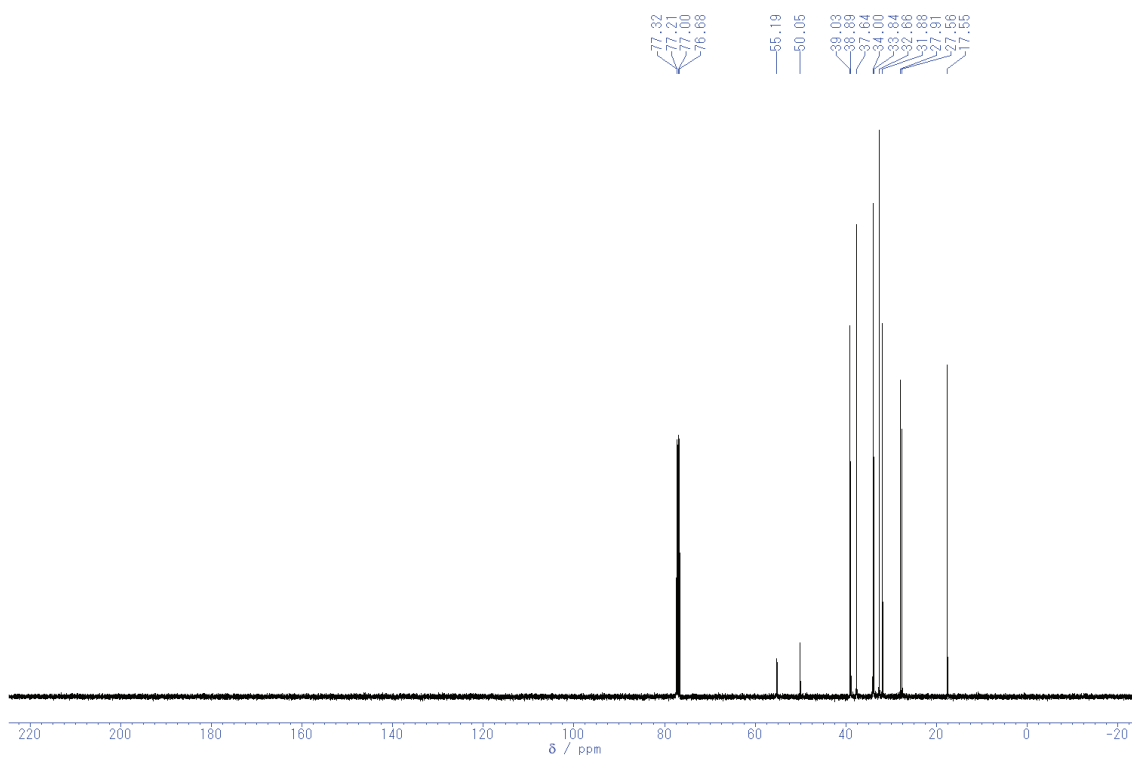


Figure S14. ¹³C NMR spectrum (400 MHz) of **13** in CDCl₃.

Variable Temperature ^1H NMR Spectra

Variable-temperature ^1H NMR (500 MHz) spectra were recorded using JEOL JNM-ECA500 NMR spectrometer in toluene- d_8 . The ^1H chemical shifts (δ scale) were determined by residual protons of the solvent (^1H , $\text{C}_6\text{D}_5\text{CD}_3$, $\delta = 2.11$ ppm). Anhydrous toluene- d_8 was used for these measurements.

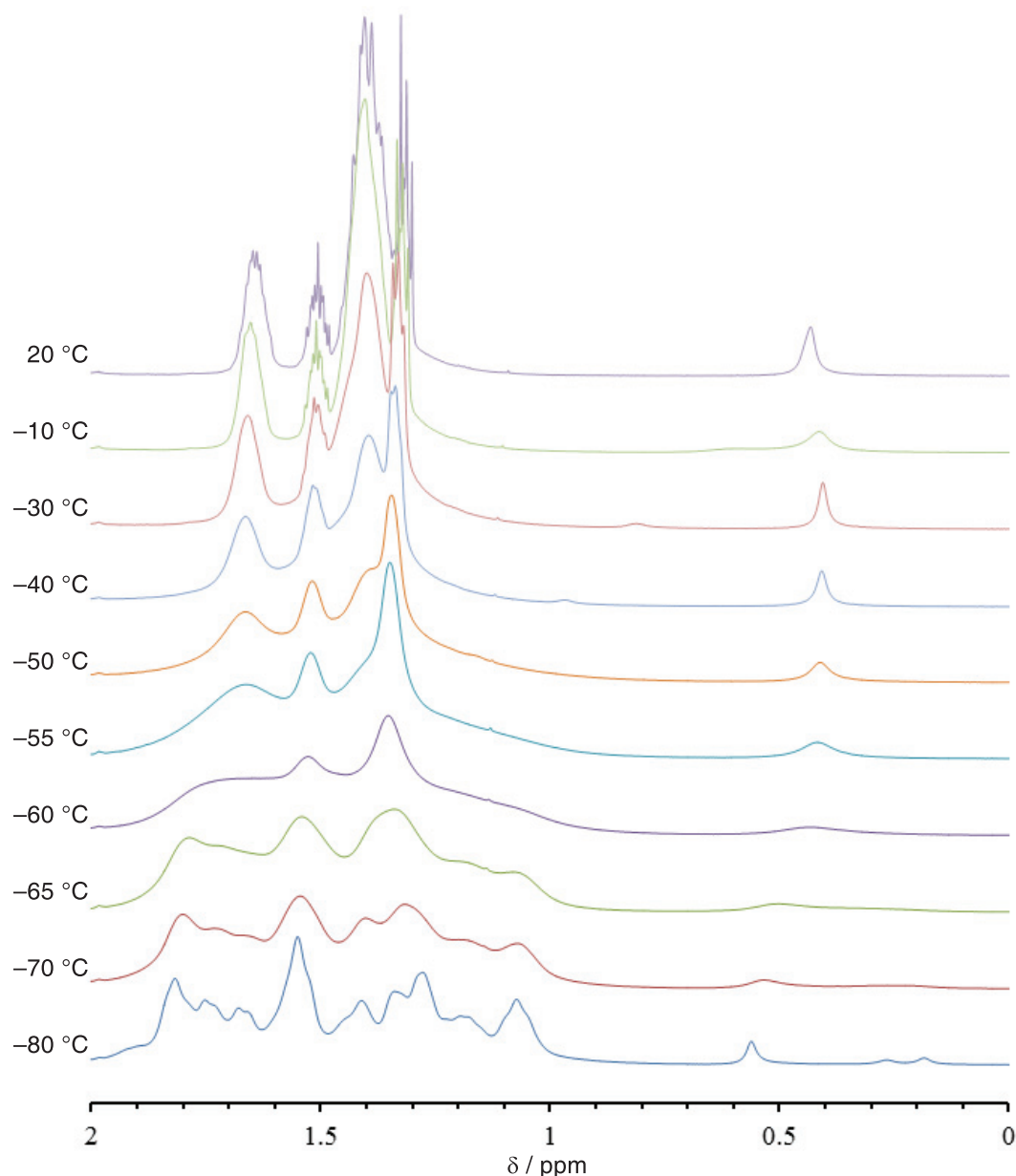
VT ^1H NMR of CPC(H) (7)

Figure S15. ^1H NMR spectrum (500 MHz) of **7** in toluene- d_8 (ca. 0.02 mmol/0.55 mL).

The secondary amine **7** showed the coalescence of the signals with lowering the temperature from -30 $^\circ\text{C}$ to -60 $^\circ\text{C}$. The broad signals gradually sharpened as the temperature dropped below -60 $^\circ\text{C}$.

VT ^1H NMR of CPC(Me) (**8**)

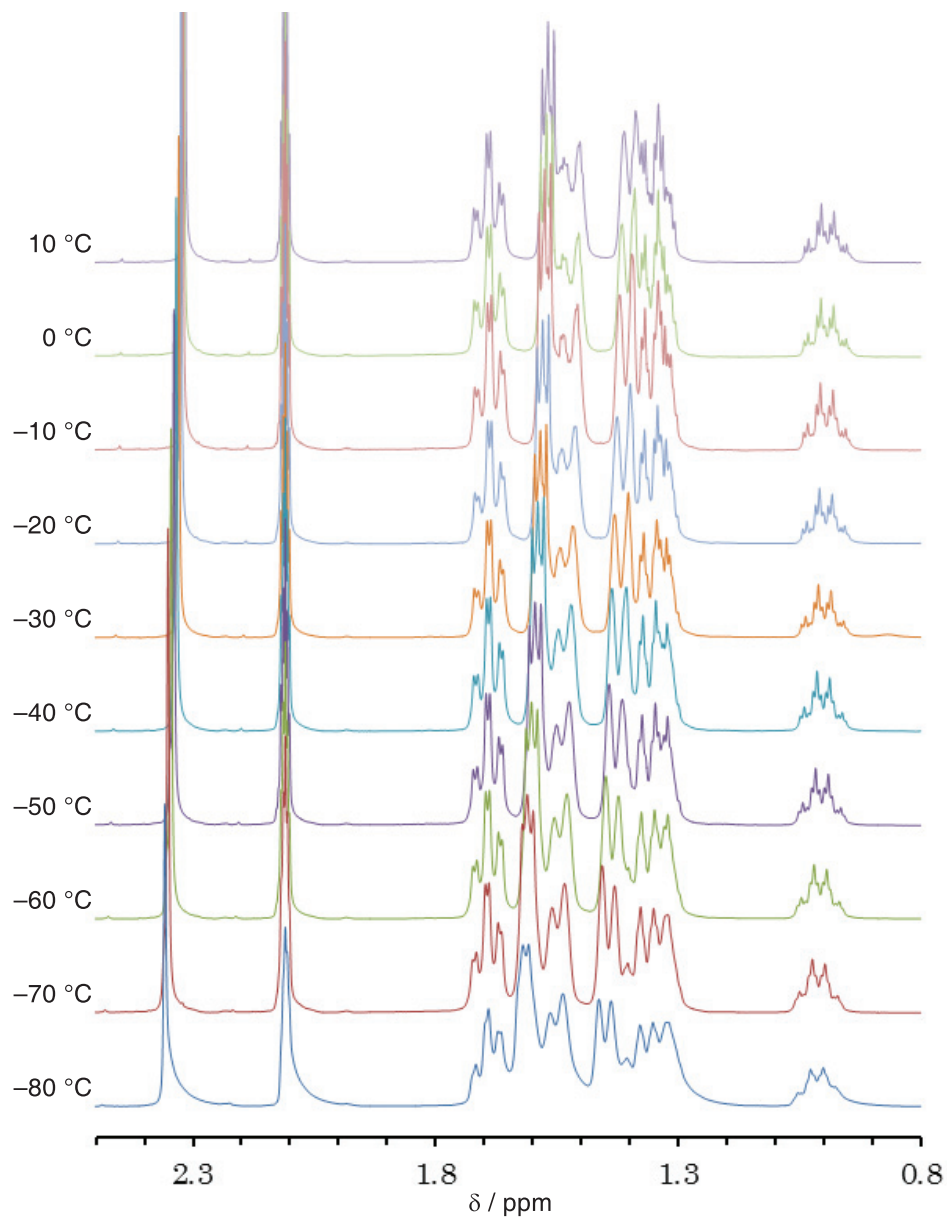


Figure S16. ^1H NMR spectrum (500 MHz) of **8** in $\text{toluene-}d_8$ (ca. 0.02 mmol/0.55 mL).

In the case of the tertiary amine **8**, no coalescence was observed between -80°C and 20°C .

Preliminary Computational Studies

General Considerations

DFT calculations were performed using the Gaussian 09 package of programs¹⁶ to estimate the relative energy gaps of possible conformational isomers **7A–F** and **8A–F**. For the conformational isomers **7A–F** and **8A–F**, the B3LYP¹⁷ hybrid functional was used with 6-31G(d,p) basis set for geometry optimization after geometry pre-optimization at the HF/6-31G(d) level of theory. All structures were optimized without any symmetry assumptions. After each geometry optimization at the B3LYP/6-31G(d,p), a frequency calculation at the same level was performed to verify that all the stationary points had no imaginary frequency. The relative energy gaps (kcal/mol) were calculated from the sum of the electronic (E) and zero-point energies (ZPE).

The energy gaps of possible conformational isomers of CPC(H) (7)

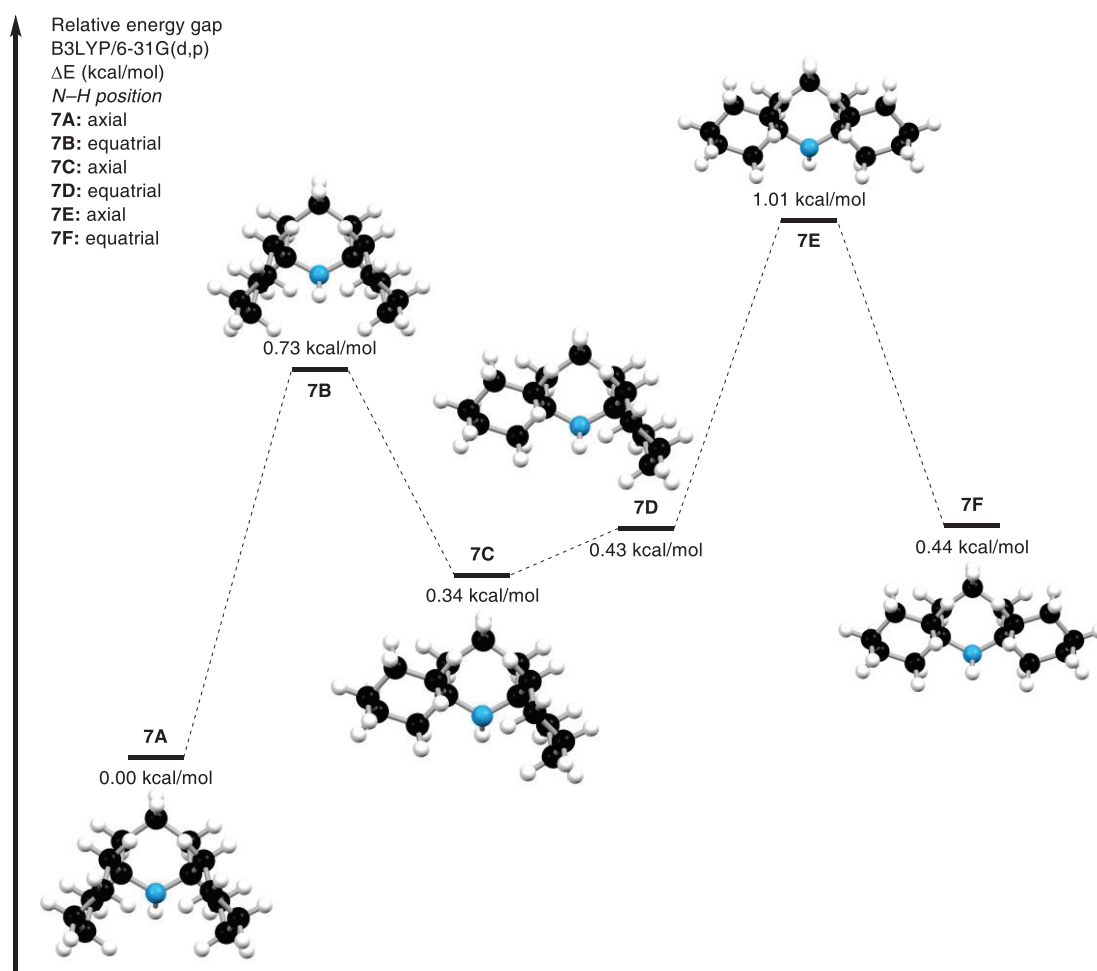


Figure S17. Relative energy gaps of possible conformational isomers **7A–F** at the level of B3LYP/6-31G(d,p).

Table S4. The electronic energies of **2A–F** at the B3LYP/6-31G(d,p) level of theory in Hartrees.

	7A	7B	7C	7D	7E	7F
E	-642.6286522	-642.6273861	-642.6285862	-642.6281033	-642.627284	-642.6280868
ZPE	0.4048	0.4047	0.405282	0.404941	0.405045	0.404931
E+ZPE	-642.2238522	-642.2226861	-642.2233042	-642.2231623	-642.222239	-642.2231558

The energy gaps between each isomer are very small (<1.01 kcal/mol).

The energy gaps of possible conformational isomers of CPC(Me) (8)

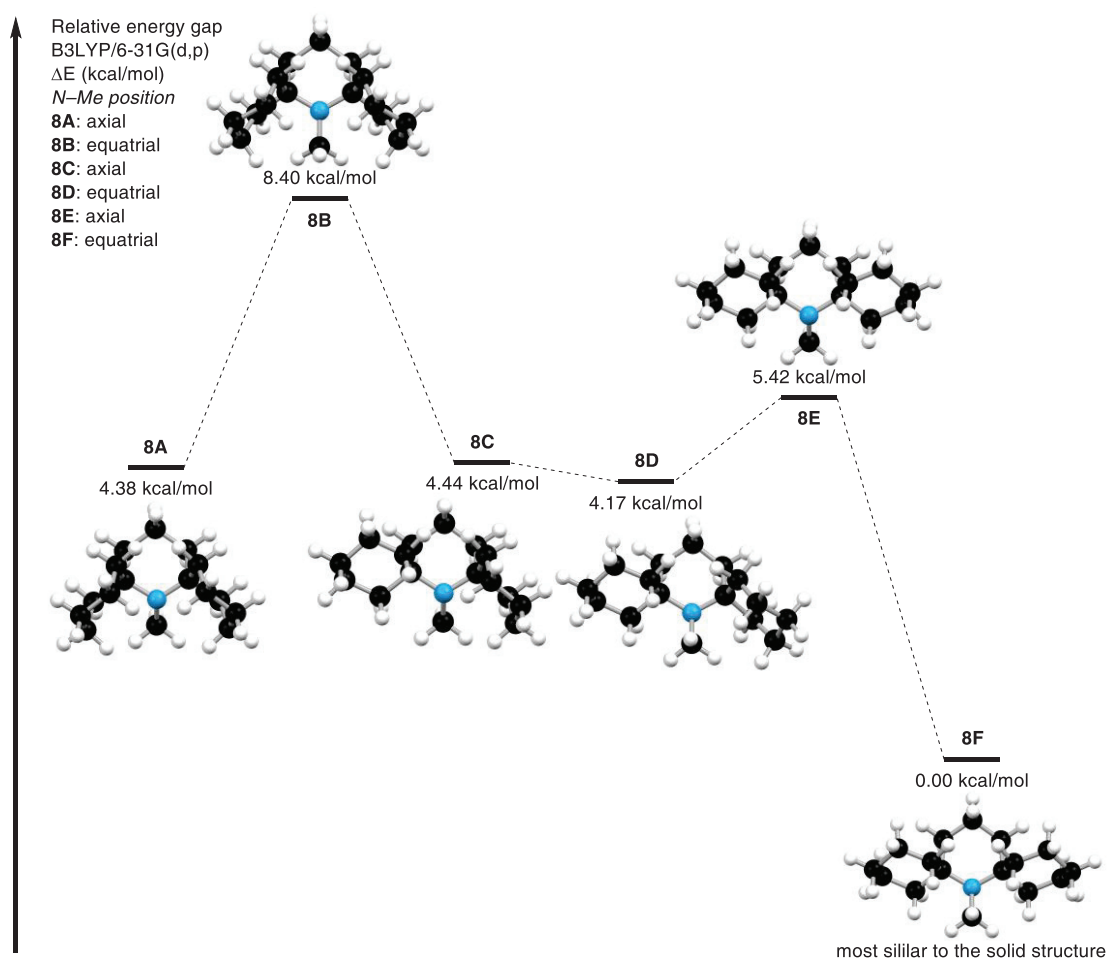


Figure S18. Relative energy gaps of possible conformational isomers **8A–F** at the level of B3LYP/6-31G(d,p).

Table S5. The electronic energies of **3A–F** at the B3LYP/6-31G(d,p) level of theory in Hartrees.

	8A	8B	8C	8D	8E	8F
E	-681.9116736	-681.9042846	-681.9113832	-681.9109826	-681.9095918	-681.9179246
ZPE	0.434457	0.433487	0.434277	0.433434	0.434041	0.433736
E+ZPE	-681.4772166	-681.4707976	-681.4771062	-681.4775486	-681.4755508	-681.4841886

In comparison to **7**, the energy gaps between conformational isomers of **8** are larger (4.17–8.40 kcal/mol).

Proposed Reaction Mechanism^{5c}

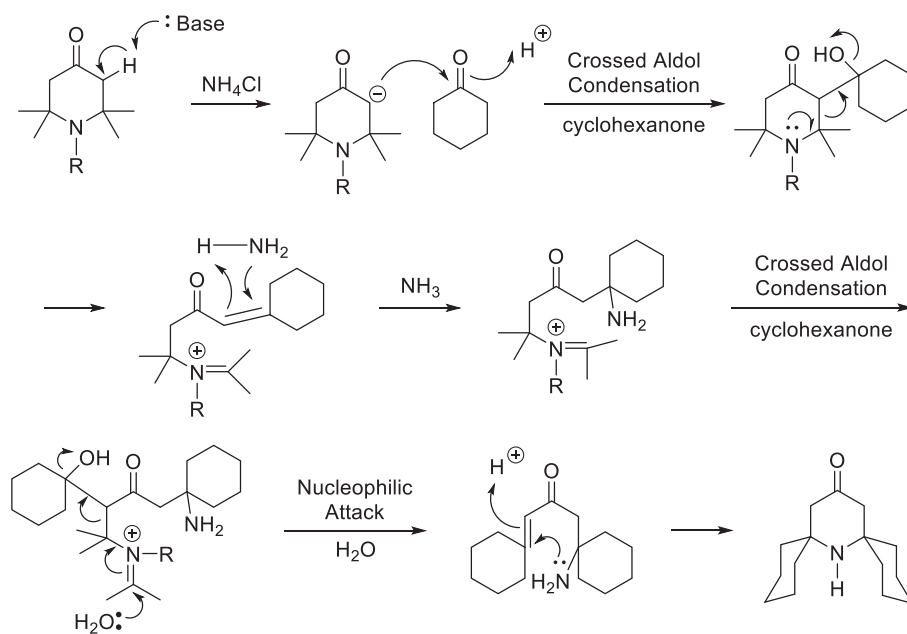


Figure S11. Proposed reaction mechanism from **1** to **4**.

References

- [1]. α -Hydrogen atom adjacent to an anionic nitrogen atom (e.g., $\text{LiN}(\text{CHMe}_2)_2$) can migrate to electrophilic substrates, see:
- (a) Nguyen, T. T. T.; Boussonnière, A.; Banaszak, E.; Castanet, A.-S.; Nguyen, K. P. P.; Mortier, J. *J. Org. Chem.* **2014**, *79*, 2775–2780.
 - (b) Gallagher, D. J.; Henderson, K. W.; Kennedy, A. R.; O'Hara, C. T.; Mulvey, R. E.; Rowlings, R. B. *Chem. Commun.* **2002**, 376–377.
 - (c) Sanchez, R.; Scott, W. *Tetrahedron Lett.* **1988**, *29*, 139–142.
 - (d) Woo, E. P.; *Tetrahedron Lett.* **1974**, *15*, 4095–4098.
- [2]. Decomposition of TMP has been reported in certain cases, see:
- (a) Kennedy, A. R.; Klett, J.; McGrath, G.; Mulvey, R. E.; Robertson, G. M.; Robertson, S. D.; O'Hara, C. T. *Inorg. Chim. Acta* **2014**, *411*, 1–4.
 - (b) Kennedy, A. R.; Leenhouts, S. M.; Liggat, J. J.; Martínez-Martínez, A. J.; Miller, K.; Mulvey, R. E.; O'Hara, C. T.; O'Keefe, P.; Steven, A. *Chem. Commun.* **2014**, *50*, 10588–10591.
 - (c) Conway, B.; Kennedy, A. R.; Mulvey, R. E.; Robertson, S. D.; Álvarez, J. G. *Angew. Chem. Int. Ed.* **2010**, *49*, 3182–3184.
- [3]. Mulvey, R. E.; Robertson, S. D. *Angew. Chem. Int. Ed.* **2013**, *52*, 11470–11487.
- [4]. Campbell, R.; Conway, B.; Fairweather, G. S.; García-Álvarez, P.; Kennedy, A. R.; Klett, J.; Mulvey, R. E.; O'Hara, C. T.; Robertson, G. M. *Dalton Trans.* **2010**, *39*, 511–519.
- [5]. (a) Ma, Z.; Huang, Q.; Bobbitt, J. M. *J. Org. Chem.* **1993**, *58*, 4837–4843.
- (b) Miura, Y.; Nakamura, N.; Taniguchi, I. *Macromolecules* **2001**, *34*, 447–455.
 - (c) Sakai, K.; Yamada, K.-i.; Yamasaki, T.; Kinoshita, Y.; Mito, F.; Utsumi, H. *Tetrahedron* **2010**, *66*, 2311–2315.
 - (d) Yamasaki, T.; Mito, F.; Ito, Y.; Pandian, S.; Kinoshita, Y.; Nakano, K.; Murugesan, R.; Sakai, K.; Utsumi, H.; Yamada, K.-i. *J. Org. Chem.* **2011**, *76*, 435–440.
- [6]. (a) Carrozza, P.; Ferri, G. Process for the Methylation of 2,2,6,6-Tetramethylpiperidin-4-one. European Patent 0,729,947, September 4, 1996.
- (b) The detailed synthetic procedure and NMR data are described in the experimental section.
- [7]. Synthesis of tetrahydro-4*H*-thiopyran-4-one, see; Rule, G. N.; Detty, R. M.; Kaeding, E. J.; Sinicropi, A., *J. Org. Chem.*, **1995**, *60*, 1665–1673.
- [8]. It was reported in ref. 5c that use of **1b** in a crossed aldol condensation improved the yield of a desired dispiro-piperidine.
- [9]. The detailed synthetic procedure and its molecular structure are described in the experimental section
- [10]. Chandrasekhar, S.; Reddy, C. R.; Babu, N. *J. Org. Chem.* **2002**, *67*, 9080–9082.
- [11]. Wolff–Kishner–Huang reduction from 2,2,6,6-tetramethylpiperidin-4-one to TMP(H), see:

- Kampmann, D.; Stuhlmu"ller, G.; Simon, R.; Cottet, F.; Leroux, F.; Schlosser, M. *Synthesis* **2005**, *2005*, 1028–1029.
- [12]. Orther, L. *Liebigs Ann. Chem.* **1928**, *459*, 217–233.
- [13]. Sheldrick, G. M. A short history of *SHELXL*. *Acta Cryst.* **2008**, *A64*, 112–122.
- [14]. H"ubebschle, C. B.; Sheldrick, G. M.; Dittrich, B. *ShelXle*: a Qt graphical user interface for *SHELXL*. *J. Appl. Cryst.* **2011**, *44*, 1281–1284.
- [15]. Persistence of Vision Raytracer (*ver.* 3.7.0); Persistence of Vision Pty. Ltd., 2016; Retrieved from <http://www.povray.org/download/>
- [16]. Gaussian 09, Revision D.01, Frisch, M. J.; Trucks, G. W.; Schlegel, H. B.; Scuseria, G. E.; Robb, M. A.; Cheeseman, J. R.; Scalmani, G.; Barone, V.; Mennucci, B.; Petersson, G. A.; Nakatsuji, H.; Caricato, M.; Li, X.; Hratchian, H. P.; Izmaylov, A. F.; Bloino, J.; Zheng, G.; Sonnenberg, J. L.; Hada, M.; Ehara, M.; Toyota, K.; Fukuda, R.; Hasegawa, J.; Ishida, M.; Nakajima, T.; Honda, Y.; Kitao, O.; H. Nakai, O.; Vreven, T.; Montgomery, J. A., Jr.; Peralta, J. E.; Ogliaro, F.; Bearpark, M.; Heyd, J. J.; Brothers, E.; Kudin, K. N.; Staroverov, V. N.; Keith, T.; Kobayashi, R.; Normand, J.; Raghavachari, K.; Rendell, A.; Burant, J. C.; Iyengar, S. S.; Tomasi, J.; Cossi, M.; Rega, N.; Millam, J. M.; Klene, M.; Knox, J. E.; Cross, J. B.; Bakken, V.; Adamo, C.; Jaramillo, J.; Gomperts, R.; Stratmann, R. E.; Yazyev, O.; Austin, A. J.; Cammi, R.; Pomelli, C.; Ochterski, J. W.; Martin, R. L.; Morokuma, K.; Zakrzewski, V. G.; Voth, G. A.; Salvador, P.; Dannenberg, J. J.; Dapprich, S.; Daniels, A. D.; Farkas, O.; Foresman, J. B.; Ortiz, J. V.; Cioslowski, J.; Fox, D. J.; Gaussian, Inc.: Wallingford CT, 2013.
- [17]. (a) Becke, A. D. Density-functional exchange-energy approximation with correct asymptotic behavior. *Phys. Rev. A: Gen. Phys.* **1988**, *38*, 3098–3100.
- (b) Lee, C.; Yang, W.; Parr, R. G. Development of the Colle-Salvetti correlation-energy formula into a functional of the electron density. *Phys. Rev. B: Condens. Matter* **1988**, *37*, 785–789.
- (c) Becke, A. D. A new mixing of Hartree-Fock and local-density-functional theories. *J. Chem. Phys.* **1993**, *98*, 1372–1377.
- (d) Becke, A. D. Density-functional thermochemistry. III. The role of exact exchange. *J. Chem. Phys.* **1993**, *98*, 5648–5652.

Chapter 3

Deprotonative-Metalation Reactions

3-1. Introduction

Sterically hindered lithium amides (Li-NR_2) show high proton affinity and poor nucleophilicity, which make Li-NR_2 useful and excellent deprotonation reagents. For example, by using sterically demanding Li-NR_2 in the deprotonation reaction of ketones, corresponding silyl enol ethers, which are storable nucleophiles utilizing in Mukaiyama aldol addition, are obtained region- and/or stereoselectively.¹ In addition, amides can be used as a base for (aromatic)C–H metalation. Direct C–H metalation is a powerful tool for synthesizing highly functionalized aromatics in fields of functional materials and pharmaceuticals.² Besides common deprotonation methods that include the employment of strong Brønsted bases such as alkyllithium and lithium amides,³ heterobimetallic heteroleptic ate compounds have attracted attention in recent years.⁴ In particular, the lithium dialkyl(amido)zincate reagents such as $[\text{Li}(\text{TMP})\text{Zn}(\text{tBu})_2]$ (TMP = 2,2,6,6-tetramethylpiperidino), first reported by Kondo and Uchiyama et al.,⁵ offer complementary reactivity and improved regio- and chemoselectivity with high functional group tolerance in certain cases.^{6,7} The steric bulk of amido ligands used in these zincate reagents have been recently shown to play a decisive role in the reactivity and regioselectivity of C–H metalation (Figure 1).^{8,9} Despite of their crucial role and wide applications in synthetic organic chemistry, the library of sterically hindered secondary amides remains rather small, with diisopropylamide (DA), 1,1,1,3,3,3-hexamethyldisilazide (HMDS), and TMP being the mostly used amides (Figure 2).¹⁰ As mentioned in chapter 2, among these reagents, TMP is preferred as it offers higher stability,^{11,12} larger steric bulk,^{10,13} and the highest basicity as the lithium amide.¹⁰

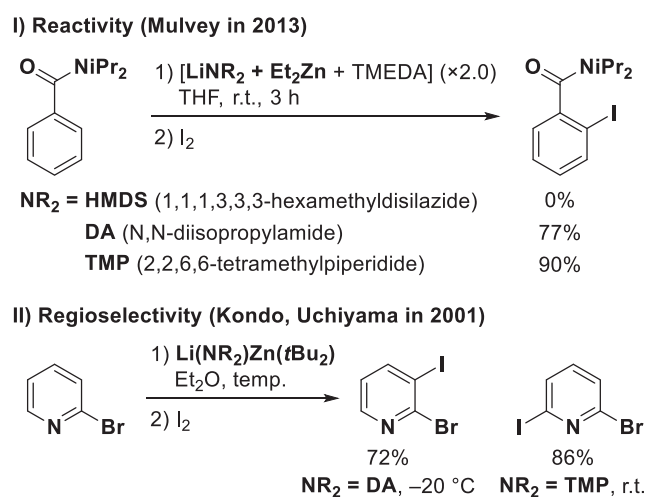
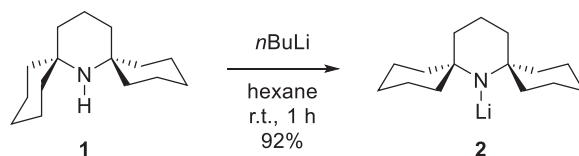


Figure 1. Selected examples demonstrating the effect of different amido ligands on reactivity and regioselectivity of C–H activation: Iodination of (I) *N,N*-diisopropylbenzamide and (II) 2-bromopyridine.

3-2. Synthesis of the Lithium Amide

Herein, to develop sterically hindered Li–NR₂ toward application for regioselective deprotonation reaction, the direct *N*-lithiation of CPC(H) (**1**) is reported. The parent amine (**1**) can be easily deprotonated by *n*BuLi in hexane at room temperature to afford the lithium amide complex (LiCPC, **2**), which crystallizes as colorless hexagonalshaped crystals (Scheme 1). The ⁷Li NMR spectrum of **2** showed a singlet at 2.75 ppm, similar to that observed for (LiTMP)_n at 2.47 ppm, which contains a mixture of tetramer and trimer of LiTMP.^{14a}



Scheme 1. *N*-lithiation of CPC(H) to afford LiCPC **2**.

A single-crystal X-ray crystallographic study revealed that **2** crystallized as an unsolvated cyclic trimer (Figure 2), which is isostructural to the previously reported (LiTMP)₃.^{14a} The structural parameters of **2** are almost identical to those observed in (LiTMP)₃.^{14a} The two cyclohexyl rings assume equatorial positions due to steric hindrance.

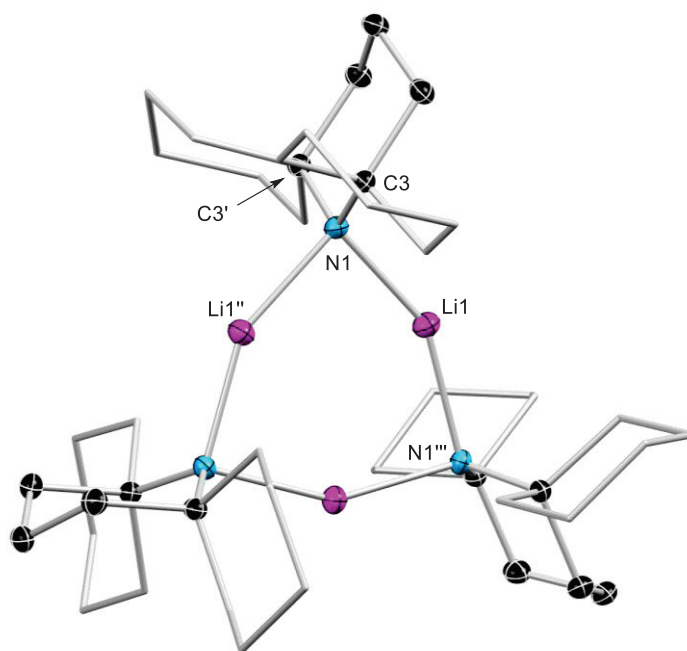
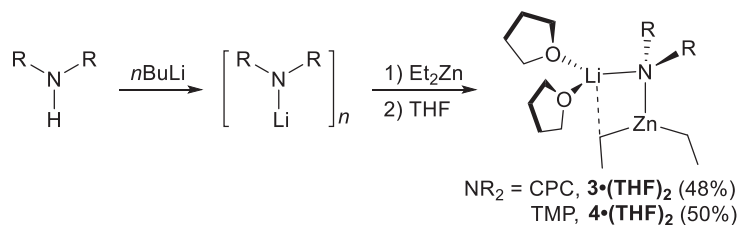


Figure 2. Molecular structure of LiCPC (**2**) obtained from single-crystal X-ray diffraction analysis. Thermal ellipsoids are displayed at 30% probability. Those of peripheral atoms and hydrogen atoms are omitted for clarity. Selected bond angles (degrees) for LiCPC (**2**): N1–Li1 2.003(3), N1–Li1'' 2.064(3); C3–N1–C3' 116.2(2), Li1–N1–Li1'' 88.7(2), N1–Li1–N1''' 151.3(2).

3-3. Syntheses of Monoamidodialkyl Zincate Complexes

Herein, syntheses and structural characterization of the lithium dialkyl(amido)zincate using both CPC and TMP for a detailed comparison are reported. The zincates $[\text{Li}(\mu\text{-NR}_2)(\mu\text{-Et})\text{Zn}(\text{Et})]$ ($\text{NR}_2 = \text{CPC}$, **3** and $\text{NR}_2 = \text{TMP}$, **4**) were obtained by addition of the commercially available ZnEt_2 to a freshly prepared lithium amide suspension (LiNR_2 , $\text{NR}_2 = \text{CPC}$ and TMP ; Scheme 2). Recrystallization from a THF/hexane solution mixture afforded the respective solvated monomeric zincates, $[(\text{THF})_2\text{Li}(\mu\text{-NR}_2)(\mu\text{-Et})\text{Zn}(\text{Et})]$ ($\text{NR}_2 = \text{CPC}$, **3**·(THF)₂ and $\text{NR}_2 = \text{TMP}$, **4**·(THF)₂) as colorless crystals in moderate yields (Scheme 2). The TMEDA coordinated lithium dialkyl(amido)zincates $[(\text{TMEDA})\text{Li}(\mu\text{-NR}_2)(\mu\text{-Et})\text{Zn}(\text{Et})]$ were also isolated for structural comparison. A recrystallization of the THF solvated zincate in neat TMEDA afforded $[(\text{TMEDA})\text{Li}(\mu\text{-NR}_2)(\mu\text{-Et})\text{Zn}(\text{Et})]$ ($\text{NR}_2 = \text{CPC}$, **3**·TMEDA and $\text{NR}_2 = \text{TMP}$, **4**·TMEDA) as needle shaped colorless crystals (Figure 3b and 3d).



Scheme 2. Preparation of THF-solvated monomeric zincates **3**·(THF)₂ and **4**·(THF)₂.

The bonding parameters of **3**·(THF)₂ and **4**·(THF)₂ in the solid state are very similar (Figure 3a and 3c). Their structures resemble those previously reported lithium dialkyl(amido)zincates.¹⁵ The amide coordinates to both metal centers. The lithium cation is stabilized by an $\alpha\text{-}(\text{CH}_2)$ group of the diethyl zinc and two THF molecules, forming a planar four-membered Li–N–Zn–C cyclic structure. The N–Zn distance of 2.062(2) Å in **3**·(THF)₂ is longer than that of **4**·(THF)₂ [2.041(2) Å], while the N–Li distances in **3**·(THF)₂ [2.022(3) Å] and **4**·(THF)₂ [2.018(5) Å] are X-ray crystallographically indistinguishable. In these TMEDA coordinated structures, the N–Li and N–Zn distances of **3**·TMEDA and **4**·TMEDA are crystallographically identical. However, in comparison to the THF-solvated analogues, the N–Li distances in **3**·TMEDA [2.058(5) Å] and **4**·TMEDA [2.042(5) Å] are marginally longer. The N–Zn distance of 2.066(2) Å in **4**·TMEDA is only slightly longer than that of **4**·(THF)₂ [2.041(2) Å], while the N–Zn distance in **3**·TMEDA [2.067(2)] is identical to that observed in **3**·(THF)₂.

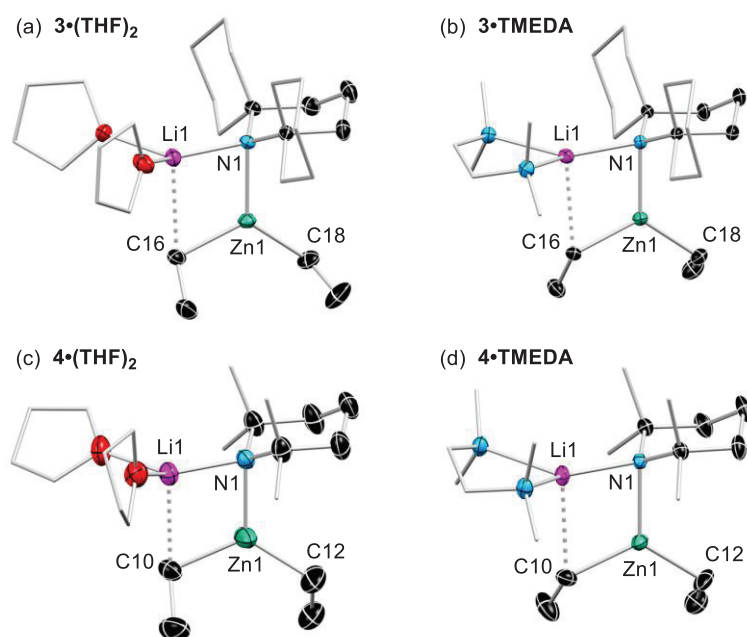


Figure 3. Molecular structures of (a) $3 \cdot (\text{THF})_2$, (b) $3 \cdot \text{TMEDA}$, (c) $4 \cdot (\text{THF})_2$, and (d) $6 \cdot \text{TMEDA}$ obtained from single-crystal X-ray diffraction analyses. Thermal ellipsoids are displayed at 30% probability. Hydrogen atoms and some carbon atoms are omitted for clarity. Structural disorders were observed in THF and TMEDA moieties in all structures as well as in ethyl moieties of $4 \cdot (\text{THF})_2$. Selected bond lengths (Angstroms) and angles (degrees) for $3 \cdot (\text{THF})_2$: N1–Li1 2.022(3), N1–Zn1 2.062(2), Li1–C16 2.635(4), Zn1–C16 2.048(2), Zn1–C18 2.009(2); C1–N1–C5 116.5(2), $\Sigma \text{LiNZnC} = 360.1$. Selected bond lengths (Angstroms) and angles (degrees) for $3 \cdot \text{TMEDA}$: N1–Li1 2.058(5), N1–Zn1 2.067(2), Li1–C16 2.652(6), Zn1–C16 2.036(3), Zn1–C18 2.004(3); C1–N1–C5 117.0(2), $\Sigma \text{LiNZnC} = 360.0$. Selected bond lengths (Angstroms) and angles (degrees) for $4 \cdot (\text{THF})_2$: N1–Li1 2.018(5), N1–Zn1 2.041(2); C1–N1–C5 114.7(2). Selected bond lengths (Angstroms) and angles (degrees) for $4 \cdot \text{TMEDA}$: N1–Li1 2.042(5), N1–Zn1 2.066(2), Li1–C10 2.649(7), Zn1–C10 2.034(4), Zn1–C12 2.005(4); C1–N1–C5 115.4(2), $\Sigma \text{LiNZnC} = 360.0$.

The ^1H and $^{13}\text{C}\{^1\text{H}\}$ spectra of $3 \cdot (\text{THF})_2$ and $4 \cdot (\text{THF})_2$ are generally unremarkable. At room temperature, only one set of signals was observed from the two ethyl moieties. The ^7Li NMR chemical shifts of $3 \cdot (\text{THF})_2$ and $4 \cdot (\text{THF})_2$ in C_6D_6 were observed at 1.42 and 1.03 ppm, respectively, lying in higher fields than those observed for the lithium amide complexes (**2**, 2.75 ppm; $(\text{LiTMP})_n$, 2.47 ppm).^{14a}

To gain a better understanding of the solution behavior in the reaction solvent THF, DOSY ^1H NMR studies of $3 \cdot (\text{THF})_2$ and $4 \cdot (\text{THF})_2$ were carried out in $\text{THF}-d_8$.^{8,16} The NMR spectrum shows that in solution, $3 \cdot (\text{THF})_2$ loses one THF on average, while $3 \cdot (\text{THF})_2$ frees both of its coordinating THF molecules from the Li atom in the zincate **4** (see Experimental Section).

3-4. Regio- and Chemoselective (Aromatic)C–H Zincations of mono/di-Substituted Benzens

As shown in Figure 1, there have been examples of C–H metalation reactions that are dependent on the zincate amido ligand. As the steric environment of the amido ligand affects the pK_a and the structure of the intermediates involved in the reaction sequence, we investigated how the newly prepared zincate **3** influenced the reactivity and/or regioselectivity of C–H metalation reactions in comparison to previously reported analogues.

We carried out the deprotonative metalation and iodination of the *tert*-butyl 3-bromobenzoate (**5**) using **3** and **4**. In compound **5**, the 2-hydrogen situated between two electron-withdrawing groups (EWG) has the highest acidity. Thus, the derivations of **5** at the 2 position are thermodynamically favored (Figure 4, Path A). With the bromine atom at the 3 position, we hypothesized that a bulky amido ligand would cast steric hindrance over the halogen, as illustrated in Figure 4 Path B, forcing the alternative facial coordination to favor the deprotonation at the 6 position.

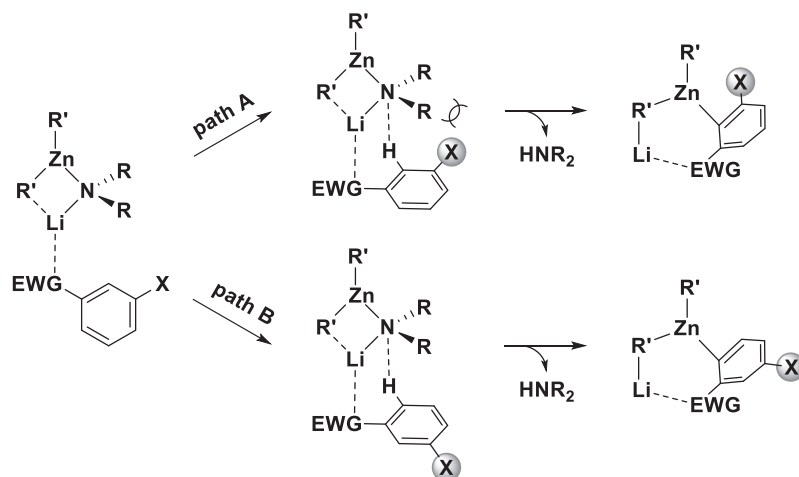
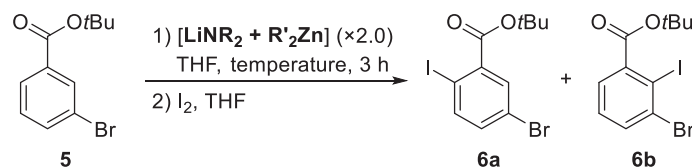


Figure 4. Proposed mechanism for deprotonative metalation of the 1,3-disubstituted benzene.¹⁷ Path A: deprotonation at the 2 position with steric repulsion between the halogen and the amido ligand. Path B: deprotonation at the 6 position without steric repulsion. EWG = electron-withdrawing groups, X = halide.

Previously, this substrate (**5**) has been used in Uchiyama's studies on alkyl ligand-dependent selectivity and reactivity of TMP–zincates.^{6a} Their study showed that the methyl–zincate favored benzyne formation (at reflux temperature), while the *tert*-butyl zincate provided the 6-iodinated product **6a** and the 2-iodinated product **6b** at room temperature in 67% and 31% yields, respectively. We carried out the same iodinating reactions to see if the newly developed amide would further promote the formation of **6a**.

The iodination reaction using **2** was carried out with Et_2Zn and $t\text{Bu}_2\text{Zn}$ independently at both elevated and reduced temperatures to optimize the yields. Parallel reactions using TMP were also performed for comparison (see Experimental Section).

Table 1. Direct C–H metalation of *tert*-butyl 3-bromobenzoate **5** with zincates.



Entry	LiNR ₂ + R' ₂ Zn	temp.	Yield (%) ^a		Ratio ^b
			6a, 6b	6a/6b	
1	LiTMP + Et ₂ Zn	0 °C	45, 21	2.1	
2	LiCPC (2) + Et ₂ Zn	0 °C	64, 11	5.8	
3	LiTMP + Et ₂ Zn	–30 °C	49 ^c , 46 ^c	1.1	
4	LiCPC (2) + Et₂Zn	–30 °C	72^c, 22^c	3.3	
5	LiTMP + <i>t</i> Bu ₂ Zn	0 °C	66 ^c , 30 ^c	2.2	
6	LiCPC (2) + <i>t</i>Bu₂Zn	0 °C	77^c, 20^c	3.9	
7	LiTMP + <i>t</i> Bu ₂ Zn	–30 °C	64, 32	2.0	
8 ^e	LiCPC (2) + <i>t</i> Bu ₂ Zn	–30 °C	60, 17	2.4	

^aIsolated yield. ^bThe ratio was calculated from isolated yield. ^cAverage value of two times. ^dReaction time was 12 h, and *tert*-butyl 3-bromobenzoate **5** was recovered in 17% yield. A shorter reaction time provided the higher yield of **5**.

In all reactions, both **6a** and **6b** were isolated. The optimized reaction conditions and results are summarized in Table 1. In combination with the Et_2Zn (Table 1, entries 1–4), the iodination of **5** at 0 °C employing Li(CPC)ZnEt₂ (**3**) afforded **6a** and **6b** in 64% and 11% yields, respectively (entry 2). Although this **6a/6b** ratio was better than that observed in the parallel reaction using LiTMP (**6a**, 45%; **6b**, 21%, entry 1), the difference in regioselectivity is not conclusive due to the low total yields (entries (1) LiTMP, 66%; (2) **2**, 75%) of the products. This is likely due to the benzyne formation, which has been observed from the reaction of **5** with Li(TMP)ZnMe₂ by Uchiyama et al.^{6,18}

The yield improved significantly when the iodination of **5** was repeated at –30 °C. In reactions employing Li(CPC)ZnEt₂ (entry 4), **6a** and **6b** were obtained in 72% and 22% yields (total yield, 94%), showing a higher regioselectivity for the 6 position. By comparison, the parallel

reactions employing $\text{Li}(\text{TMP})\text{ZnEt}_2$ afforded **6a** and **6b** in close to equal amounts, 49% and 46%, respectively (total yield, 95%). In the case of using LiNR_2 and Et_2Zn , the metalated intermediate, generated by C–H metalation at the 2 position on the aromatic ring, might decompose through the benzyne formation. This decomposition can be suppressed at lower temperatures or by using $t\text{Bu}_2\text{Zn}$. Uchiyama et al. observed this benzyne formation from the reaction of **5** with $\text{Li}(\text{TMP})\text{ZnMe}_2$ but no benzyne formation with $\text{Li}(\text{TMP})\text{Zn}(t\text{Bu})_2$.^{6a} Therefore, the yields of **6b** were higher at $-30\text{ }^\circ\text{C}$ (entry 3, 46%; entry 4, 22%) than those at $0\text{ }^\circ\text{C}$ (entry 1, 21%; entry 2, 11%), and the ratios **8a/8b** were apparently lower at $-30\text{ }^\circ\text{C}$ (entry 3, 1.1; entry 4, 3.3) than those at $0\text{ }^\circ\text{C}$ (entry 1, 2.1; entry 2, 5.8).

Similar regioselectivity can be achieved using $\text{Li}(\text{CPC})\text{Zn}(t\text{Bu})_2$ at $0\text{ }^\circ\text{C}$ (**6a**, 77%; **6b**, 20%, entry 6), moderately improved from the reaction with $\text{Li}(\text{TMP})\text{Zn}(t\text{Bu})_2$, (**6a**, 66%; **6b**, 30%, entry 5). The regioselectivity is more affected by the alkyl ligands of zinc in the TMP zincates than in the CPC zincates. With both alkyl zinc agents, the CPC zincates consistently offered higher regioselectivity for the 6 position (kinetic product) in comparison to the TMP zincates.

3-5. Conclusion and Outlook

In conclusion, a direct *N*-lithiation of CPC(H) (**1**) provides the corresponding bulky amide (**2**), which may be a useful addition to the currently rather small library of sterically hindered secondary amide reagents. A preliminary reaction study on the iodination of the *tert*-butyl 3-bromobenzoate (**5**) with $\text{Li}(\text{CPC})\text{ZnR}_2$ showed a moderately improved regioselectivity for the 6 position in comparison to that with the $\text{Li}(\text{TMP})\text{ZnR}_2$, which suggested a slightly larger (at least comparable) steric bulk of CPC in comparison to the TMP. Applications of the more sterically hindered bases is future subject.

Experimental Section

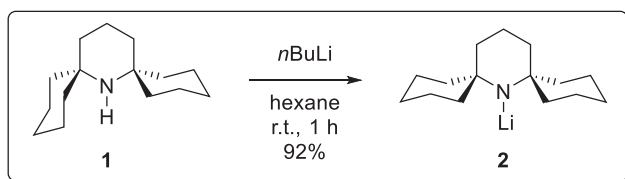
General Considerations.

All syntheses were carried out under inert atmosphere with standard Schlenk and glovebox techniques unless otherwise stated. THF, hexane and toluene were freshly distilled from Na/benzophenone prior to use. Hexane was distilled from sodium followed by drying over potassium mirror and degassed three times using freeze–pump–thaw cycling and stored in an argon-filled glovebox for washing and recrystallization of **3**·(THF)₂ and **4**·(THF)₂. 2,2,6,6-Tetramethylpiperidine (TMP(H)) were distilled from CaH₂ and stored over 4 Å molecular sieves. TMEDA was distilled from CaH₂. ZnCl₂ was dried by heating in vacuo. 1-Phenylnaphthalene (PhN) was distilled from sodium. C₆D₆ and C₄D₈O (THF-*d*₈) were distilled from sodium followed by drying over potassium mirror and degassed three times using freeze–pump–thaw cycling and stored in an argon-filled glovebox for NMR measurements of **2**, **3**·(THF)₂, **4**·(THF)₂, **3**·TMEDA, **4**·TMEDA, and *t*Bu₂Zn. Other chemicals were used as supplied. Column chromatography was carried out using Kanto silica gel 60N (spherical, neutral).

General Measurements.

¹H NMR (400 MHz), ¹³C NMR (100 MHz), and ⁷Li NMR (155 MHz) spectra were recorded using a JEOL EX-400 or AL-400 NMR spectrometer. The ¹H and ¹³C NMR chemical shifts (δ scale) are determined by residual protons of the solvent (¹H, CDCl₃, δ = 7.26 ppm; C₆D₆, δ = 7.20 ppm; C₄D₈O, δ = 3.58 ppm) or the solvent itself (¹³C, CDCl₃, δ = 77.0 ppm; C₆D₆, δ = 128.0 ppm; C₄D₈O, δ = 67.4 ppm). The ⁷Li NMR chemical shifts are referenced to LiCl in D₂O at 0 ppm. Melting points were measured with a Yanagimoto micromelting point apparatus and are uncorrected.

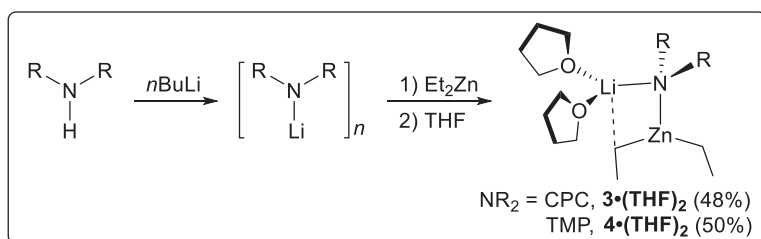
Synthesis of LiCPC (**2**).



n-Butyllithium (1.60 M in hexane, 0.35 mL, 0.56 mmol) was added dropwise to a hexane (5.0 mL) solution of **1** (125 mg, 0.562 mmol) at 0 °C with no stirring. The still reaction mixture stood at ambient temperature for 1 h, from which colorless crystals were obtained. The reaction mixture was centrifuged at 20 °C for 2 min at a speed of 3000 rpm. The supernatant was removed by syringe. The remaining crystals were washed with hexane (5 mL), and the washing was separated and removed as described above. The remaining solid in a small amount of hexane was filtered under argon atmosphere to give LiCPC (**2**) (118 mg, 0.517 mmol, 92%) as colorless crystals suitable for X-ray crystallographic analysis. ¹H NMR (C₆D₆, 400 MHz): δ = 2.09–1.98 (2H, m), 1.80–1.13

(20H, m), 1.00–0.83 ppm (4H, m). ^{13}C NMR (C_6D_6 , 100 MHz): δ = 54.26 (C), 45.80 (CH_2), 39.70 (CH_2), 32.54 (CH_2), 28.69 (CH_2), 23.53 (CH_2), 20.29 (CH_2), 14.44 ppm (CH_2). ^7Li NMR (C_6D_6 , 155 MHz, LiCl in D_2O): δ = 2.75 ppm.

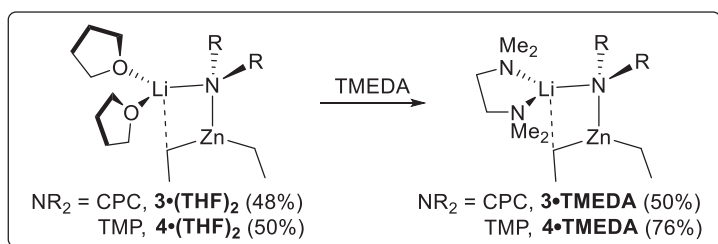
THF-Coordinated Zincate Complexes, 3·(THF)₂ and 4·(THF)₂.



n-Butyllithium (1.63 M in hexane, 1.25 mL, 2.04 mmol for $\mathbf{3}\cdot(\text{THF})_2$, or 1.85 mL, 3.02 mmol for $\mathbf{4}\cdot(\text{THF})_2$) was added dropwise to **1** (neat, 443 mg, 2.00 mmol for $\mathbf{3}\cdot(\text{THF})_2$) or TMP(H) (neat, 0.500 mL, 2.96 mmol for $\mathbf{4}\cdot(\text{THF})_2$) at -78°C . After stirring at -78°C for 1 h, diethyl zinc (1.06 M in hexane, 2.00 mL, 2.12 mmol for $\mathbf{3}\cdot(\text{THF})_2$, or 3.00 mL, 3.18 mmol for $\mathbf{4}\cdot(\text{THF})_2$) was added and the resultant slurry was warmed to ambient temperature. THF (3.0 mL for $\mathbf{3}\cdot(\text{THF})_2$, or 2.0 mL for $\mathbf{4}\cdot(\text{THF})_2$) was then added to the reaction mixture to give a homogeneous solution and concentrated under reduced pressure. The resultant solution was stored at -80°C for 1 day, from which two phases formed. The top layer is a solvent mixture of THF and hexane, which is removed using a syringe. The bottom phase is frozen $\mathbf{3}\cdot(\text{THF})_2$ or $\mathbf{4}\cdot(\text{THF})_2$ in THF, which was stored at -30°C for 1 day under argon atmosphere to afford $\mathbf{3}\cdot(\text{THF})_2$ or $\mathbf{4}\cdot(\text{THF})_2$ as a white solid. This was filtered and washed with hexane (3×2 mL) to afford pure $\mathbf{3}\cdot(\text{THF})_2$ (473 mg, 0.955 mmol, 48%) or $\mathbf{4}\cdot(\text{THF})_2$ (620 mg, 1.49 mmol, 50%). Recrystallization from hexane at -30°C gave crystals suitable for X-ray crystallographic analysis.

$\mathbf{3}\cdot(\text{THF})_2$. ^1H NMR (C_6D_6 , 400 MHz): δ = 3.46 (8H, m), 2.35 (2H, d, J = 12 Hz), 2.13 (2H, m), 1.91 (6H, t, J = 8 Hz), 1.84–1.00 (30H, m), 0.58 ppm (4H, q, J = 8 Hz). ^{13}C NMR (C_6D_6 , 100 MHz): δ = 68.27 (CH_2), 55.47 (C), 46.23 (CH_2), 41.69 (CH_2), 35.71 (CH_2), 26.93 (CH_2), 25.40 (CH_2), 24.42 (CH_2), 24.04 (CH_2), 18.64 (CH_2), 13.80 (CH_3), 5.81 ppm (CH_2). ^7Li NMR (C_6D_6 , 155 MHz, LiCl in D_2O): δ = 1.42 ppm.

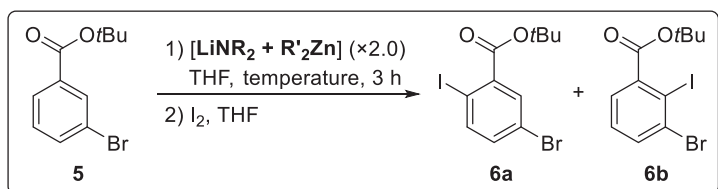
$\mathbf{4}\cdot(\text{THF})_2$. ^1H NMR (C_6D_6 , 400 MHz): δ = 3.42 (8H, m), 2.08–1.65 (10H, m), 1.48 (6H, s), 1.38–1.02 (16H, m), 0.51 ppm (4H, q, J = 8 Hz). ^{13}C NMR (C_6D_6 , 100 MHz): δ = 68.27 (CH_2), 52.79 (C), 41.04 (CH_2), 36.19 (CH_3), 32.01 (CH_3), 25.32 (CH_2), 20.05 (CH_2), 13.56 (CH_3), 5.24 ppm (CH_2). ^7Li NMR (C_6D_6 , 155 MHz, LiCl in D_2O): δ = 1.03 ppm.

TMEDA-Coordinated Zincate Complexes, **3**·TMEDA and **4**·TMEDA.

Recrystallization of **3**·(THF)₂ (175 mg, 0.354 mmol) or **4**·(THF)₂ (154 mg, 0.370 mmol) from neat TMEDA afforded **3**·TMEDA (82.3 mg, 0.176 mmol, 50%) or **4**·TMEDA (109 mg, 0.282 mmol, 76%) as colorless crystals suitable for X-ray crystallographic analysis.

3·TMEDA. ¹H NMR (C₆D₆, 400 MHz): δ = 2.36–0.83 (48H, m), 0.41 ppm (4H, q, 3J = 7.8 Hz). ¹³C NMR (C₆D₆, 100 MHz): δ = 57.17 (CH₂), 55.46 (C), 46.84 (CH₃), 43.49 (CH₂), 43.14 (CH₂), 33.03 (CH₂), 26.36 (CH₂), 24.23 (CH₂), 23.62 (CH₂), 18.63 (CH₂), 14.34 (CH₃), 6.27 ppm (CH₂). ⁷Li NMR (C₆D₆, 155 MHz, LiCl in D₂O): δ = 0.75 ppm.

4·TMEDA. ¹H NMR (C₆D₆, 400 MHz): δ = 2.16–1.71 (26H, m), 1.65–1.46 (2H, m), 1.25 (12H, s), 0.32 ppm (4H, q, 3J = 7.8 Hz). ¹³C NMR (C₆D₆, 100 MHz): δ = 57.19 (CH₂), 52.91 (C), 46.79 (CH₃), 38.66 (CH₂), 35.99 (CH₃), 33.70 (CH₃), 20.00 (CH₂), 14.24 (CH₃), 5.59 ppm (CH₂). ⁷Li NMR (C₆D₆, 155 MHz, LiCl in D₂O): δ = 0.70 ppm.

Deprotonative Metalation of **5**.General Procedure A with [Li(NR₂)ZnEt₂].⁸

For each 4 mmol of [Li(NR₂)ZnEt₂] (NR₂ = CPC, **3** and NR₂ = TMP, **4**) prepared, *n*-butyllithium (1.54 M in hexane, 2.65 mL, 4.08 mmol) was added to R₂N(H) (neat, 4.03 mmol) dropwise at room temperature. The resulting pale yellow suspension was stirred at room temperature for 15 min, and then THF (10 mL) was added, followed by Et₂Zn (1.06 M in hexane, 3.85 mL, 4.08 mmol). The resulting pale orange solution was stirred for 15 min at room temperature. After addition of *tert*-butyl 3-bromobenzoate (**5**) (514 mg, 2.00 mmol) at the reaction temperature (from –30 °C to room temperature), the reaction mixture solution was stirred for 3 h, during which the color of the solution changed to dark orange. To trap the metalated intermediate, iodine (4.09 g, 16.1 mmol) in THF (16.1 mL) was added slowly to the reaction solution at the reaction temperature. After stirring for 8 h, the reaction solution was quenched by addition of Na₂S₂O₃ (satd aq.) and a small amount of

NH₄Cl (satd aq.) and then extracted with AcOEt (× 4). (In some cases, solids were generated which were removed by filtration before extraction.) The combined organic layer was washed with saturated aqueous NaCl solution, dried over MgSO₄, and dried under reduced pressure. The residue was purified by column chromatography (silica gel) with hexane/AcOEt (15:1) as the eluent to separate *tert*-butyl 5-bromo-2-iodobenzoate (**6a**) (pale yellow oil, *R_f* = 0.59) and *tert*-butyl 3-bromo-2-iodobenzoate (**6b**) (pale yellow oil, *R_f* = 0.42).

6a. ¹H NMR (400 MHz, CDCl₃): δ = 7.78 (1H, d, ⁴*J* = 0.8 Hz), 7.77 (1H, d, ³*J* = 5.1 Hz), 7.23 (1H, dd, ³*J* = 8.6 Hz, ⁴*J* = 2.7 Hz), 1.61 ppm (9H, s).

6b. ¹H NMR (400 MHz, CDCl₃): δ = 7.68 (1H, dd, ³*J* = 8.1 Hz, ⁴*J* = 1.7 Hz), 7.35 (1H, dd, ³*J* = 7.8 Hz, ⁴*J* = 1.7 Hz), 7.23 (1H, t, ³*J* = 8.0 Hz), 1.61 ppm (9H, s).

*General Procedure B with [Li(NR₂)Zn(*t*Bu)₂].^{6a}*

For each 4 mmol of [Li(NR₂)Zn(*t*Bu)₂] (NR₂ = CPC, TMP) prepared, *n*-butyllithium (1.54 M in hexane, 2.65 mL, 4.08 mmol) was added dropwise to R₂N(H) (4.03 mmol) in THF (10 mL) at -78 °C. The resulting pale orange solution was stirred at room temperature for 30 min before a THF solution (10 mL) of *t*Bu₂Zn (790 mg, 4.40 mmol) was added at -78 °C. The resulting pale orange solution was stirred for 30 min at 0 °C. After addition of *tert*-butyl 3-bromobenzoate (**5**) (514 mg, 2.00 mmol) at the reaction temperature (from -30 °C to room temperature), the reaction mixture solution was stirred for the reaction time (3–36 h), during which the color of the solution changed to dark orange. To trap the metalated intermediate, iodine (3.55 g, 14.0 mmol) in THF (14.0 mL) was added slowly to the reaction solution at the reaction temperature. After stirring for 12 h, the reaction solution was quenched by addition of Na₂S₂O₃ (satd aq.) and a small amount of NH₄Cl (satd aq.) and then extracted with CHCl₃ (×4). (In some cases, solids were generated which were removed by filtration before extraction.) The combined organic layer was washed with saturated aqueous NaCl solution, dried over MgSO₄, and dried under reduced pressure. The residue was purified as described for general procedure A to give **6a** and **6b**.

NMR Spectra

NMR Spectra of LiCPC (2)

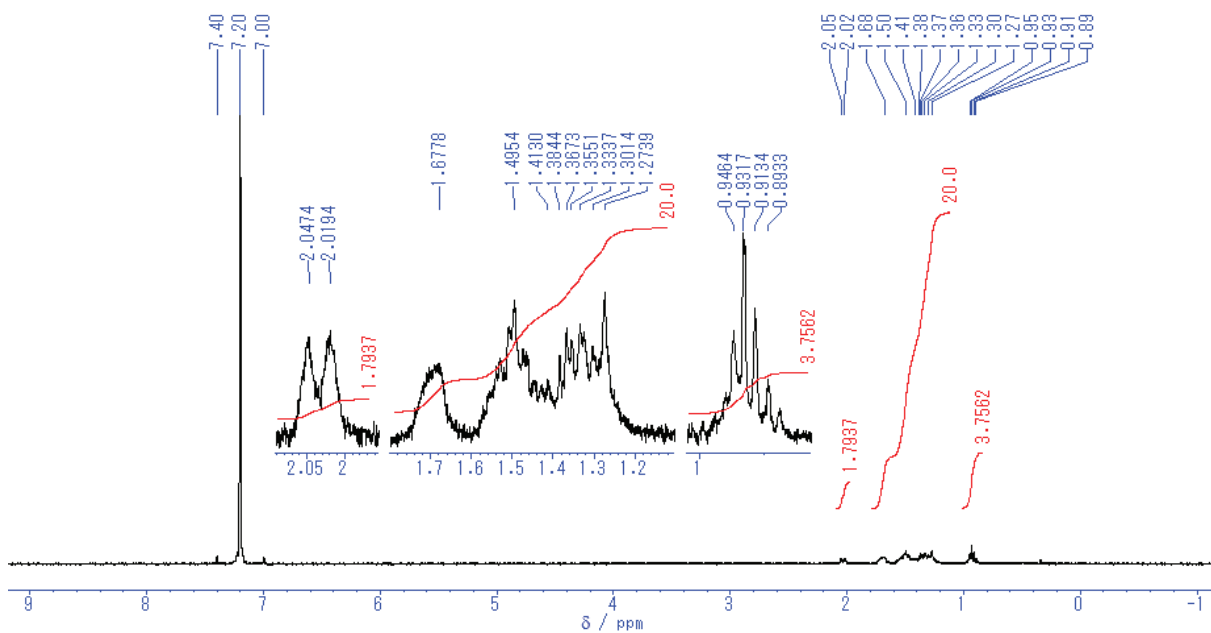


Figure S1. ^1H NMR spectrum (400 MHz) of **2** in C_6D_6 .

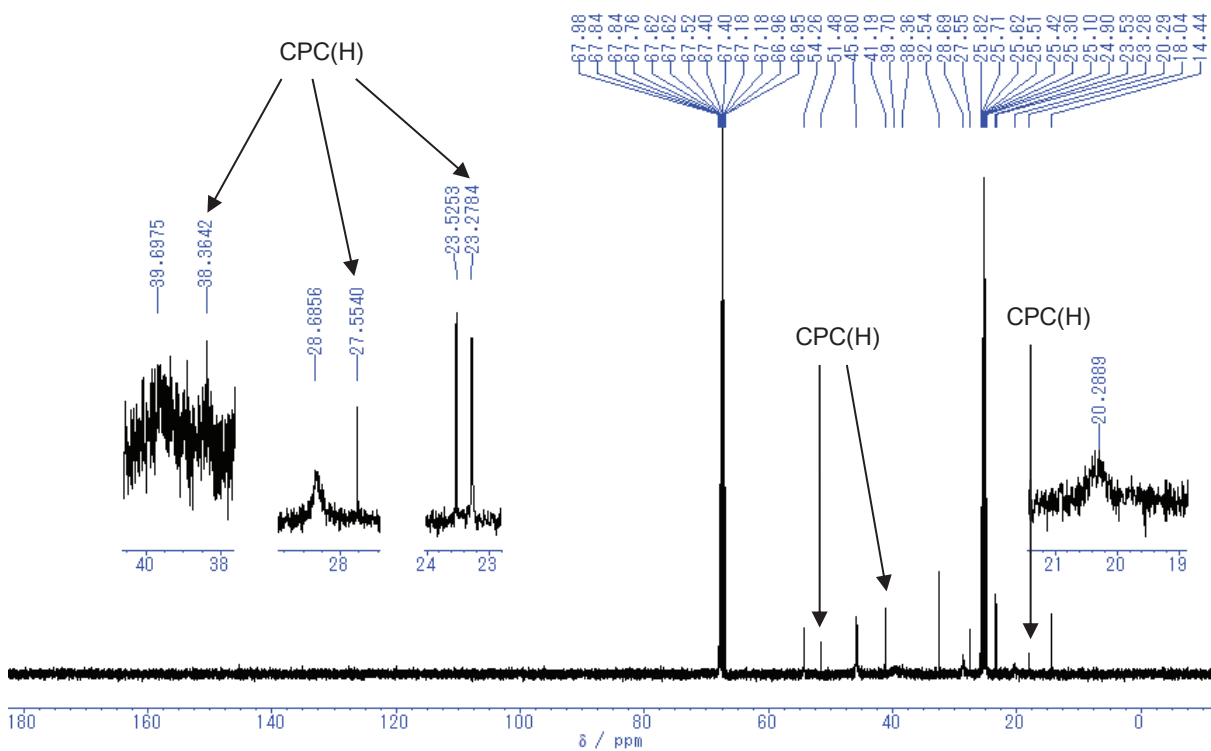


Figure S2. $^{13}\text{C}\{^1\text{H}\}$ NMR spectrum (100 MHz) of **2** in $\text{C}_4\text{D}_8\text{O}$.

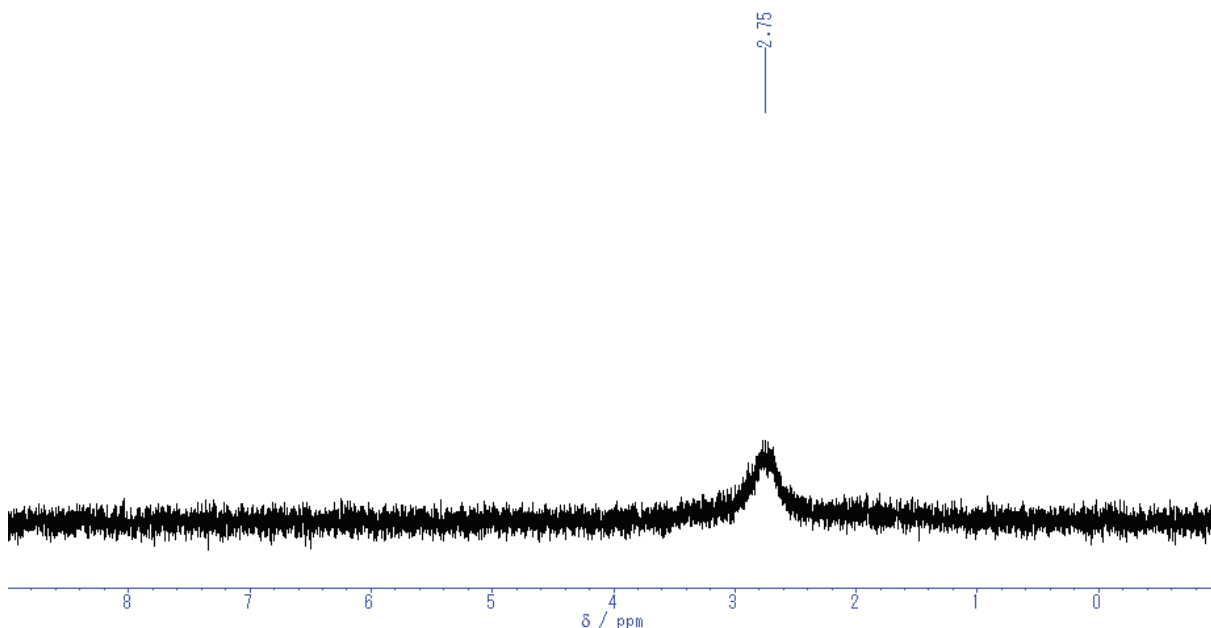


Figure S3. ^7Li NMR spectrum (155 MHz, LiCl in D_2O) of **2** in C_6D_6 .

NMR Spectra of $[(\text{THF})_2\text{Li}(\mu\text{-CPC})(\mu\text{-Et})\text{Zn}(\text{Et})] \cdot 3 \cdot (\text{THF})_2$

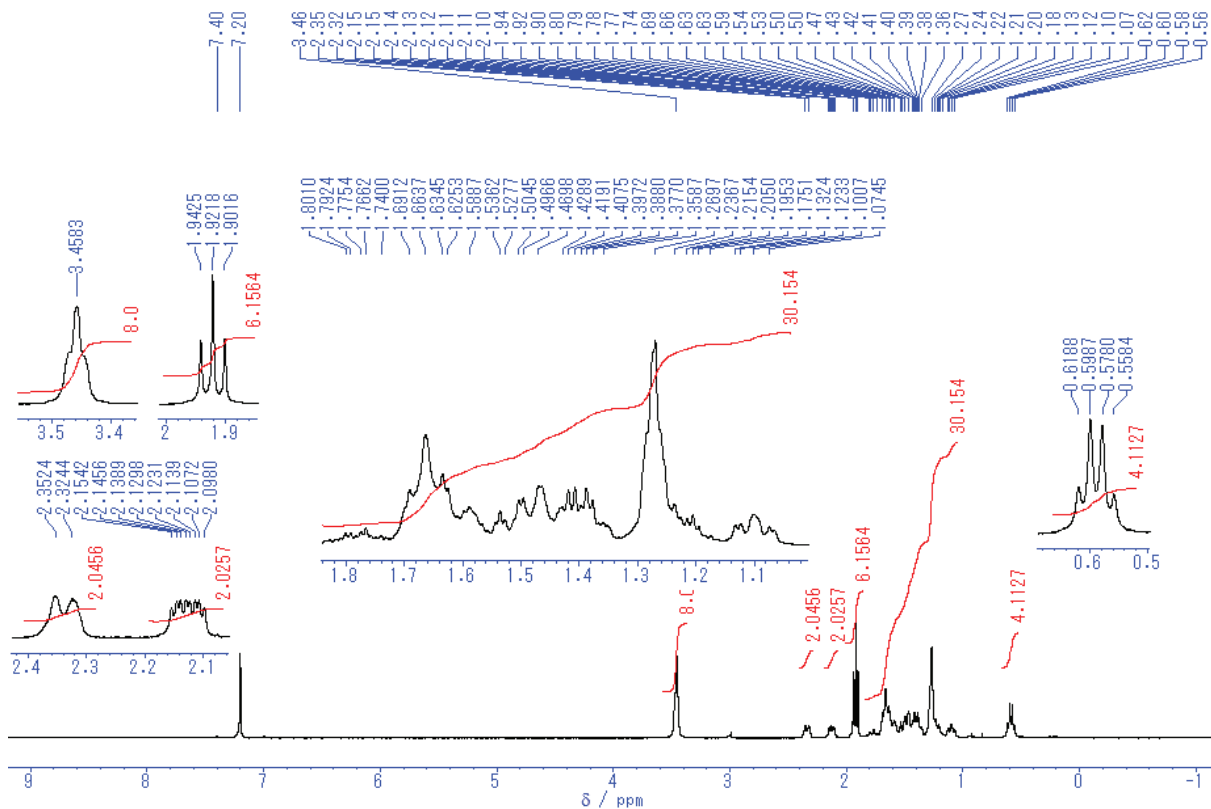


Figure S4. ^1H NMR spectrum (400 MHz) of $\mathbf{3} \cdot (\text{THF})_2$ in C_6D_6 .

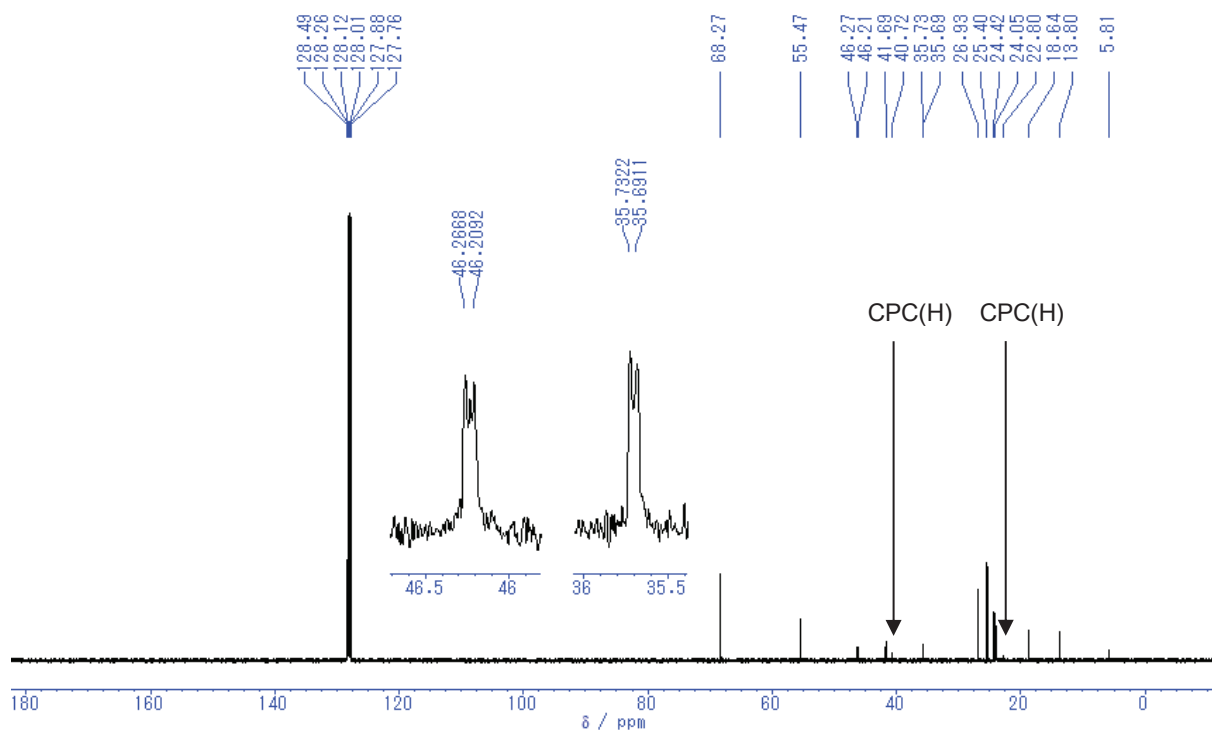


Figure S5. $^{13}\text{C}\{^1\text{H}\}$ NMR spectrum (100 MHz) of $3\cdot(\text{THF})_2$ in C_6D_6 .

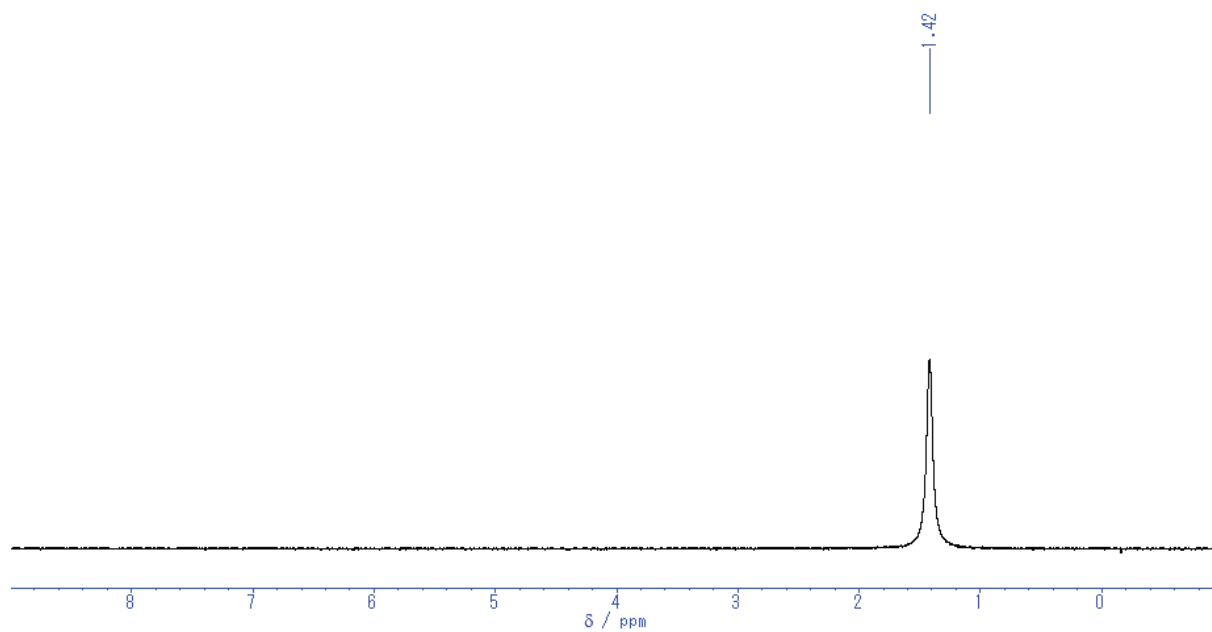


Figure S6. ^7Li NMR spectrum (155 MHz, LiCl in D_2O) of $3\cdot(\text{THF})_2$ in C_6D_6 .

NMR Spectra of $[(\text{THF})_2\text{Li}(\mu\text{-TMP})(\mu\text{-Et})\text{Zn}(\text{Et})] \cdot 4 \cdot (\text{THF})_2$

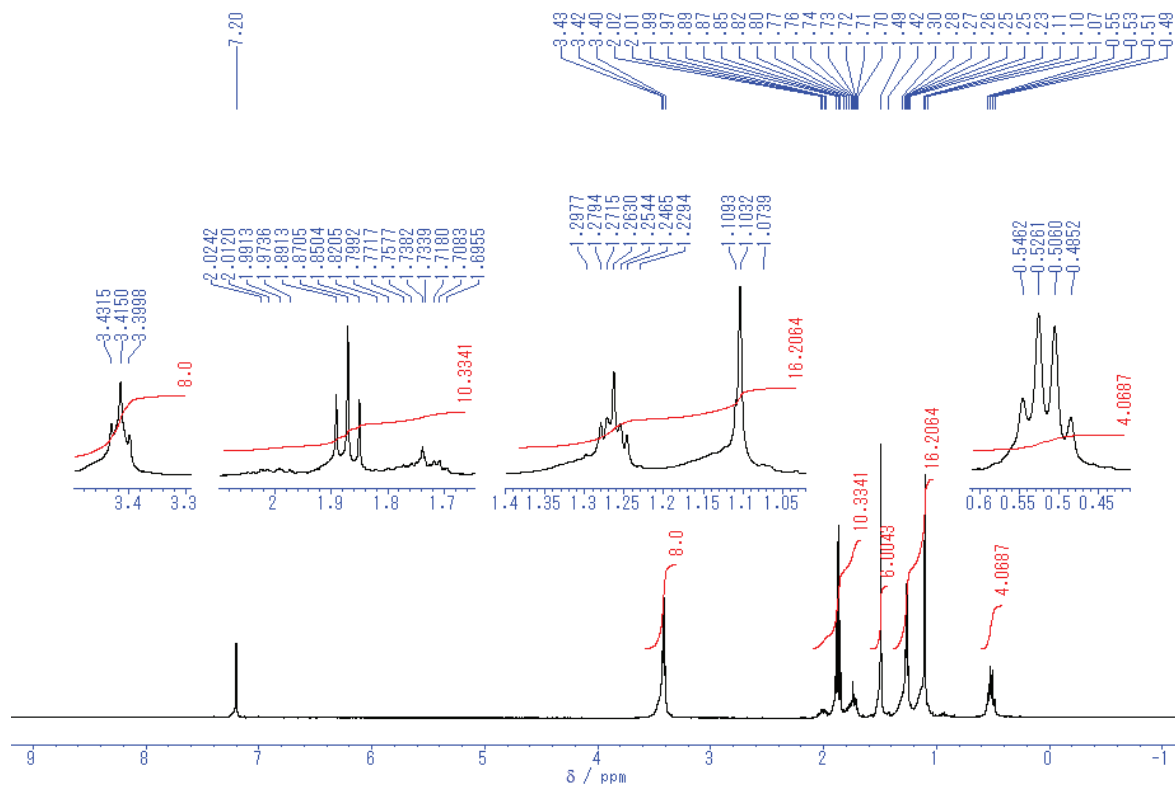


Figure S7. ^1H NMR spectrum (400 MHz) of $4 \cdot (\text{THF})_2$ in C_6D_6 .

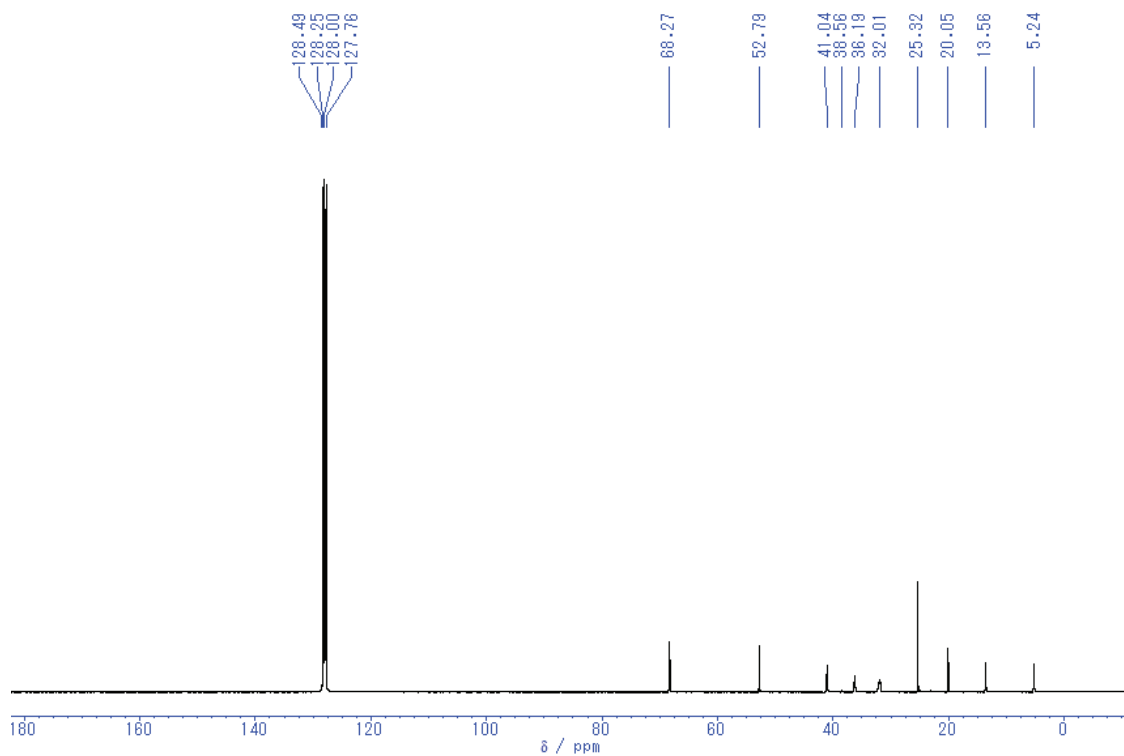


Figure S8. $^{13}\text{C}\{^1\text{H}\}$ NMR spectrum (100 MHz) of $4 \cdot (\text{THF})_2$ in C_6D_6 .

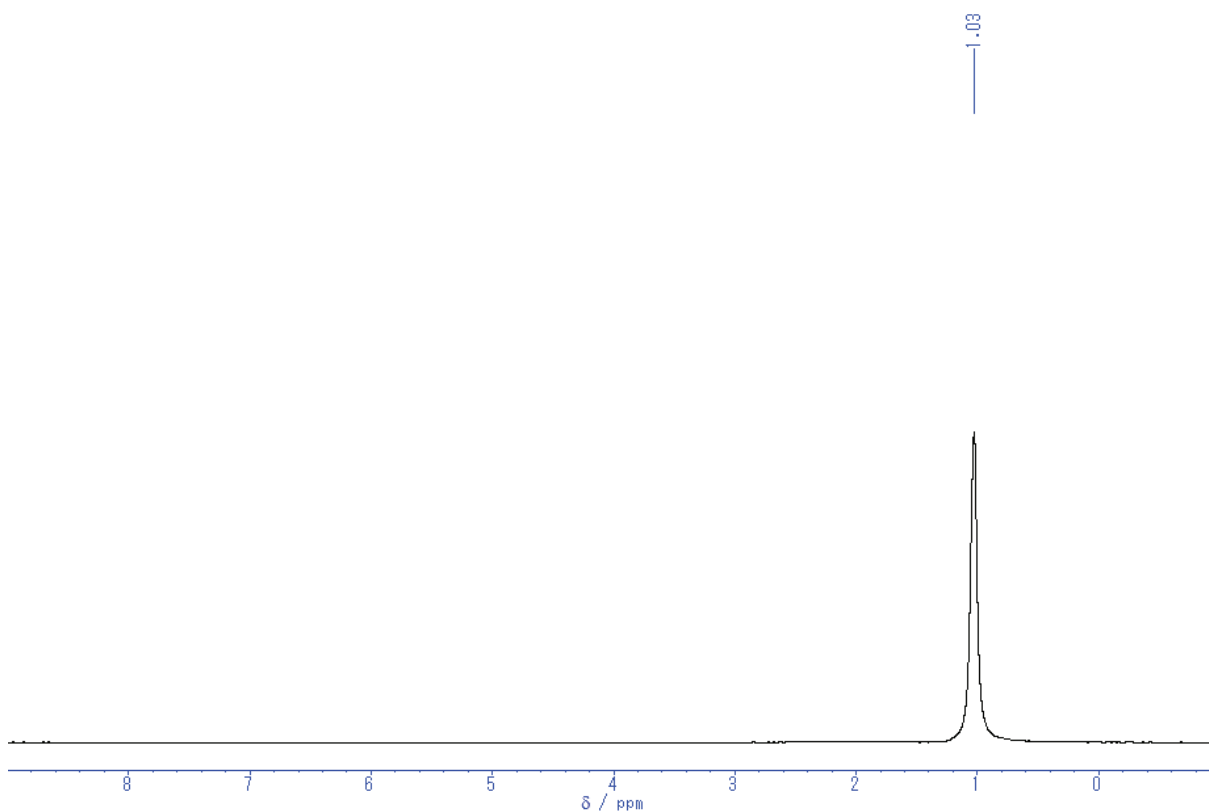


Figure S9. ^7Li NMR spectrum (155 MHz, LiCl in D_2O) of $4 \cdot (\text{THF})_2$ in C_6D_6 .

NMR Spectra of $[(\text{TMEDA})\text{Li}(\mu\text{-CPC})(\mu\text{-Et})\text{Zn}(\text{Et})] (3 \cdot \text{TMEDA})$

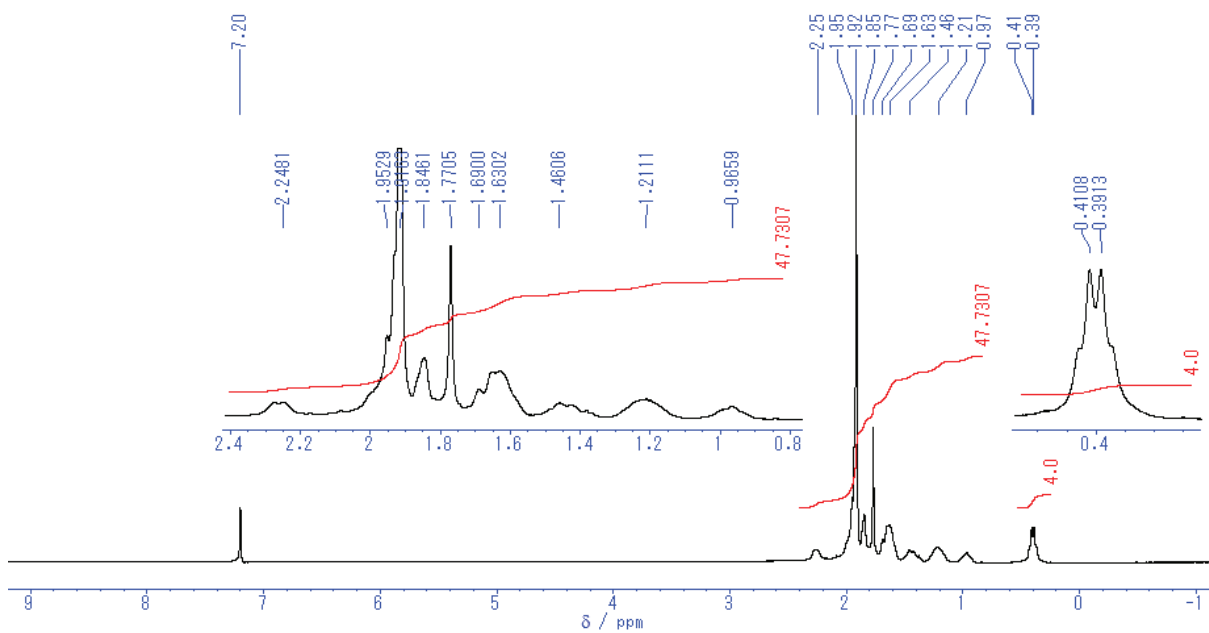


Figure S10. ^1H NMR spectrum (400 MHz) of $3 \cdot \text{TMEDA}$ in C_6D_6 .

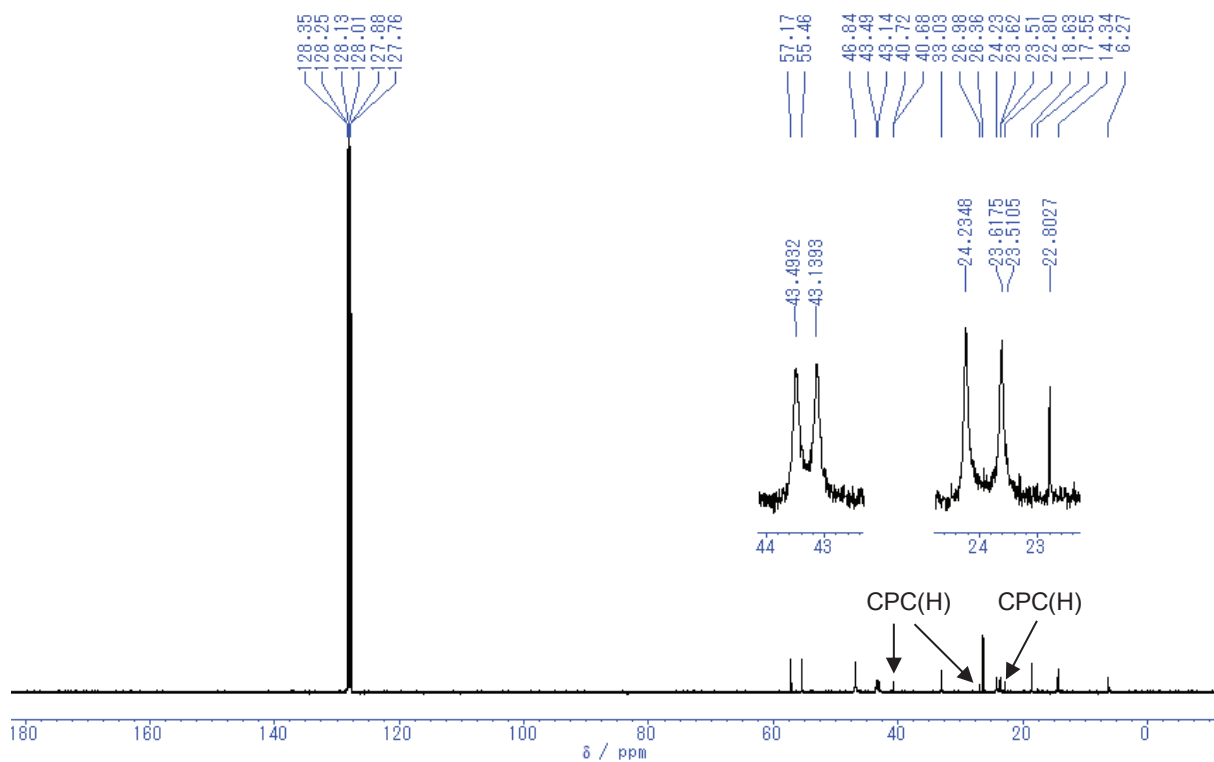


Figure S11. $^{13}\text{C}\{^1\text{H}\}$ NMR spectrum (100 MHz) of $3\cdot\text{TMEDA}$ in C_6D_6 .

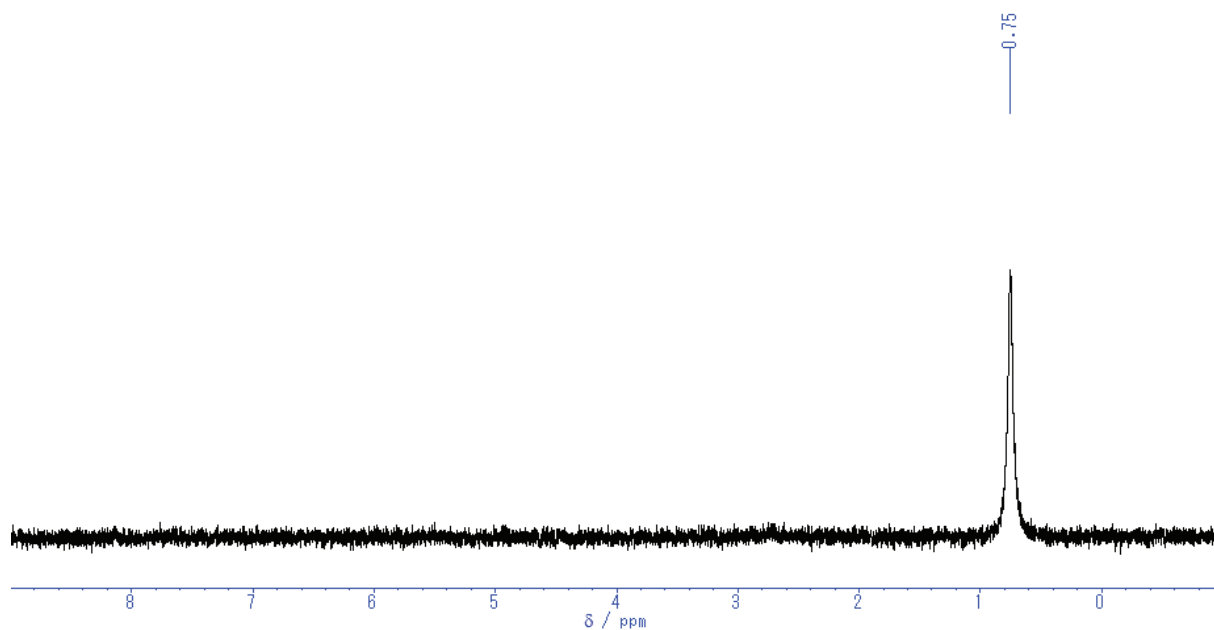


Figure S12. ^7Li NMR spectrum (155 MHz, LiCl in D_2O) of $3\cdot\text{TMEDA}$ in C_6D_6 .

NMR Spectra of $[(\text{TMEDA})\text{Li}(\mu\text{-TMP})(\mu\text{-Et})\text{Zn}(\text{Et})]$ (**4·TMEDA**)

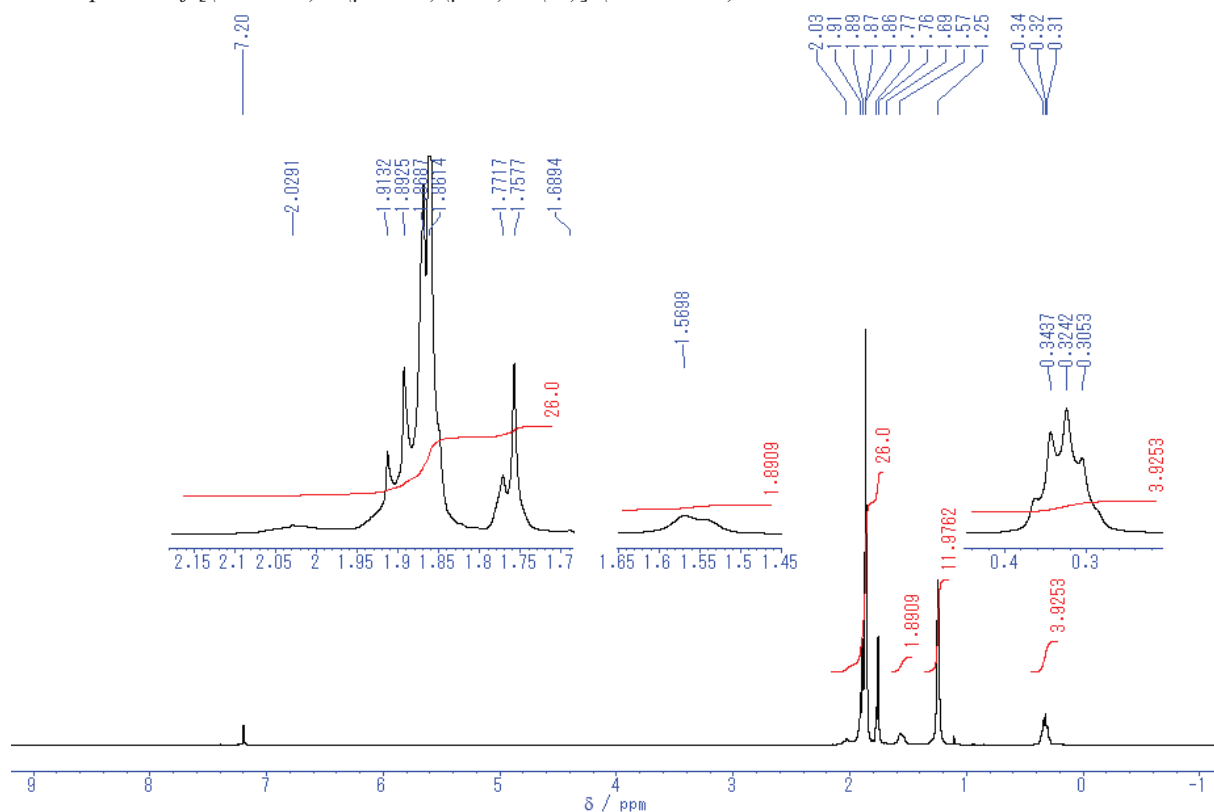


Figure S13. ^1H NMR spectrum (400 MHz) of **4·TMEDA** in C_6D_6 .

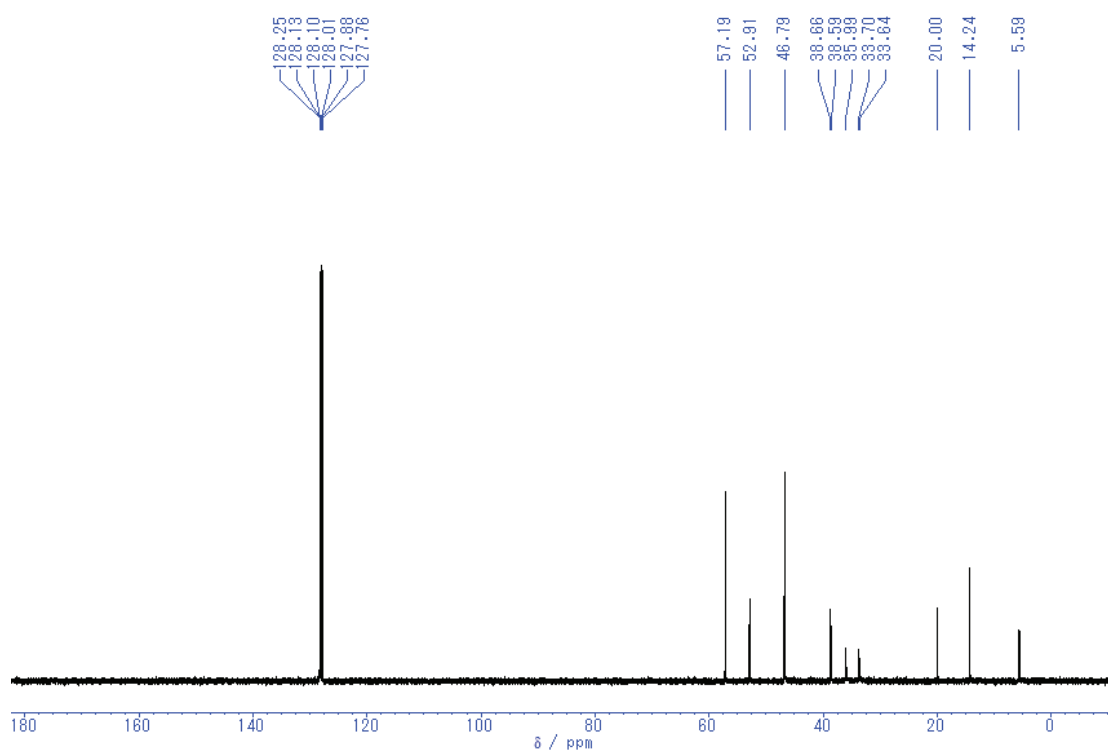


Figure S14. $^{13}\text{C}\{^1\text{H}\}$ NMR spectrum (100 MHz) of **4·TMEDA** in C_6D_6 .

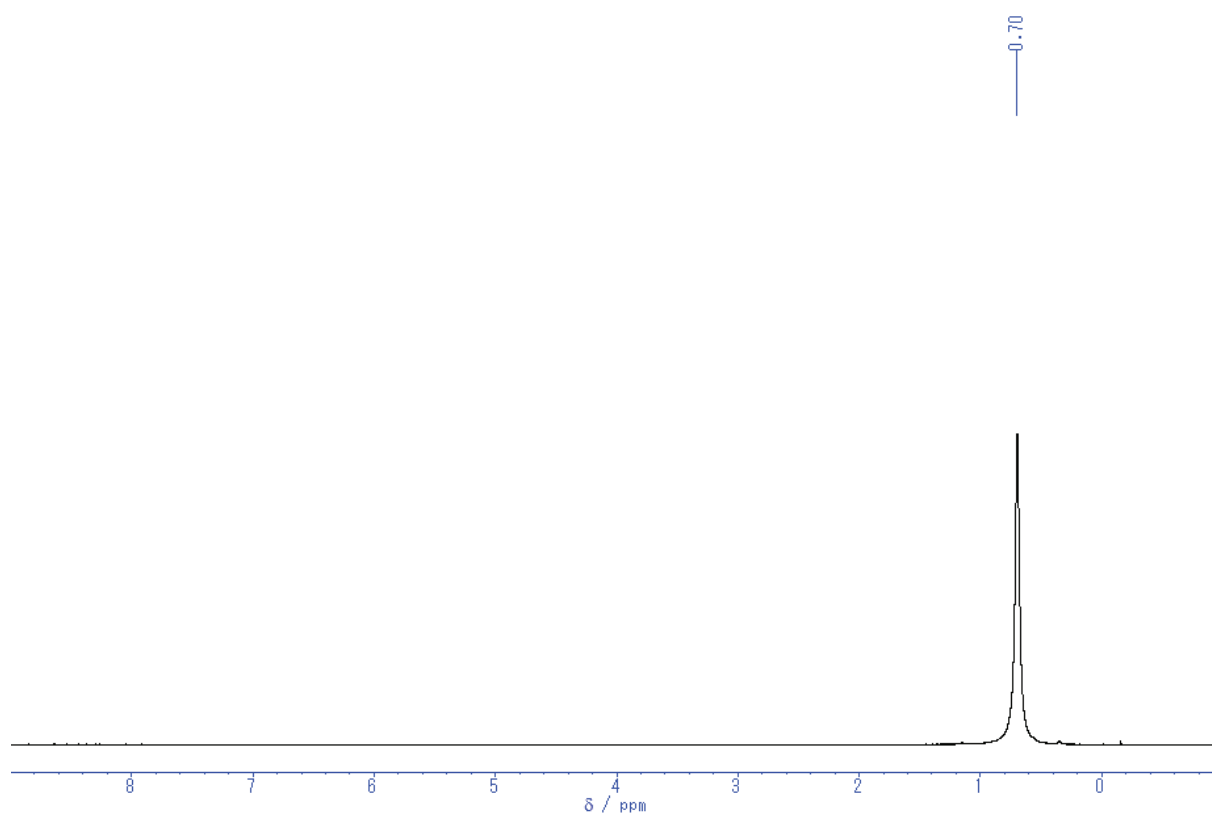


Figure S15. ${}^7\text{Li}$ NMR spectrum (155 MHz, LiCl in D_2O) of $4\cdot\text{TMEDA}$ in C_6D_6 .

Crystal Structure Determination

Crystals suitable for X-ray structural determination were mounted on a *Bruker SMART APEXII* CCD diffractometer. Samples were irradiated with graphite monochromated Mo-K α radiation ($\lambda=0.71073$ Å) at 173 K for data collection. The data were processed using the *APEX* program suite. All structures were solved by the *SHELXT* program (*ver.* 2014/5). Refinement on F^2 was carried out by full-matrix least-squares using the *SHELXL* in the *SHELX* software package (*ver.* 2014/7)¹⁹ and expanded using Fourier techniques. All non-hydrogen atoms were refined using anisotropic thermal parameters. The hydrogen atoms were assigned to idealized geometric positions and included in the refinement with isotropic thermal parameters. The *SHELXL* was interfaced with *ShelXle* GUI (*ver.* 742) for most of the refinement steps.²⁰ The pictures of molecules were prepared using *Pov-Ray* 3.7.0.²¹ The crystallographic data are summarized in Table S1 and S2.

Table S1. Crystallographic data.

	2₃^[a]	3·(THF)₂	4·(THF)₂
Formula	C ₁₅ H ₂₆ LiN	C ₂₁ H ₄₄ LiNO ₂ Zn	C ₂₇ H ₅₂ LiNO ₂ Zn
Mol wt	227.31	414.88	495.00
Crystal system	Hexagonal	monoclinic	monoclinic
Space group	<i>P6/mcc</i>	<i>P2₁/n</i>	<i>P2₁/c</i>
Color	colorless	colorless	colorless
Habit	plate	plate	plate
Cryst dimens, mm	0.12 × 0.11 × 0.05	0.15 × 0.14 × 0.06	0.26 × 0.16 × 0.06
<i>a</i> , Å	15.6814(7)	11.2358(13)	9.5012(7)
<i>b</i> , Å	15.6814(7)	18.399(2)	18.7387(14)
<i>c</i> , Å	22.5674(10)	12.1072(14)	16.3221(12)
α , deg	90	90	90
β , deg	90	104.549(2)	104.3260(10)
γ , deg	120	90	90
<i>V</i> , Å ³	4806.0(5)	2422.7(5)	2815.6(4)
<i>Z</i>	12	4	4
<i>D</i> _{calc} , g cm ⁻³	0.942	1.137	1.168
Abs coeff, mm ⁻¹	0.053	1.026	0.894
<i>F</i> (000)	1512	904	1080

Chapter 3. Deprotonative-Metalation Reactions

Temp, K	173(2)	173(2)	173(2)
Reflections	26065	14116	15919
Independent	1979	5521	6459
<i>R</i> _{int}	0.0332	0.0248	0.0256
Parameters	82	374	383
<i>R</i> ₁ [<i>I</i> > 2σ(<i>I</i>)]	0.0471	0.0562	0.0370
<i>wR</i> ₂ (all data)	0.1591	0.1759	0.0976
Goodness of fit	1.184	1.020	1.028
solv for crystallization	hexane	hexane, −30 °C	hexane, −30 °C

CCDC-1491873 (**2**), 1491874 (**3**·(THF)₂) and 1491875 (**4**·(THF)₂) contain the supplementary crystallographic data. These data can be obtained free of charge from the Cambridge Crystallographic Data Centre via www.ccdc.cam.ac.uk/data_request/cif

[a] In this crystal structure, there are disordered solvent molecules, and their contribution to the scattering values have been removed by using the PLATON SQUEEZE program (*ver.* 1.16).²²

Table S2. Crystallographic data.

	3 ·TMEDA	4 ·TMEDA
Formula	C ₁₉ H ₄₄ LiN ₃ Zn	C ₂₅ H ₅₂ LiN ₃ Zn
Mol wt	386.88	467.00
Crystal system	monoclinic	monoclinic
Space group	<i>Cc</i>	<i>P2₁/c</i>
Color	colorless	colorless
Habit	needle	needle
Cryst dimens, mm	0.10 × 0.09 × 0.01	0.13 × 0.09 × 0.03
<i>a</i> , Å	8.5884(12)	9.7336(10)
<i>b</i> , Å	25.543(3)	17.1347(18)
<i>c</i> , Å	10.5895(14)	16.1465(17)
<i>α</i> , deg	90	90

Chapter 3. Deprotonative-Metalation Reactions

β , deg	103.379(2)	100.1190(10)
γ , deg	90	90
V , Å ³	2285.0(5)	2651.1(5)
Z	4	4
D_{calc} , g cm ⁻³	1.125	1.170
Abs coeff, mm ⁻¹	1.080	0.942
$F(000)$	848	1024
Temp, K	173(2)	173(2)
Reflections	6681	15472
Independent	3951	6191
R_{int}	0.0189	0.0576
Parameters	267	325
$R_1 [I > 2\sigma(I)]$	0.0297	0.0534
wR_2 (all data)	0.0687	0.1214
Goodness of fit	1.027	1.010
solv for crystallization	TMEDA, -30 °C	TMEDA, -30 °C

CCDC-1491876 (**3·TMEDA**) and 1491877 (**4·TMEDA**) contain the supplementary crystallographic data. These data can be obtained free of charge from the Cambridge Crystallographic Data Centre via www.ccdc.cam.ac.uk/data_request/cif

¹H Diffusion-Ordered Spectroscopy NMR Analysis

Instrumental details

All measurements were carried out with 3 mm NMR tubes (Wilmad-LabGlass) filled with argon (sealed). The Diffusion-Ordered Spectroscopy (DOSY) NMR experiments were performed on JEOL JNM-ECA500 NMR spectrometer operating at 500 MHz for proton resonance under Delta (*ver.* 5.0.4) and equipped with a 50H3X/FG3 probe. ¹H-DOSY experiments were performed with the BPPSTE (Bipolar Pulse Pairs STimulated Echo) pulse sequence. The gradient amplitude was changed from 0.3 G cm⁻¹ to 50.3 G cm⁻¹ in 51 steps for **3**·(THF)₂, and from 0.3 G cm⁻¹ to 35.3 G cm⁻¹ in 51 steps for **4**·(THF)₂. The measurement conditions for ¹H-DOSY were: diffusion time, 0.1 s; field gradient pulse width, 1 ms; relaxation delay, 7.0 s; duration of the 90° pulse, 4.4 μs.

*Sample preparation*²³

All samples were prepared in a glovebox filled with argon. The solvated zincate **3**·(THF)₂ (23.8 mg) or **4**·(THF)₂ (19.9 mg) was dissolved in THF-*d*₈ along with 1,2,3,4-tetraphenyl-naphthalene (TPhN, 14.6 mg), 1-phenyl-naphthalene (PhN, 13.2 μL) and tetramethylsilane (TMS, 19.1 μL) as inert reference standards. The solution surface was 3.0 cm from the bottom of the NMR tube. The ¹H-DOSY NMR data was recorded at 27 °C without spinning.

Analysis

Linear calibration graphs were prepared by plotting log D versus log FW and log D versus log V, in which log D was calculated from the diffusion coefficients of the internal standards (FW= formula weight; V= volume). The FW_{DOSY} and V_{DOSY} of the species in THF-*d*₈ were estimated from the average value of the diffusion coefficients for the signals corresponding to a zincate (**3** or **4**) using the calibration equation. To determine the volumes of the standards used and candidate zincates **3**·(THF)_n and **4**·(THF)_n (n= 0, 1, 2), DFT calculations were carried out. The volumes used for creating graphs (logD versus logV) were average values of volumes from four independent calculations.

Chapter 3. Deprotonative-Metalation Reactions

DOSY NMR study of 3·(THF)₂

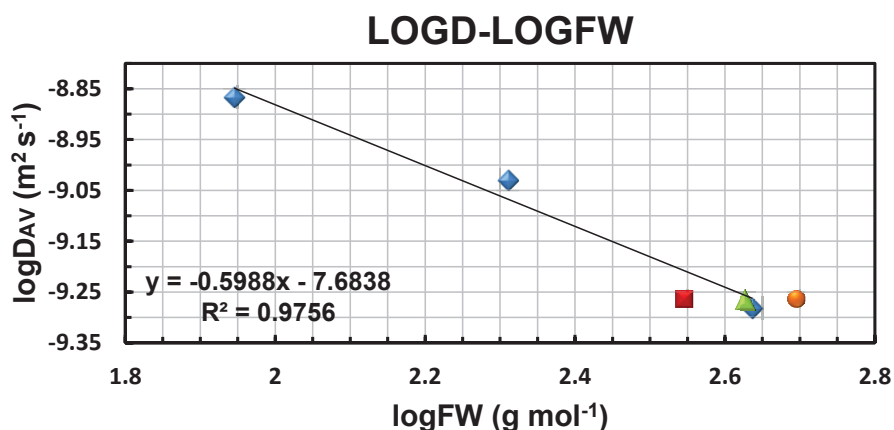
Table S3 shows the D_{AV} for each standard and also their FW and volumes, and Table S4 shows FW and volumes of candidate CPC-zincate $3 \cdot (THF)_n$ ($n = 0, 1, 2$). The D_{AV} values are average values of the diffusion coefficients obtained for each signal which corresponds to the inert standard. Graph S1 shows the observed D_{AV} for **3** versus log FW of candidate CPC-zincate on the linear calibration graph of log D versus log FW. Graph S2 shows the observed D_{AV} for **3** versus log V of candidate CPC-zincate on the linear calibration graph of log D versus log V. In both graphs, square, triangle and circle mean $n = 0, 1$ and 2 respectively.

Table S3. Diffusion coefficients of internal standards and their FW and volumes in THF- d_8 .

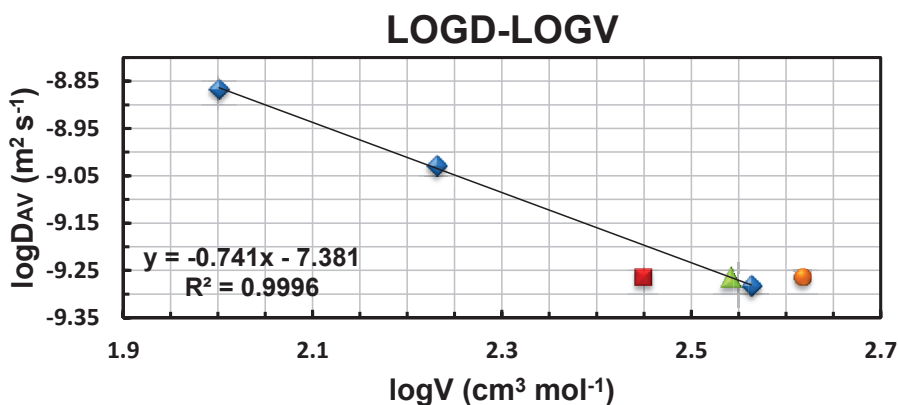
Compound	$10^{-10} D_{AV}$ ($m^2 s^{-1}$)	logD	FW ($g mol^{-1}$)	logFW	V ($cm^3 mol^{-1}$)	logV
TPhN	5.22	-9.282336985	432.57	2.636056397	365.8	2.563243701
PhN	9.34	-9.029504238	204.27	2.310204589	170.1	2.230704314
TMS	13.6	-8.866751783	88.23	1.945616279	100.3	2.001300933

Table S4. FW and volumes of candidate CPC-zincates in THF- d_8 .

Compound	FW ($g mol^{-1}$)	logFW	V ($cm^3 mol^{-1}$)	logV
(THF) ₂ Li(CPC)ZnEt ₂	495.04	2.694640292	414.3	2.617314933
(THF)Li(CPC)ZnEt ₂	422.93	2.626268492	348.1	2.541704023
Li(CPC)ZnEt ₂	350.82	2.545084344	281.1	2.448860846



Graph S1. log D – log FW representation from the ¹H DOSY NMR data obtained for candidate CPC-zincate and the standards TPhN, PhN, TMS at 27 °C in THF-*d*₈.



Graph S2. log D – log V representation from the ¹H DOSY NMR data obtained for candidate CPC-zincate and the standards TPhN, PhN, TMS at 27 °C in THF-*d*₈.

From the Graph S1 and S2, **3**·THF (*n* = 1, triangle) best fits the calibration (black line). The D_{AV} for **3** which was calculated from *D* values for the signals corresponding to the components of **3** was $D_{AV} = 5.45 \times 10^{-10}$ (m² s⁻¹). This D_{AV} could convert to log *D* = -9.263654341. Assigning this log *D* to *y* in linear calibration equations for log *D* versus log FW and log *D* versus log *V*, FW and volume for chemical species corresponding to **3**·(THF)₂ dissolved in THF-*d*₈ were estimated to be $FW_{DOSY} = 434.88$ (g mol⁻¹) and $V_{DOSY} = 347.29$ (cm³ mol⁻¹) respectively. Table S5 shows the FW and *V*, and Error_{FW}, Error_V between calculated data and DOSY data.

Table S5. FW, V and errors between calculated data and DOSY data.

Compound	FW (g mol ⁻¹)	Error _{FW} (%)	V (cm ³ mol ⁻¹)	Error _V (%)
(THF) ₂ Li(CPC)ZnEt ₂	495.04	12.2	414.3	16.2
(THF)Li(CPC)ZnEt ₂	422.93	2.8	348.1	0.2
Li(CPC)ZnEt ₂	350.82	24.0	281.1	23.5

From the DOSY study for **3**·(THF)₂ in THF-*d*₈, **3**·THF showed a much smaller error in comparison to **3**·(THF)₂ and **3**. This indicates that **3** could form an ate complex with Et₂Zn in THF-*d*₈ and one THF molecule coordinated to the Li center on average.

DOSY NMR study of **4**·(THF)₂

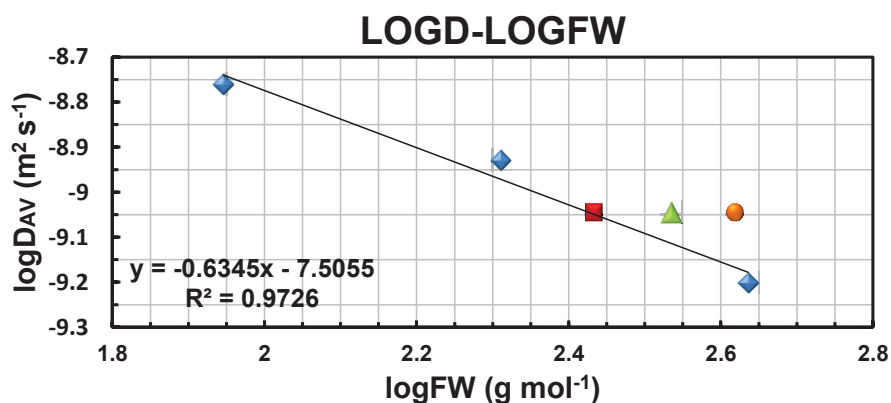
Table S6 shows the D_{AV} for each standard and also their FW and volumes, and Table S7 shows FW and volumes of candidate TMP-zincate **4**·(THF)_n (n = 0, 1, 2). Graph S3 shows the observed D_{AV} for **4** versus log FW of candidate TMP-zincate on the linear calibration graph of log D versus log FW. Graph S4 shows the observed D_{AV} for **4** versus log V of candidate TMP-zincate on the linear calibration graph of log D versus log V. In both graphs, square, triangle and circle mean n = 0, 1 and 2 respectively.

Table S6. Diffusion coefficients of internal standards and their FW and volumes in THF-*d*₈.

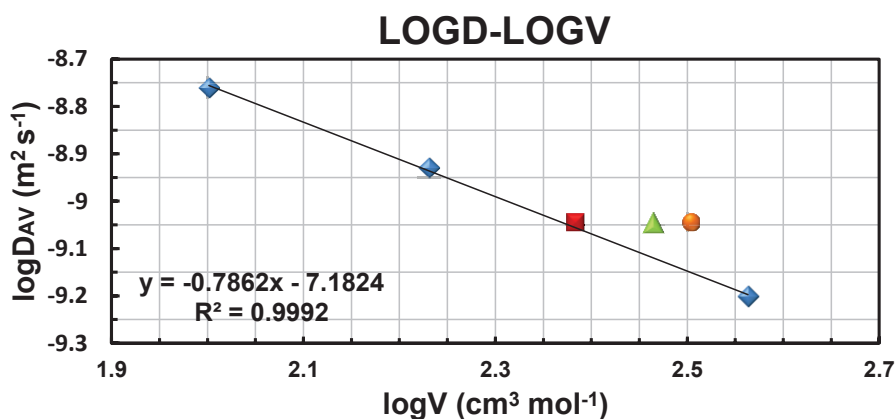
Compound	10 ⁻¹⁰ D _{AV} (m ² s ⁻¹)	logD	FW (g mol ⁻¹)	logFW	V (cm ³ mol ⁻¹)	logV
TPhN	6.30	-9.200543826	432.57	2.636056397	365.8	2.563243701
PhN	11.8	-8.928868228	204.27	2.310204589	170.1	2.230704314
TMS	17.4	-8.760080186	88.23	1.945616279	100.3	2.001300933

Table S7. FW and volumes of candidate TMP-zincates in THF-*d*₈.

Compound	FW (g mol ⁻¹)	logFW	V (cm ³ mol ⁻¹)	logV
(THF) ₂ Li(TMP)ZnEt ₂	414.91	2.694640292	318.8	2.617314933
(THF)Li(TMP)ZnEt ₂	342.80	2.626268492	291.5	2.541704023
Li(TMP)ZnEt ₂	267.69	2.545084344	241.5	2.448860846



Graph S3. log D – log FW representation from the ¹H DOSY NMR data obtained for candidate TMP-zincate and the standards TPhN, PhN, TMS at 27 °C in THF-*d*₈.



Graph S4. log D – log V representation from the ¹H DOSY NMR data obtained for candidate TMP-zincate and the standards TPhN, PhN, TMS at 27 °C in THF-*d*₈.

From the Graph S3 and S4, **4** ($n=0$, square) best fits the calibration (black line). The D_{AV} for **4** which was calculated from D values for the signals corresponding to the components of **4** was $D_{AV} = 9.04 \times 10^{-10}$ (m² s⁻¹). This D_{AV} could convert to $\log D = -9.043978441$. Assigning this $\log D$ to y in linear calibration equations for $\log D$ versus $\log FW$ and $\log D$ versus $\log V$, FW and volume for chemical species corresponding to **4**·(THF)₂ dissolved in THF-*d*₈ were estimated to be $FW_{DOSY} = 265.89$ (g mol⁻¹) and $V_{DOSY} = 233.25$ (cm³ mol⁻¹) respectively. Table S8 shows the FW and V , and $Error_{FW}$, $Error_V$ between calculated data and DOSY data.

Table S8. FW, V and error between calculated data and DOSY data.

Compound	FW (g mol ⁻¹)	Error _{FW} (%)	V (cm ³ mol ⁻¹)	Error _V (%)
(THF) ₂ Li(TMP)ZnEt ₂	414.91	35.9	318.8	26.8
(THF)Li(TMP)ZnEt ₂	342.80	22.4	291.5	20.0
Li(TMP)ZnEt ₂	267.69	1.8	241.5	3.4

From the DOSY study for **4**·(THF)₂ in THF-*d*₈, **4** showed a smaller error than **4**·(THF)₂ and **4**·(THF). This indicates that **4** could form ate complex with Et₂Zn in THF-*d*₈ and no THF molecules coordinated to the Li center on average.

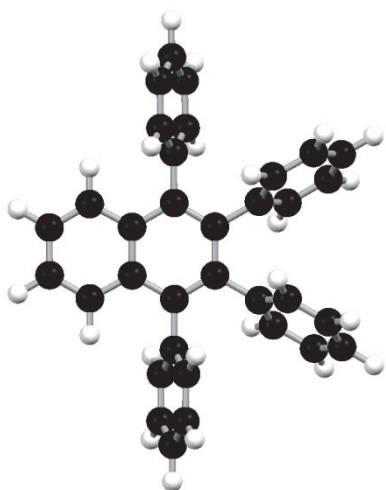
DFT calculations

General considerations

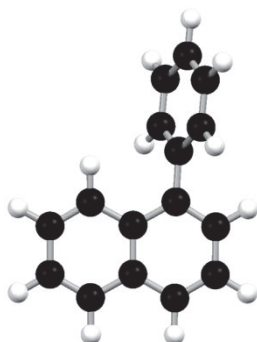
DFT calculations were performed using the Gaussian 09 package of programs²⁴ to estimate the volumes of inert reference standards, TPhN, PhN and TMS, and candidate zincates, **3**·(THF)_n and **4**·(THF)_n (n= 0, 1, 2) for DOSY analysis. For TPhN, PhN, TMS, **3**·(THF)_n and **4**·(THF)_n (n= 0, 1, 2), the B3LYP²⁵ hybrid functional was used with 6-311G(d,p) basis set for geometry optimization. For PhN and TMS, the HF/6-31G(d) level of theory was used for geometry pre-optimization. For TPhN, Spartan'04²⁶ was used for geometry pre-optimization. All structures were optimized without any symmetry assumptions. After each geometry optimization at the B3LYP/6-311G(d,p) level of theory, a frequency calculation at the same level was performed to verify that all the stationary points had no imaginary frequency. The volume for each species were determined by DFT calculations of all optimized structures using volume keyword at the same level of B3LYP/6-311G(d,p).

Optimized structures for DOSY analysis

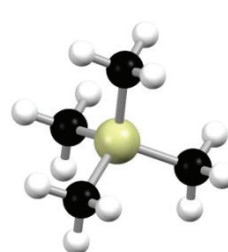
TPhN



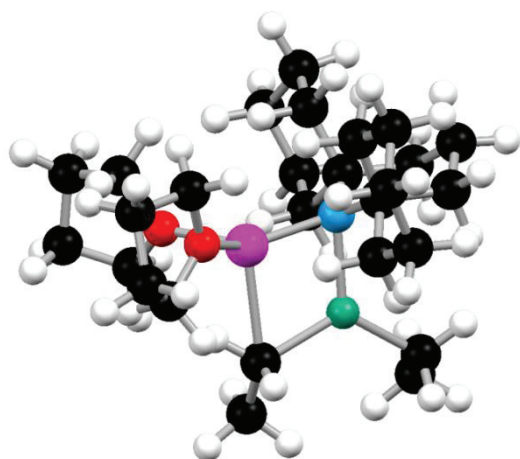
PhN



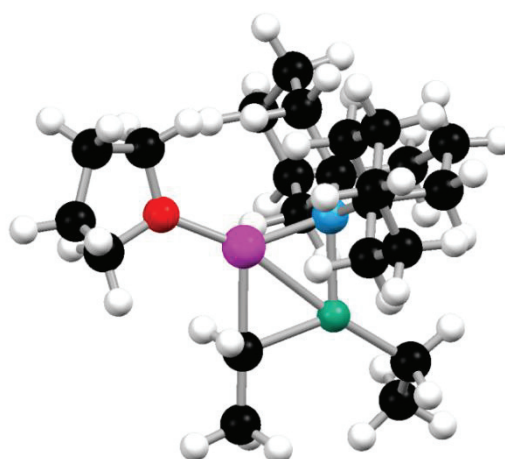
TMS



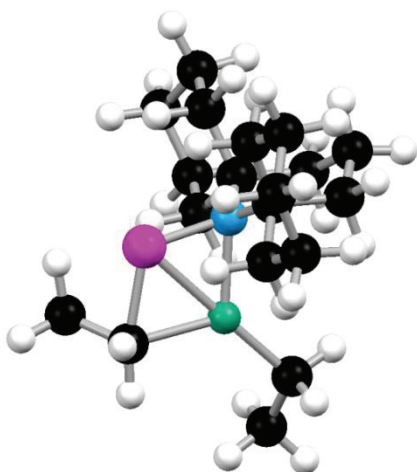
3·(THF)₂



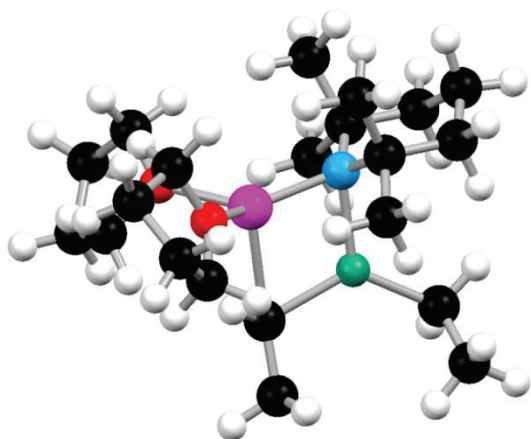
3·THF



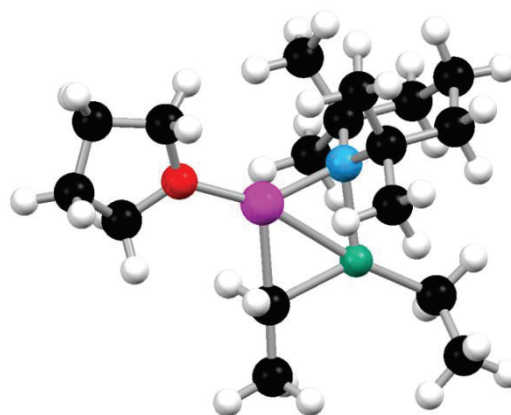
3



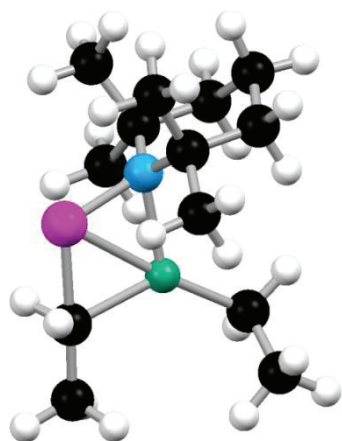
4·(THF)₂



4·THF



4



Volume of each species

	TPhN	PhN	TMS	3·(THF) ₂	3·THF	3	4·(THF) ₂	4·THF	4
1st	333.693	180.216	104.246	405.624	338.422	288.372	292.099	309.515	250.611
2nd	382.675	163.255	100.712	395.224	359.574	294.853	332.929	261.435	216.821
3rd	382.675	161.134	100.712	388.29	363.099	239.77	295.239	294.49	247.795
4th	364.307	175.976	95.411	468.028	331.372	301.333	354.915	300.5	250.611
Average	365.8375	170.1453	100.2703	414.2915	348.1168	281.082	318.7955	291.485	241.4595

References

- [1]. Hall, P. L.; Gilchrist, J. H.; Collum, D. B. *J. Am. Chem. Soc.* **1991**, *113*, 9571–9574.
- [2]. (a) Board, J.; Cosman, J. L.; Rantanen, T.; Singh, S. P.; Snieckus, V. *Platinum Met. Rev.* **2013**, *57*, 234–258.
(b) Snieckus, V. *Chem. Rev.* **1990**, *90*, 879–933.
- [3]. (a) Schlosser, M. Organometallic Chemistry. In *Organometallics in Synthesis, Third Manual*; Schlosser, M., Ed.; John Wiley & Sons, Inc., 2013; pp 1–222.
(b) Clayden, J. In *Organolithiums: Selectivity for Synthesis*; Baldwin, J. E., Williams, R. M., Eds.; Tetrahedron Organic Chemistry Series 23; Elsevier Science Ltd., 2002; pp 1–375.
Common utility alkyl lithium and lithium amide reagents (*n*-BuLi, *s*-BuLi, *t*-BuLi, LiDA, LiHMDS and LiTMP): (c) In *Handbook of reagents for organic synthesis: acidic and basic reagents*; Reich, H. J., Rigby, J. H., Eds.; Wiley, 1999; pp 66–74 (*n*-BuLi), 74–80 (*s*-BuLi), 81–87 (*t*-BuLi), 213–221 (LiDA), 221–224 (LiHMDS), 232–234 (LiTMP).
- [4]. (a) Martínez-Martínez, A. J.; Kennedy, A. R.; Mulvey, R. E.; O'Hara, C. T. *Science* **2014**, *346*, 834–837.
(b) Mulvey, R. E.; Robertson, S. D. Modern Developments in Magnesium Reagent Chemistry for Synthesis. In *Alkaline-Earth Metal Compounds: Oddities and Applications*; Harder, S., Ed.; Topics in Organometallic Chemistry 45; Springer GmbH, 2013; pp 103–139.
(c) Mulvey, R. E.; Mongin, F.; Uchiyama, M.; Kondo, Y. *Angew. Chem. Int. Ed.* **2007**, *46*, 3802–3824.
(d) Mulvey, R. E. *Acc. Chem. Res.* **2009**, *42*, 743–755.
(e) Haag, B.; Mosrin, M.; Ila, H.; Malakhov, V.; Knochel, P. *Angew. Chem. Int. Ed.* **2011**, *50*, 9794–9824.
(f) Harford, P. J.; Peel, A. J.; Chevallier, F.; Takita, R.; Mongin, F.; Uchiyama, M.; Wheatley, A. E. H. *Dalton Trans.* **2014**, *43*, 14181–14203.
(g) Snégaroff, K.; L'Helgoual'ch, J.-M.; Bentabed-Ababsa, G.; Nguyen, T. T.; Chevallier, F.; Yonehara, M.; Uchiyama, M.; Derdour, A.; Mongin, F. *Chem. - Eur. J.* **2009**, *15*, 10280–10290.
- [5]. Kondo, Y.; Shilai, M.; Uchiyama, M.; Sakamoto, T. *J. Am. Chem. Soc.* **1999**, *121*, 3539–3540.
- [6]. (a) Uchiyama, M.; Miyoshi, T.; Kajihara, Y.; Sakamoto, T.; Otani, Y.; Ohwada, T.; Kondo, Y. *J. Am. Chem. Soc.* **2002**, *124*, 8514–8515.
(b) Uchiyama, M.; Kobayashi, Y.; Furuyama, T.; Nakamura, S.; Kajihara, Y.; Miyoshi, T.; Sakamoto, T.; Kondo, Y.; Morokuma, K. *J. Am. Chem. Soc.* **2008**, *130*, 472–480.
- [7]. Computational studies on the differences between heteroleptic lithium zincates and alkyl lithium reagents are reported in the following paper. Uchiyama, M.; Matsumoto, Y.; Usui, S.; Hashimoto, Y.; Morokuma, K. *Angew. Chem. Int. Ed.* **2007**, *46*, 926–929.

- [8]. Armstrong, D. R.; Garden, J. A.; Kennedy, A. R.; Leenhouts, S. M.; Mulvey, R. E.; O'Keefe, P.; O'Hara, C. T.; Steven, *Chem. - Eur. J.* **2013**, *19*, 13492–13503.
- [9]. Imahori, T.; Uchiyama, M.; Sakamoto, T.; Kondo, Y. *Chem. Commun.* **2001**, 2450–2451.
- [10]. Mulvey, R. E.; Robertson, S. D. *Angew. Chem. Int. Ed.* **2013**, *52*, 11470–11487.
- [11]. α -Hydrogen atom adjacent to an anionic nitrogen atom (e.g., $\text{LiN}(\text{CHMe}_2)_2$) can migrate to electrophilic substrates. (a) Nguyen, T. T. T.; Boussonnière, A.; Banaszak, E.; Castanet, A.-S.; Nguyen, K. P. P.; Mortier, J. *J. Org. Chem.* **2014**, *79*, 2775–2780.
(b) Gallagher, D. J.; Henderson, K. W.; Kennedy, A. R.; O'Hara, C. T.; Mulvey, R. E.; Rowlings, R. B. *Chem. Commun.* **2002**, 376–377.
(c) Sanchez, R.; Scott, W. *Tetrahedron Lett.* **1988**, *29*, 139–142.
(d) Woo, E. P.; Mak, K. T. *Tetrahedron Lett.* **1974**, *15*, 4095–4098.
- [12]. Decomposition of TMP has been reported in some cases. (a) Kennedy, A. R.; Klett, J.; McGrath, G.; Mulvey, R. E.; Robertson, G. M.; Robertson, S. D.; O'Hara, C. T. *Inorg. Chim. Acta* **2014**, *411*, 1–4.
(b) Kennedy, A. R.; Leenhouts, S. M.; Liggat, J. J.; Martínez-Martínez, A. J.; Miller, K.; Mulvey, R. E.; O'Hara, C. T.; O'Keefe, P.; Steven, A. *Chem. Commun.* **2014**, *50*, 10588–10591.
(c) Conway, B.; Kennedy, A. R.; Mulvey, R. E.; Robertson, S. D.; Álvarez, J. G. *Angew. Chem. Int. Ed.* **2010**, *49*, 3182–3184.
- [13]. Campbell, R.; Conway, B.; Fairweather, G. S.; García-Álvarez, P.; Kennedy, A. R.; Klett, J.; Mulvey, R. E.; O'Hara, C. T.; Robertson, G. M. *Dalton Trans.* **2010**, *39*, 511–519.
- [14]. A cyclic trimer $(\text{LiTMP})_3$ and a cyclic tetramer $(\text{LiTMP})_4$: (a) Hevia, E.; Kennedy, A. R.; Mulvey, R. E.; Ramsay, D. L.; Robertson, S. D. *Chem. - Eur. J.* **2013**, *19*, 14069–14075.
A cyclic tetramer $(\text{LiTMP})_4$. (b) Lappert, M. F.; Slade, M. J.; Singh, A.; Atwood, J. L.; Rogers, R. D.; Shakir, R. *J. Am. Chem. Soc.* **1983**, *105*, 302–304.
- [15]. The THF coordinated zincate $[(\text{THF})\text{Li}(\text{TMP})\text{Zn}(\text{tBu})_2]$: (a) Clegg, W.; Dale, S. H.; Hevia, E.; Honeyman, G. W.; Mulvey, R. E. *Angew. Chem. Int. Ed.* **2006**, *45*, 2370–2374.
(b) Uchiyama, M.; Matsumoto, Y.; Nobuto, D.; Furuyama, T.; Yamaguchi, K.; Morokuma, K. *J. Am. Chem. Soc.* **2006**, *128*, 8748–8750.
TMEDA coordinated zincates: (c) See ref 8.
(d) Barley, H. R. L.; Clegg, W.; Dale, S. H.; Hevia, E.; Honeyman, G. W.; Kennedy, A. R.; Mulvey, R. E. *Angew. Chem. Int. Ed.* **2005**, *44*, 6018–6021.
(e) See ref 11.
(f) Clegg, W.; García-Álvarez, J.; García-Álvarez, P.; Graham, D. V.; Harrington, R. W.; Hevia, E.; Kennedy, A. R.; Mulvey, R. E.; Russo, L. *Organometallics* **2008**, *27*, 2654–2663.
(g) Graham, D. V.; Hevia, E.; Kennedy, A. R.; Mulvey, R. E. *Organometallics* **2006**, *25*, 3297–3300.

- (h) Saßmannshausen, J.; Klett, J.; Kennedy, A. R.; Parkinson, J. A.; Armstrong, D. *New J. Chem.* **2013**, *37*, 494–501.
- A no solvent-coordinated zincate: (i) See ref 19a.
- [16]. (a) Li, D.; Keresztes, I.; Hopson, R.; Williard, P. G. *Acc. Chem. Res.* **2009**, *42*, 270–280.
- (b) Armstrong, D. R.; Kennedy, A. R.; Mulvey, R. E.; Parkinson, J. A.; Robertson, S. D. *Chem. Sci.* **2012**, *3*, 2700–2707.
- (c) García-Álvarez, P.; Mulvey, R. E.; Parkinson, J. A. *Angew. Chem. Int. Ed.* **2011**, *50*, 9668–9671.
- [17]. The reaction pathways of deprotonative metalation of monosubstituted benzenes are proposed in these papers: (a) Kondo, Y.; Morey, J. V.; Morgan, J. C.; Naka, H.; Nobuto, D.; Raithby, P. R.; Uchiyama, M.; Wheatley, A. E. H. *J. Am. Chem. Soc.* **2007**, *129*, 12734–12738.
- (b) Clegg, W.; Conway, B.; Hevia, E.; McCall, M. D.; Russo, L.; Mulvey, R. E. *J. Am. Chem. Soc.* **2009**, *131*, 2375–2384.
- [18]. Computational studies about benzyne formations with a methyzincate and a *tert*-butyl-zincate (see ref 6b).
- [19]. Sheldrick, G. M. A short history of *SHELX*. *Acta Cryst.* **2008**, *A64*, 112–122.
- [20]. Hübschle, C. B.; Sheldrick, G. M.; Dittrich, B. *ShelXle*: a Qt graphical user interface for *SHELXL*. *J. Appl. Cryst.* **2011**, *44*, 1281–1284.
- [21]. Persistence of Vision Raytracer (*ver.* 3.7.0); Persistence of Vision Pty. Ltd., 2016; Retrieved from <http://www.povray.org/download/>
- [22]. PLATON for Windows Taskbar (*ver.* 1.16); (a) Speck, A. L. Structure validation in chemical crystallography. *Acta Cryst.* **2009**, *D65*, 148–155.
- (b) Speck, A. L. *PLATON, A Multipurpose Crystallographic Tool*, Utrecht University, Utrecht, The Netherlands, 2011.
- [23]. Armstrong, D. R.; Garden, J. A.; Kennedy, A. R.; Leenhouts, S. M.; Mulvey, R. E.; O'Keefe, P.; O'Hara, C. T.; Steven, A. *Chem. - Eur. J.* **2013**, *19*, 13492–13503.
- [24]. Gaussian 09, Revision D.01, Frisch, M. J.; Trucks, G. W.; Schlegel, H. B.; Scuseria, G. E.; Robb, M. A.; Cheeseman, J. R.; Scalmani, G.; Barone, V.; Mennucci, B.; Petersson, G. A.; Nakatsuji, H.; Caricato, M.; Li, X.; Hratchian, H. P.; Izmaylov, A. F.; Bloino, J.; Zheng, G.; Sonnenberg, J. L.; Hada, M.; Ehara, M.; Toyota, K.; Fukuda, R.; Hasegawa, J.; Ishida, M.; Nakajima, T.; Honda, Y.; Kitao, O.; H. Nakai, O.; Vreven, T.; Montgomery, J. A., Jr.; Peralta, J. E.; Ogliaro, F.; Bearpark, M.; Heyd, J. J.; Brothers, E.; Kudin, K. N.; Staroverov, V. N.; Keith, T.; Kobayashi, R.; Normand, J.; Raghavachari, K.; Rendell, A.; Burant, J. C.; Iyengar, S. S.;

Tomasi, J.; Cossi, M.; Rega, N.; Millam, J. M.; Klene, M.; Knox, J. E.; Cross, J. B.; Bakken, V.; Adamo, C.; Jaramillo, J.; Gomperts, R.; Stratmann, R. E.; Yazyev, O.; Austin, A. J.; Cammi, R.; Pomelli, C.; Ochterski, J. W.; Martin, R. L.; Morokuma, K.; Zakrzewski, V. G.; Voth, G. A.; Salvador, P.; Dannenberg, J. J.; Dapprich, S.; Daniels, A. D.; Farkas, O.; Foresman, J. B.; Ortiz, J. V.; Cioslowski, J.; Fox, D. J.; Gaussian, Inc.: Wallingford CT, 2013.

[25].(a) Becke, A. D. *Phys. Rev. A: Gen. Phys.* **1988**, *38*, 3098–3100.

(b) Lee, C.; Yang, W.; Parr, R. G. *Phys. Rev. B: Condens. Matter* **1988**, *37*, 785–789.

(c) Becke, A. D. *J. Chem. Phys.* **1993**, *98*, 1372–1377.

(d) Becke, A. D. *J. Chem. Phys.* **1993**, *98*, 5648–5652.

[26].(a) Spartan'04, *Wavefunction Inc.*, Irvine, CA, 92612 USA, 2004.

(b) Kong, J.; White, C. A.; Krylov, A. I.; Sherrill, D.; Adamson, R. D.; Furlani, T. R.; Lee, M. S.; Lee, A. M.; Gwaltney, S. R.; Adams, T. R.; Ochsenfeld, C.; Gilbert, A. T. B.; Kedziora, G. S.; Rassolov, V. A.; Maurice, D. R.; Nair, N.; Shao, Y.; Besley, N. A.; Maslen, P. E.; Dombroski, J. P.; Daschel, H.; Zhang, W.; Korambath, P. P.; Baker, J.; Byrd, E. F. C.; Van Voorhis, T.; Oumi, M.; Hirata, S.; Hsu, C.-P.; Ishikawa, N.; Florian, J.; Warshel, A.; Johnson, B. G.; Gill, P. M. W.; Head-Gordon, M.; Pople, J. A. Q-Chem 2.0: A High-Performance Ab Initio Electronic Structure Program Package. *J. Comput. Chem.* **2000**, *21*, 1532–1548.

Chapter 4

Syntheses of Low Oxidation-State Boron Species and Their Reactivity

4-1. Introduction

Diboranes(4) (R_2B-BR_2) with a boron–boron (B–B) single bond have become indispensable reagents for Suzuki–Miyaura reaction and other coupling reactions toward functional materials and pharmaceuticals¹ since the first synthesis of electron-precise diborane(4) (B_2Cl_4) by Stock and co-workers in 1925.² Despite the diverse investigations of diboranes(4), the chemistry of neutral $(R-B)_n$ species without polyhedral structures (up to $n = 6$) still lags behind (Figure 1). The synthetic challenge is mainly due to the inherent electron-deficiency and low electronegativity of the boron atom, which favor formation of hypercoordinate boron compounds with multicenter 2-electron bonds.

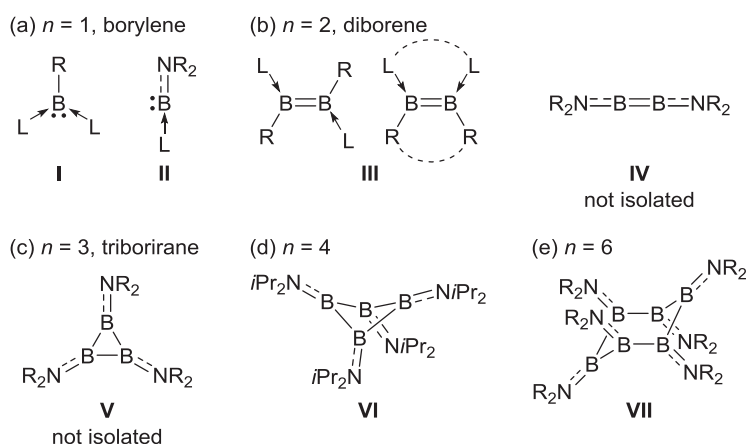


Figure 1. Selected examples of reported electron-precise $(R-B)_n$ with classical structures.

To date, besides the kinetic stabilization from steric bulk of the substituents, the most effective approach to isolation of neutral $(R-B)_n$ species is by introducing one or more neutral Lewis base ligands (L; L = carbenes, phosphines, CO, isocyanides) to the boron centers. Recently, several metal-free borylenes ($R-B:$) ($n = 1$, Figure 1a, **I** and **II**)^{3,4} and diborenes ($R-B=B-R$) ($n = 2$, Figure 1b, **III**)^{5,6} have been isolated with one or two Lewis base ligands as Lewis adducts, which exhibited new reactivity that was unexpected of the usually electron-deficient boron compounds (Figure 2).^{3,5,7–10}

An alternative approach that has been explored to access these highly reactive neutral $(R-B)_n$ species is by the use of amino-substituents. The lone pair of electrons from nitrogen is expected to compensate the electron-deficiency of the boron center in the form of π -bond as opposed to a σ -bond from a Lewis base ligand. Recently, Bertand, Stephan and co-workers,^{4d} and Hudnall and co-workers^{4k} demonstrated that with an employment of an amino group, the number of additional Lewis base ligand required to isolate borylenes can be reduced to one (Figure 1a, **II**). Also, computational work^{11a} on a NBBN skeleton in diaminodiborene **IV** showed significant shortening of N–B indicating the π -electron donation and three consecutive π -bond similar to [3]cumulene, which

was different from isolated Lewis base-stabilized diborenes.¹¹ The singlet electronic state, unlike triplet electronic-state of $\text{RB}=\text{BR}$ ($\text{R} = \text{H}$, phenyl) was also estimated by calculations.^{11a,12} In addition, computational work on the triborirane (triboracyclopropane) **V**¹³ (Figure 1c) showed stability similar to [3]radialene ($\text{R}_2\text{C}=\text{C}$)₃, which should be synthetically accessible. However, despite of these sporadic reports, the diaminodiborene **IV** (Figure 1b)¹⁴ and triborirane **V**¹⁵ have not been isolated for structural characterization. Their existence has been proposed based on mass-spectrometric data.¹⁶ The larger cyclic catenated analogues **VI**^{14b} and **VII**,^{15c,17} which can be regarded formally as the oligomers of **IV** and/or **V**, were isolated (Figure 1d, e).

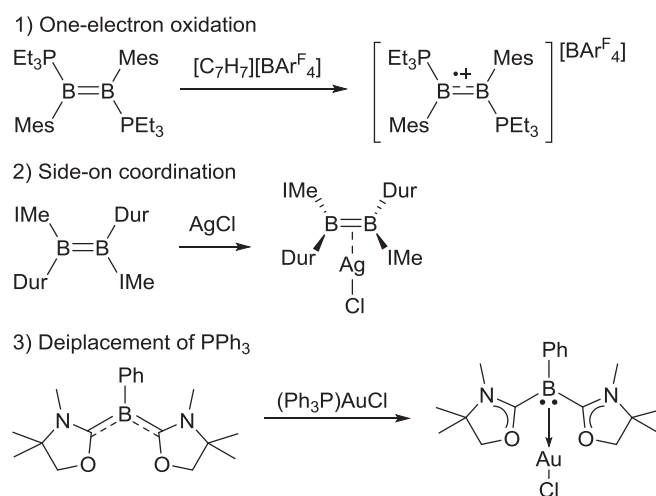
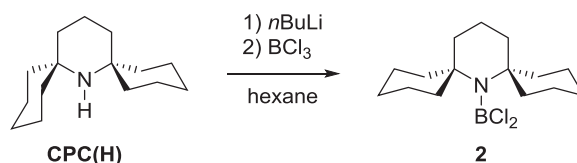


Figure 2. Unique reactivities of diborenes and borylene similar to those of amines and phosphines. $\text{Ar}^{\text{F}} = 3,5\text{-(CF}_3)_2\text{C}_6\text{H}_3$, Dur = 2,3,5,6-Me₄C₆H, IMe = 1,3-Me₂imidazol-2-ylidene.

To prevent oligomerization of the generated $(\text{R}_2\text{N}-\text{B})_n$ species, a much more sterically hindered amino-substituent is necessary. Therefore, we aim to synthesize and isolate the ligand-free diaminodiborene **IV** and/or triborirane **V** by employing TMP and our CPC substituents, and also aim to reveal their reactivity and electronic behavior.

4-2. Syntheses of Aminodichlorodiboranes

Herein, syntheses of (TMP)BCl₂ (**1**)^{18,19} and (CPC)BCl₂ (**2**) are reported. A starting material **1** was synthesized according to the previously reported procedure.²⁰ Another starting material **2** was synthesized according to the modified procedure reported in ref. 20 (Scheme 1). The *N*-lithiation of prepared amine CPC(H) by *n*BuLi and subsequent the reaction with BCl₃ were carried out in hexane solution. The insoluble precipitate was filtered and the filtrate was concentrated under reduced pressure. The resulting solution was stored at -30 °C. Desired aminodichloroborane **2** was obtained as colorless crystals in 77% yield. Compound **1** can be also synthesized by this method.



Scheme 1. Synthesis of (CPC)BCl₂ (**2**).

The ¹¹B NMR of **2** was observed at $\delta = 35.1$ ppm comparable to that of **1** ($\delta = 33.1$ ppm). The ¹³C NMR spectrum showed six signals, which indicated that the rapid ring flipping of piperidine and cyclohexyl rings in **2** was occurred in the solution state. The molecular structure of **2** was confirmed by single-crystal X-ray diffraction analysis (Figure 3). The short bond distance of B1–N1 (1.394(2) Å) indicated the strong N→B π -donation.

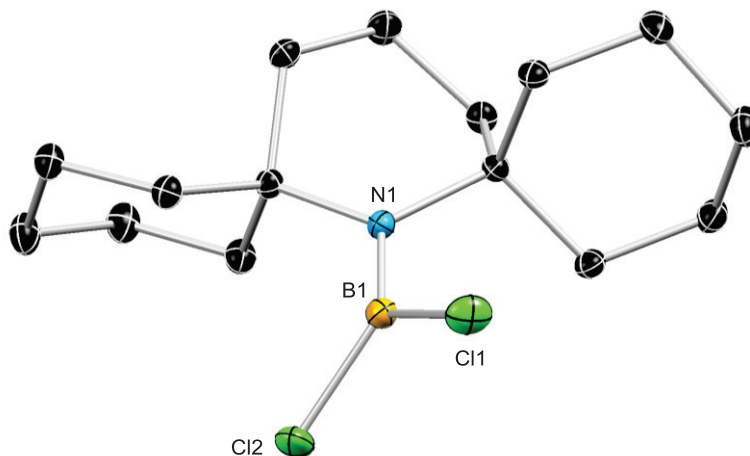


Figure 3. Molecular structures of **2** obtained from single-crystal X-ray diffraction analysis. Thermal ellipsoids are displayed at 30% probability. Hydrogen atoms are omitted for clarity. Selected bond lengths (Angstroms) and angles (degrees) for **2**: B1–N1 1.394(2), B1–Cl1 1.791(2), B1–Cl2 1.790(2); N1–B1–Cl1 124.4(2), N1–B1–Cl2 124.9(2), Cl1–B1–Cl2 110.73(8).

4-3. Attempts to Synthesize Ligand-Free Diaminodiborenes

Herein, attempts to synthesize the desired ligand-free diaminodiborenes through the reduction of prepared **1** and **2** with alkaline metal reductants are reported. Before the beginning of experiments, we preliminarily estimated the relative energies between a diaminodiborene **IV** and its dimerized tetrahedral cluster by DFT calculations. In the case of the TMP-substituted diborene (**IV-TMP**), the type-B conformation (**IV-TMP-B**) was slightly stable than the type-A conformation (**IV-TMP-A**), and the tetrahedral cluster was most stable with the relative energy gap of -16.39 kcal mol⁻¹ in comparison to **IV-TMP-A**. In contrast, the type-A conformation of the CPC-substituted diborene (**IV-CPC-A**) was slightly stable than the type-B conformation (**IV-CPC-B**), and the tetrahedral cluster was most unstable with the relative energy gap of $+5.31$ kcal mol⁻¹ in comparison to **IV-CPC-A**. Therefore, newly prepared CPC-substituent may be more suitable for the isolation of the diaminodiborene.

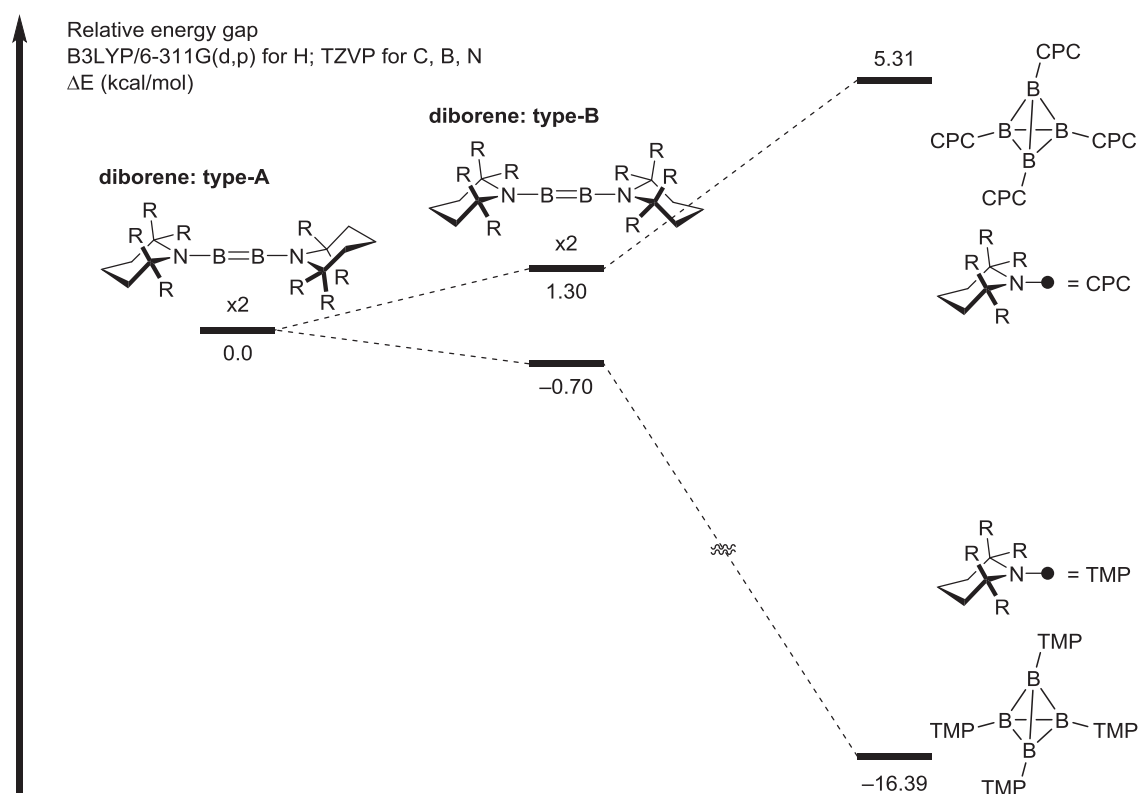
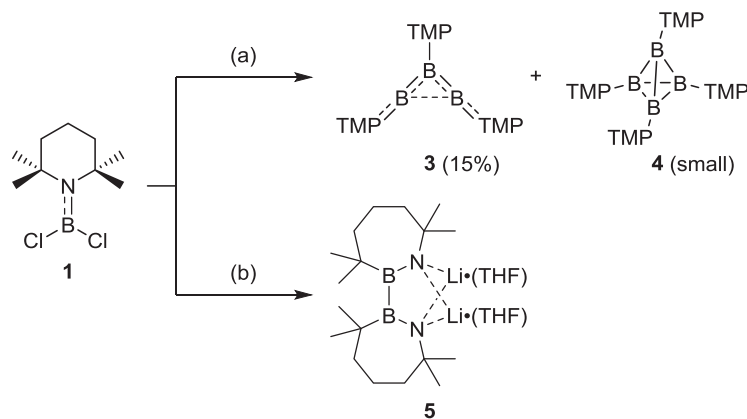


Figure 4. Relative energy gaps estimated by DFT calculations. All structures were optimized with the B3LYP functional using the 6-311 basis set for H atom and TZVP for C, B and N atoms. The relative energy gaps (kcal/mol) were calculated from the sum of the electronic and zero-point energies.

First, to establish the reaction condition and method, the reduction of **1** was carried out. Two or more than two equivalents of potassium in various organic solvents above ambient temperature only provided unidentifiable mixtures. Two equivalents of potassium graphite prepared prior to use in THF at room temperature also provided red colored complex mixture. Two equivalents of sodium in THF at room temperature afforded a red oily mixture. In the case of DME as the solvent, a triaminotriborane(3) **3** was obtained in around 15% yield associated with a small amount of yellow crystals **4**¹³ (Scheme 2). Compound **3** might be formed by borylene coordination to the desired diborene similar to the cheletropic reaction,^{21,22} and a dimerization of the diborene might form tetrahedral cluster **4**^{14a,b} (Figure 5). The details of structural parameters and further attempt to synthesize **3** selectively are described in the next section 4-4. The previously reported tetrahedral cluster **4** was characterized by a single-crystal X-ray diffraction analysis (Figure S25).



Scheme 2. Reduction of **1**. (a) Na, DME, r.t., 18 h; (b) Li, THF, r.t., 12 h. DME.

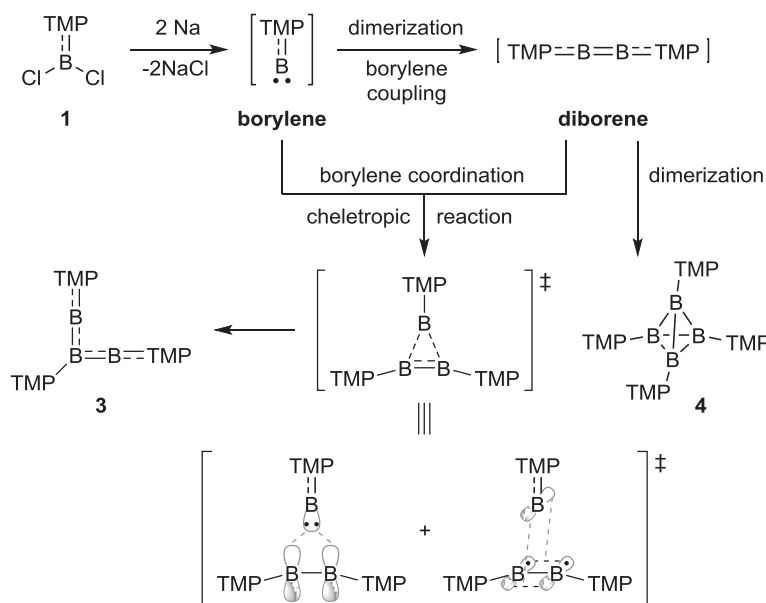


Figure 5. Proposed reaction mechanism to afford **3** and **4**.

In contrast to the reduction with sodium, the reduction of **1** with excess of Li afforded a small amount of dianion species **5** as colorless crystals (Scheme 2), which could be characterized by a single-crystal X-ray diffraction only (Figure 6).

The solid-state structure of **5** was shown in Figure 6. The boron atom inserted into a C–N bond of the TMP substituent. The bond length of B1–B2 (1.791(3) Å) is relatively longer than that of typical B–B single bond (1.697–1.728 Å) in neutral diboranes (R')(R₂N)B–B(NR₂)(R').²³ The shorter N–B bond length (N1–B1 1.403(2) Å) due to N→B π-interactions indicated partial double-bond characters.²⁴ Based on these structural features, **5** can be viewed as an unusual 1,4-diaza-2,3-diborabutadiene.

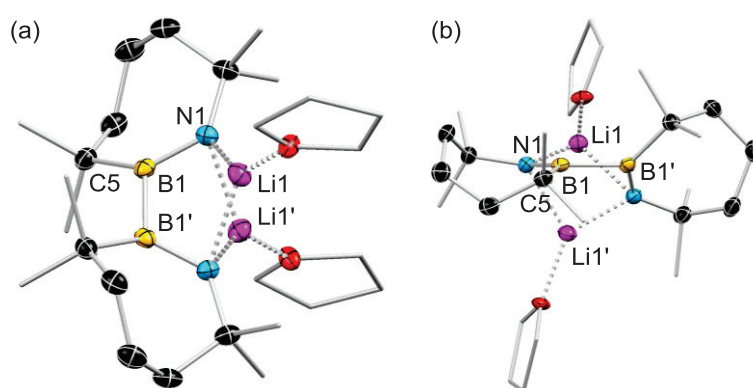
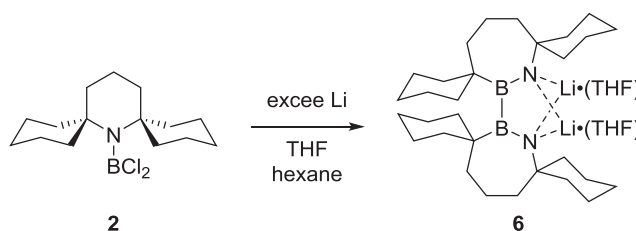


Figure 6. Molecular structure of **5** obtained by single-crystal X-ray diffraction analysis. (a) Top view and (b) side view of **5**. Thermal ellipsoids are displayed at 30% probability. Those of peripheral atoms are omitted for clarity. Structural disorder was observed in THF moieties. Hydrogen atoms are omitted for clarity. Selected bond lengths [Angstroms] and angles [degrees]: B1–B1' 1.791(3), B1–N1 1.403(2), B1–C5 1.651(2), N1–Li1 1.938(3), N1–Li1' 2.073(3); N1–B1–B' 110.73(8), N1–B1–C5 125.4(2), C5–B1–B1' 122.07(9).

For the reduction of (CPC)BCl₂ **2**, using excess of Li in THF and hexane at room temperature also afforded a small amount of dianion species **6** as colorless crystals (Scheme 3). The ¹¹B{¹H} NMR spectra showed a broad single signal at δ = 49.5 ppm, which was upfield shifted as compared to that observed for 2,3-diborabutadienes (57, 58 ppm).⁴³



Scheme 3. Reduction of **2** with Li.

The molecular structure of **6** was confirmed by a single-crystal X-ray diffraction analysis. The solid-state structure shown in Figure 7 was similar to that of **5**. The boron atom inserted into a C–N bond of the CPC substituent. Note that the bond length of B1–B1' (1.855(3) Å) was significantly elongated as compared to that of **5** (1.791(3) Å) and that of typical B–B single bond (1.697–1.728 Å) in neutral diboranes (R')(R₂N)B–B(NR₂)(R'),²³ which may be due to the larger steric hindrance of cyclohexyl rings in **6** than methyl groups in **5** or the electrostatic repulsion of the π -charges on the boron atoms as described for 2,3-diboratabutadiene, whereas this length was comparable to that of the reported 2,3-diboratabutadiene.⁴³ The shorter N–B bond length (N1–B1 1.406(2) Å) due to N→B π -interactions indicated partial double-bond characters.²⁴ Based on these structural features, **6** can be also viewed as an unusual 1,4-diaza-2,3-diborabutadiene.

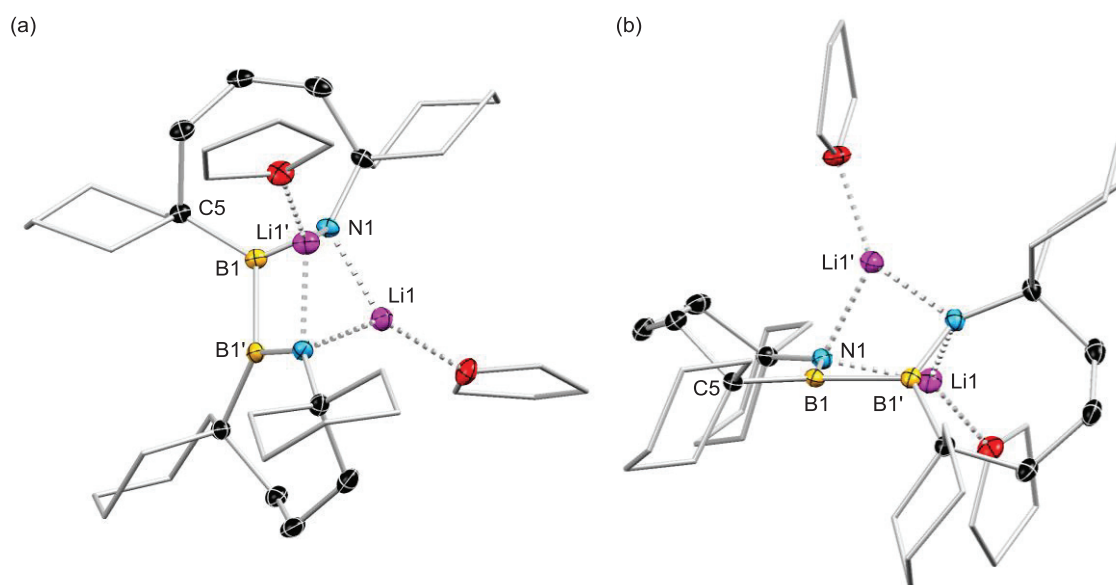


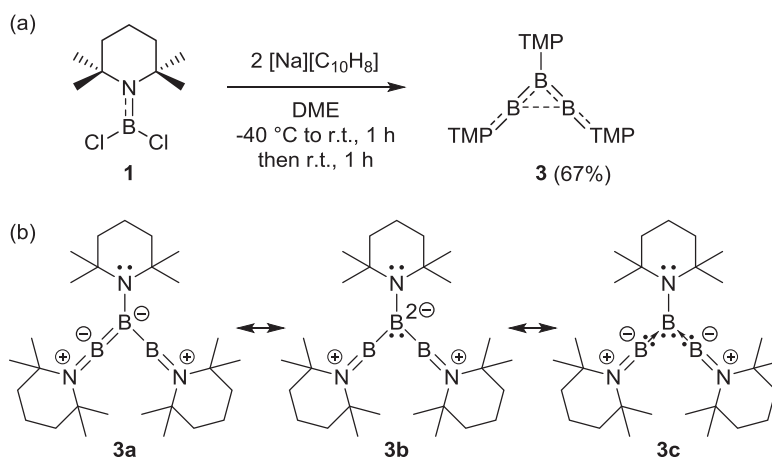
Figure 7. Molecular structure of **6** obtained by single-crystal X-ray diffraction analysis. (a) Top view and (b) side view of **6**. Thermal ellipsoids are displayed at 30% probability. Those of peripheral atoms are omitted for clarity. Structural disorder was observed in THF moieties. Hydrogen atoms are omitted for clarity. Selected bond lengths [Angstroms] and angles [degrees]: B1–B1' 1.855(3), B1–N1 1.406(2), B1–C5 1.656(2), N1–Li1 1.928(3), N1–Li1' 2.056(3); N1–B1–B1' 108.49(8), N1–B1–C5 125.4(2), C5–B1–B1' 124.94(9).

We also preliminary tried to trap and/or isolate the reaction intermediates aminoborylenes and diaminodiborenes by conducting the reductions in the presence of 2,3-dimethylbutadiene, diphenylacetylene, PMe_3 , $(\text{Me}_2\text{S})\text{AuCl}$ or elemental sulfur, but failed.

In order to synthesize desired diaminodiborenes **IV**, the different synthetic approach should be required, such as the reduction of 1,2-X₂-1,2-(CPC)₂-diborane(4) as reported by Siebert.^{14b}

4-4. Syntheses of Triaminotriboranes(3) and Naphthalene-Adducts

Because a triaminotriborane(3) **3** has the promise to show the unique reactivity, we aim to synthesize **3** and its CPC derivative selectively, and reveal their properties. Herein, the synthesis of triaminotriboranes(3) and diborene–naphthalene adducts, and computational studies for them are reported. Since a triaminotriborane(3) **3** was obtained from the reduction of the aminodichloroborane **1** by using sodium in DME, we attempted to use sodium naphthalenide as a reductant. In THF solution at $-78\text{ }^{\circ}\text{C}$, the reduction reaction only formed oily mixture product. In contrast, the reaction in DME at $-40\text{ }^{\circ}\text{C}$ allowed isolation of **3** as dark purple crystals in 67% yield (Scheme 4a).



Scheme 4. (a) Synthesis of triaminotriborane(3) **3** and (b) its selected resonance forms. $[\text{Na}][\text{C}_{10}\text{H}_8]$ = sodium naphthalenide.

An X-ray crystallographic study of **3** revealed an unexpected triaminotriborane(3) structure, in which three $(\text{R}_2\text{N}-\text{B}:)$ units catenated into a bent B_3 chain structure (Figure 8), which also can be viewed as a bis(borylene)-stabilized borylene **3c** (Scheme 4b) and represents the first structurally authenticated example of $(\text{R}-\text{B})_3$ chain.^{25,26} Compound **3** was thermally stable below around $120\text{ }^{\circ}\text{C}$ in the solid state and around $60\text{ }^{\circ}\text{C}$ in the hexane solution under argon atmosphere.

The solid-state structure of **3** is shown in Figure 7. There are three independent molecules in the asymmetric unit of **3**. The structure is comparable to optimized structure of C_{2v} symmetric $(\text{BH})_3$ ²⁷ rather than triboracyclopropenyl dianion $[(\text{Cy}_2\text{N}-\text{B})_3]^{2-}$ (Cy = cyclohexyl).^{15d} The terminal boron atoms (B1 and B3) are divalent; each adopts a linear geometry. The central B2 atom is trivalent with a planar geometry, bound to the amino-substituent and the two terminal $[\text{B}(\text{NR}_2)]$ units. The bond lengths between the central boron atom and the terminal boron atoms (B1–B2 avg. 1.561 \AA , B2–B3 avg. 1.558 \AA) are similar to those observed in Lewis base-stabilized neutral diborenes ($1.524\text{--}1.593\text{ \AA}$),^{6a–g,i,j,m} indicating double bond characters along the B_3 chain. The distance between terminal boron atoms (B1 \cdots B3 avg. 2.177 \AA) was significantly longer than those of typical B–B single bonds in triboranes(5) ($1.68\text{--}1.755\text{ \AA}$),²⁸ neutral diboranes(4) $(\text{R}')(\text{R}_2\text{N})\text{B}-\text{B}(\text{NR}_2)(\text{R}')$

(1.697–1.728 Å),²³ the three-membered ring oxadiborirane (1.601(7) Å)²⁹ and the azadiboriridine (1.610(3) Å),³⁰ suggesting the absence of any σ -bond between B1 and B3. Meanwhile, the longer B1 \cdots B3 distance is in the region of some interacted boron atoms such as transition metal bis(borylene) complexes (1.972–1.982 Å)³¹ and singlet diradical 1,3-dibora-2,4-diphosphoniocyclobutane-1,3-diyls (R₂PBR')₂ (2.57 Å).³² In **3**, this weak interaction may exist through π -orbitals (see later).

Furthermore, all boron and nitrogen atoms were in the same plane and the terminal TMP rings were perpendicular to the B₃ plane. The short bond lengths of N1–B1 (avg. 1.380 Å) and N3–B3 (avg. 1.382 Å)³³ and linear geometry of the B1 and B3 centers^{4d,k,34} are evident of strong in plane N \rightarrow B π -interactions due to the electron deficiency of the two-coordinate terminal boron atoms. By contrast, the significantly longer bond length of N2–B2 (avg. 1.481 Å) and the mildly pyramidal geometry of N2 (avg. $\Sigma_N = 352^\circ$) indicate a weak N2 \rightarrow B2 π -donation, with the nitrogen lone pair more localized around the N1 atom.³³

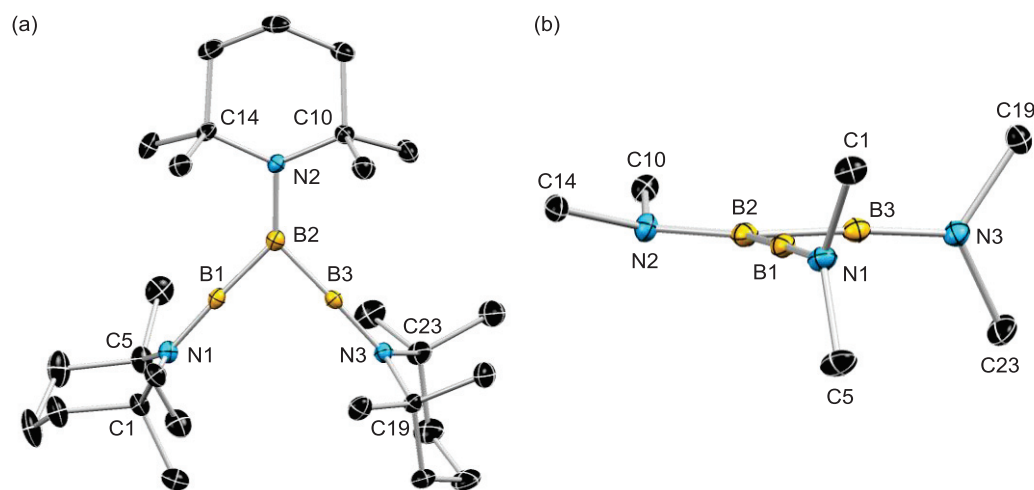


Figure 8. Molecular structure of **3** obtained from single-crystal X-ray diffraction analysis. (a) A top view of **3** and (b) a side view of (C₂NB)₃ skeleton in **3**. Thermal ellipsoids are displayed at 30% probability. Hydrogen atoms are omitted for clarity. There are three independent molecules in the asymmetric unit of **3**, and one of these is shown. Average values of selected bond lengths [Å] and angles [°]: B1–B2 1.561, B2–B3 1.558, B1 \cdots B3 2.177, N1–B1 1.380, N2–B2 1.481, N3–B3 1.382; B1–B2–B3 88.5, N1–B1–B2 176.1, N3–B3–B2 176.4.

Variable-temperature (VT) NMR experiments were carried out with a solution sample of **3** (see Figures S7–S11). At -80°C , the ¹¹B NMR spectrum showed two broad signals at $\delta = -4.8$ and 77.6 ppm (half-width $h_{1/2} = 1700$ and 6200 Hz, respectively), assigned to the central and terminal boron nuclei of **3**, respectively. The negative chemical shift of $\delta = -4.8$ ppm is comparable to those

of nucleophilic Lewis base stabilized borylenes (-32.2 – 0.8 ppm).^{4b,c,e,g,h,j,l,m} The chemical shift $\delta = 77.6$ ppm is comparable to those of low-coordinate silaborene^{34b} and azaborataallene,^{4d} and the quite large half-width is similar to that of dimesitylborinium cation ($h_{1/2} = 5000$ Hz).³⁵ The two signals starts to coalesce at around -5 °C. At room temperature, only one broad signal was observed at $\delta = 51.7$ ppm. Similarly, the $^{13}\text{C}\{^1\text{H}\}$ NMR spectrum obtained at 20 °C showed four signals, whereas that at -80 °C showed eight signals, assigned to the central and terminal TMP substituents. These results revealed a rapid change of the boron environments in solution at room temperature, which may be due to intramolecular bond rearrangement of the $[(\text{R}_2\text{N})\text{B}]$ fragments (Figure 9). The solid-state ^{11}B magic angle spinning NMR spectrum of **3** at room temperature showed two signals at around $\delta = -5.5$ and 68.5 ppm (see Figure S12), thus confirming that **3** at room temperature in the solid state retains the open-form structure that was revealed by the single-crystal X-ray crystallographic study.

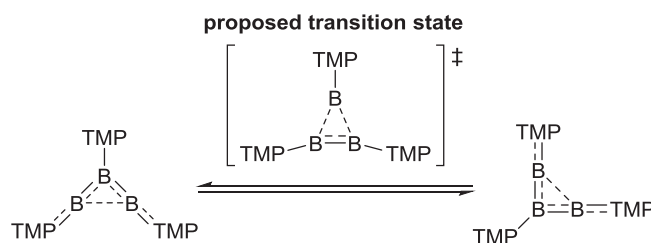


Figure 9. Plausible intramolecular bond rearrangement of **3** via a proposed transition state in C_6D_6 solution.

The UV/Vis spectrum of **3** as a solution in hexane showed two absorption bands at $\lambda_{\text{max}} = 329$ and 532 nm (see Figure S23). The absorption at the longer wave length is characteristic of Lewis base stabilized diborenes.^{6c,e} The electrochemical properties of **3** were measured by cyclic voltammetry (CV) in THF by using 100 mm $[\text{nBu}_4\text{N}][\text{PF}_6]$ as the supporting electrolyte (see Figure S24). A single reversible reduction event was observed for **3** at $E_{1/2} = -0.94$ V (vs. ferrocene/ferrocenium).

Structure optimization of **3** at the B3LYP/6-31G(d) level of theory reproduced its solid-state structure. Therefore, to obtain more insight into the electronic structure, bonding, and properties, we used the optimized structure **3**^{opt}. By using the gauge-independent atomic orbital (GIAO) method at the B3LYP/6-311+G(2d,p) level, the calculated ^{11}B chemical shifts of **3**^{opt} were $\delta_{\text{B}} = -8.0$, 86.1 , and 86.3 ppm for the central and terminal boron nuclei, respectively, in good agreement with the experimental data (see Table S8).

Frontier orbitals at the CAM-B3LYP/6-31+G(d) level of theory are shown in Figure 10. The orbitals are similar to those for a reported borylene dicarbonyl complex.^{4g} The HOMO was mainly found to lie out of the plane of the B_3 chain, which indicated that the delocalization of two

π -electrons on the B₃ chain offered multiple-bonding character in B1–B2 and B2–B3. The LUMO+2, LUMO+3, and LUMO+4 in the plane of the B₃ chain indicated π -antibonding between terminal nitrogen and boron atoms. Inherent empty p-orbitals on the terminal boron atoms mainly contributed to LUMO+9.

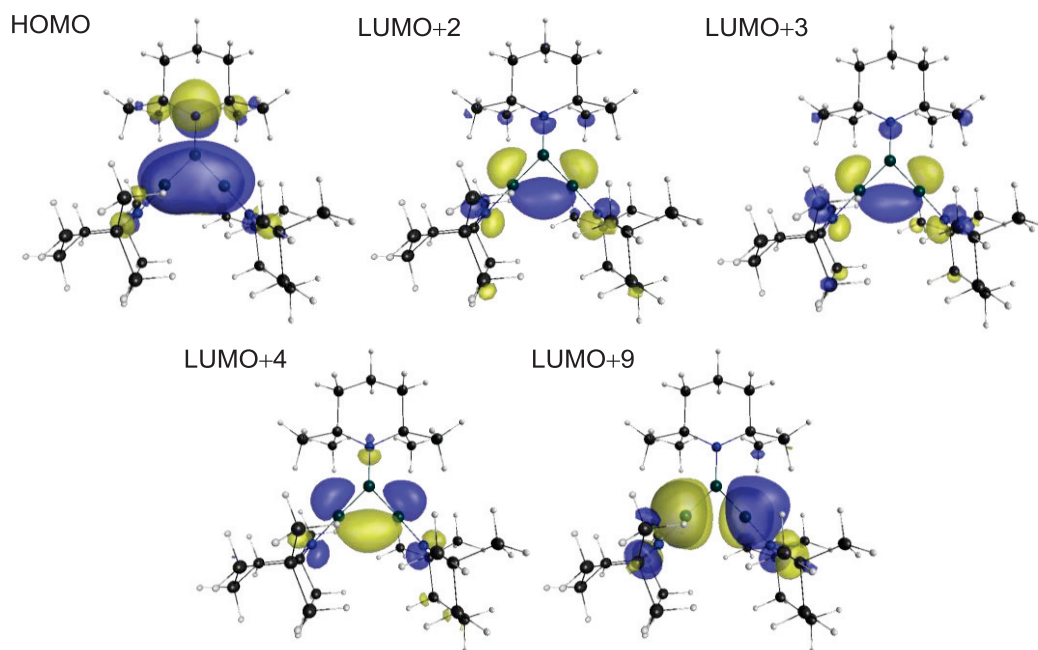


Figure 10. Frontier orbitals of the model compound 3^{opt} at the CAMB3LYP/6-31+G(d) level of theory with a contour value of 0.03 atomic units.

The calculation for **3** at the B3LYP/6-311G(d) level of theory showed similar frontier orbitals (Figure S32). The central boron atom bearing the three σ -bonds has the electron density in the both HOMO and HOMO–1, which indicate that the central boron atom is electron-rich. The LUMO and LUMO+1 was mainly found as inherent vacant p-orbitals of B1 and B3 and the π -antibonding between terminal nitrogen and boron atoms respectively, which imply the terminal boron atoms have the electron-accepting property.

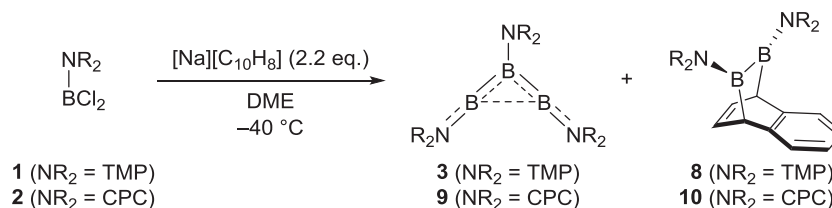
Wiberg bond indices (WBI) and natural charges were estimated by natural bond orbital (NBO) calculations at the same level of theory (see Table S11). The WBI values for B1–B2 and B2–B3 are both 1.36, thus confirming the partial double-bond character caused by the three-center two-electron (3c-2e) π -bond mentioned above. The WBI of 0.42 between B1 and B3 may be explained by the conjugated π -orbitals of all boron atoms (Figure 9, HOMO). Weak N2→B2 π -donation was also suggested by the small WBI of 0.84 and the small rotational energies along the N2–B2 bond (see Tables S11 and S14). As expected, only the central boron atom B2 has an unusual negative charge of -0.57 .³⁶ The nucleus-independent chemical shift (NICS)³⁷ calculated at 1 Å above the center of the B₃ chain plane of 3^{opt} (-12.5 ppm) at the B3LYP/6-311+G(d,p) level of

theory indicates π -delocalization, and is similar to those of allyl cation (-12.4 ppm) and B_3H_3 (C_{2v} : -11.8 ppm,³⁸ see Table S13).³⁹ The small diradical character (γ)⁴⁰ of $\mathbf{3}^{opt}$ estimated as $\gamma = 0.013$ by the spin-projected (P)UHF method with the 6-31+G(d) basis set rules out open-shell character (see Figure 36).

A time-dependent density functional theory (TD-DFT) calculation of $\mathbf{3}^{opt}$ at the CAM-B3LYP/6-31+G(d) level of theory revealed good agreement between the molecular structures in the solid and solution (see Table S9). The two absorption bands at $\lambda_{max} = 329$ and 532 nm (molar absorption coefficients $\epsilon = 2935$ and 168 , respectively) were assigned as B–B π -bond-related absorptions, which were confirmed by TD-DFT calculations for $\mathbf{3}^{opt}$; the absorption at 532 nm was a forbidden transition (main components of $\lambda_{calc} = 333$ nm: HOMO \rightarrow LUMO+9; $\lambda_{calc} = 557$ nm: HOMO \rightarrow LUMO+2, LUMO+3, and LUMO+4; oscillator strength: $f = 0.1568$ and 0.0010 , respectively).

The influence of the steric bulkiness of amino substituents on the geometry of triaminotriborane($\mathbf{3}$) was revealed by computational studies. The molecular structure of a model compound, $(Me_2N-B)_3$ ($\mathbf{7}^{opt}$), optimized at the B3LYP/6-31++G(d,p) level of theory is quite different from that of $\mathbf{3}$ (see Figure S28c). The B1–B2 and B2–B3 bond lengths are elongated to 1.629 Å, whereas B1 and B3 clearly form a σ -bond (B1–B3 1.763 Å). All N–B bonds have double-bond character and deviate from the B_3 ring plane. The structural discrepancy between $\mathbf{3}$ and $\mathbf{7}^{opt}$ reflects the significance of the large steric repulsion between TMP substituents.

In a large scale synthesis of $\mathbf{3}$, especially under the higher concentration, the diborene–naphthalene adduct $\mathbf{8}$ was obtained as a minor product accompanying with $\mathbf{3}$ as a major product (Scheme 5). This adduct $\mathbf{8}$ can be considered as a product obtained from the cycloaddition reaction between a diaminodiborene and naphthalene,^{42,44} which indicate the generation of a desired diaminodiborene in this system. The case of the reduction of (CPC)BCl₂ $\mathbf{2}$ instead of $\mathbf{1}$ also provided the naphthalene adduct $\mathbf{10}$ accompanying with the triaminotriborane($\mathbf{3}$) $\mathbf{9}$. The poor solubility of $\mathbf{9}$ in organic solvents and contamination of $\mathbf{10}$ may be the reason of the low isolated yield of $\mathbf{9}$ (38%). The molecular structure of $\mathbf{9}$ was preliminary confirmed by a single-crystal X-ray analysis. However, because the quality of data was not enough to discuss about the structural parameters, re-measurement are required. The NMR measurements for $\mathbf{9}$ are also needed. The naphthalene adduct $\mathbf{8}$ and $\mathbf{10}$ were structurally characterized by single-crystal X-ray analyses (Figure 11).



Scheme 5. Synthesis of $\mathbf{3}$ in a large scale and synthesis of $\mathbf{9}$.

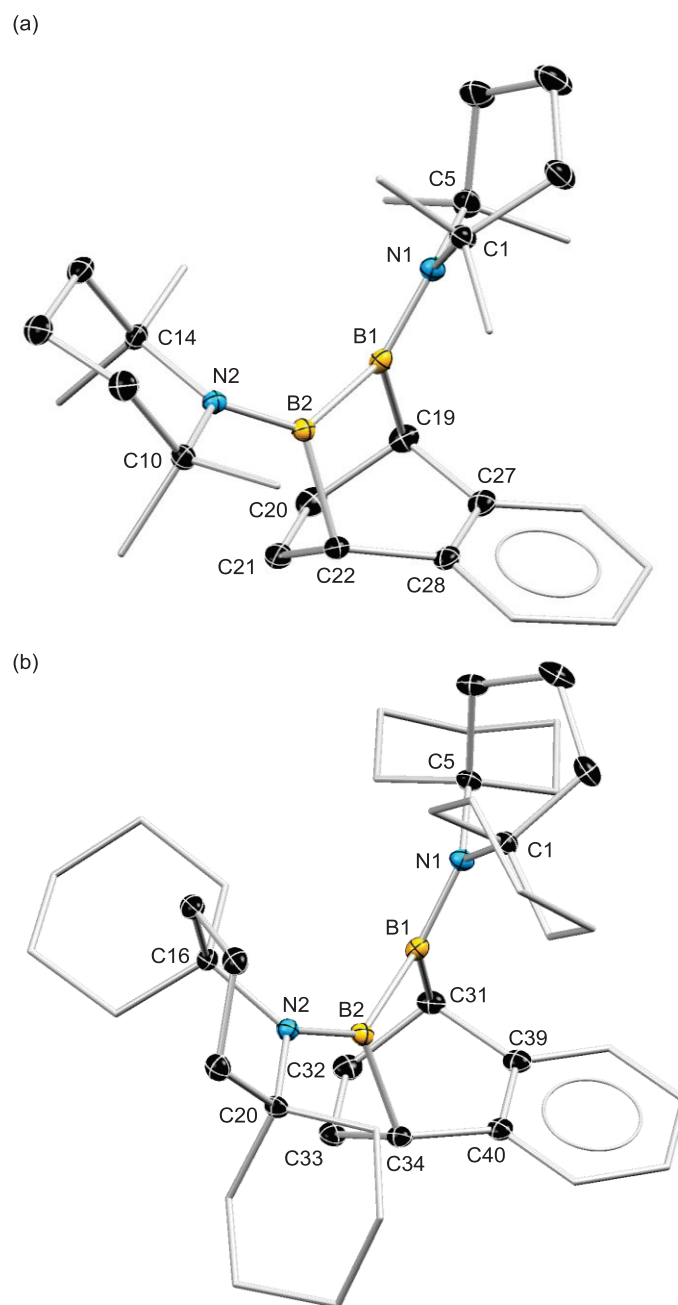


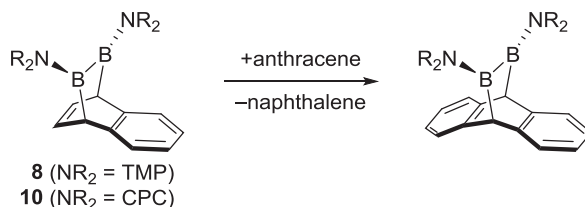
Figure 11. Molecular structures of (a) **8** and (b) **10** obtained from single-crystal X-ray diffraction analyses. Thermal ellipsoids are displayed at 30% probability. Those of peripheral atoms and hydrogen atoms are omitted for clarity. Selected bond lengths [\AA] and angles [$^\circ$] for **8**: B1–B2 1.750(2), B1–N1 1.420(2), B2–N2 1.438(2), B1–C19 1.640(2), B2–C22 1.636(2), C19–C20 1.512(2), C19–C27 1.527(2), C20–C21 1.332(2), C21–C22 1.520(2), C22–C28 1.510(2), C27–C28 1.400(2); N1–B1–B2 130.81(9), N2–B2–B1 131.47(9), C1–N1–C5 117.21(9), C1–N1–B1 119.73(8), C5–N1–B1 122.90(9), C14–N2–C10 117.08(8), C14–N2–B2 119.62(8), C10–N2–B2 121.41(8); N1–B1–B2–N2 55.4(2). Selected bond lengths [\AA] and angles [$^\circ$] for **10**: B1–B2 1.764(2), B1–N1

1.427(2), B2–N2 1.430(2), B1–C31 1.646(2), B2–C34 1.641(2), C31–C32 1.510(2), C31–C39 1.525(2), C32–C33 1.334(2), C33–C34 1.518(2), C34–C40 1.503(2), C39–C40 1.402(2); N1–B1–B2 132.2(2), N2–B2–B1 133.6(2), C1–N1–C5 117.40(9), C1–N1–B1 120.3(1), C5–N1–B1 122.3(1), C16–N2–C20 115.5(1), C16–N2–B2 122.6(1), C20–N2–B2 121.2(1); N1–B1–B2–N2 53.4(2).

The solid-state molecular structures of **8** and **10** are shown in Figure 11. The both compounds showed similar structures, in which bond alternations are observed for borylated bent C₆ rings (**8**, C20–C21 1.332(2) Å; **10**, C32–C33 1.334(2) Å) as drawn in Scheme 5. The short bond lengths of N–B (**8**, 1.420(2), 1.438(2) Å; **10**, 1.427(2), 1.430(2) Å) indicate that N→B π -interactions. The bond lengths of B1–B2 (**8**, 1.7503(2) Å; **10**, 1.764(2) Å) are comparable to those observed in typical B–B single bonds in triboranes(5) (1.68–1.755 Å)²⁸ and neutral diboranes(4) (R')(R₂N)B–B(NR₂)(R') (1.697–1.728 Å),²³ but a little bit longer than those observed in reported aromatic adducts bearing a NMe₂ substituent on a boron atom (1.719–1.728).⁴¹ The elongation of B1–B2 bond lengths in **8** and **10** are most likely due to the larger steric hindrance of TMP and CPC substituents in **8** and **10** than NMe₂ substituent in reported adduct, respectively. This phenomenon is also observed for larger torsion angles of N1–B1–B2–N2 (**8**, 55.4(2) °; **10**, 53.4(2) °) in comparison to those observed in reported adducts (39.4–46.3 °).

As compared the structure between **8** and **10**, in the molecular structure of **8**, one piperidine ring at the B1 atom is distorted and another one has a chair conformation. In contrast, all piperidin rings in **10** are distorted. For the bond lengths of B–C (Å), those observed in **10** (B1–C31 1.646(2), B2–C34 1.641(2)) are slightly longer than those observed in **10** (B1–C19 1.640(2), B2–C22 1.636(2)).

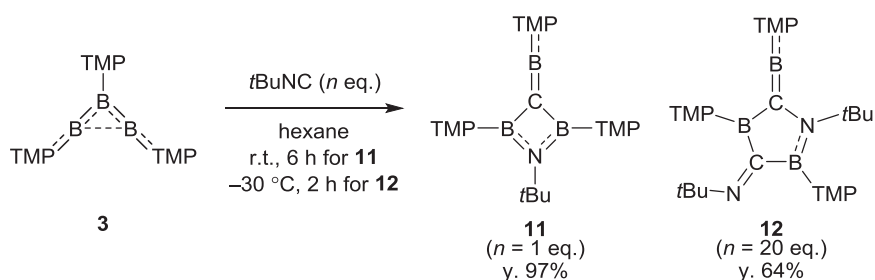
Since the amount of **8** in hand is small and the isolation of minor product **10** is hard, the characterization of **8** and **10** by NMR measurements and elemental analyses are future subjects. To obtain the adducts **8** and **10** as major products, the high concentration of the reaction solution and the addition of excess amount of naphthalene may be useful. The adducts **8** and **10** may exchange the naphthalene to other aromatics accompanying with the generation of diaminodiborenes as intermediates (Scheme 6).



Scheme 6. Plausible reactivity of **8** and **10**. Exchange reaction of aromatics.

4-5. Facile Cleavage of a Carbon-Nitrogen Triple Bond in *tert*-Butyl Isocyanide Using a Triaminotriborane(3)

As mentioned above, (TMP-B)₃ **3** have the promise to act as a electrophile. To reveal the electrophilicity of **3**, we investigated the reaction with *tert*-butyl isocyanide (Scheme 7). The reaction with 1 equivalent of *t*BuNC at room temperature afforded the 4-membered ring product **11** as colorless crystals in 97% yield, in which a carbon-nitrogen (C–N) triple bond in isocyanide was completely cleaved (Figure 12). In general, the cleavage of a strong C–N triple bond requires to use transition metal complexes.⁴⁵ Recently, Yamashita and co-workers demonstrated the facile cleavage of a isocyanide C–N triple bond by use of a highly Lewis acidic asymmetric diborane(4) (pin)B–B(Mes) (pin = pinacolato, Mes = 2,4,6-Me₃C₆H₂).^{46,47} To the best of our knowledge, our result is a second example to completely cleave a C–N triple bond using a boron compound without transition metals. In contrast, using 20 equivalents of *t*BuNC provided the 5-membered ring product **12** as yellow crystals in 64%, in which two C–N triple bonds were partially cleaved (Figure 12). In the presence of excess amount of pyridine, only the same products were obtained. Further addition of excess amount of *t*BuNC to the hexane solution of **11** resulted in no reaction.



Scheme 7. Reaction of **3** with *tert*-butyl isocyanide.

The solid-state structure of **11** and **12** are shown in Figure 12. In the both structures, the exocyclic boron atoms B2 are divalent and adopt linear geometries (C1–B2–N2: **11**, 178.4(2) °; **12**, 174.1(2) °). The short bond lengths of C1–B2 (**11**, 1.381(2) Å; **12**, 1.406(2) Å), and B2–N2 (**11**, 1.375(2) Å; **12**, 1.373(2) Å) are similar to those observed in 1-aza-2-borataallene (C–B 1.391–1.424 Å; B–N 1.349–1.363 Å)^{34a,d} and aminoborylene (C–B 1.401(5) Å; B–N 1.382(5) Å),^{4d} which indicate C–B double bonds and strong N→B π -interactions between C1–B2 and B2–N2, respectively. The slightly shorter bond lengths of C1–B2 in **12** imply that the bond may be a little bit stronger in **11** than that in **12**. In the molecular structure of **11**, the 4-membered ring buckled only slightly into a butterfly conformation. The TMP rings attached to endocyclic boron atoms B1 and B3 were perpendicular to the trigonal planes of the boron atoms. The longer bond lengths of B1–N1 (1.473(2) Å) and B3–N3 (1.468(2) Å) indicate the weak N3→B3 π -donation. The slightly shorter bond lengths of B1–N4 (1.456(2) Å) and B3–N4 (1.460(2) Å) imply the delocalization of the nitrogen electron lone pair into partially vacant p-orbitals of B1 and B3. The bond lengths of C1–B1 (1.577(2) Å) and

C1–B3 (1.579(2) Å) are remarkably shorter than those observed in C–B single bonds of 1,2,4-azadiboretidine (1.645–1.647 Å)⁴⁸ which indicates partial double bond characters in C1–B1 and C1–B3. The atomic distances between B1 and B3 (2.027(2) Å), and C1 and N4 (2.249(2) Å) are comparable to those observed in 1,2,4-azadiboretidine⁴⁸ and mean that there are no σ -bonds between them. In the molecular structure of **12**, one isocyanide C–N triple bond was incorporated as an exocyclic imine (C2–N5 1.292(2) Å) and another one was incorporated as an endocyclic amine (C1–N4 1.512(2) Å). The 5-membered ring distorted into an envelope conformation. The TMP ring on B3 was perpendicular to the trigonal plane of B3 atom. The moderate short bond lengths of B1–N1 (1.429(2) Å) and B3–N4 (1.428(2) Å) imply soft N→B π -interactions. The significantly longer bond length of B3–N3 (1.477(2) Å) indicates the weak N3→B3 π -donation.

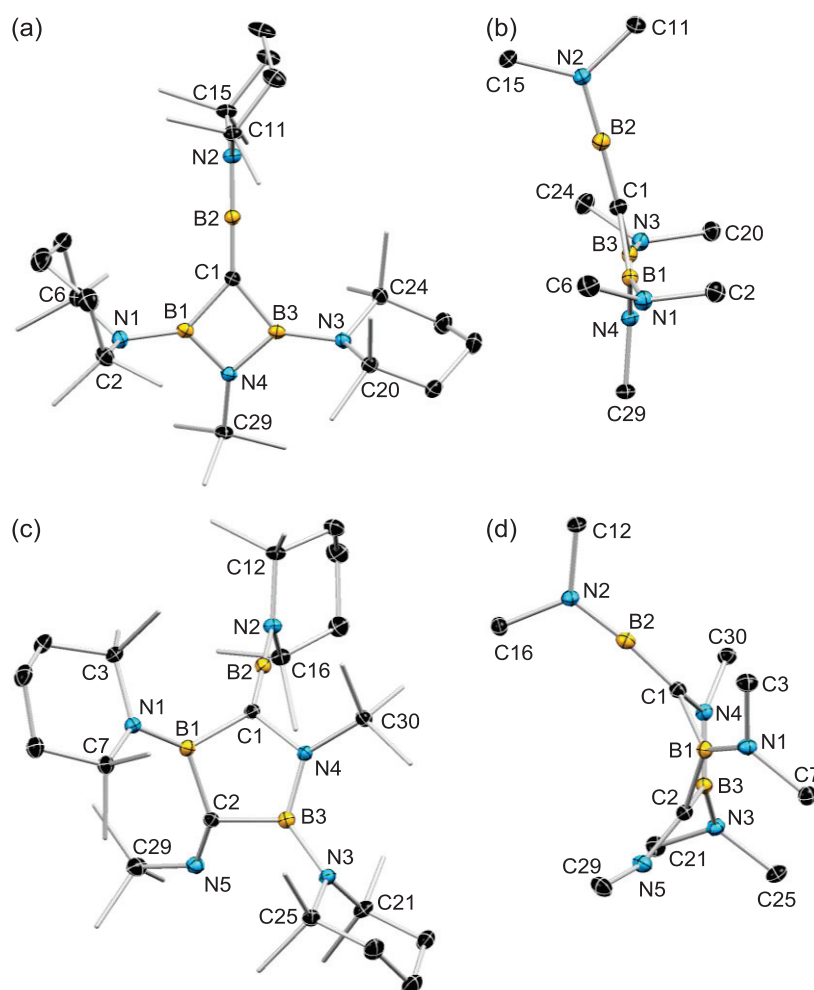


Figure 12. Molecular structures of **11** and **12** obtained from single-crystal X-ray diffraction analyses. (a) A front view of **11** and (b) a side view of partial skeleton of **11**, (c) a front view of **12** and (d) a side view of partial skeleton of **12**. Thermal ellipsoids are displayed at 30% probability. Those of peripheral atoms and hydrogen atoms are omitted for clarity. Selected bond lengths [Å] and angles [°] for **11**: C1–B1 1.577(2), C1–B2 1.381(2), C1–B3 1.579(2), B1–N1 1.473(2), B2–N2 1.375(2),

B3–N3 1.468(2), B1–N4 1.456(2), B3–N4 1.460(2); C1–B2–N2 178.4(2). Selected bond lengths [Å] and angles [°] for **12**: C1–B1 1.606(2), C1–B2 1.406(2), B1–N1 1.429(2), B2–N2 1.373(2), B3–N3 1.477(2), C1–N4 1.512(2), B3–N4 1.428(2), B1–C2 1.602(2), B3–C2 1.619(2), C2–N5 1.292(2); C1–B2–N2 174.1(2).

The ^{11}B NMR spectrum of **11** showed only one signals at $\delta = 43.3$ ppm, which is most likely due to the overlapping of signals corresponding to exo- and endocyclic boron atoms. This signal was upfield shifted as compared to those of 1-aza-2-borataallene ($\delta = 46.3, 59.2$ ppm)^{34a,d,49} and aminoborylenes ($\delta = 62, 83.7$ ppm).^{4d,k} The ^{13}C NMR spectrum of **11** could be assigned to one *t*Bu and two different TMP substituents. For the 5-membered ring product **12**, the three boron atoms were observed at $\delta = 53.9, 49.6$ and 32.4 ppm by ^{11}B NMR measurement.

Structure optimization of **11** and **12** at the B3LYP-6-31G(d) level of theory reproduced their solid-state structures. Frontier orbitals of the optimized structure **11**^{opt} at the same level of theory are shown in Figure 13. The HOMO–1 and HOMO–3 were orthogonal two π -orbitals at C1–B2 and B2–N2 bonds, which were expected for cumulated π -orbitals. The HOMO–5 lying out of the plane of the central 4-membered ring indicated two electron π -delocalization to provide partial double bond characters in C1–B1, C1–B3, B1–N4 and B3–N4. The LUMO and LUMO+2 were orthogonal two inherent vacant p-orbitals at B2 atom. Inherent vacant p-orbitals on endocyclic boron atoms mainly contributed to LUMO+1.

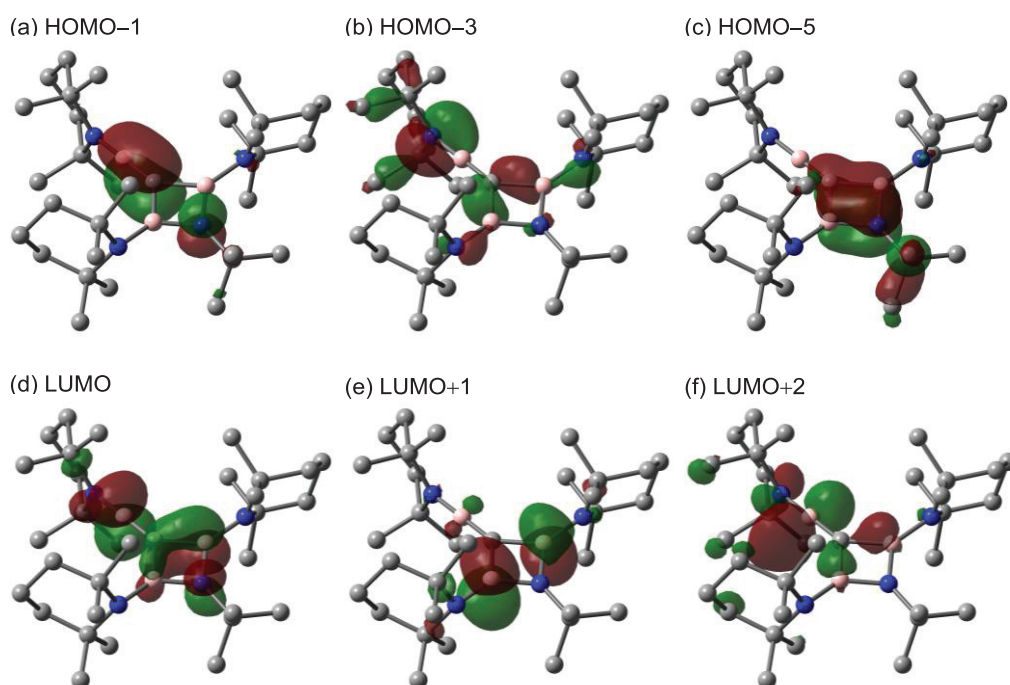


Figure 13. Frontier orbitals of **11**^{opt} at the B3LYP/6-31G(d) level of theory with a contour value of 0.05 atomic units. H atoms are omitted for clarity.

Frontier orbitals of the optimized structure $\mathbf{12}^{\text{opt}}$ at the B3LYP/6-31G(d) level of theory are shown in Figure 14. As observed in $\mathbf{11}^{\text{opt}}$, two orthogonal π -orbitals were found to lie at C1–B2 and B2–N2 bonds as HOMO–1 and HOMO–5, respectively. The HOMO–3 and HOMO–6 indicated the N→B π -interaction between N1 and B1 atoms and imine π -bond, respectively.

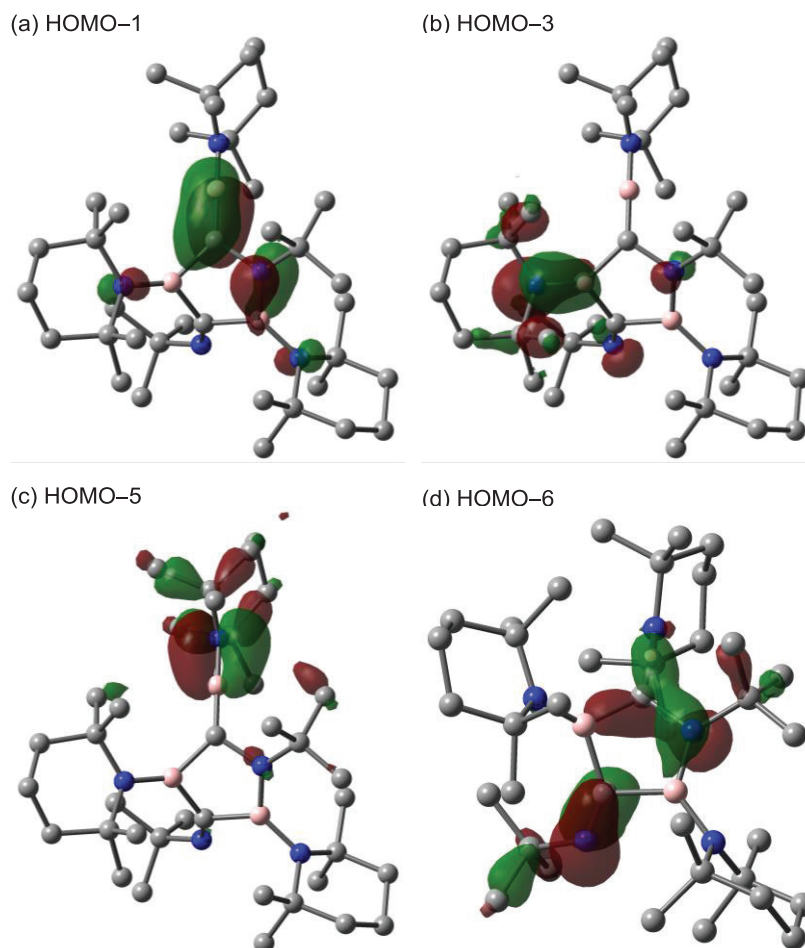


Figure 14. Frontier orbitals of $\mathbf{12}^{\text{opt}}$ at the B3LYP/6-31G(d) level of theory with a contour value of 0.05 atomic units. H atoms are omitted for clarity.

To assign ^{11}B NMR spectra, GIAO calculations for $\mathbf{11}^{\text{opt}}$ and $\mathbf{12}^{\text{opt}}$ were carried out at the B3LYP/6-311+G(2d,p) level. The calculated ^{11}B chemical shifts of $\mathbf{11}^{\text{opt}}$ were $\delta_{\text{B}} = 42.3, 44.3$ and 42.1 ppm for B1, B2 and B3 atoms, selectively, which supported that only one signal was observed experimentally for $\mathbf{11}$ ($\delta_{\text{B}} = 43.3$ ppm). The calculated ^{11}B chemical shifts of $\mathbf{12}^{\text{opt}}$ were $\delta_{\text{B}} = 51.5, 53.7$ and 31.7 ppm for B1, B2 and B3 atoms, selectively, in good agreement with the experimental data (see Table S8).

The plausible reaction mechanism was shown in Figure 15. First, a isocyanide coordinates to a terminal boron atom in $(\text{TMP-B})_3$ followed by $\text{TMP-B}=\text{B-TMP}$ migration. The double cyclization through the nucleophilic addition of an imine nitrogen atom to a cationic boron center,

and the reaction between iminium and B–B double bond, forms a spiro-intermediate. In the case of using only one equivalent of isocyanide, further cyclization and ring opening, where a C–N bond is completely cleaved, affords the 4-membered ring product **11**. In contrast, in the presence of excess isocyanide, it coordinates to a more Lewis acidic boron atom in a CBB ring than that in a CBN ring. Finally, cyclization and ring opening provides the 5-membered ring product **12**. The further [2+2] cycloaddition reaction between exocyclic C–B double bonds in **11** and **12** may be suppressed due to the large steric hindrance of TMP substituents.^{34a,50} The computational study to support this mechanism is in progress by Dr. Kishi and Prof. Dr. Nakano.

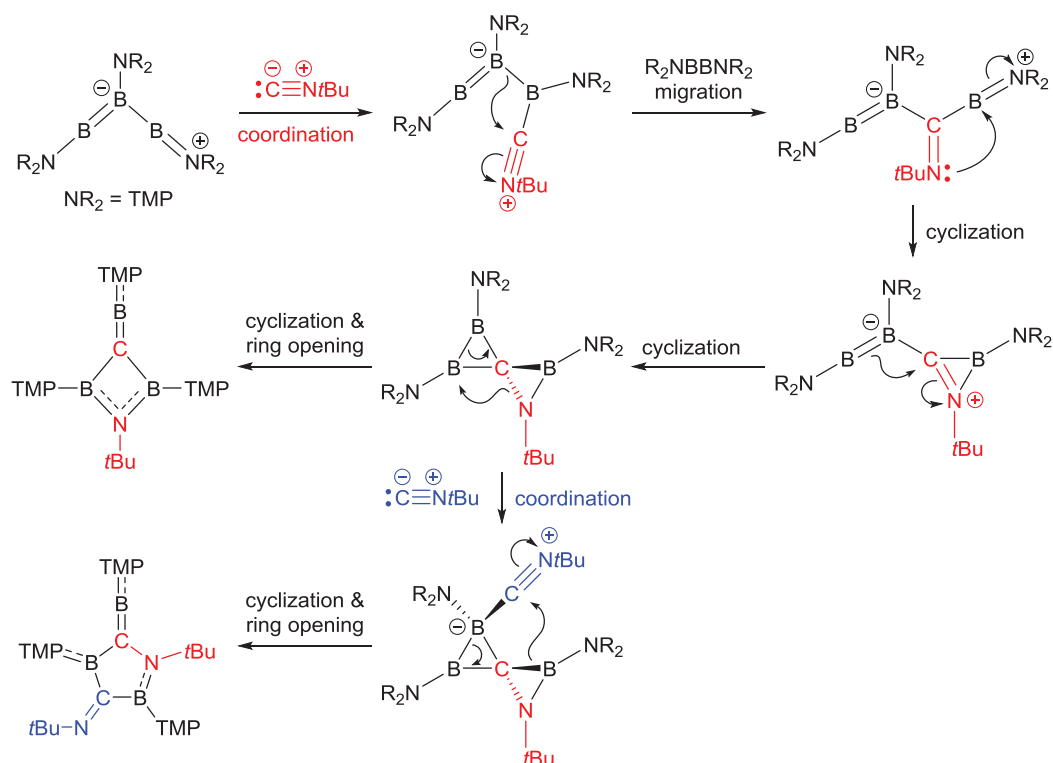


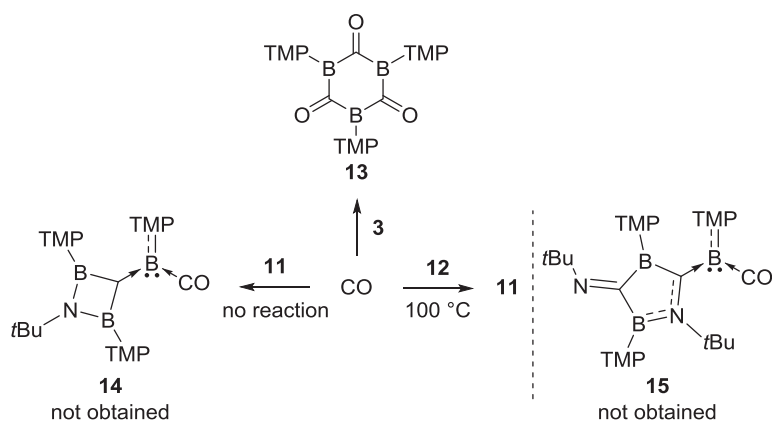
Figure 15. Plausible reaction mechanism.

The reaction with cyclohexyl isocyanide (CyNC) was also preliminary investigated. The hexane solution including **3** and 1 or 6 equivalents of CyNC was stirred at room temperature for 36 hours, then concentrated and stored at $-30\text{ }^\circ\text{C}$, which provided dark red solution and red solid in contrast to the case of using tBuNC . Further reaction study may allow us to isolate and confirm the reaction product.

The high reactivity of a triaminotriborane(3) **3** to the nucleophile of isocyanide have proved that the terminal boron atoms are the electron-accepting.

4-6. Reaction of Low-Coordinate Boron Species with Carbon Monoxide

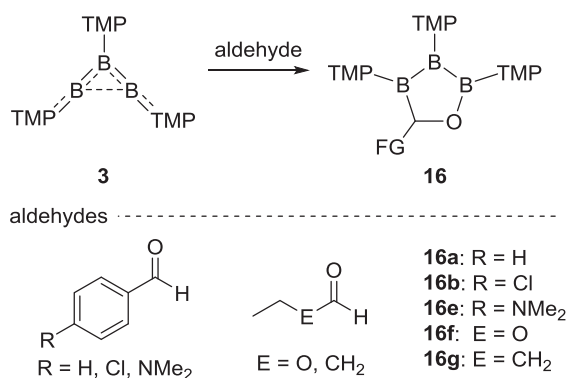
We have also investigated about the reaction of $(\text{TMP-B})_3$ (**3**), **11** and **12** with carbon monoxide, CO (Scheme 8). In the case of using **3**, the reaction at room temperature for 72 hours proceeded cleanly and formed a crystalline yellow solid. The $^{11}\text{B}\{^1\text{H}\}$ NMR of the crude product showed only one signal at $\delta = 59.9$ ppm. Also, the four ^{13}C NMR signals assigned to one TMP substituent were observed. These results indicate that the obtained product may be a 6-membered ring, 1,3,5-tris(2,2,6,6-tetramethylpiperidin-1-yl)-1,3,5-triborinane-2,4,6-trione **13**. Recrystallization of the crude product is in progress, and the molecular structure will be confirmed by single-crystal X-ray diffraction analysis. For the reaction of **11** and **12**, as reported by Bertrand, Stephan and co-workers,^{4d} since these compounds may be viewed as carbene-stabilized aminoborylenes, the preliminary reactions with CO were investigated (Scheme 8). In the case of using compound **11**, no reaction was observed, even after the heating at 100 °C for 21 hours. However, the reaction of **12** with CO at 100 °C for 55 hours showed one $^{11}\text{B}\{^1\text{H}\}$ NMR signals at $\delta = 43.4$ ppm. This chemical shift was significantly downfield shifted as compared to that of $(\text{cAAC})(\text{CO})[\text{BN}(\text{SiMe}_3)_2]$ ($\delta = -3.4$ ppm).^{4d} These results of NMR measurements were not correspond to the desired compound **15**. Recrystallization of the obtained product afforded colorless crystals, assigned to **11** by the X-ray diffraction analysis. Further investigation about the thermolysis of **12** into **11** in the absence of CO gas is future subject. As reported by Nöth and co-workers, and Paetzold and co-workers,^{34a,d,48} the C–B double bonds in **11** and **12** may show similar reactivities. The detailed investigation about the reaction of **11** and **12** other reagent is also future subject.

Scheme 8. Reactions of $(\text{TMP-B})_3$, **11** and **12** with CO.

4-7. Metal-Free Direct 1,2-Diborylation Reaction of Aldehydes Using a Triaminotriborane(3)

To date, a few methods of the 1,2-diborylation reaction of carbon–oxygen double bonds have been reported. For the transition metal catalyzed diborylation, Sadighi and co-workers firstly succeeded the 1,2-diborylation of aldehydes by using a (carbine)copper(*Ot*Bu) catalyst.⁵¹ A subsequent report by Clark and co-workers represented that reaction of ketones with similar method.⁵² On the other hand, the metal-free 1,2-borylation of C–O double bonds have been also discovered. In 2002, Paetzold and co-workers reported that tri-*tert*-butylazadiboriridine reacted with aldehydes to provide the 5-membered ring products similar to **16**.⁵³ Kinjo and co-workers reported the reaction of 1,3,2,5-diazadiborinine and acetophenone, and also found that the product can act as a catalytic active species in the hydroboration of ketones with HB(*pin*).⁵⁴ Herein, the metal-free direct 1,2-borylation of aldehydes is described.

The reaction of (TMP–B)₃ (**3**) with aldehydes have also been investigated (Scheme 9). The mixture of benzaldehyde and **3** in organic solvents at room temperature provided the 1,2-diborylated 5-membered ring product, 1,2,3,4-oxatriborolane **16a** in 40% yield. This is the first example of the isolation and structural identification of 1,2,3,4-oxatriborolane. Instead of benzaldehyde, using 4-chlorobenzaldehyde also afforded the 1,2-borylated cyclic compound **16b** in 80% yield. The isolated yield of **16a** was decreased due to the recrystallization. Surprisingly, compounds **16a** and **16b** were stable in air. The reaction with the aldehyde bearing the electron-donating NMe₂ group at the *para*-position afforded unidentifiable sticky solid. The reaction with butyraldehyde completely consumed **3**, but showed the unidentifiable ¹H NMR spectrum. In contrast, in the case of using ethyl formate, no reaction was observed.



Scheme 9. Reaction of **3** with aldehydes.

The molecular structures of **16a** and **16b** are shown in Figure 16, which were similar structures to each other. In the both structures, central 5-membered rings distorted into envelope conformations. All TMP rings were almost parallel to the trigonal planes of the attached boron atoms. The bond lengths of B1–B2 and B2–B3 (**16a**, 1.727(2), 1.722(2) Å; **16b**, 1.718(2), 1.737(2) Å) were comparable to those observed in B–B single bonds in triboranes(5) (1.68–1.755 Å).²⁸

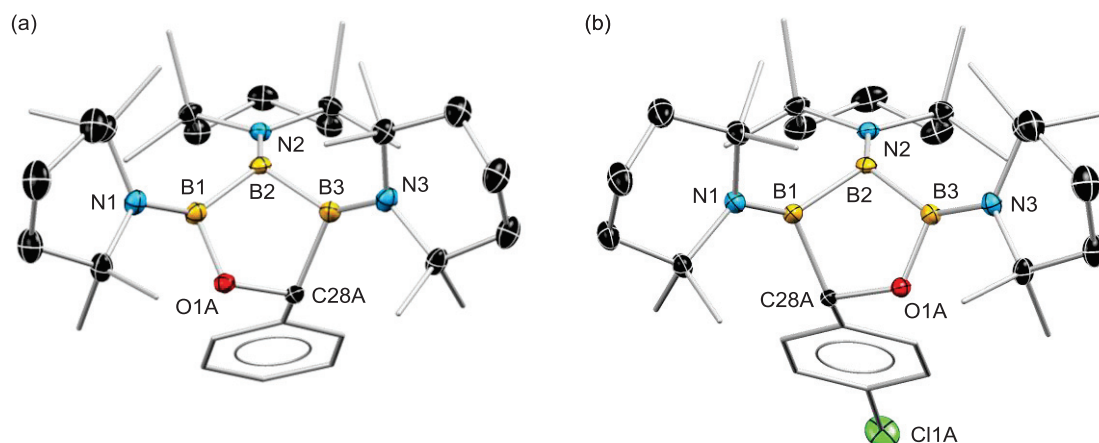


Figure 16. Molecular structures of (a) **16a** and (b) **16b** obtained from single-crystal X-ray diffraction analyses. Thermal ellipsoids are displayed at 30% probability. Those of peripheral atoms and hydrogen atoms are omitted for clarity. Structural disorder was observed in ArC(H)O moieties in **16a** and **16b**. Selected bond lengths [Å] and angles [°] for **16a**: B1–B2 1.727(2), B2–B3 1.722(2), B1–N1 1.428(2), B2–N2 1.417(2), B3–N3 1.432(2), B1–O1A 1.384(2), B3–O1B 1.342(3), B3–C28A 1.695(3), B1–C28B 1.778(6), O1A–C28A 1.456(2), O1B–C28B 1.459(6); B1–B2–B3 90.45(9). Selected bond lengths [Å] and angles [°] for **16b**: B1–B2 1.718(2), B2–B3 1.737(2), B1–N1 1.422(2), B2–N2 1.416(2), B3–N3 1.428(2), B3–O1A 1.400(2), B1–O1B 1.318(7), B1–C28A 1.674(3), B3–C28B 1.802(10), O1A–C28A 1.454(2), O1B–C28B 1.480(12); B1–B2–B3 90.4(2).

The $^{11}\text{B}\{^1\text{H}\}$ NMR spectra of **16a** and **16b** in C_6D_6 showed three signals at the almost same chemical shifts (**16a**, $\delta = 58.0, 51.3, 39.4$ ppm; **16b**, $\delta = 57.9, 51.3, 39.3$ ppm), similar to those observed for 2,3,4,5-tetra-*tert*-butyl-1,3,2,4-oxazadiborolidine ($\delta = 63.2, 39.3$ ppm).⁵³ To assign ^{11}B NMR spectra, GIAO calculations should be required. The protons attached to aromatic rings were identified by ^1H NMR measurements. The ^1H NMR spectra also showed characteristic singlet signals (**16a**, 5.93 ppm; **16b**, 5.77 ppm) which could be assigned to Ar(O)CH. Further reactions with various aldehydes (4-Me and 4-OMe-benzaldehyde, 1,4-phthalaldehyde) and acetophenone are future subjects. In contrast to the good reactivity with benzaldehyde, in the case of using 1 equivalent of benzophenone, no reaction was observed. This can be concluded that the large steric hindrance between the additional phenyl- and TMP-substituent disfavor the formation of the 5-membered ring. Due to its steric recognition, a triaminotriborane(3) **3** may show a high aldehyde affinity.

These direct 1,2-diborylation reaction using a triaminotriborane(3) **3** indicated the ambiphilic property as observed for 1,3,2,5-diazadiborinine reported by Kinjo.⁵⁴

4-7. Reaction of a Triaminotriborane(3) with Other Multiple Bonds

Herein, the reaction study of a triaminotriborane(3) **3** with other multiple bond compounds is reported. Compound **3** was stable under the nitrogen atmosphere and also stable in MeCN or PhCN solution with the color change to red solution. For the reaction with C–C multiple bonds, we used 2-norbornene, 2,5-norbornadiene, 2,3-dimethylbutadiene, diphenylacetylene and phenylacetylene as reactants. As the results, except for phenylacetylene, all C–C multiple bond compounds showed ^1H and/or $^{11}\text{B}\{^1\text{H}\}$ NMR signals only corresponding to **3** and their-selves. In the reaction with phenylacetylene (PhCCH), compound **3** reacted with 1 equivalent of PhCCH in C_6D_6 , which showed four broad signals ($\delta = 80, 54, 50, 42$ ppm) and one sharp signal ($\delta = -20$ ppm) in $^{11}\text{B}\{^1\text{H}\}$ NMR. After 74 hours at room temperature, the signal at $\delta = -20$ ppm was decreased and the new broad signal was observed at $\delta = 16$ ppm, the similar $^{11}\text{B}\{^1\text{H}\}$ NMR signals were also observed by using of the excess amount of PhCCH ($\delta = 54, 50, 42, 16$ ppm). From these reactions, the orange sticky solid was obtained. Furthermore, we investigated the reaction with C–C π -electrons in aromatic ring, but no reactions were observed with 1-methylpyrrole, furan and anthracene.

On the other hand, the reaction with $\text{E}=\text{C}=\text{E}$ ($\text{E} = \text{O}, \text{NCy}, \text{S}$) was also studied. Although no reaction was observed in the reaction with N,N' -dicyclohexylcarbodiimide or carbon disulfide, compound **3** reacted with undried carbon dioxide in C_6D_6 and the dark purple solution changed to the pale yellow solution immediately after shaking the NMR tube, in which **3** was consumed. The removal of volatiles provided a pale yellow oil.

In addition, we also investigated about the reaction with heteroatoms multiple bonds. Unfortunately, a triaminotriborane(3) **3** was stable in the presence of an iminoborane ($t\text{Bu}-\text{B}=\text{N}-t\text{Bu}$) and no reaction was observed.

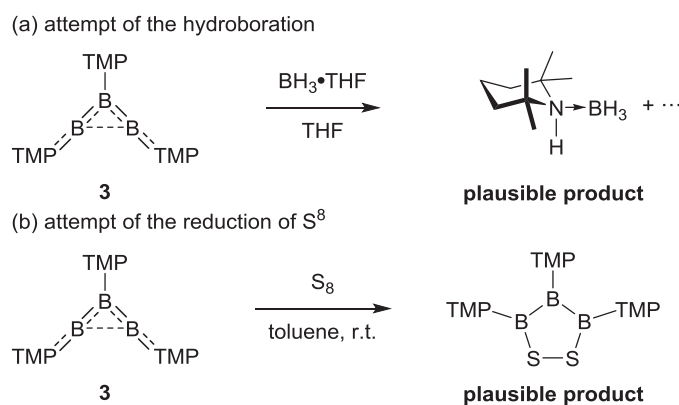
4-8. Reactions of a Triaminotriborane(3) with Heteroatom Single Bonds

Herein, the reaction of **3** with dihydrogen, B–H bonds and elemental sulfur (S_8) is reported (Scheme 10). Recently, the activation of the relatively strong H–H bond in dihydrogen by using diboranes(4),⁵⁵ boryllithium,⁵⁶ (cAAC)aminoborylene^{4d} and B–B multiple bond species^{5,6j} have been reported. Then, we attempted the reaction of **3** with dihydrogen. Under the H_2 atmosphere which was dried passed through the dry and reduction column, the hexane solution of **3** at room temperature had not changed the color even after 54 hours. The heating at 60°C for 86 hours allowed to proceed the reaction and changed the color to colorless solution. The resulting product showed three sharp signals at $\delta = 47.8, 44.6$ and 40.2 ppm in $^{11}\text{B}\{^1\text{H}\}$ NMR no lock. The two proton-couplings were observed at $\delta = 44.6$ ppm as a doublet ($J_{\text{BH}} = 115$ Hz) and at $\delta = 40.2$ ppm as a triplet ($J_{\text{BH}} = 120$ Hz). To confirm the product, the detailed modification of the reaction condition is needed.

As reported by Braunschweig and co-workers,^{5,6e,57} the hydroboration with 9-BBN and HB(cat) can proceed for a B=B bond to form a new B–B single bond. Based on these insights, we

tried the hydroboration of **3**. In the case of using a $\text{BH}_3 \cdot \text{THF}$ complex in THF solution, the reaction solution gradually changed to the colorless solution over 3 hours, and showed several $^{11}\text{B}\{^1\text{H}\}$ NMR signals, at least observed at $\delta = 36.8, 17.2, -0.9, -5.8, -7.8, -14.1, -15.8$ and -21.0 ppm. The B–H couplings were also observed at $\delta = 36.8$ (t, $J_{\text{BH}} = 128$ Hz), 17.2 (d, $J_{\text{BH}} = 128$ Hz), -14.1 (d, $J_{\text{BH}} = 128$ Hz) and -21.0 (q, $J_{\text{BH}} = 102$ Hz). The major signal observed at $\delta = -21.0$ ppm was corresponding to that observed for a $\text{TMP}(\text{H}) \cdot \text{BH}_3$ adduct, which was separately prepared from the stoichiometric mixture of $\text{TMP}(\text{H})$ and a $\text{BH}_3 \cdot \text{THF}$ complex in THF ($\delta = -21.1$ ppm, q, $J_{\text{BH}} = 96$ Hz).⁵⁸ In contrast to BH_3 , the reaction with purified 9-BBN at room temperature offered no reaction in C_6D_6 or DME. Although new ^1H and $^{11}\text{B}\{^1\text{H}\}$ NMR signals were observed as minor signals after the heating at 40°C for 68 hours, compound **3** was still a major product. The poor reactivity with 9-BBN is most likely due to the large steric repulsion between them.

In addition, the reaction with elemental sulfur (S_8) was investigated. The addition of toluene and 1 equivalent of S_8 to a toluene solution of a triaminotriborane(**3**) at room temperature provided the colorless solution after 10 minutes. After the filtration and removal of volatiles, the yellow solid was obtained without **3**. The crude product showed two major signals at $\delta = 46.9$ and 25.7 ppm, one small signal at $\delta = 40.4$ ppm and one shoulder peak at around $\delta = 53$ ppm in $^{11}\text{B}\{^1\text{H}\}$ NMR. As the reported reaction using isolated diborenes an elemental chalcogen, our B–B multiple bond chemical species **3** reacted with S_8 and formed the BBBSS 5-membered ring.⁵⁹ Further reaction study of **3** with chalcogen compounds (E^0 , REER, REH; E = S, Se, Te) is future subject.



Scheme 10. Reaction studies of **3** using (a) BH_3 and (b) S_8 .

4-9. Reaction of a Triaminotriborane(3) with Other Nucleophiles

Herein, the reactions of **3** with various nucleophiles are described. First, the reaction with **3** and amines and pyridines were investigated by NMR measurements. Although **3** did not react with Et₂NH even after the addition of excess of Et₂NH, one equivalent of piperidine gradually decolorized the reaction solution to pink. After the addition of excess amount of piperidine, the color changed to colorless which showed at least three ¹¹B{¹H} NMR signals at $\delta = 50.7, 42.4$ and 40.5 ppm. For the reaction with a primary amine, *t*BuNH₂, the solution also gradually decolorized to pink. After the addition of excess of *t*BuNH₂, compound **3** was completely consumed to afford a complex mixture. In the reaction using NH₃ gas without drying, the solution immediately changed to colorless and offered four ¹¹B{¹H} NMR signals ($\delta = 54, 49.2, 37.5, 27.5$ ppm). The one B–H bond formation was indicated by the proton-coupled ¹¹B NMR signal observed at $\delta = 27.5$ ppm with the coupling constant of $J_{\text{BH}} = 141$ Hz. After the removal of volatiles, unidentifiable colorless sticky solid was obtained. These results using amines, compound **3** can react with less sterically hindered amines. In contrast to the reaction with amines and NH₃, no reaction was observed with pyridine and DMAP at room temperature.

In addition, we tried to synthesize pentacoordinate phosphorus compounds bearing two P–B bonds as an apical and equatorial bond. As the results, compound **3** could not show any reactivity with PR₃ (R = Ph, Cy, Me, OMe).

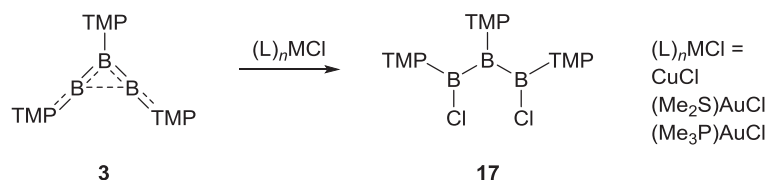
The reaction of **3** and dry MeOH was also preliminary investigated. In deuterated-benzene, compound **3** immediately reacted with 1 equivalent of MeOH and completely consumed accompanying with the color change to yellow, which showed three broad signals at $\delta = 48.6, 37.6$ and 30.8 ppm and one sharp signal at $\delta = 18.4$ ppm. After 10 hours at room temperature, the solution changed to colorless. The signals observed at $\delta = 37.6$ ppm was upfield shifted to $\delta = 34.6$ ppm by the addition of excess of MeOH. The crude product was colorless oily solid and any crystals were not obtained, as well as the same reaction was carried out in hexane solvent.

As the other nucleophiles, the reaction with *t*BuOK, NaNH₂ and PhLi were investigated. Surprisingly, no signal change was observed by ¹¹B{¹H} NMR measurement (no lock) in the presence of excess amount of *t*BuOK in DME solution. In contrast, the reaction with NaNH₂ in DME and C₆D₆ solution showed several ¹¹B NMR signals, in which one B–H coupling was observed at $\delta = -21.3$ ppm with the coupling constant of $J_{\text{BH}} = 71$ Hz. For the reaction with isolated PhLi in DME at -30 °C, the reaction solution darkened and offered several ¹¹B{¹H} NMR signals in the both negative and positive region, in which most of compound **3** remained.

4-10. One-Electron Chemical Reductions of Coinage Metal Complexes Using a Triaminotriborane(3)

As the recent studies that demonstrate the electron-rich characters of neutral diborenes and borylenes,⁷⁻¹⁰ the inference, based on the computational study for **3** to imply its electron-rich property, led us to use **3** with transition metal complexes aiming to form **3**-coordinated or an aminoborylene (TMP-B:) coordinated metal complexes.

The reaction of **3** with coinage metal complexes (L)_nMCl (M = Cu, Au; L = SMe₂; n = 0, 1) in the mixed solution of hexane and Et₂O formed the dark colored precipitate and changed to the colorless solution at room temperature after 24 hours (Scheme 11). Recrystallization of the resulting white solid afforded the suitable colorless crystals of 1,3-Cl₂-1,2,3-TMP₃-triborane(5) (**17**) for X-ray analysis. These reactions also proceeded under the dark condition. The reaction with (Me₃P)AuCl, no reaction was observed. In the case of (Ph₃P)AuCl, dark red solution and solid were formed, but not characterized. Recently, Kinjo and co-workers reported the chlorination of the borylene with coinage metal chlorides,^{7c} GeCl₂, PhPCl₂ and Ph₂BiCl,^{7e} Braunschweig and co-workers reported the formation of 1,3-Cl₂-1,2,3-(NCy₂)₃-triborane(5) from the reaction of [(Cy₂N-B)₃]²⁻ and PbCl₂.^{15d} In these reactions, it is reasonable to conclude that the electron transfer from the electron-rich boron species afforded those chlorinated products. Then, similar electron transfer from **3** to CuCl and (Me₂S)AuCl were expected. In contrast, the lowered Lewis acidity of the Au center in (Me₃P)AuCl, due to the strong σ-coordination by PMe₃, may be the reason of no reaction with **3**.



Scheme 11. One-electron chemical reductions of coinage metal complexes.

The solid-state structure of **17** is shown in Figure 17. The structural conformation is comparable to those of the previously reported 1,3-X₂-1,2,3-(NR₂)₃triboranes(5) (X = Cl, R = Cy,²⁵ X = Br, R = Me;²⁸ X = I, R = Me²⁸). All boron atoms and N₂ atom were in the same plane, and all TMP rings were almost parallel to the trigonal planes of the attached boron atoms. The trigonal planes of B1 and B3 atoms were perpendicular to the plane of the B₃ chain. The bond lengths (Å) of B–B bonds (1.745(3), 1.734(3)), B–N bonds (1.415(3), 1.427(3), 1.413(3)) and B–Cl bonds (1.846(3), 1.860(3)) in **17** were longer than those observed in the reported 1,3-X₂-1,2,3-(NR₂)₃triboranes(5). These elongations are most likely due to the larger steric hindrance of TMP-substituents than those of NCy₂- and NMe₂-substituents. The bond angle B1–B2–B3 (102.8(2)°) was narrow as compared to those observed in 1,3-X₂-1,2,3-(NR₂)₃triboranes(5).

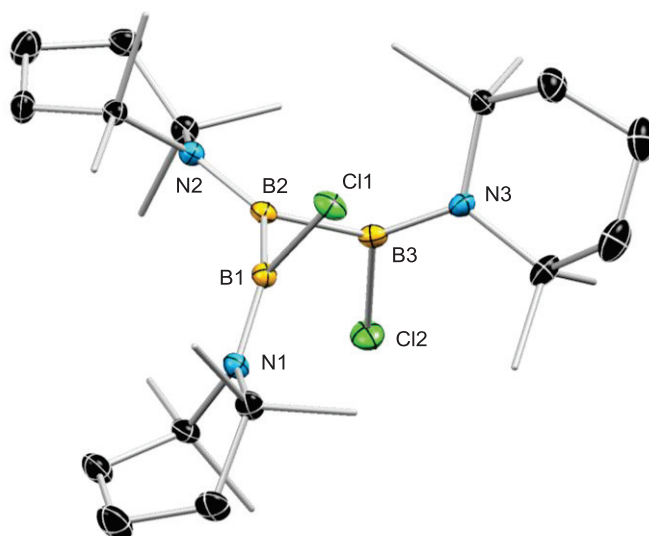


Figure 17. Molecular structure of **17** obtained from single-crystal X-ray diffraction analysis. Thermal ellipsoids are displayed at 30% probability. Those of peripheral atoms and hydrogen atoms are omitted for clarity. Selected bond lengths [\AA] and angles [$^\circ$]: B1–B2 1.745(3), B2–B3 1.734(3), B1–N1 1.415(3), B2–N2 1.427(3), B3–N3 1.413(3), B1–Cl1 1.846(2), B3–Cl2 1.860(2); B1–B2–B3 102.8(2), N1–B1–B2 135.1(2), N1–B1–Cl1 117.4(2), B2–B1–Cl1 107.1(2), N2–B2–B1 127.8(2), N2–B2–B3 129.3(2), N3–B3–B2 129.8(2), N3–B3–Cl2 118.0(2), Cl3–B3–B2 111.0(2).

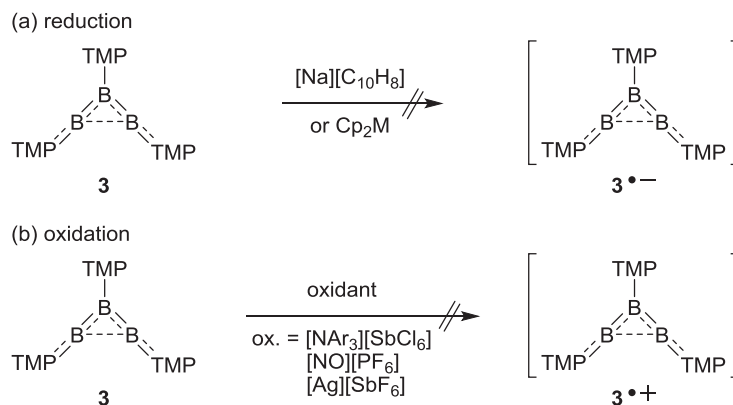
The reaction of **3** with other transition metals was also investigated. In the case of using $\text{Ni}(\text{cod})_2$ in toluene, no reaction was observed as expected. The reaction of **3** with one half equivalent of $[\text{IrCl}(\text{coe})_2]_2$ at room temperature in C_6D_6 also showed no reaction. Even after the heating at $40\text{ }^\circ\text{C}$ for 15 hours, almost all of **3** remained.

These results prove that a triaminotriborane(3) **3** is an electron-donating as well as an electron-accepting.

4-11. One-Electron Chemical Oxidations or Reductions of a Triaminotriborane(3)

As the cyclic voltammetry predicted, the reduction of compound **3** to provide a corresponding radical anion $3^{\bullet-}$ may be able to be isolated. Therefore, we preliminary tried to reduce **3** using sodium naphthalenide and metallocenes (Cp_2M ; Cp = cyclopentadienyl, M = Fe, Co) (Scheme 12). The mixture of **3** and the freshly prepared sodium naphthalenide in DME was stored at $-30\text{ }^\circ\text{C}$. All volatiles were removed *in vacuo*, and red oil was obtained without any crystals. In contrast, the reaction with Cp_2M did not proceed, even when using the highly reducing Cp_2Co were used.⁶⁰ The use of the stronger reducing reagent such as bis(pentamethylcyclopentadienyl)cobalt(II), and the detailed modification of the reaction condition may be required for the reduction of **3**.⁶⁰

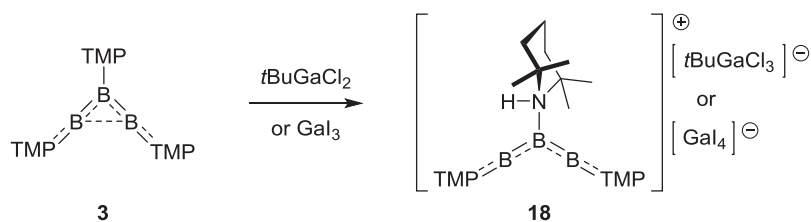
On the other hand, since the one-electron reduction of metal chlorides using **3** occurred, we investigated the chemical oxidation of **3** preliminary. The oxidation using an aminium radical salt $[\text{N}(2,4\text{-Br}_2\text{C}_6\text{H}_3)_3][\text{SbCl}_6]$ in a mixture of toluene and MeCN at $-30\text{ }^\circ\text{C}$ provided an orange solid with messy ^1H NMR spectrum. The reaction with a nitrosonium salt $[\text{NO}][\text{PF}_6]$ at room temperature also afforded an orange solid with messy ^1H NMR spectrum. The ^{19}F (376 MHz) chemical shifts were observed at $\delta = -67.11$ and -69.03 ppm as a result of doublet. In the reaction with a silver salt $[\text{Ag}][\text{SbF}_6]$, the black precipitate was generated. The filtration and drying afforded the pale orange and white solids with two major broad ^{19}F signals at $\delta = -66.75$ and -76.22 ppm. All of these resulting products could not be characterized.

Scheme 12. One-electron redox reactions of **3**.

4-12. Reaction of a Triaminotriborane(3) with Electrophiles

In order to confirm whether **3** can act as a σ -donating aminoborylene ($R_2N-B:$) or not, we tried to react with several electrophiles.^{3,7c-e} As mentioned above, the reaction with $(L)_nMCl$ ($M = Cu, Au$) offered the one electron transfer from **3** to the metal center, but did not provide $(R_2N-B:)MCl$. First, LiOTf was used as an electrophile instead of transition metals, however only no reaction was observed. For the preliminary reaction with a $GeCl_2$ •dioxane complex, compound **3** was rapidly consumed at room temperature in THF- d_8 , and two signals and one shoulder peak in $^{11}B\{^1H\}$ NMR in THF- d_8 were observed at $\delta = 51.8$ and 46.0 ppm and at $\delta = 55.9$ ppm, respectively (versus $BF_3 \cdot Et_2O$ in C_6D_6). After 32 hours at that temperature, almost same NMR spectra were observed. The removal of volatiles *in vacuo* afforded insoluble red-orange solid. We have not be able to conclude that the chlorination of **3** to form the triborane(5) **17** happened or not, as reported by Kinjo and co-workers.^{7e}

Furthermore, according to the formation of the σ -complex between a borylene and GaI_3 reported by Braunschweig and co-workers,^{7d} we investigated the reaction with gallium species as electrophiles. The reaction with $tBuGaCl_2$ or GaX_3 ($X = Cl, I$), the yellow solution and gray mud were always formed in non-polar solvents. Although the use of $GaCl_3$ afforded no crystals, $tBuGaCl_2$ and GaI_3 provided a small amount of the yellow crystals, confirmed as protonated analogues **18a** and **18b** by single X-ray diffraction analyses (Scheme 13). The detailed structural parameters and computational studies of **18a** will be described in section 4-13. The quality of data of **18b** was not enough to discuss about the structure parameters. The reaction with GaI_3 also provided a small amount of $[TMP(H)_2][GaI_4]$ salt as colorless crystals together with **18b**. The similar salt $[TMP(H)_2][Cl]$ was obtained as colorless crystals from the reaction with $AlCl_3$. These salts were only characterized by X-ray analyses, at which the crystals of **18b** and $[TMP(H)_2][GaI_4]$ were separated under the microscope to measure the X-ray diffractions. These cation species **18** may be formed through the electron transfer from **3** to gallium reagents following the decomposition of 3^{*+} .^{4a}



Scheme 13. Reaction of **3** with gallium electrophiles to form protonated analogues **18**.

4-13. Syntheses of Cationic Bent Boron Chains Connected By Boron–Boron Multiple Bonds

Herein, the detailed molecular structural character and computational studies of **18a**, and attempts to synthesize the similar cation analogues are represented. The solid-state structure of **18a** by single-crystal X-ray diffraction analysis is shown in Figure 18. Structural disorder was observed in whole cation moiety (TMP–B)₃•H⁺. As shown in the solid-state structure of **3**, all boron nitrogen atoms in **18a** were in the same plane, and the terminal boron atoms are divalent with a linear geometry and the central boron atom adopts a trigonal planar geometry. The molecular structure of **18a** differed from that of **3** in that all TMP rings were perpendicular to the B₃ plane, which can be explained as follows; (i) the loss of the moderate stabilization that was originated from the interactions between the central nitrogen lone pair electrons and B–B–B π -orbitals as observed in **3** (Figure 19), (ii) the relaxation of the steric repulsion between the central and terminal TMP-substituents. In addition, it is noteworthy that double bond characters were observed in B–B bonds (B1–B2, 1.560 Å; B2–B3, 1.554 Å)^{6a–g,l,j,m} and the atomic distances between the terminal boron atoms (B1···B3, 2.409 Å) in **18a** were elongated in comparison to that observed in **3** (B1···B3, 2.177 Å). Naturally, the bond angle of B1–B2–B3 (101.4 °) in **18a** was larger than that observed in **3** (B1–B2–B3, 88.5 °). The bond length of N2–B2 (1.587 Å) was remarkably elongated as compared to that observed in **3** (1.481 Å). These molecular structural features allowed us to consider **18a** as a TMP(H)-coordinated borenium ion.⁶¹

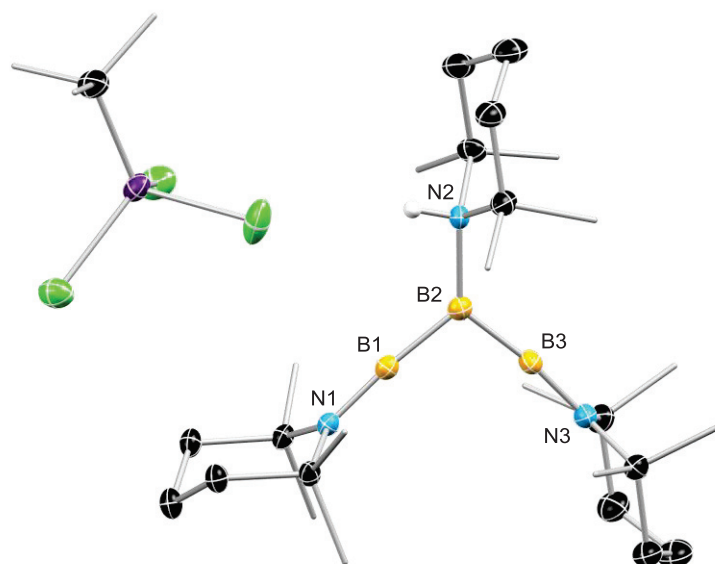


Figure 18. Molecular structure of **18a** obtained from single-crystal X-ray diffraction analysis. Thermal ellipsoids are displayed at 30% probability. Structural disorder was observed in whole cation moiety. Those of peripheral atoms and hydrogen atoms, except N–H, are omitted for clarity. Average values of selected bond lengths [Å] and angles [°]: B1–B2 1.560, B2–B3 1.554, B1–N1 1.343, B2–N2 1.587, B3–N3 1.361; B1–B2–B3 101.4.

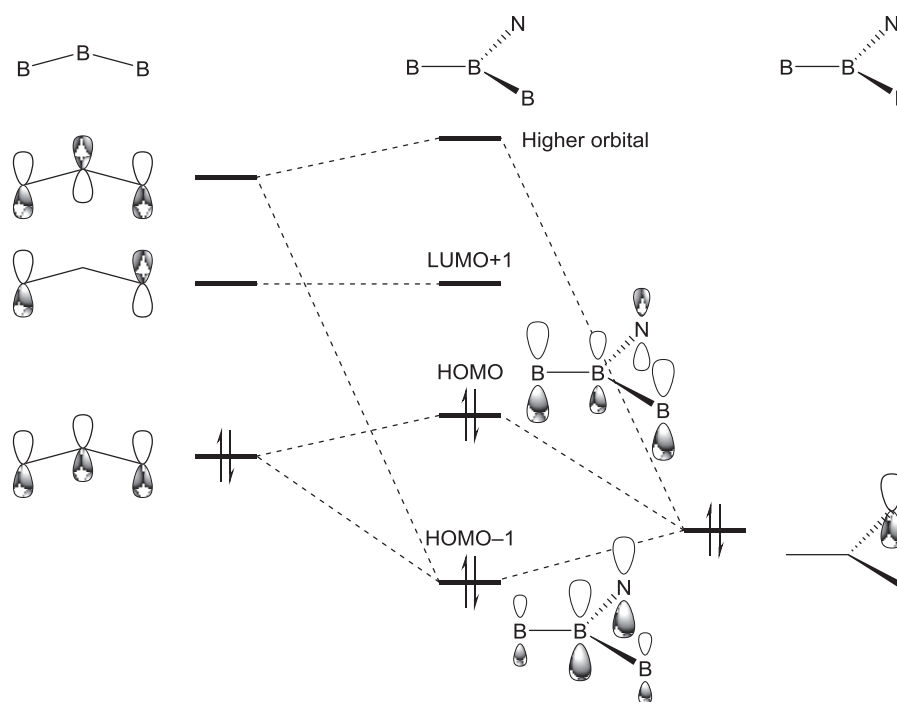


Figure 19. Molecular orbital diagram to describe the stabilization for **3**.

The $^{11}\text{B}\{^1\text{H}\}$ NMR spectrum with a solution sample of **18a** showed two broad signals at $\delta = 79.2$ and -2.8 ppm (half-width $h_{1/2}$ will be estimated) at room temperature. These signals are comparable to those observed for **3** at -80 °C ($\delta = 77.6, -4.8$ ppm), which supports the change of the boron environments of **3** in solution at room temperature. Note that the negative chemical shifts at $\delta = -2.8$ ppm is in the region of those of neutral Lewis base stabilized borylenes (-32.2 – 0.8 ppm)^{4b,c,e,g,h,j,l,m} although **18a** can be viewed as a borenium ion.

To reveal the electronic structure of **18a**, we conducted the computational studies for its counter cation moiety. The structure optimization at the B3LYP/6-31+G(d) level of theory represented **18^{opt}** with similar structural parameters observed in **18a**. The double bond characters were observed in B–B bonds (1.567 and 1.561 Å), and the atomic distance between terminal boron atoms was slightly elongated to 2.472 in **18^{opt}**. The $^{11}\text{B}\{^1\text{H}\}$ NMR spectrum of **18a** ($\delta_{\text{B}} = 79.2, -2.8$ ppm) was reproduced by the GIAO calculation of **18^{opt}** at the B3LYP/6-311+G(2d,p) level of theory, in which calculated chemical shifts were observed at $\delta_{\text{B}} = 80.9, 80.0$ and -4.2 ppm for the terminal and central boron atoms, respectively.

Frontier orbitals of **18^{opt}** at the B3LYP/6-31+G(d) level of theory are similar to those for **3^{opt}** and a reported borylene^{4g} (Figure 20). The HOMO lying out of plane of the B₃ chain offered the B–B double bond characters. The N→B π -interactions between terminal boron and nitrogen atoms were found in HOMO–1 and HOMO–2 as bonding interactions, and in LUMO as an anti-bonding interaction. The LUMO+1 was mainly constructed by inherent vacant p-orbitals on the terminal

boron atoms.

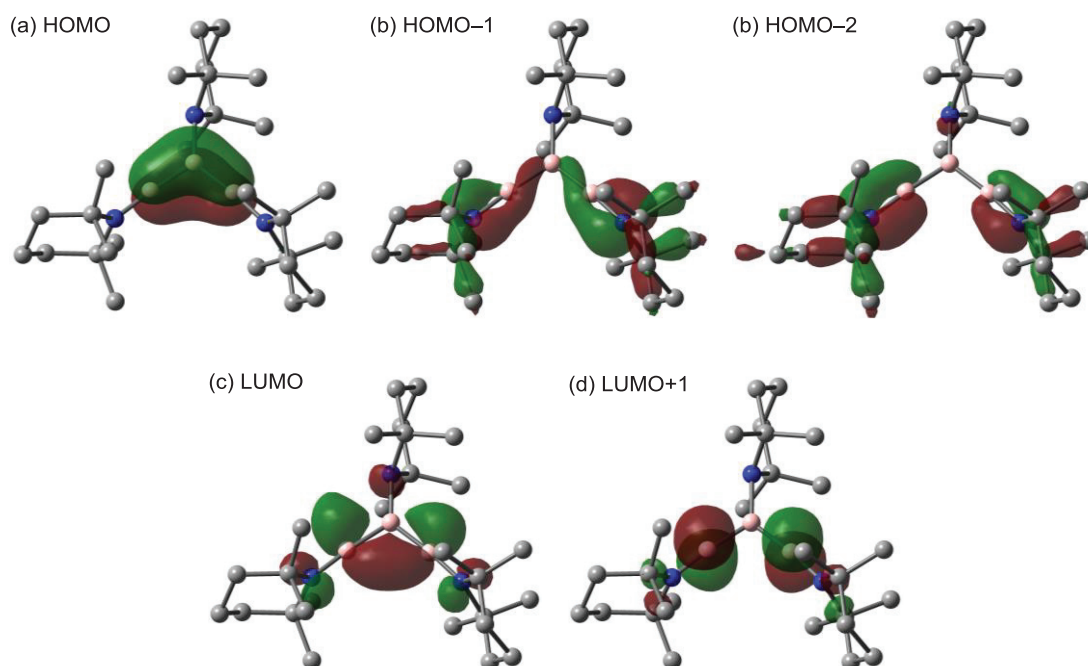


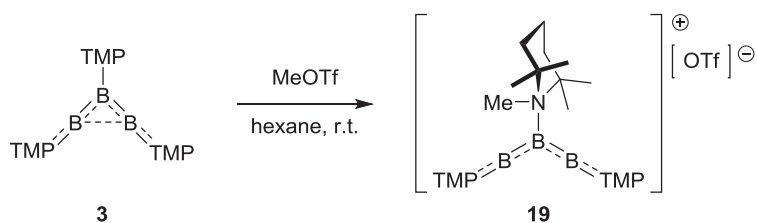
Figure 20. Frontier orbitals of 18^{opt} at the B3LYP/6-31G+(d) level of theory with a contour value of 0.05 atomic units. H atoms are omitted for clarity.

WBIs and natural charges were also estimated by NBO calculations at the CAM-B3LYP/6-31+G(d) level of theory. The WBI values for B1–B2 and B2–B3 were both 1.39 implying the double bond characters. As expected, in comparison to 3^{opt} , the smaller WBI value (0.21) was obtained for the longer atomic distance between terminal boron atoms. The decrease of WBI value was also observed for N2–B2 bond (0.68). For the natural charge, surprisingly, a negative charge of the central boron atom in 18^{opt} (–0.86) was increased as compared to that of 3^{opt} (–0.57). In contrast, the B1 and B3 atoms have the higher natural charges of 0.98 and 1.01. These can be considered as follow; (i) an electrostatic repulsion between the central nitrogen lone pair electrons and the occupied B–B–B π -orbital, which constructs HOMO and increases its energy level (Figure19), distributes the electron density on the B2 atom to the terminal B1 and B3 atoms in **3**, (ii) the loss of that repulsion in 18^{opt} offered the higher negative charge on the central B2 atom.

Electron deficient boron cations have been used as Lewis acids in organic reactions,⁶¹ and compound **18a** may show the unique reactivity. However, as the preparation of enough amount of **18a** to investigate the reactivity due to the poor reproducibility for its synthesis with *t*BuGaCl₂ (section 4-12), we tried to synthesize **18** directly from **3**. The preliminary estimation of the small rotational energy along the central N–B bond and electron distribution at the nitrogen atom of the central TMP-substituent in **3** indicate that the nitrogen lone pair electrons possess Lewis basicity.

Then, we tried to protonate the nitrogen in **3**. At first, a diethyl ether solution of HCl was used as a proton source, in which a dark yellow solid was obtained without ^{11}B chemical shifts. In contrast, the protonation reaction with a prepared pyridine hydrochloride (Py•HCl) in a toluene and MeCN solution prepared the yellow solid with the several ^{11}B chemical shifts, in which the signals similar those of **18a** were observed at $\delta = 77.4$ and -5.17 ppm. Unfortunately, the isolation of a desired protonated species was not succeeded. The other protonation reagents such as $[\text{H}(\text{OEt}_2)_2][\text{BAr}^{\text{F}}_4]$ ($\text{Ar}^{\text{F}}_4 = \text{C}_6\text{F}_5$ or $3,5\text{-(CF}_3)_2\text{-C}_6\text{H}_3$)⁶² should be needed.

Then, we attempted to synthesize the *N*-methylated analogue **19** using the nitrogen favored MeOTf. The reaction of **3** with MeOTf at room temperature immediately proceeded and afforded a yellow solid with the ^{11}B chemical shifts at $\delta = 76.2$ and -3.6 ppm (Scheme 14). Recrystallization of the crude solid from THF at room temperature provided yellow crystals.



Scheme 14. Protonation or methylation reactions of **3**.

The solid-state structure of **19** without a counter anion (OTf) is shown in Figure 21. This data have a problem about a Flack parameter and further analysis is required. This temporary structure of **19** is comparable to **18a** with the multiple-bond characters in B–B bonds.

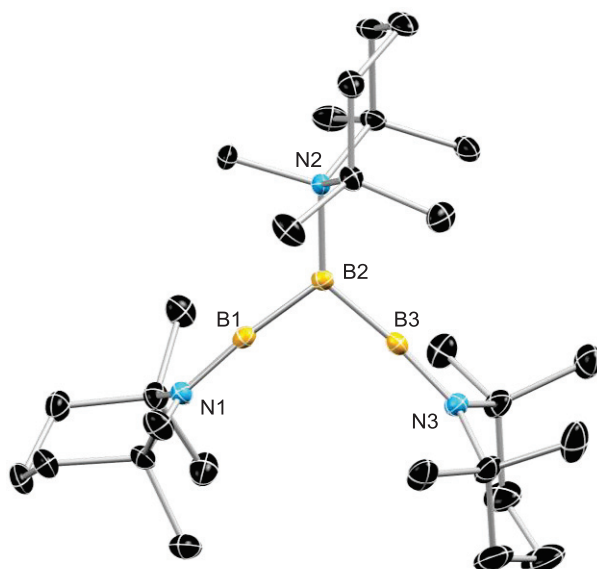


Figure 21. Molecular structure of **19** obtained from single-crystal X-ray diffraction analysis. Thermal ellipsoids are displayed at 30% probability. Hydrogen atoms and counter anion (OTf) are

omitted for clarity. There are two independent molecules in the asymmetric unit of **19**, and one of these is shown. Average values of selected bond lengths [\AA] and angles [$^\circ$]: B1–B2 1.554, B2–B3 1.550, B1–N1 1.360, B2–N2 1.579, B3–N3 1.362; B1–B2–B3 99.3.

The computational studies for **19** also offered the similar frontier orbitals (Figure 22), WBI values and natural charges to those of **18^{opt}**. Further modification of the reaction condition to synthesize **19** and experimental studies to reveal the reactivity and electronic property are future subjects.

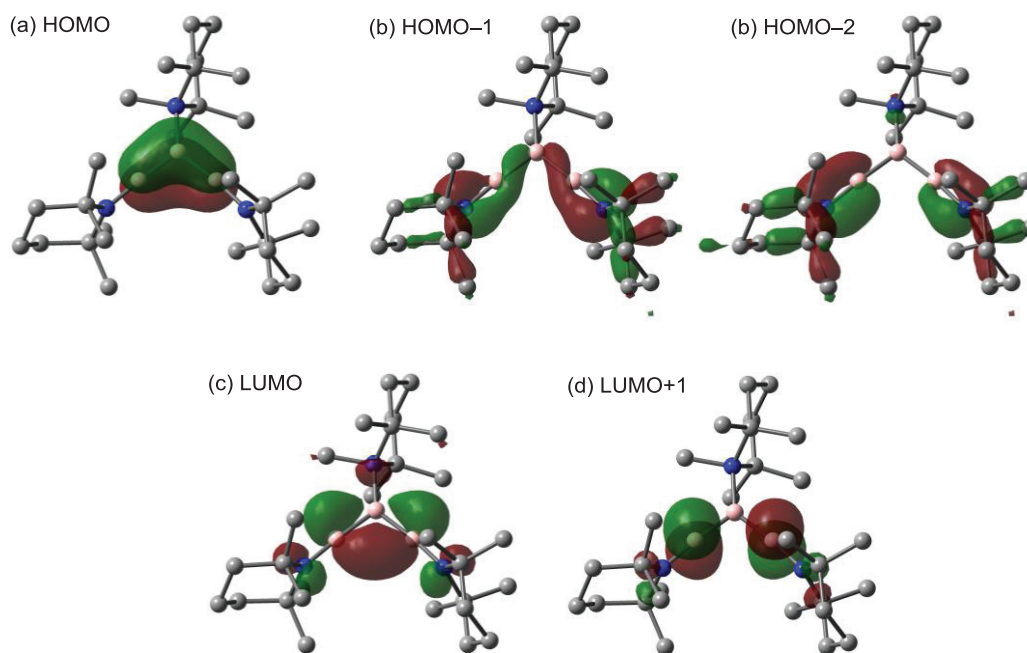


Figure 22. Frontier orbitals of **19^{opt}** at the B3LYP/6-31G+(d) level of theory with a contour value of 0.05 atomic units. H atoms are omitted for clarity.

4-14. Conclusion and Outlook

In conclusion, the chemical reduction of an aminodihloroborane is sensitive to the reductants, solvent, and amino-substituent. Sodium naphthalenide in DME afforded triaminotriboranes(3) **3** in good yield and **9** in low yield; sterically hindered amino-substituents TMP or CPC were essential for kinetic stabilization. When these reduction reactions were carried out under the higher concentration in large scale, the diborene-naphthalene adducts **8** and **10** were obtained accompanying with **3** and **9**. An excess of lithium in THF provided dianionic species **5** and **6**, which can be considered 1,4-diaza-2,3-diborabutadienes. As experimental and computational studies revealed, compounds **3** and **9** are homocatenated boron chain connected by B–B multiple bonds originating from three-center two-electron π -bonds, and can be viewed as bis(borylene)-stabilized borylenes and **3** is the first structurally authenticated example of a (R–B)₃ chain.

The reaction study of **3** and nucleophiles and electrophiles has also been investigated. In the reaction of **3** and one equivalent of *t*BuNC, a carbon–nitrogen triple bond in the isocyanide was facilely and completely cleaved to afford **11**. To the best of our knowledge, this is the second example of the metal-free C–N triple bond scission. The use of excess amount of *t*BuNC provided a different product **12** possessing the isocyanide C–N bonds. Those products **11** and **12** have rare 1-aza-2-borataallene moieties. Thermolysis of **12** to **11** was preliminary observed, but the detailed investigation should be required. The reaction of **3** with CO gas provided a single product and further characterizations are in progress. In addition, compound **3** allowed the direct metal-free 1,2-diborylation of aldehydes under the mild condition and form the air stable BBBOC 5-membered rings **16**, which were the first isolation of 1,2,3,4-oxatriborolanes. The reactions with phenylacetylene, BH₃•THF, elemental sulfur and various nucleophiles were carried out, but failed to characterize those products.

Furthermore, a triaminotriborane(3) **3** has showed the reactivity with electrophiles. The metal centers in the coinage metal chlorides were reduced by the electron transfer from **3**, and the chlorinated triborane(5) **17** was obtained. The reaction with gallium electrophiles provided the cation analogues of **3** serendipitously, which led us to use nitrogen favored MeOTf to synthesize a similar cation analogue. The reaction was succeeded and afforded **19**. The X-ray crystallographic analysis of **19** revealed the double bond characters in B–B bonds.

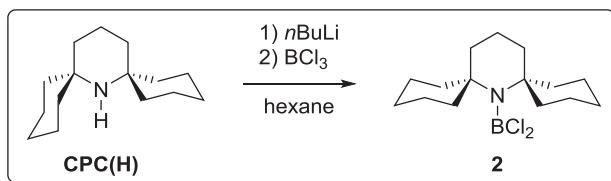
These reactivities of **3** with nucleophiles and electrophiles are certain evidences that **3** is an ambiphilic chemical species. Further detailed reaction studies of **3** are demanded. In addition, cation analogues of **3** also have the promise to demonstrate the unique reactivity. These reaction studies are future subjects. On the other hand, to achieve the initial goal toward the synthesis of a diaminodiborene and the reveal of its hidden properties, other synthetic approach and/or development of more sterically hindered amino-substituent(s) are essential.

Experimental Section

General Procedure

All syntheses were carried out under inert atmosphere with standard Schlenk and glovebox techniques unless otherwise stated. Tetrahydrofuran (THF) was freshly distilled from Na/benzophenone prior to use. 1,2-Dimethoxyethane (DME) and hexane were distilled from Na and stored over 4 Å molecular sieves in an argon-filled glovebox. 2,2,6,6-Tetramethylpiperidine (TMP(H)) was distilled from CaH₂ and stored over 4 Å molecular sieves. *n*-BuLi solution and BCl₃ solution were used as supplied. C₆D₆, toluene-*d*₈ and THF-*d*₈ were distilled from sodium followed by drying over potassium mirror and degassed three times using freeze–pump–thaw cycling and stored over 4 Å molecular sieves in an argon-filled glovebox for NMR measurements. (TMP)BCl₂ (**1**) was synthesized according to the previously reported procedure.²⁰ ¹H NMR (400 MHz), ⁷Li NMR (155 MHz) NMR, ¹¹B NMR (128 MHz), ¹³C NMR (100 MHz), and ¹⁹F NMR (376 MHz) spectra were recorded using a JEOL AL-400 NMR spectrometer. The ¹H and ¹³C NMR chemical shifts (δ scale) are determined by residual protons of the solvent (¹H, C₆D₆, δ = 7.20 ppm; toluene-*d*₈, δ = 2.08 ppm) or the solvent itself (¹³C, C₆D₆, δ = 128.0 ppm; toluene-*d*₈, δ = 137.48 ppm). The ¹¹B NMR chemical shifts are referenced to BF₃•Et₂O at 0 ppm. The ⁷Li NMR chemical shifts are referenced to LiCl in D₂O at 0 ppm. The ¹⁹F NMR chemical shifts are referenced to LiCl in D₂O at 0 ppm. The variable temperature ¹¹B NMR (160 MHz) spectra of **3** in toluene-*d*₈ were recorded using a JEOL JNM-ECA500 NMR spectrometer. The ¹¹B magic angle spinning (MAS) NMR spectrum of **3** was recorded using a JEOL JNM-ECA600 NMR spectrometer with the MAS rate of 17 kHz. Melting point was determined on Optimelt (SRS) and was uncorrected. Mass spectrum was measured on a JEOL JMS-700 mass spectrometer.

Synthesis of (CPC)BCl₂ (**2**)



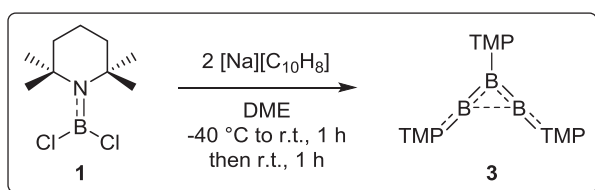
n-BuLi solution (1.64 M in *n*-hexane, 24.4 mL, 40.0 mmol) was added to a hexane (80 mL) solution of CPC(H) (8.86 g, 40.0 mmol) at -78 °C. The reaction solution was warmed to ambient temperature, then stirred for one hour. BCl₃ heptane solution (1.0 M, 40.0 mL, 40.0 mmol) was added dropwise to the pale yellow suspended hexane solution at -78 °C. The resulting white suspension was warmed to ambient temperature, then stirred for one hour. The insoluble precipitate was filtered and the filtrate was concentrated under reduced pressure. The resulting solution was stored at -30 °C, which afforded desired aminodichloroborane **2** was obtained as colorless crystals (9.32 g, 30.9 mmol, 77%). Mp. ¹H NMR (C₆D₆, 400 MHz): δ = 2.72–2.53 (m, 4H), 1.60–1.30 (m,

14H), 1.29–1.00 ppm (m, 8H); $^{13}\text{C}\{^1\text{H}\}$ NMR (C_6D_6 , 100 MHz): $\delta = 60.69$ (C), 37.81 (CH_2), 26.13 (CH_2), 25.21 (CH_2), 24.23 (CH_2), 12.86 ppm (CH_2); $^{11}\text{B}\{^1\text{H}\}$ NMR (C_6D_6 , 128 MHz): $\delta = 35.07$ ppm (s).

Preparation of sodium naphthalenide

After the addition of sodium (52.0 mg, 2.23 mmol) to naphthalene (283 mg, 2.21 mmol) in 7.4 mL of DME, the resultant dark-green solution was stirred for 1 h.

Synthesis of (TMP-B)₃ (3)



Procedure A (sodium naphthalenide):

Freshly prepared sodium naphthalenide solution was added dropwise to **1** (222 mg, 1.00 mmol) in 15.0 mL of DME at $-40\text{ }^\circ\text{C}$. After warming the dark-green reaction solution to room temperature over 1 h, the deep-red-purple solution was stirred for 1 h at room temperature. After removal of the solvent, naphthalene was sublimed at $40\text{ }^\circ\text{C}$ for 15 h in full vacuum. The resultant deep-purple solid was dissolved in hexane, and insoluble solid was filtered and washed with hexane. After concentration, the dark-purple filtrate was stored at $-30\text{ }^\circ\text{C}$ for 1 day to afford crystalline dark-purple solid **3** (102 mg, 0.224 mmol, 67%). ^1H NMR (C_6D_6 , 400 MHz): $\delta = 1.63$ – 1.49 ppm (m, 54H); ^{13}C NMR (C_6D_6 , 100 MHz): $\delta = 55.11$ (C), 40.76 (CH_2), 32.55 (CH_3), 18.12 ppm (CH_2); ^{11}B NMR (C_6D_6 , 128 MHz): $\delta = 51.7$ ppm (br s); mp: 118.5 – $120.1\text{ }^\circ\text{C}$ (dec.); HRMS (FAB⁺) calcd for $\text{C}_{27}\text{H}_{54}\text{B}_3\text{N}_3$ [M^+]: 453.4597, found: 453.4580.

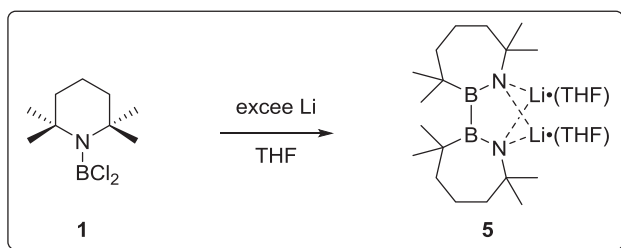
*: In a larger scale reaction under higher concentration condition, in which the reduction of **1** (1.33 g, 6.01 mmol) in 40 mL of DME was carried out by using sodium naphthalenide prepared from sodium (0.287 g, 12.5 mmol) and naphthalene (1.59 g, 12.4 mmol) in 15 mL of DME, the naphthalene adduct **8** was included in the crude product. Recrystallization in hexane at $-30\text{ }^\circ\text{C}$ was required several times to remove **8** from **3**, which decreased the isolated yield of **3** (0.245 g, 0.451 mmol, 23%).

Procedure B (sodium):

Sodium (110 mg, 4.78 mmol) was added to **1** (447 mg, 2.01 mmol) in 20.0 mL of DME. The reaction solution was stirred at room temperature for 1 day. After concentration under reduced pressure, hexane was added to the deep-pink solution, and insoluble solid was filtered off and

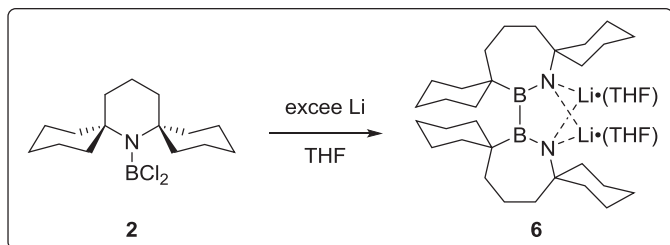
washed with hexane. After removal of the solvent, the red oily product was stored at room temperature for 3 day to afford as red-purple crystals in oil. The crystals was gathered and washed with cooled hexane. Compound **3** was obtained as red-purple crystals (46.2 mg, 0.102 mmol, 15%) associated with a small amount of yellow crystalline (TMP-B)₄ (**4**). Compound **4** was previpusly reported and fully characterized.^{14a,b}

Synthesis of dianionic diborane (5)



Lithium pieces (168 mg, 24.2 mmol) was added to **1** (229 mg, 1.03 mmol) in 15.0 mL of THF. The reaction mixture was stirred at room temperature for 12 h. After concentration under reduced pressure, hexane was added to the orange solution, and residual Li and insoluble solid were filtered off and washed with hexane. After concentration, the orange solution was stored at -30 °C for 1 day to afford trace amount of **5** as colorless crystals.

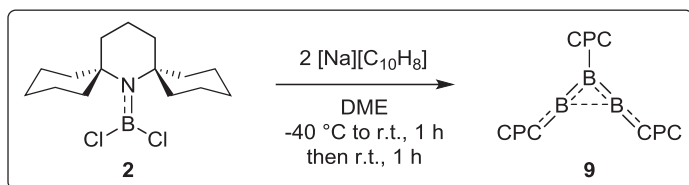
Synthesis of dianionic diborane (6)



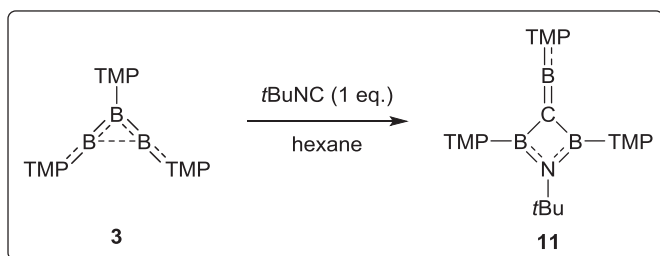
Lithium pieces (28.6 mg, 4.12 mmol) was added to **2** (122 mg, 0.403 mmol) in 5.0 mL of THF and 5.0 mL of hexane. The reaction mixture was stirred at room temperature for 12 h. After concentration under reduced pressure, hexane was added to the yellow suspension, and residual Li and insoluble solid were filtered off and washed with hexane. After concentration, the yellow solution was stored at -30 °C to afford trace amount of colorless solid which was filtered. The yellow filtrate was concentrated again and stored at -30 °C to afford a white solid. This solid was gathered and washed with pre-cooled hexane by decantation. The resulting white solid (16.3 mg) showed a single signal for ⁷Li and ¹¹B{¹H} NMR measurements as shown later, and was recrystallized from THF at room temperature to afford small amount of **6** as colorless crystals. ⁷Li NMR (C₆D₆, 155 MHz, LiCl in D₂O): δ = 1.25 ppm (s); ¹¹B NMR (C₆D₆, 128 MHz): δ = 49.5 ppm

(br, s).

Synthesis of (CPC-B)₃ (9)



Synthesis of 11 (Using 1 equivalent of *t*BuNC)

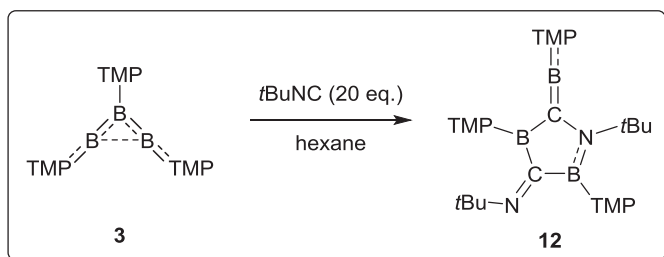


11:

1,1'-(1-(tert-butyl)-3-((2,2,6,6-tetramethylpiperidin-1-yl)boranylidene)-1,2,4-azadiboretidine-2,4-diyl)bis(2,2,6,6-tetramethylpiperidine)

A *n*-hexane (3.0 mL) solution of *tert*-BuNC (4.2 mg, 51 μmol) was added dropwise to a *n*-hexane (1.0 mL) solution of (TMP-B)₃ (23.2 mg, 51.2 μmol) in three portions every 2 hours with stirring. Each addition took 20 minutes. After the stirring for 2 hours from the last portion, the colorless solution was dried under reduced pressure. Recrystallization from toluene at -30 °C afforded **11** (26.7 mg, 49.8 μmol, 97%) as colorless crystals suitable for X-ray crystallographic analysis. Mp. ¹H NMR (toluene-*d*₈, 400 MHz): δ = 1.89–1.16 ppm (m); ¹¹B{¹H} NMR (toluene-*d*₈, 128 MHz): δ = 43.3 ppm (s); ¹³C{¹H} NMR (toluene-*d*₈, 100 MHz): δ = 54.11 (C), 51.88 (C), 51.60 (C), 39.88 (CH₃), 39.24 (CH₂), 33.35 (CH₂), 32.83 (CH₃), 30.29 (CH₃), 19.33 (CH₂), 17.86 ppm (CH₂). One carbon atom with adjacent three boron atoms was not observed, due to the quadrupole moments of boron atoms. Anal. Calcd for C₃₂H₆₃B₃N₄: C, 71.67; H, 11.84; N, 10.45. Found: C, 71.29; H, 11.64; N, 10.23.

Synthesis of 12 (Using 20 equivalents of *tert*-BuNC)



12:

(3*E*)-*N*,1-di-*tert*-butyl-2,4-bis(2,2,6,6-tetramethylpiperidin-1-yl)-5-((2,2,6,6-tetramethylpiperidin-1-yl)boraneylidene)-1,2,4-azadiborolidin-3-imine

A pre-cooled ($-30\text{ }^{\circ}\text{C}$) *n*-hexane (2.0 mL) solution of $(\text{TMP-B})_3$ (23.9 mg, 52.7 μmol) was added dropwise to a *n*-hexane (1.0 mL) solution of *tert*-BuNC (84.2 mg, 1.01 mmol) at $-30\text{ }^{\circ}\text{C}$. After the stirring for 3 hours at $-30\text{ }^{\circ}\text{C}$, the yellow solution was dried under reduced pressure.

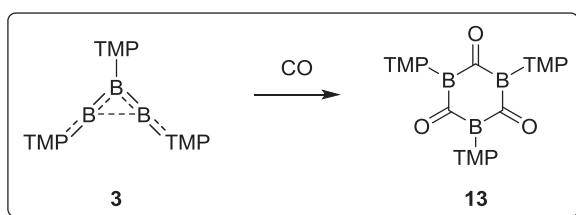
Recrystallization from toluene at $-30\text{ }^{\circ}\text{C}$ afforded **12** (26.7 mg, 49.8 μmol , 97%) as yellow crystals suitable for X-ray crystallographic analysis. Mp. $^{11}\text{B}\{^1\text{H}\}$ NMR (toluene- d_8 , 128 MHz): $\delta = 53.9$, 49.6, 32.4 ppm (s). Anal. Calcd for $\text{C}_{37}\text{H}_{72}\text{B}_3\text{N}_5$: C, 71.74; H, 11.724; N, 11.31. Found: C, 71.71; H, 11.76; N, 11.15.

Reaction With CO

General Procedure.

Toluene solution of $(\text{TMP-B})_3$, **11** or **12** were degassed using freeze-pump-thaw cycling, the CO gas was added without drying into a flask or NMR tube.

Using $(\text{TMP-B})_3$, **3**

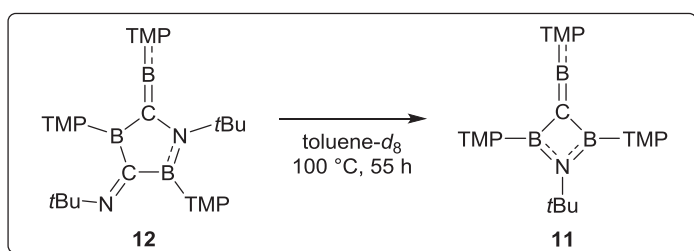


A toluene (mL) solution of $(\text{TMP-B})_3$ (mg, μmol) in a flask was used. After the stirring at room temperature for 72 hours, the reaction solution was dried in full vacuum. The crystalline yellow solid (mg) was obtained with small amount of toluene. $^{11}\text{B}\{^1\text{H}\}$ (C_6D_6 , 128 MHz): $\delta = 59.9$ ppm (s, br); $^{13}\text{C}\{^1\text{H}\}$ (C_6D_6 , 160 MHz): $\delta = 203.24$ (C), 137.88 (C, toluene), 129.34 (CH, toluene), 128.56 (CH, toluene) 125.70 (CH, toluene), 54.39 (C), 40.22 (CH_2), 32.06 (CH_3), 21.45 (CH_3 , toluene), 18.12 ppm (CH_2).

Using **11**

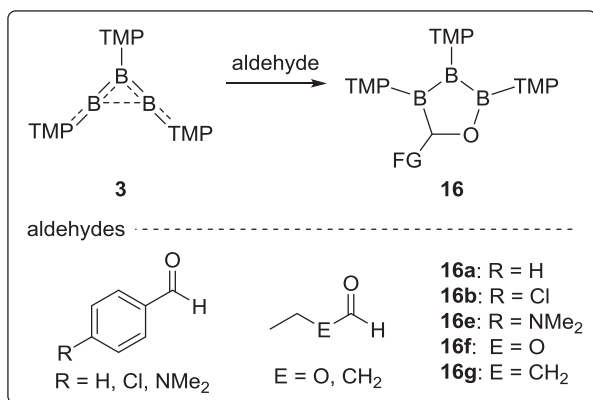
The reaction of **11** (21.0 mg, 39.2 μmol) with CO in toluene- d_8 (0.6 mL) was monitored by ^1H and $^{11}\text{B}\{^1\text{H}\}$ NMR measurements. No reaction was observed, even after the heating at 100 $^\circ\text{C}$ for 21 hours.

Using **12**



The reaction of **12** (31.3 mg, 50.5 μmol) with CO in toluene- d_8 (0.6 mL) was monitored by ^1H and $^{11}\text{B}\{^1\text{H}\}$ NMR measurements. After the heating at 60 $^\circ\text{C}$ for 11 hours, no reaction was observed. Further heating at 100 $^\circ\text{C}$ for 55 hours completely consumed **12** and afforded **11**.

Reaction of $(\text{TMP-B})_3$ With Aldehydes



General Procedure.

Aldehydes (mmol) solution in organic solvents were added to a *n*-hexane (0.30 mL) solution of $(\text{TMP-B})_3$ (22.7 mg, 50.1 μmol) at room temperature. The resulting purple solution was stirred at the same temperature. After removal of solvents under reduced pressure, the solid or yellow oil was obtained.

Using benzaldehyde (product 16a).

A *n*-hexane (mL) solution of benzaldehyde (mg, μmol) was used. After the stirring of the reaction solution for 4 hours, the resulting colorless solution was dried under reduced pressure. Recrystallization from toluene at -30 $^\circ\text{C}$ afforded **7a** (mg, μmol , %) as colorless crystals suitable for X-ray crystallographic analysis. Mp not yet. ^1H (toluene- d_8 , 400 MHz): δ = ppm (); $^{11}\text{B}\{^1\text{H}\}$

(C₆D₆, 128 MHz): δ = 58.0 (br, s), 51.3 (br, s), 39.4 ppm (br, s); ¹³C{¹H} (toluene-*d*₈, 160 MHz): δ = ppm (). Anal. Calcd for C₃₄H₆₀B₃N₃O: C, 73.01; H, 10.81; N, 7.51. Found: C, 72.75; H, 10.84; N, 7.41.

Using 4-chlorobenzaldehyde (product **16b**).

A toluene (0.4 mL) solution of 4-chlorobenzaldehyde (mg, μ mol) was used. After the stirring of the reaction solution for 6 hours, the resulting colorless solution was dried under reduced pressure. Recrystallization from toluene at -30 °C afforded **7b** (mg, μ mol, %) as colorless crystals suitable for X-ray crystallographic analysis. Mp not yet. ¹H (toluene-*d*₈, 400 MHz): δ = ppm (); ¹¹B{¹H} (C₆D₆, 128 MHz): δ = 57.9 (br, s), 51.3 (br, s), 39.3 ppm (br, s); ¹³C{¹H} (toluene-*d*₈, 160 MHz): δ = ppm (). Anal. Calcd for C₃₄H₅₉B₃N₃OCl: C, 68.78; H, 10.02; N, 5.97. Found: C, 69.10; H, 10.11; N, 6.98. Remeasurement.

Using 4-(dimethylamino)benzaldehyde.

A toluene (mL) solution of 4-(dimethylamino)benzaldehyde (mg, μ mol) was used. After the stirring of the reaction solution for 6 hours, the resulting yellow solution was dried under reduced pressure. The obtained yellow oily solid showed messy ¹H NMR spectrum.

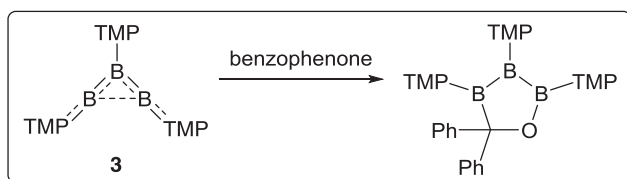
Using butyraldehyde.

A *n*-hexane (0.20 mL) solution of butyraldehyde (mg, μ mol) was used. After the stirring of the reaction solution for 15 hours, the resulting colorless solution was dried under reduced pressure. The obtained pale yellow oil showed unassignable ¹H NMR spectrum without signals corresponding to those of (TMP-B)₃.

Using ethyl formate.

The reaction of (TMP-B)₃ (22.8 mg, 50.3 μ mol) with ethyl formate (3.9 mg, 53 μ mol) in a C₆D₆ solution (0.5 mL) at room temperature was monitored by ¹H NMR measurement. No reaction was observed, even after the addition of excess amount of ethyl formate (13.5 mg, 182 μ mol).

Reaction of (TMP-B)₃ With Ketons.

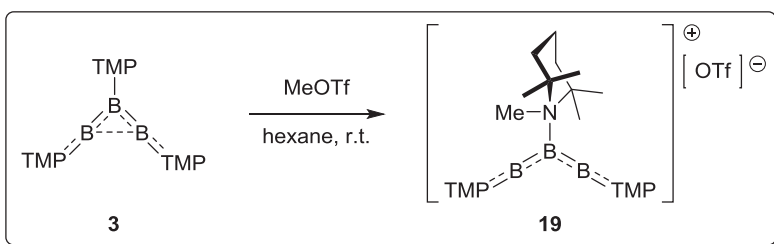
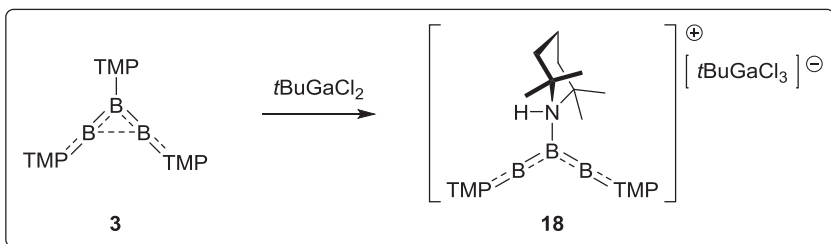
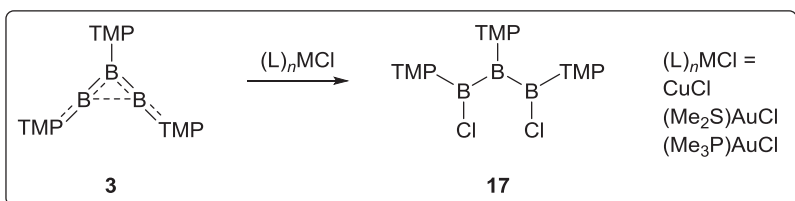


Using Benzophenone.

The reaction of (TMP-B)₃ (22.7 mg, 50.1 μ mol) with benzophenone (9.6 mg, 53 μ mol) in

a C₆D₆ solution (0.5 mL) at room temperature was monitored by ¹H NMR measurement. No reaction was observed, even after the heating at 40 °C for 18 hours.

Reaction With Coinage Metal Complexes



NMR Spectra

NMR Spectra of 2

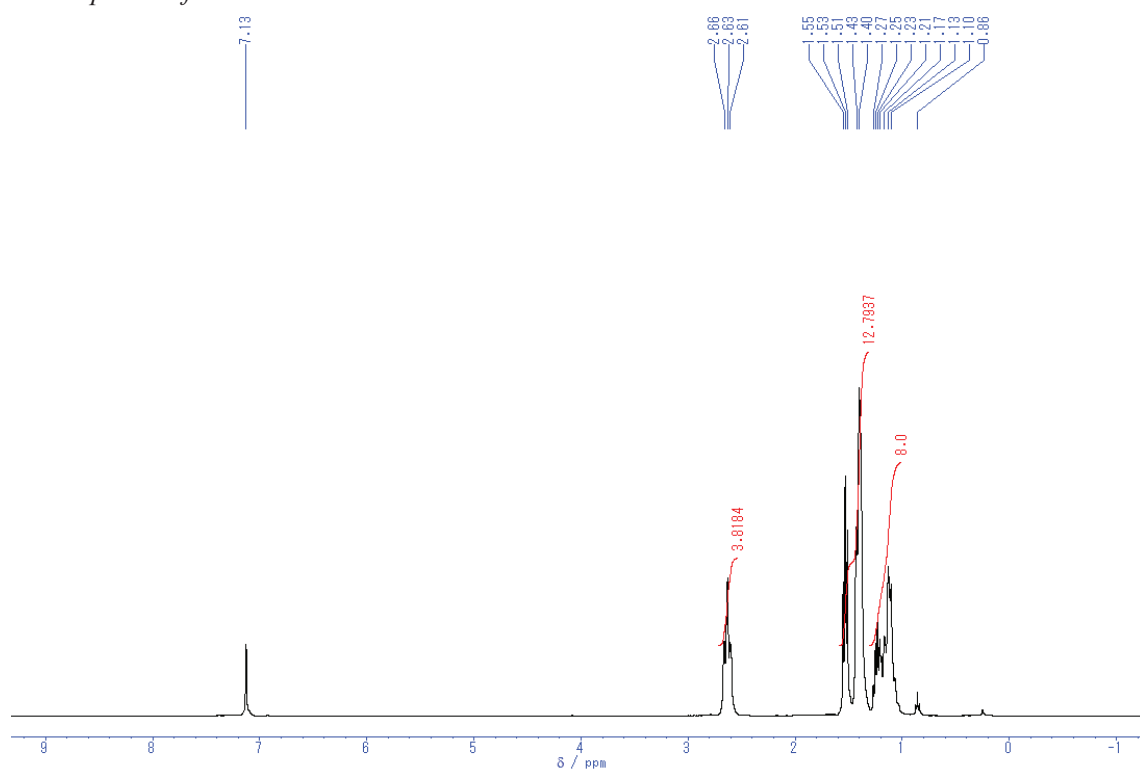


Figure S1. ^1H NMR spectrum (400 MHz) of **2** in C_6D_6 at room temperature.

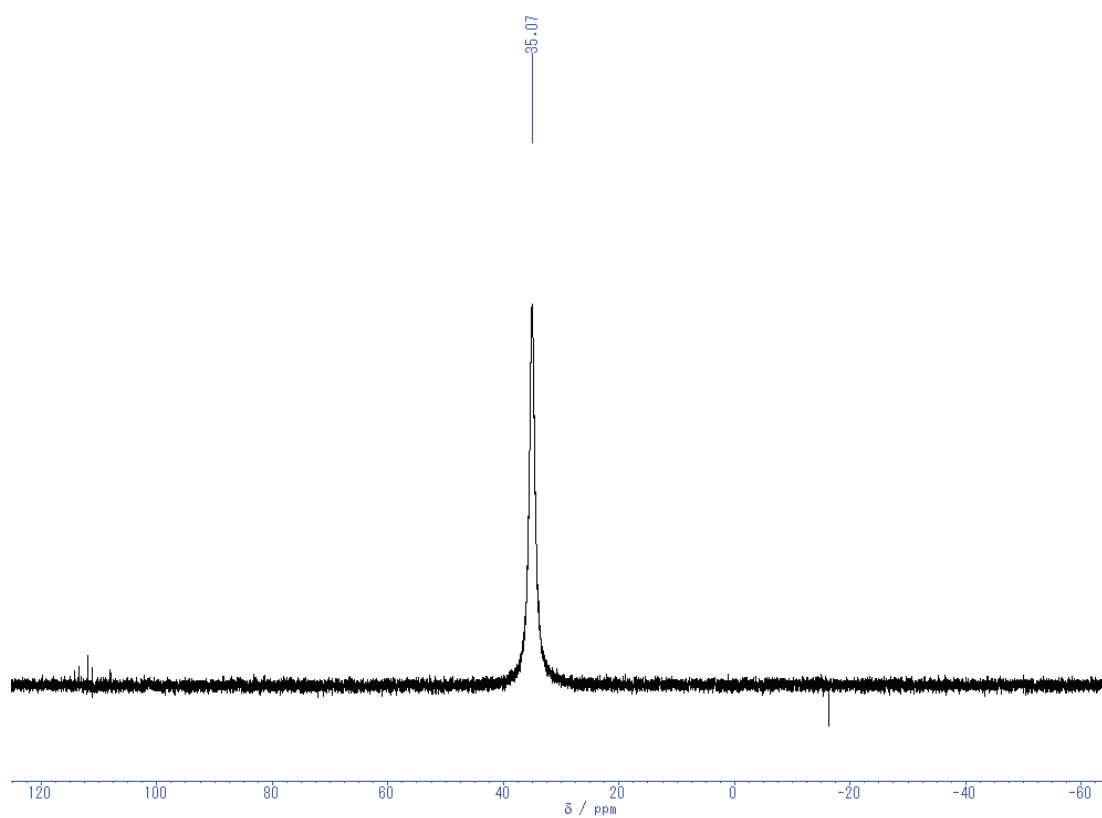


Figure S2. $^{11}\text{B}\{^1\text{H}\}$ NMR spectrum (128 MHz) of **2** in C_6D_6 at room temperature.

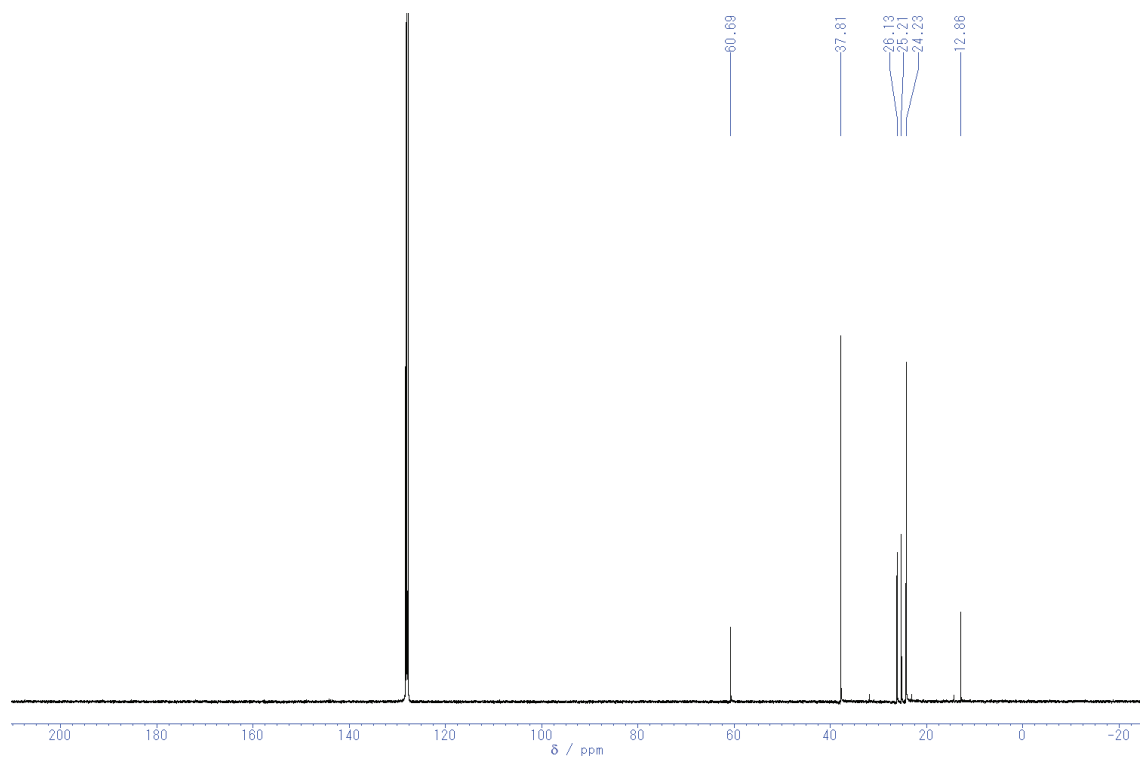


Figure S3. $^{13}\text{C}\{^1\text{H}\}$ NMR spectrum (100 MHz) of **2** in C_6D_6 at room temperature.

NMR Spectra of **3**

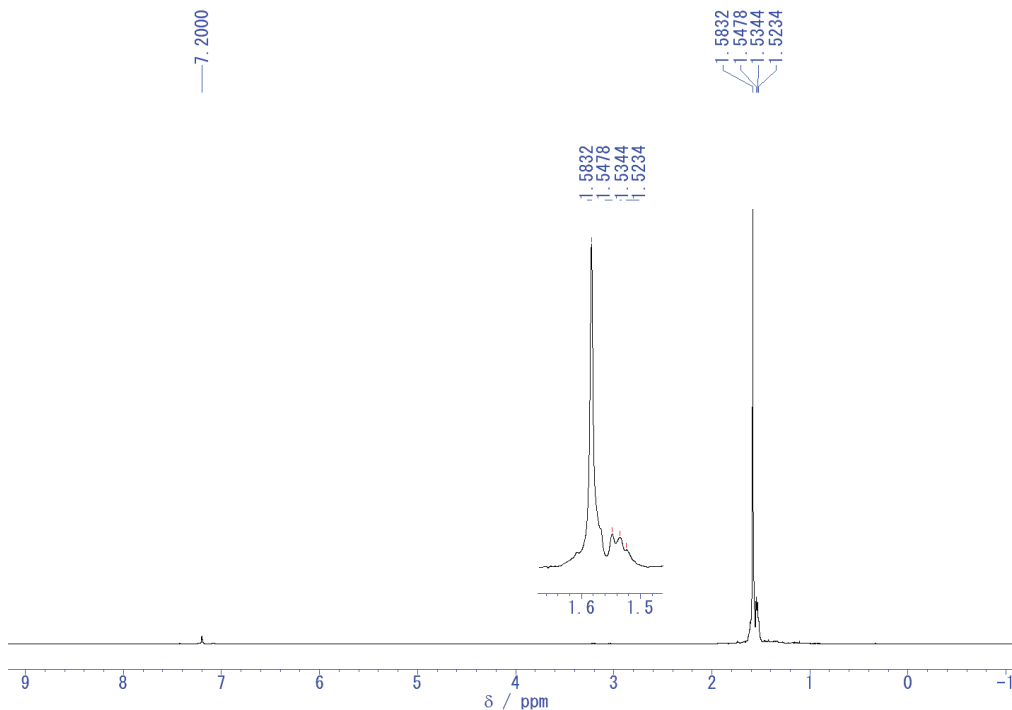


Figure S4. ^1H NMR spectrum (400 MHz) of **3** in C_6D_6 at room temperature.

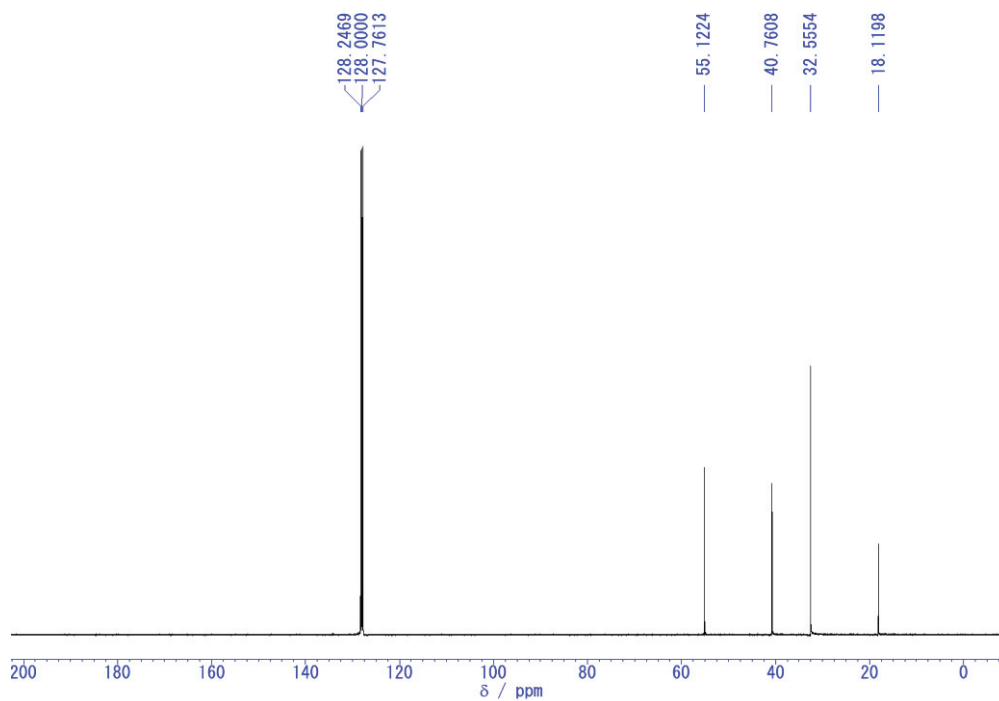


Figure S5. $^{13}\text{C}\{^1\text{H}\}$ NMR spectrum (100 MHz) of **3** in C_6D_6 at room temperature.

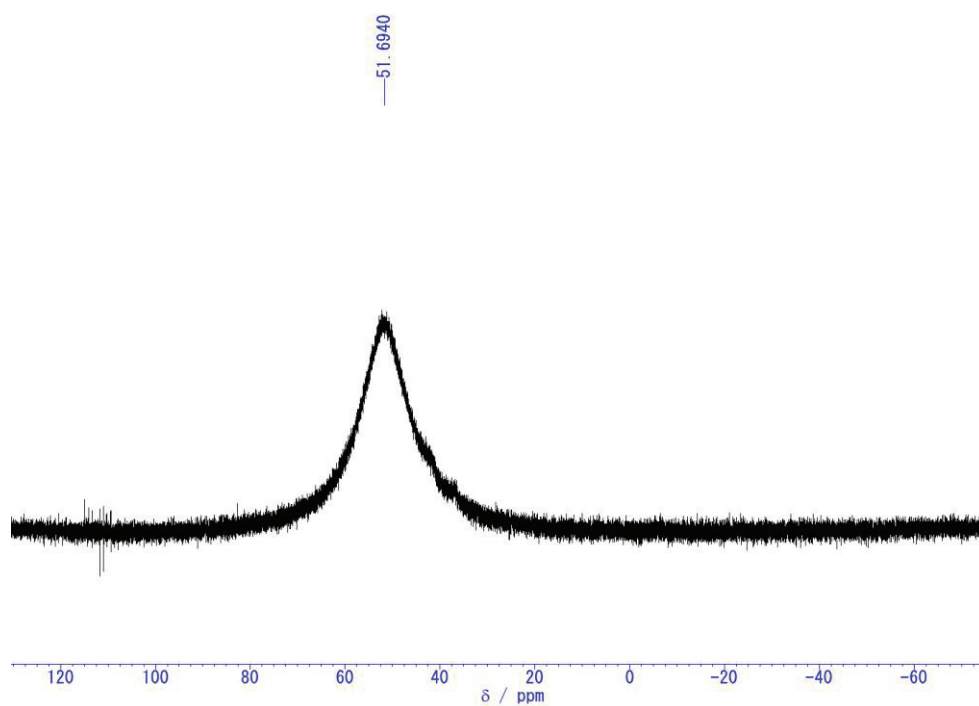


Figure S6. $^{11}\text{B}\{^1\text{H}\}$ NMR spectrum (128 MHz) of **3** in C_6D_6 at room temperature.

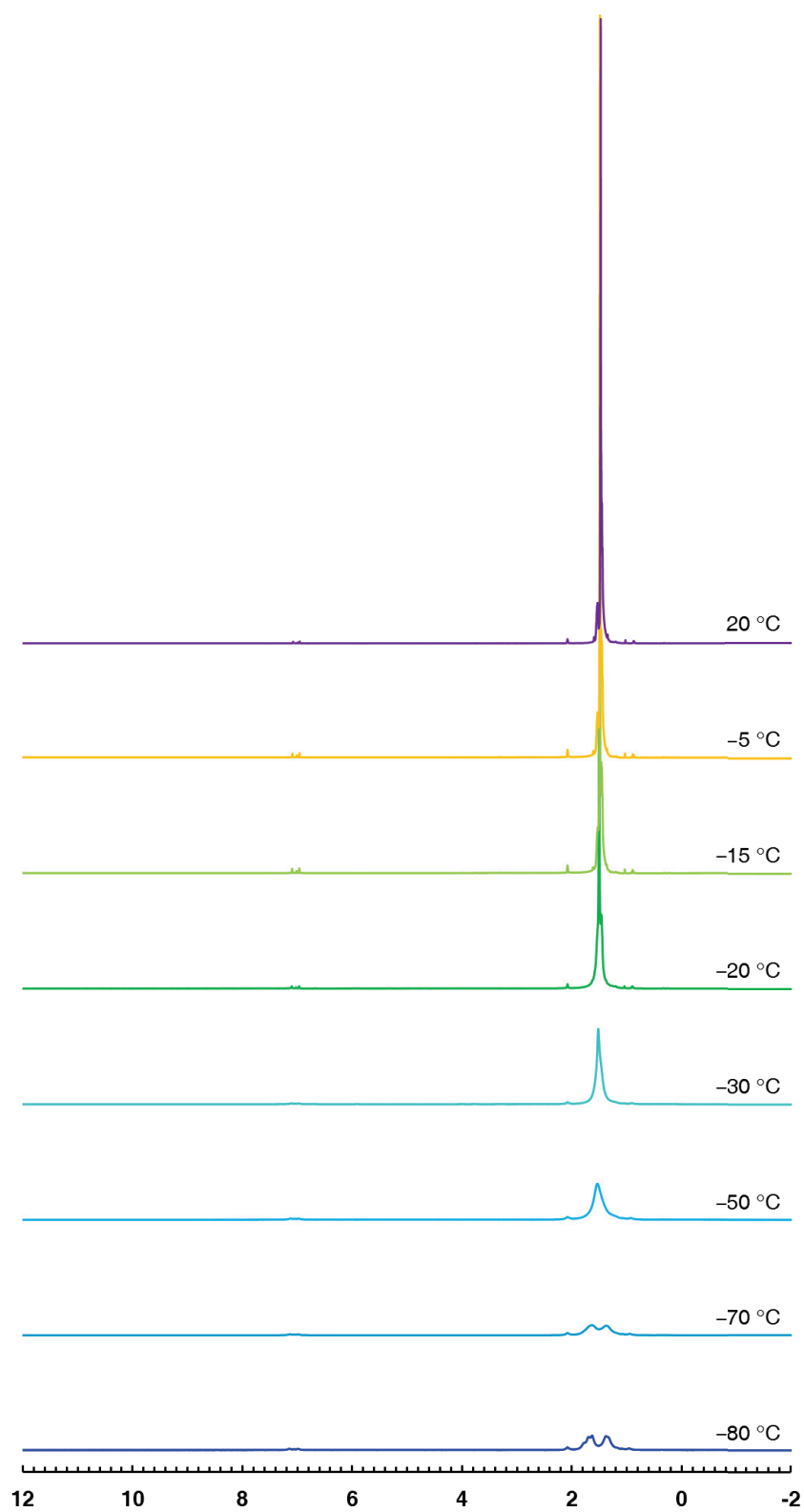


Figure S7. ¹H NMR spectra (500 MHz) of **3** in toluene-*d*₈ drawn in ppm.

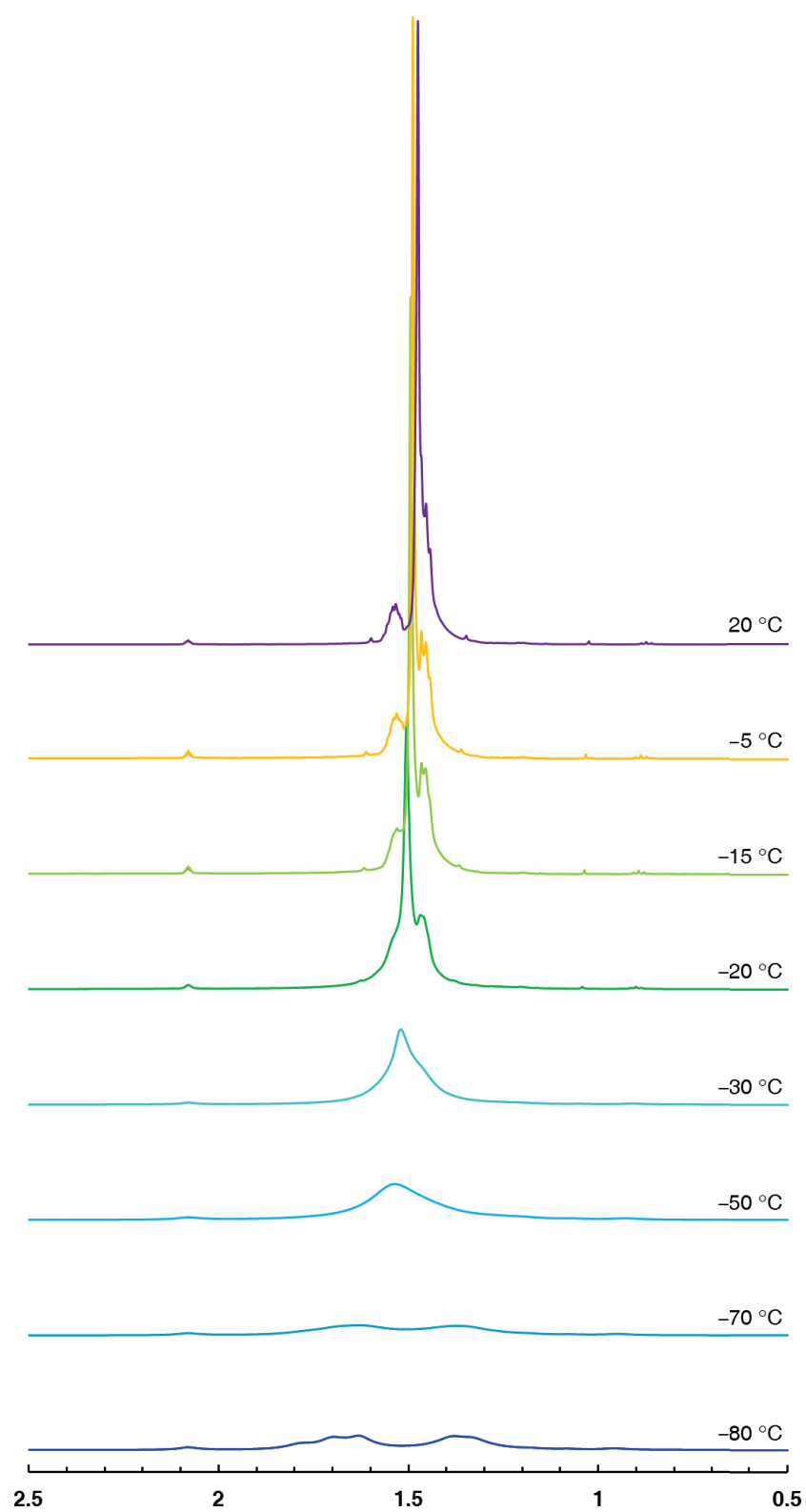


Figure S8. Selected region of ^1H NMR spectra (500 MHz) of **3** in $\text{toluene-}d_8$ drawn in ppm.

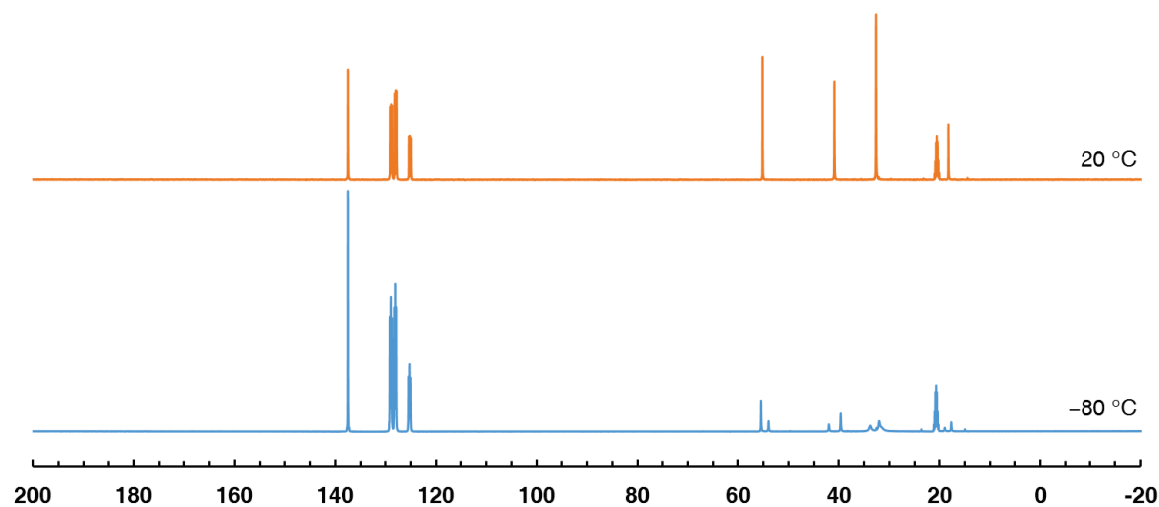


Figure S9. $^{13}\text{C}\{^1\text{H}\}$ NMR spectra (126 MHz) of **3** in toluene- d_8 drawn in ppm.

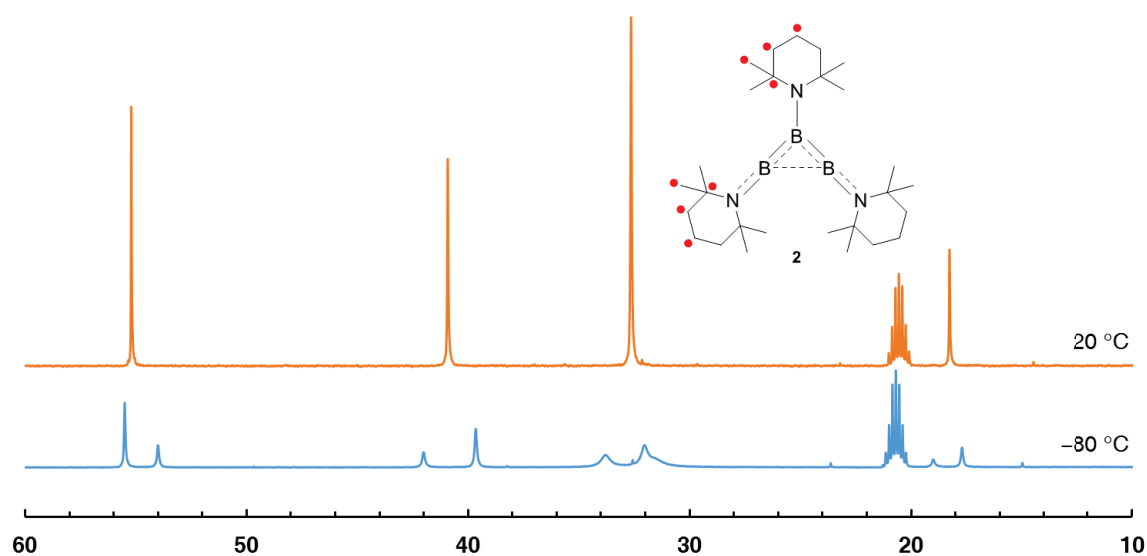


Figure S10. Selected region of $^{13}\text{C}\{^1\text{H}\}$ NMR spectra (126 MHz) of **3** in toluene- d_8 drawn in ppm.

The $^{13}\text{C}\{^1\text{H}\}$ NMR spectrum showed four signals at $\delta = 55.21, 40.92, 32.64$ and 18.27 ppm at $20\text{ }^\circ\text{C}$. By contrast, at $-80\text{ }^\circ\text{C}$, the $^{13}\text{C}\{^1\text{H}\}$ NMR spectrum showed eight signals at $\delta = 55.50, 54.00, 42.01, 39.66, 33.80, 32.03, 19.00$ and 17.70 ppm, which also could be assigned as the terminal and central boron substituents that was revealed by the single crystal X-ray crystallographic study.

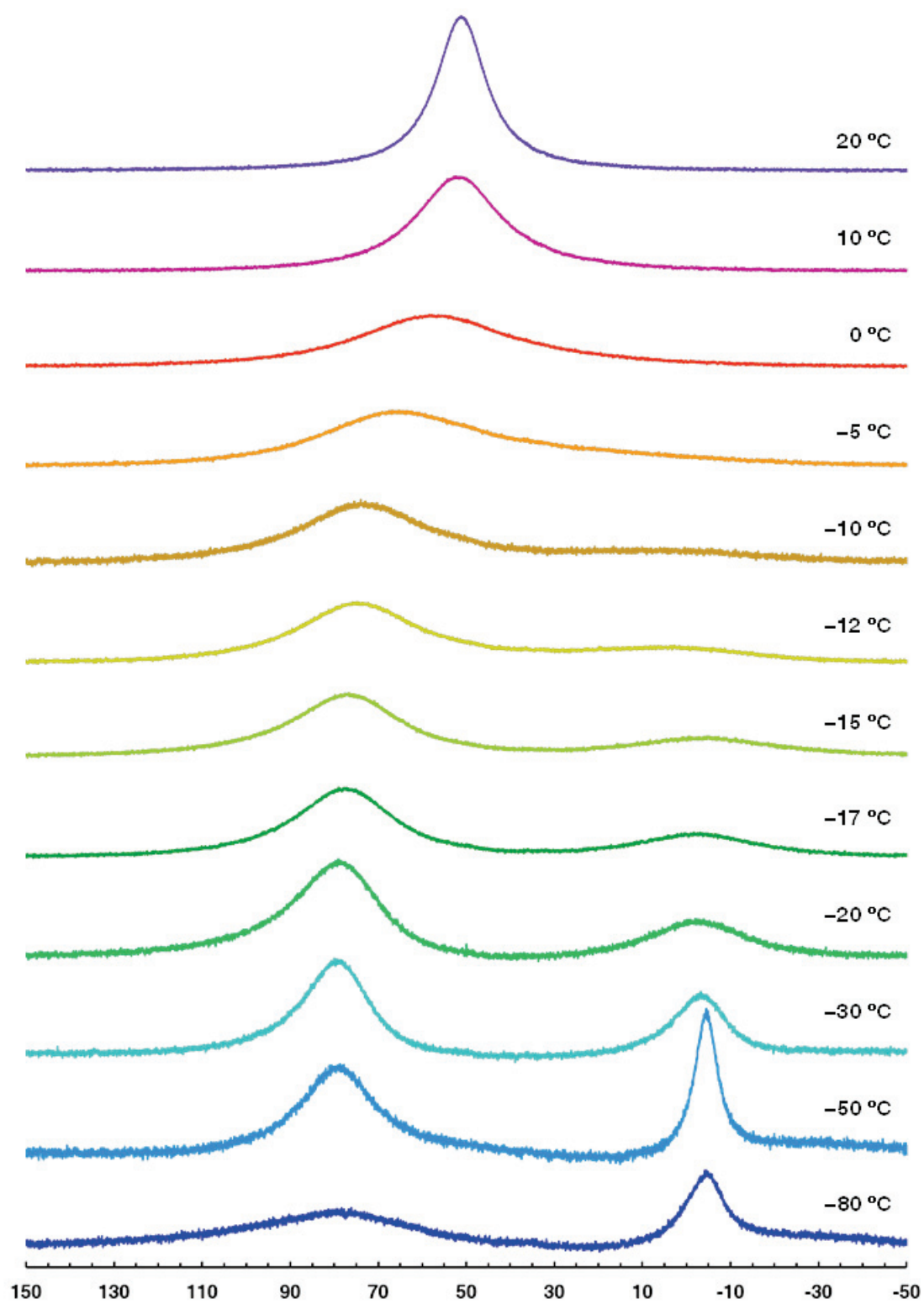


Figure S11. ^{11}B NMR spectra (160 MHz) of **3** in $\text{toluene-}d_8$ drawn in ppm.

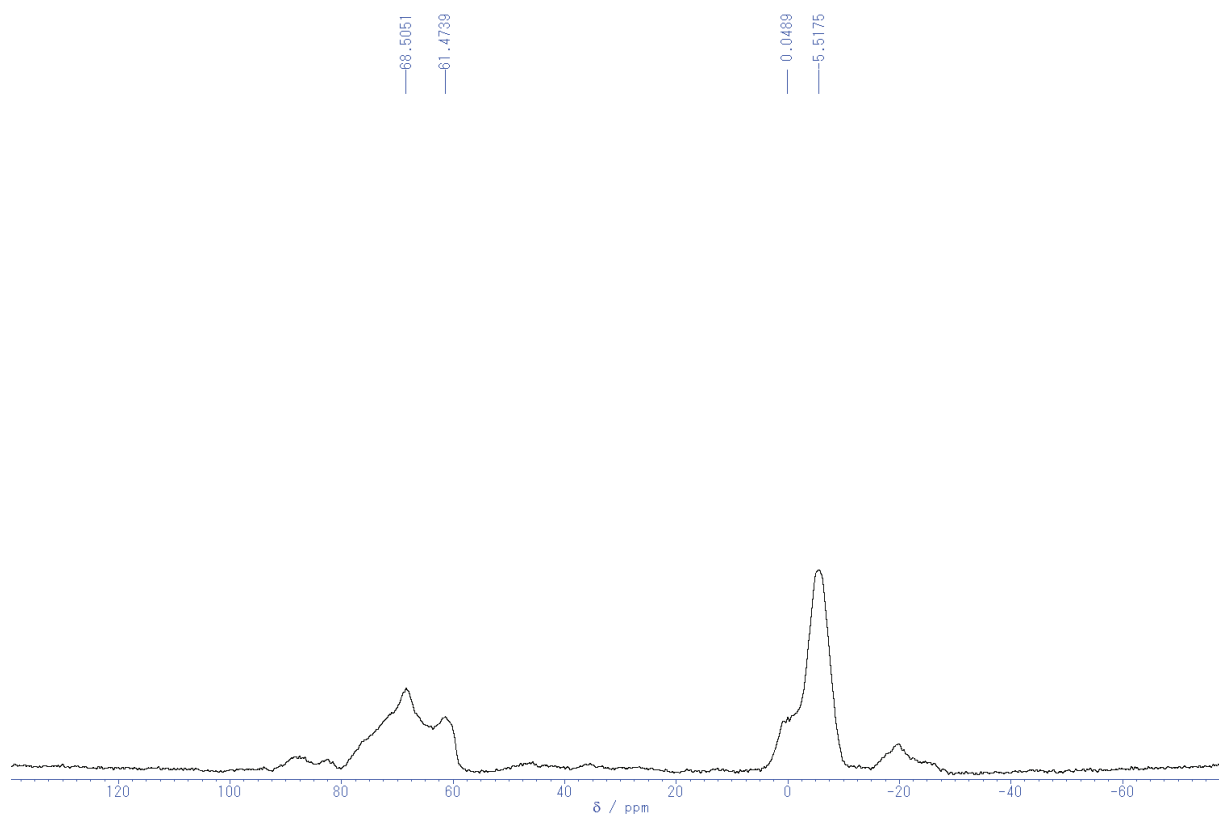


Figure S12. ^{11}B MAS NMR spectrum of **3**.

NMR Spectra of 6

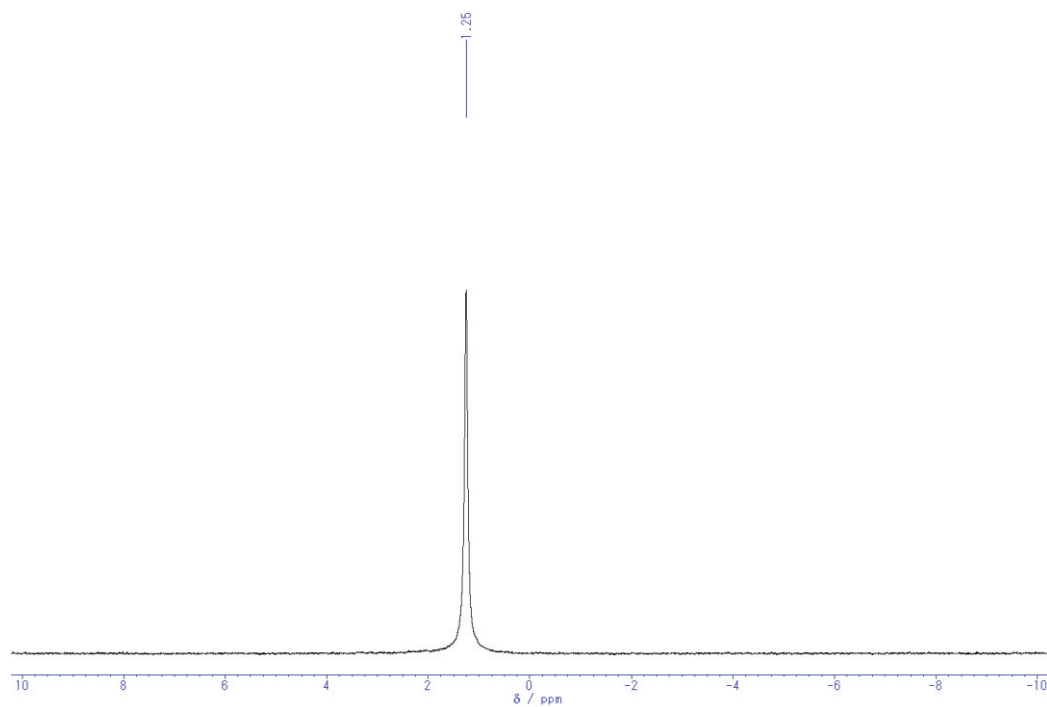


Figure S6. $^{11}\text{B}\{^1\text{H}\}$ NMR spectrum (128 MHz) of **3** in C_6D_6 at room temperature.

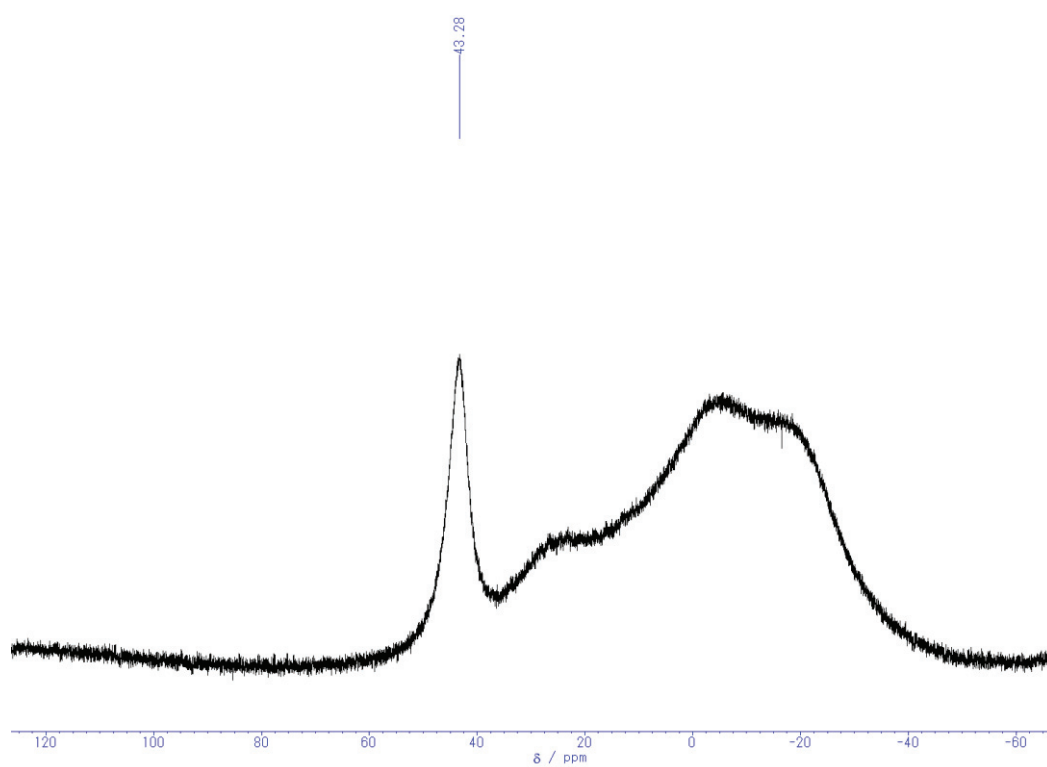


Figure S16. $^{11}\text{B}\{^1\text{H}\}$ NMR spectrum (128 MHz) of **11** in toluene- d_8 at room temperature.

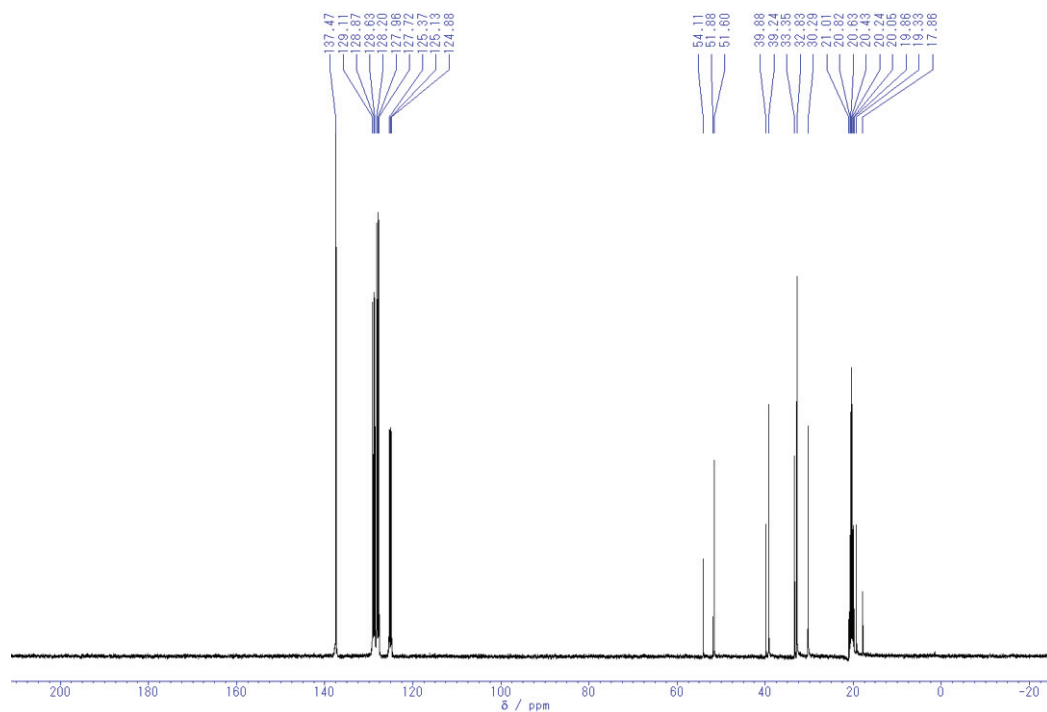


Figure S17. $^{13}\text{C}\{^1\text{H}\}$ NMR spectrum (100 MHz) of **11** in toluene- d_8 at room temperature.

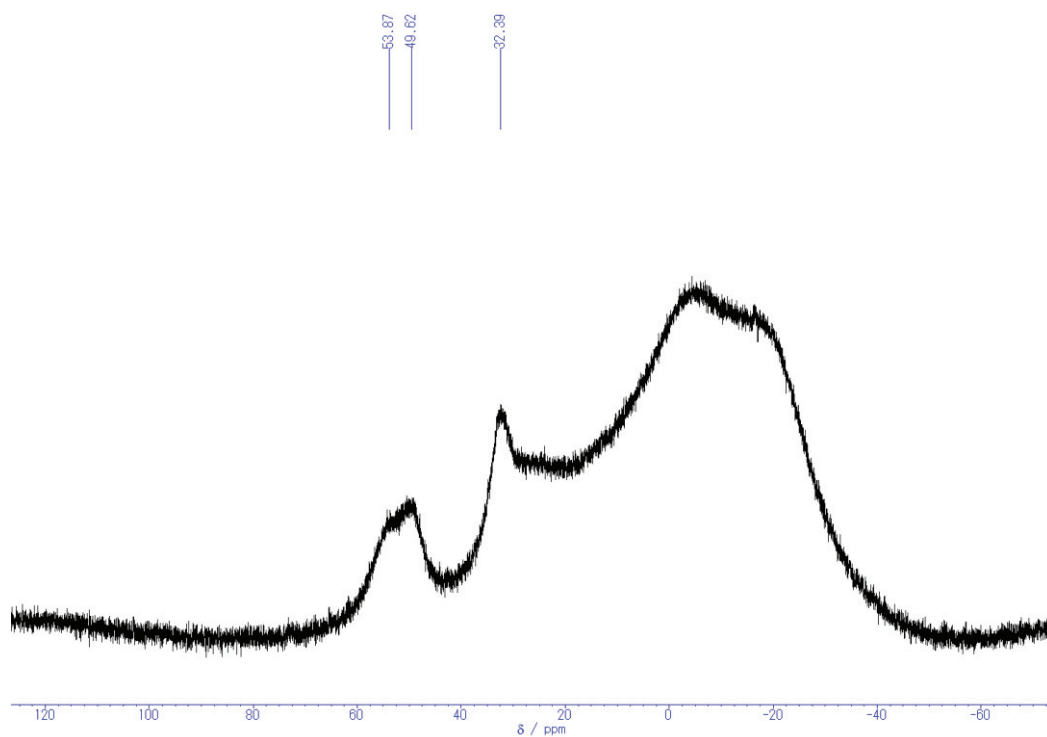


Figure S18. $^{11}\text{B}\{^1\text{H}\}$ NMR spectrum (128 MHz) of **12** in toluene- d_8 at room temperature.

NMR Spectra of the reaction of 3 with CO

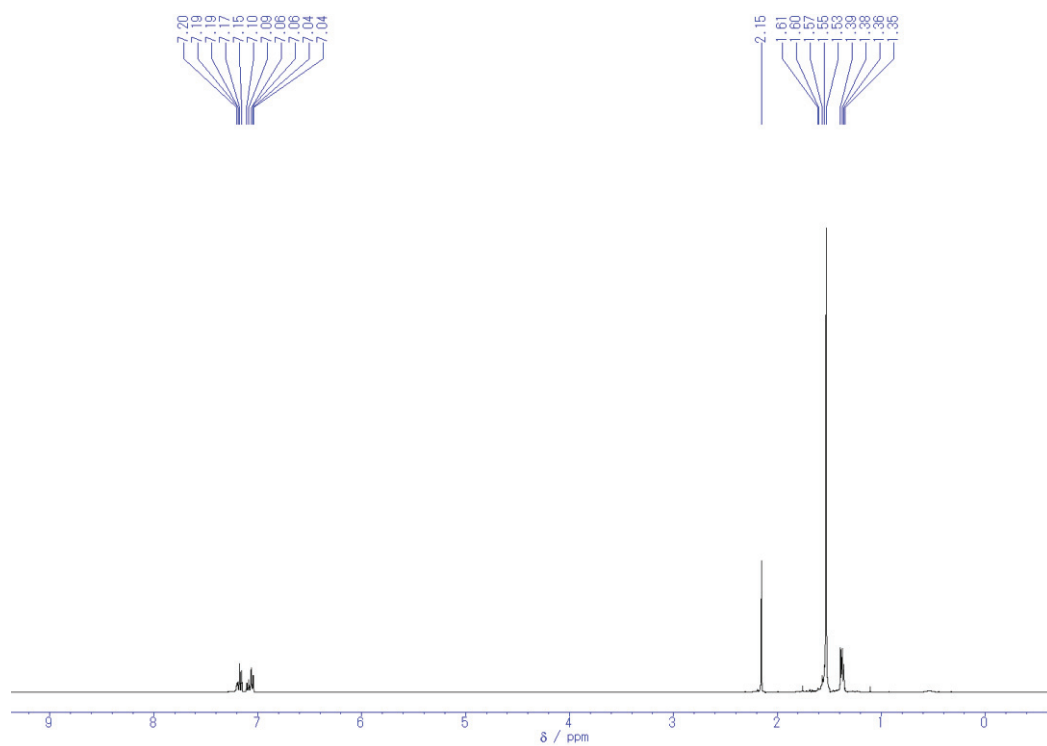


Figure S19. ^1H NMR spectrum (400 MHz) of the crude product in C_6D_6 at room temperature.

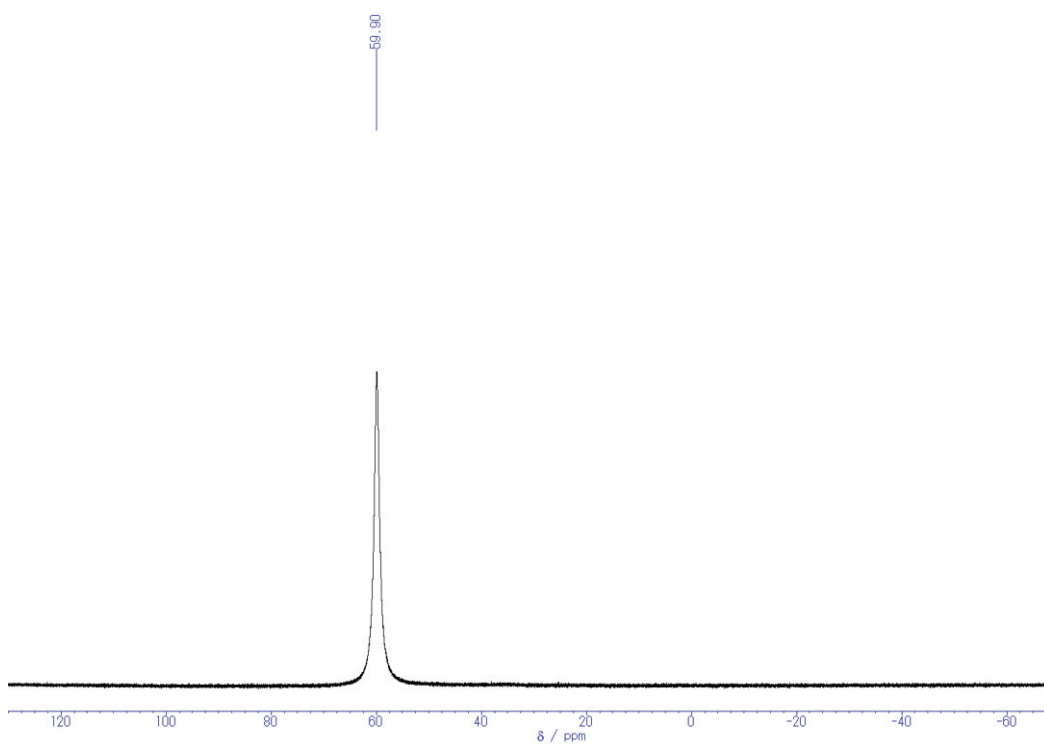


Figure S20. $^{11}\text{B}\{^1\text{H}\}$ NMR spectrum (128 MHz) of the crude product in C_6D_6 at room temperature.

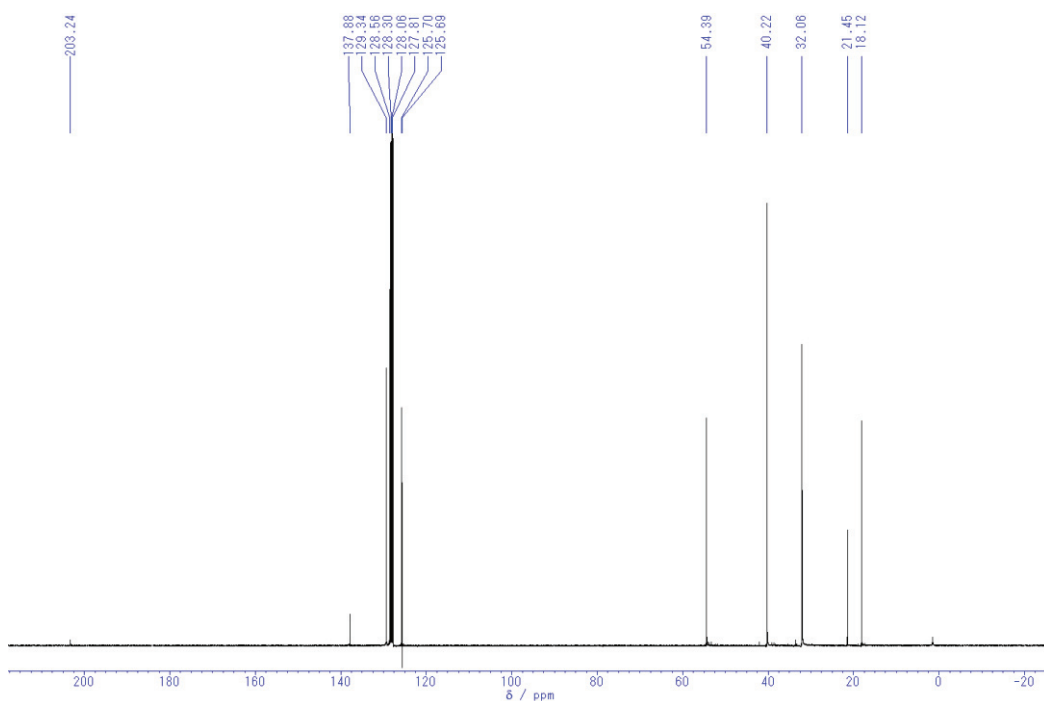


Figure S21. $^{13}\text{C}\{^1\text{H}\}$ NMR spectrum (100 MHz) of the crude product in C_6D_6 at room temperature.

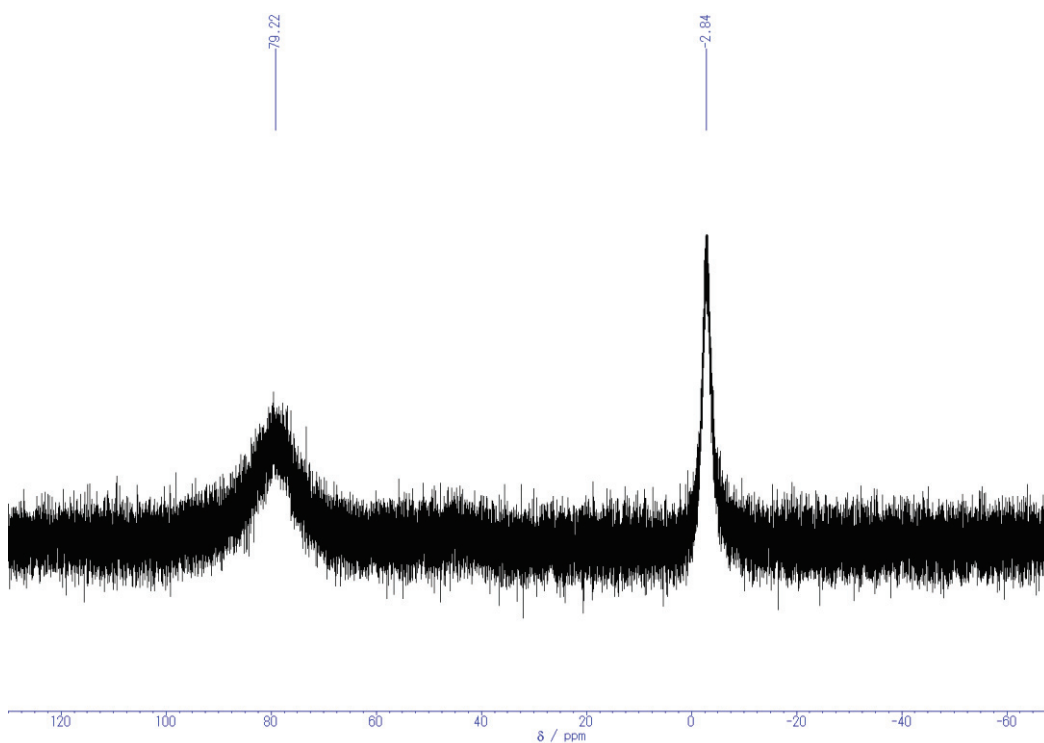


Figure S22. $^{11}\text{B}\{^1\text{H}\}$ NMR spectrum (128 MHz) of **18a** in toluene- d_8 at room temperature.

UV/Vis spectrometry

UV/Vis spectrum of 1.0 mM solution of **3** in hexane was recorded on DT-MINI-2-GS (Ocean Optics) in a glovebox filled with argon at room temperature. The obtained spectrum was illustrated in in Figure S23.

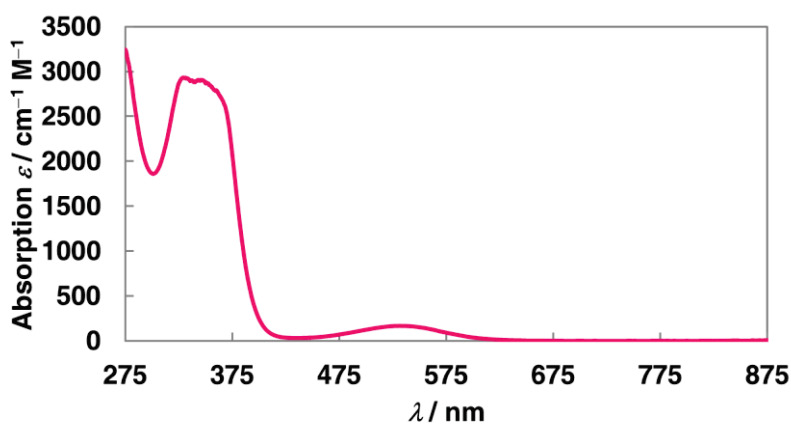


Figure S23. UV/Vis spectrum of **3** in hexane.

Cyclic Voltammetry

Cyclic voltammetric measurement of **3** (1.0 mM) was performed by using an ALS 600D potentiostat/galvanostat in THF solution containing 100 mM of $[n\text{Bu}_4\text{N}][\text{PF}_6]$ with a scan rate of 50 mV/s in a glovebox filled with argon at room temperature. A three electrode cell, which was equipped with a glassy carbon disk working electrode, a Pt wire counter electrode, and Ag/0.01 M AgNO₃ reference electrode, was used. The half wave potentials of **2** was compensated with that of ferrocene/ferrocenium redox cycle, which is +0.216 V (vs. Ag/Ag⁺). The cyclic voltammogram is illustrated in Figure S24.

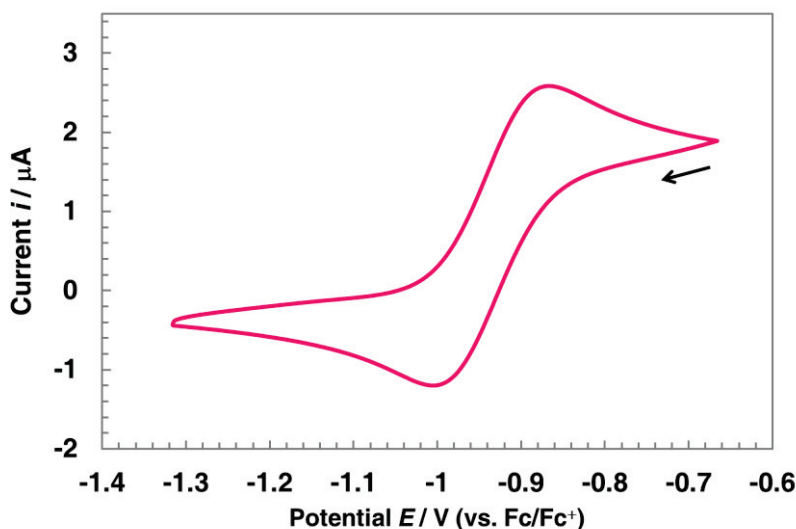


Figure S24. Cyclic voltammogram of a 1.0 mM solution of **3** in THF using 100 mM of $[n\text{Bu}_4\text{N}][\text{PF}_6]$ as the supporting electrolyte.

Crystal Structure Determination

Crystals suitable for X-ray structural determination were mounted on a *Bruker SMART APEXII* CCD diffractometer. Samples were irradiated with graphite monochromated Mo- $K\alpha$ radiation ($\lambda = 0.71073 \text{ \AA}$) at 173 K for data collection. The data were processed using the *APEX* program suite. All structures were solved by the *SHELXT* program (ver. 2014/5). Refinement on *F*² was carried out by full-matrix least-squares using the *SHELXL* in the *SHELX* software package (ver. 2014/7)⁶² and expanded using Fourier techniques. All non-hydrogen atoms were refined using anisotropic thermal parameters. The hydrogen atoms were assigned to idealized geometric positions and included in the refinement with isotropic thermal parameters. The *SHELXL* was interfaced with *ShelXle* GUI (ver. 742) for most of the refinement steps.⁶³ The pictures of molecules were prepared using *Pov-Ray* 3.7.0.⁶⁴

Chapter 4. Syntheses of Low Oxidation-State Boron Species and Their Reactivity

Table S1. Crystallographic data of **2**, **3** and **4**.

	2	3	4
Formula	C ₁₅ H ₂₆ BNCl ₂	C ₂₇ H ₅₄ B ₃ N ₃	C ₃₆ H ₇₂ B ₄ N ₄
Mol wt	302.08	453.18	604.24
Crystal system	monoclinic	monoclinic	orthorhombic
Space group	<i>P</i> 2 ₁ / <i>c</i>	<i>I</i> 2/ <i>a</i>	<i>F</i> dd2
Color	colorless	dark purple	yellow
Habit	Block	block	block
Cryst dimens, mm	0.136 × 0.124 × 0.058	0.292 × 0.151 × 0.071	0.231 × 0.082 × 0.062
<i>a</i> , Å	11.1018(14)	28.8885(19)	20.783(5)
<i>b</i> , Å	16.550(2)	11.4061(8)	32.639(7)
<i>c</i> , Å	8.8159(11)	52.932(5)	10.865(3)
<i>α</i> , deg	90	90	90
<i>β</i> , deg	102.720(2)	91.122(2)	90
<i>γ</i> , deg	90	90	90
<i>V</i> , Å ³	1580.1(3)	17438(2)	7370(3)
<i>Z</i>	4	24	8
<i>D</i> _{calc} , g cm ⁻³	1.270	1.036	1.089
Abs coeff, mm ⁻¹	0.398	0.058	0.061
<i>F</i> (000)	648	6048	2688
Temp, K	173(2)	173(2)	173(2)
Reflections	9061	46891	2129
Independent	3533	18652	2129
<i>R</i> _{int}	0.0190	0.0373	?
Parameters	172	928	208
<i>R</i> ₁ [<i>I</i> > 2σ(<i>I</i>)]	0.0326	0.0587	0.0786
<i>wR</i> ₂ (all data)	0.0857	0.1432	0.1973
Goodness of fit	1.035	1.043	1.064
solv for crystallization	hexane, -30 °C	hexane, -30 °C	hexane, -30 °C

CCDC-1560986 (**3**) and 1560987 (**4**) contain the supplementary crystallographic data. These data can be obtained free of charge from the Cambridge Crystallographic Data Centre via www.ccdc.cam.ac.uk/data_request/cif

Table S2. Crystallographic data of **5** and **6**.

	5	6
Formula	C ₂₆ H ₅₂ B ₂ Li ₂ N ₂ O ₂	C ₃₈ H ₆₈ B ₂ Li ₂ N ₂ O ₂
Mol wt	460.21	620.44
Crystal system	monoclinic	orthorhombic
Space group	<i>C2/c</i>	<i>Pbcn</i>
Color	colorless	colorless
Habit	block	block
Cryst dimens, mm	0.098 × 0.083 × 0.049	0.218 × 0.142 × 0.123
<i>a</i> , Å	22.360(2)	18.4770(17)
<i>b</i> , Å	9.4013(10)	10.8615(10)
<i>c</i> , Å	16.5222(17)	18.5761(17)
α , deg	90	90
β , deg	121.4890(10)	90
γ , deg	90	90
<i>V</i> , Å ³	2961.8(5)	3728.0(6)
<i>Z</i>	4	4
<i>D</i> _{calc} , g cm ⁻³	1.032	1.105
Abs coeff, mm ⁻¹	0.061	0.065
<i>F</i> (000)	1016	1368
Temp, K	173(2)	173(2)
Reflections	8344	20681
Independent	3292	4242
<i>R</i> _{int}	0.0189	0.0318
Parameters	204	254
<i>R</i> ₁ [<i>I</i> > 2σ(<i>I</i>)]	0.0490	0.0511
<i>wR</i> ₂ (all data)	0.1475	0.1509
Goodness of fit	1.043	1.054
solv for crystallization	THF, -30 °C	THF

CCDC-1560988 (**5**) contain the supplementary crystallographic data. These data can be obtained free of charge from the Cambridge Crystallographic Data Centre via www.ccdc.cam.ac.uk/data_request/cif

Table S3. Crystallographic data of **8** and **10**.

	8	10
Formula	C ₂₈ H ₄₄ B ₂ N ₂	C ₄₀ H ₆₀ B ₂ N ₂
Mol wt	430.27	590.52
Crystal system	monoclinic	monoclinic
Space group	<i>P2₁/c</i>	<i>P2₁/c</i>
Color	colorless	colorless
Habit	block	block
Cryst dimens, mm	0.237 × 0.184 × 0.163	0.141 × 0.078 × 0.025
<i>a</i> , Å	14.765(2)	17.9761(10)
<i>b</i> , Å	10.5347(14)	18.4993(10)
<i>c</i> , Å	17.297(2)	10.0847(6)
α , deg	90	90
β , deg	108.656(2)	93.6680(10)
γ , deg	90	90
<i>V</i> , Å ³	2549.1(6)	3346.7(3)
<i>Z</i>	4	4
<i>D</i> _{calc} , g cm ⁻³	1.121	1.172
Abs coeff, mm ⁻¹	0.063	0.066
<i>F</i> (000)	944	1296
Temp, K	173(2)	173(2)
Reflections	15100	18701
Independent	6059	7391
<i>R</i> _{int}	0.0257	0.0227
Parameters	297	397
<i>R</i> ₁ [<i>I</i> > 2σ(<i>I</i>)]	0.0439	0.0433
<i>wR</i> ₂ (all data)	0.1226	0.1094
Goodness of fit	1.051	1.028
solv for crystallization	hexane, toluene	hexane, -30 °C

Table S4. Crystallographic data of **11** and **12**.

	11	12
Formula	C ₃₂ H ₆₃ B ₃ N ₄	C ₃₇ H ₇₂ B ₃ N ₅
Mol wt	536.29	619.42
Crystal system	monoclinic	monoclinic
Space group	<i>P2₁/c</i>	<i>P2₁/c</i>
Color	colorless	yellow
Habit	block	block
Cryst dimens, mm	0.318 × 0.264 × 0.167	0.291 × 0.237 × 0.192
<i>a</i> , Å	11.4749(9)	11.4601(7)
<i>b</i> , Å	17.7259(14)	14.3085(9)
<i>c</i> , Å	16.5190(13)	23.4954(14)
<i>α</i> , deg	90	90
<i>β</i> , deg	93.5080(10)	94.1000(10)
<i>γ</i> , deg	90	90
<i>V</i> , Å ³	3353.7(5)	3842.8(4)
<i>Z</i>	4	4
<i>D</i> _{calc} , g cm ⁻³	1.062	1.071
Abs coeff, mm ⁻¹	0.060	0.061
<i>F</i> (000)	1192	1376
Temp, K	173(2)	173(2)
Reflections	18644	21948
Independent	7420	8528
<i>R</i> _{int}	0.0235	0.0200
Parameters	367	424
<i>R</i> ₁ [<i>I</i> > 2σ(<i>I</i>)]	0.0430	0.0428
<i>wR</i> ₂ (all data)	0.1206	0.1151
Goodness of fit	1.026	1.040
solv for crystallization	toluene, -30 °C	toluene, -30 °C

Table S5. Crystallographic data of **16a**, **16b** and **17**.

	16a	16b	17
Formula	C ₃₄ H ₆₀ B ₃ N ₃ O	C ₃₄ H ₅₉ B ₃ N ₃ OCl	C ₂₇ H ₅₄ B ₃ N ₃ Cl ₂
Mol wt	559.28	593.72	524.06
Crystal system	triclinic	triclinic	orthorhombic
Space group	<i>P</i> $\bar{1}$	<i>P</i> $\bar{1}$	<i>Pbca</i>
Color	colorless	colorless	colorless
Habit	block	block	block
Cryst dimens, mm	0.178 × 0.078 × 0.073	0.163 × 0.133 × 0.096	0.185 × 0.129 × 0.070
<i>a</i> , Å	8.9251(5)	8.8804(7)	14.8879(12)
<i>b</i> , Å	11.8795(7)	12.2199(10)	11.8412(9)
<i>c</i> , Å	16.1786(10)	16.4403(13)	33.911(3)
<i>α</i> , deg	85.4570(10)	88.3980(10)	90
<i>β</i> , deg	81.1190(10)	78.2730(10)	90
<i>γ</i> , deg	80.9100(10)	79.3030(10)	90
<i>V</i> , Å ³	1670.86(17)	1716.4(2)	5978.2(8)
<i>Z</i>	2	2	8
<i>D</i> _{calc} , g cm ⁻³	1.112	1.149	1.165
Abs coeff, mm ⁻¹	0.065	0.142	0.238
<i>F</i> (000)	616	648	2288
Temp, K	173(2)	173(2)	173(2)
Reflections	18995	8896	33658
Independent	7371	6545	7172
<i>R</i> _{int}	0.0168	0.0145	0.0280
Parameters	455	473	328
<i>R</i> ₁ [<i>I</i> > 2σ(<i>I</i>)]	0.0468	0.0427	0.0563
<i>wR</i> ₂ (all data)	0.1192	0.1065	0.1678
Goodness of fit	1.035	1.031	1.026
solv for crystallization	toluene, -30 °C	toluene, -30 °C	hexane

Table S6. Crystallographic data of **18a**, **19**.

	18a	19
Formula	C ₃₁ H ₆₄ B ₃ N ₃ Cl ₃ Ga	C ₂₉ H ₅₇ B ₃ F ₃ N ₃ O ₃ S
Mol wt	687.35	617.26
Crystal system	monoclinic	monoclinic
Space group	<i>P2₁/c</i>	<i>P2₁</i>
Color	yellow	yellow
Habit	block	block
Cryst dimens, mm	0.150 × 0.102 × 0.056	0.171 × 0.142 × 0.053
<i>a</i> , Å	10.8758(5)	8.5979(6)
<i>b</i> , Å	28.6889(13)	30.348(2)
<i>c</i> , Å	12.41086(6)	13.4042(9)
α , deg	90	90
β , deg	93.8540(10)	94.8560(10)
γ , deg	90	90
<i>V</i> , Å ³	3863.6(3)	3485.0(4)
<i>Z</i>	4	4
<i>D</i> _{calc} , g cm ⁻³	1.182	1.176
Abs coeff, mm ⁻¹	0.943	0.141
<i>F</i> (000)	1472	1336
Temp, K	173(2)	173(2)
Reflections	22660	20620
Independent	9121	15134
<i>R</i> _{int}	0.0235	0.0144
Parameters	703	783
<i>R</i> ₁ [<i>I</i> > 2σ(<i>I</i>)]	0.0412	0.0386
<i>wR</i> ₂ (all data)	0.1106	0.0939
Goodness of fit	1.041	1.034
solv for crystallization	THF, hexane, -30 °C	THF

Table S7. Crystallographic data of [TMP(H)₂][GaI₄] and [TMP(H)₂][Cl].

	[TMP(H) ₂][GaI ₄]	[TMP(H) ₂][Cl]
Formula	C ₉ H ₂₀ NGaI ₄	C ₉ H ₂₀ NCl
Mol wt	687.35	177.71
Crystal system	orthorhombic	orthorhombic
Space group	<i>Pca</i> 2 ₁	<i>Pnnm</i>
Color	colorless	colorless
Habit	needle	needle
Cryst dimens, mm	0.252 × 0.087 × 0.012	0.200 × 0.179 × 0.111
<i>a</i> , Å	14.7957(8)	9.8859(10)
<i>b</i> , Å	7.9916(4)	11.0289(12)
<i>c</i> , Å	16.0035(9)	9.7023(10)
α , deg	90	90
β , deg	90	90
γ , deg	90	90
<i>V</i> , Å ³	1892.27(18)	1057.85(19)
<i>Z</i>	4	4
<i>D</i> _{calc} , g cm ⁻³	2.526	1.116
Abs coeff, mm ⁻¹	7.960	0.308
<i>F</i> (000)	1296	392
Temp, K	173(2)	173(2)
Reflections	10810	5817
Independent	4456	1335
<i>R</i> _{int}	0.0248	0.0170
Parameters	149	63
<i>R</i> ₁ [<i>I</i> > 2σ(<i>I</i>)]	0.0214	0.0267
<i>wR</i> ₂ (all data)	0.0536	0.0814
Goodness of fit	1.038	1.136
solv for crystallization	THF, hexane, -30 °C	toluene

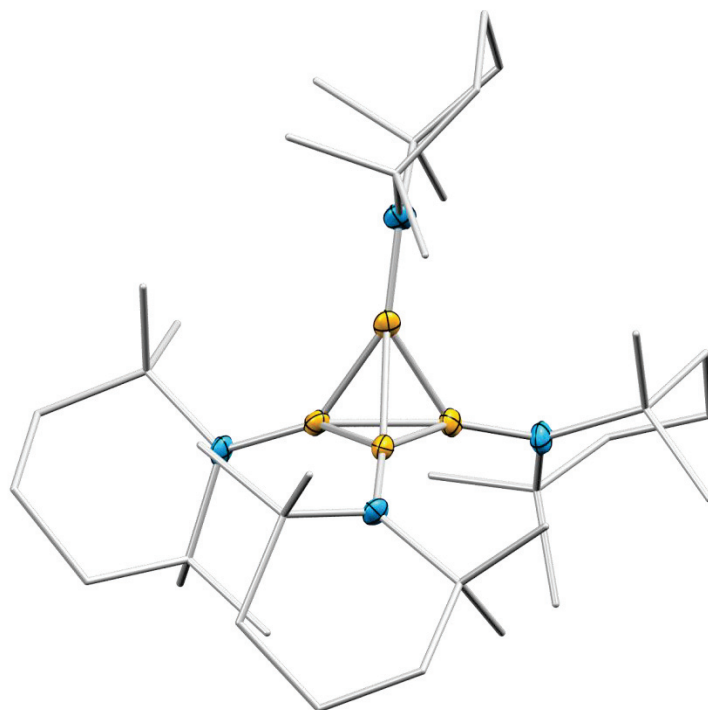


Figure S25. Molecular structure of **4** obtained from a single-crystal X-ray diffraction analysis. Thermal ellipsoids are displayed at 30% probability. Hydrogen atoms are omitted for clarity.

Molecular structure of **4** shown in Figure S13 was a same structure as the reported tetrahedral boron cluster.^{14b}

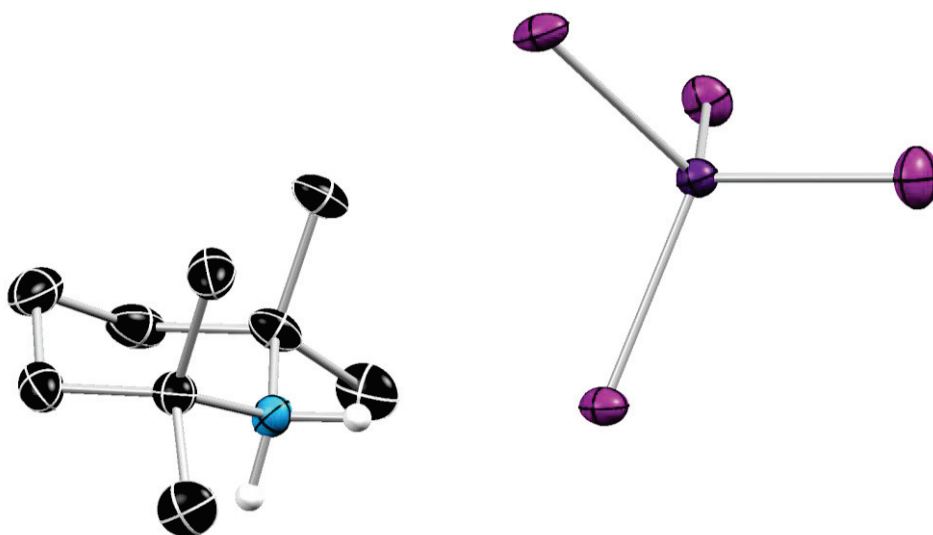


Figure S26. Molecular structure of [TMP(H)₂][GaI₄] obtained from a single-crystal X-ray diffraction analysis. Thermal ellipsoids are displayed at 30% probability. Hydrogen atoms expect for N-H are omitted for clarity.

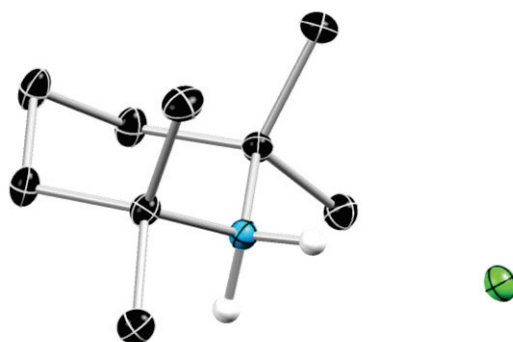


Figure S27. Molecular structure of $[\text{TMP}(\text{H})_2][\text{Cl}]$ obtained from a single-crystal X-ray diffraction analysis. Thermal ellipsoids are displayed at 30% probability. Hydrogen atoms except for *N*-H are omitted for clarity.

Computational Details

Structural Optimization

All calculations were performed in the gas phase using the *Gaussian 09* program package (Rev. B.01⁶⁵ for **3**^{opt}, **7** and **7**^{opt}, Rev. D.01⁶⁶ for allyl cation, B_3H_3 , **IV-TMP-A**, **IV-TMP-B**, **IV-CPC-A**, **IV-CPC-B**, $(\text{TMP-B})_4^{\text{opt}}$, $(\text{CPC-B})_4^{\text{opt}}$, **11**^{opt}, **12**^{opt}, **18**^{opt} and **19**^{opt}. The structure optimizations of **3**^{opt}, **11**^{opt} and **12**^{opt} were carried out with the B3LYP functional⁶⁷ using the 6-31G(d) basis set. The structure optimizations of **18**^{opt} and **19**^{opt} were carried out with the B3LYP functional using the 6-31+G(d) basis set. The structure optimizations of **IV-TMP-A**, **IV-TMP-B**, **IV-CPC-A**, **IV-CPC-B**, $(\text{TMP-B})_4^{\text{opt}}$ and $(\text{CPC-B})_4^{\text{opt}}$ were carried out with the B3LYP functional using the 6-311G(d,p) basis set for the H atoms and TZVP basis set for the C, B, N atoms (Figure S29). The other structure optimizations were carried out with the B3LYP functional using the 6-31++G(d,p) basis set. For diaminodiborenes, the HF/6-31G(d) level of theory was used for geometry pre-optimization. Structure optimizations of **3**, **4**, **11**, **12**, **18a** and **19** obtained from single-crystal X-ray diffraction analyses provided **3**^{opt}, $(\text{TMP-B})_4^{\text{opt}}$, **11**^{opt}, **12**^{opt}, **18**^{opt} and **19**^{opt}, respectively (Figure S28a, S29e, S30a, S30b, S30c and S30d). The molecular structures of **3** and **4**²⁰ obtained from single-crystal X-ray diffraction analyses were used as initial structures of a model compound in which TMP substituents were replaced by *N,N*-dimethylamino substituents and of $(\text{CPC-B})_4^{\text{opt}}$ in which TMP substituents were replaced by CPC-substituents. A structure optimization of the model compound using fixed coordinates of C, N and B without any symmetry assumptions provided **7** (Figure S28b). A structure optimization of the model compound without any fixed coordinates and symmetry assumptions provided **7**^{opt} (Figure S28c). The allyl cation $[\text{C}_3\text{H}_3]^+$ was structurally optimized without any symmetry assumptions (Figure S28d). The B_3H_3 molecule was optimized with C_{2v} symmetry (Figure S28e). After each geometry optimization, a frequency

calculation at the same level was performed to verify that all the stationary points had no imaginary frequency. Selected frontier orbitals of 3^{opt} , **7** and 7^{opt} were shown in Figure S31 and S32, Figure S33 and Figure S34, respectively.

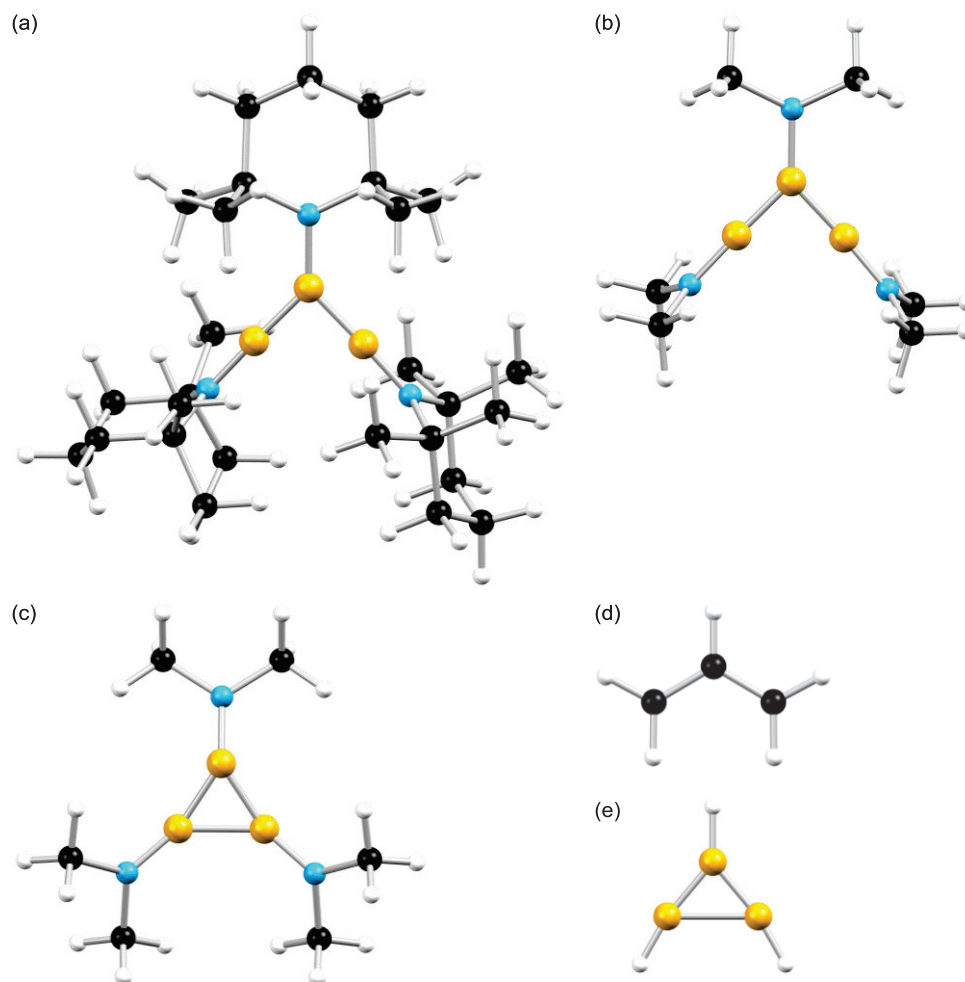


Figure S28. Calculated molecular structures of (a) 3^{opt} , (b) **7**, (c) 7^{opt} , (d) allyl cation and (e) C_{2v} -symmetric B_3H_3 .

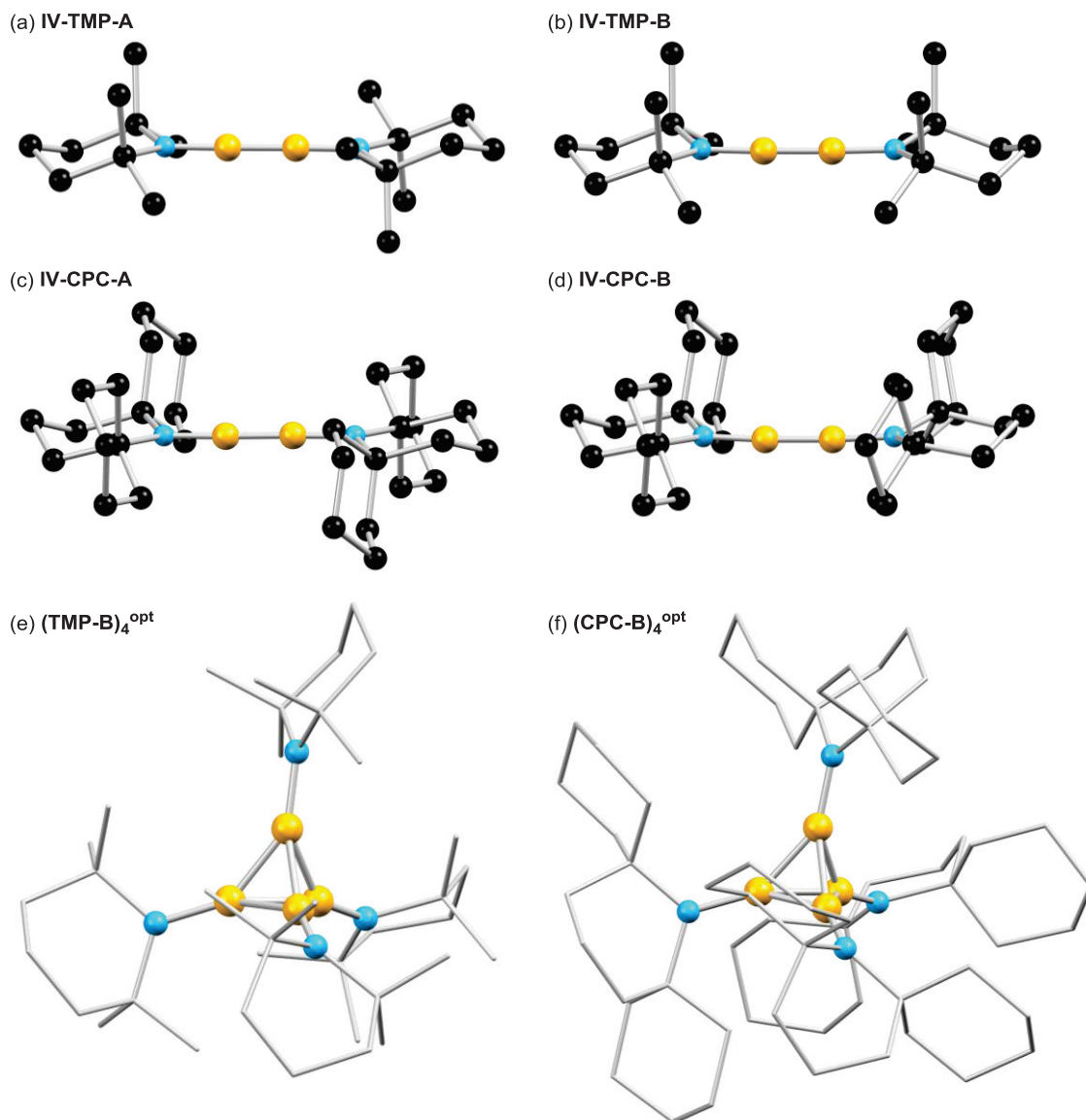


Figure S29. Calculated molecular structures of (a) IV-TMP-A, (b) IV-TMP-B, (c) IV-CPC-A, (d) IV-CPC-B, (e) (TMP-B)₄^{opt} and (f) (CPC-B)₄^{opt}.

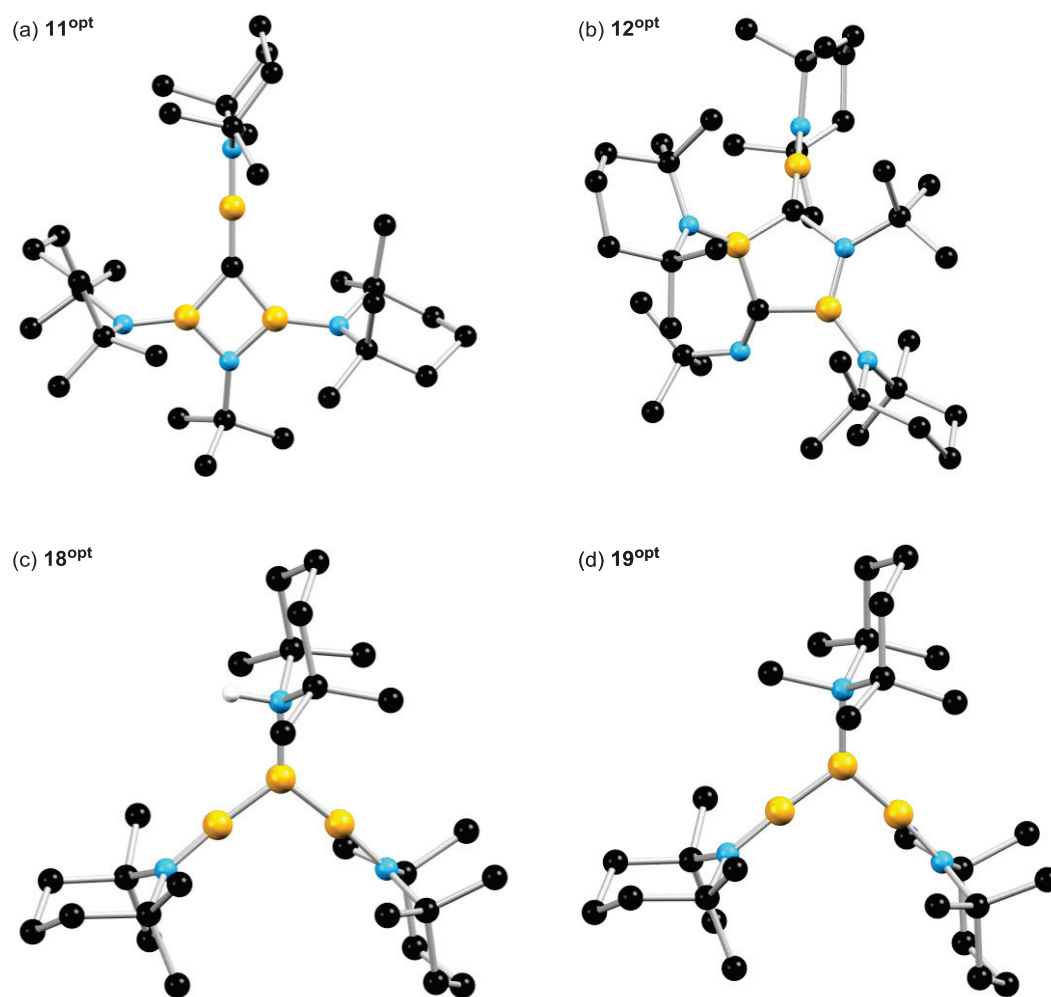


Figure S30. Calculated molecular structures of (a) 11^{opt} , (b) 12^{opt} , (c) 18^{opt} and (d) 19^{opt} .

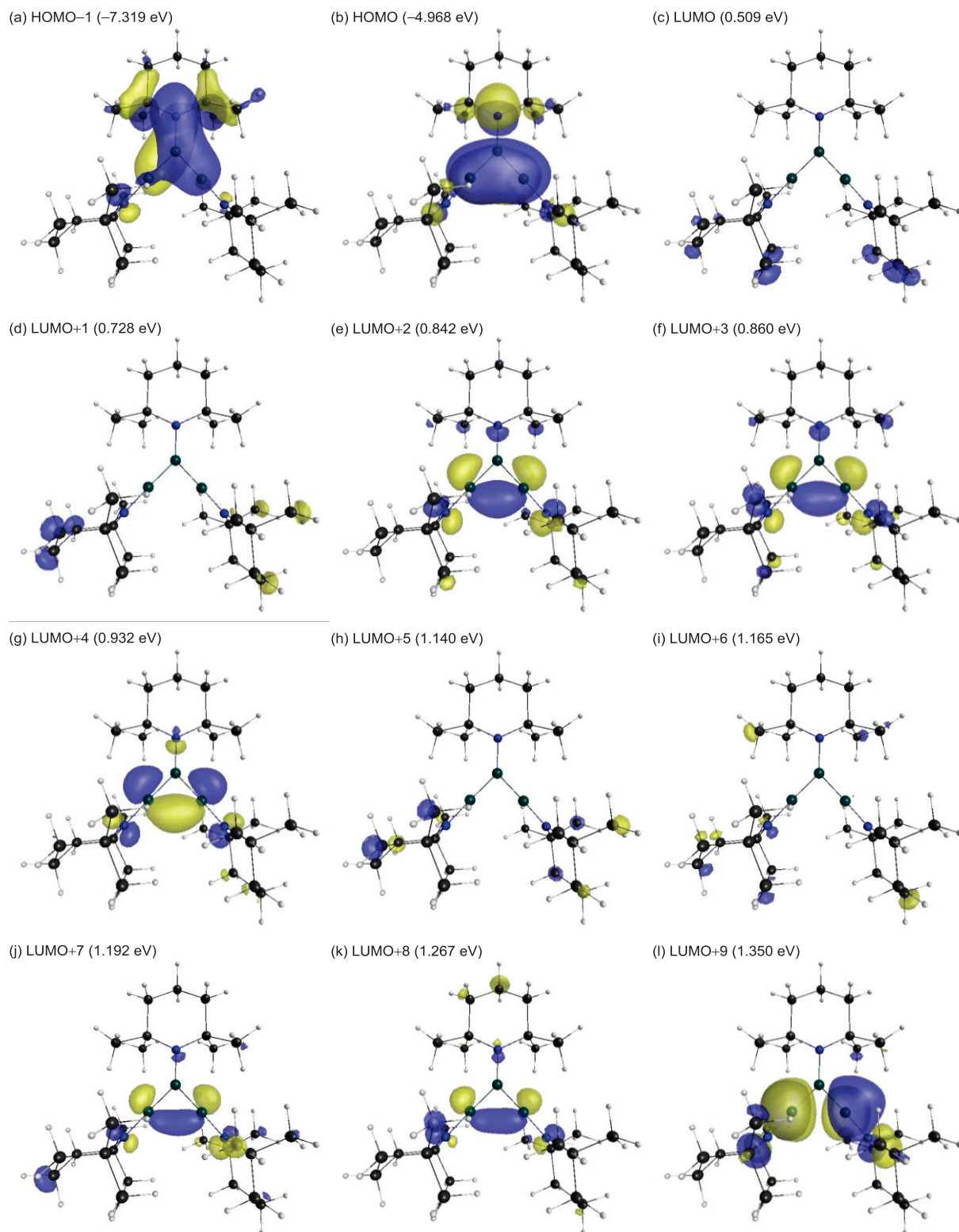


Figure S31. Selected frontier orbitals of 3^{opt} at the CAM-B3LYP/6-31+G(d) level of theory.

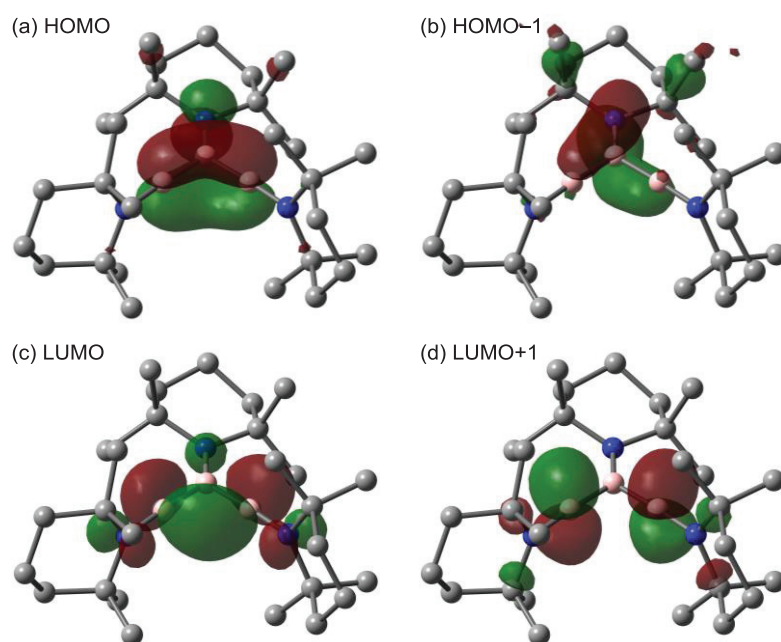


Figure S32. Selected frontier orbitals of 3^{opt} at the B3LYP/6-31G(d) level of theory.

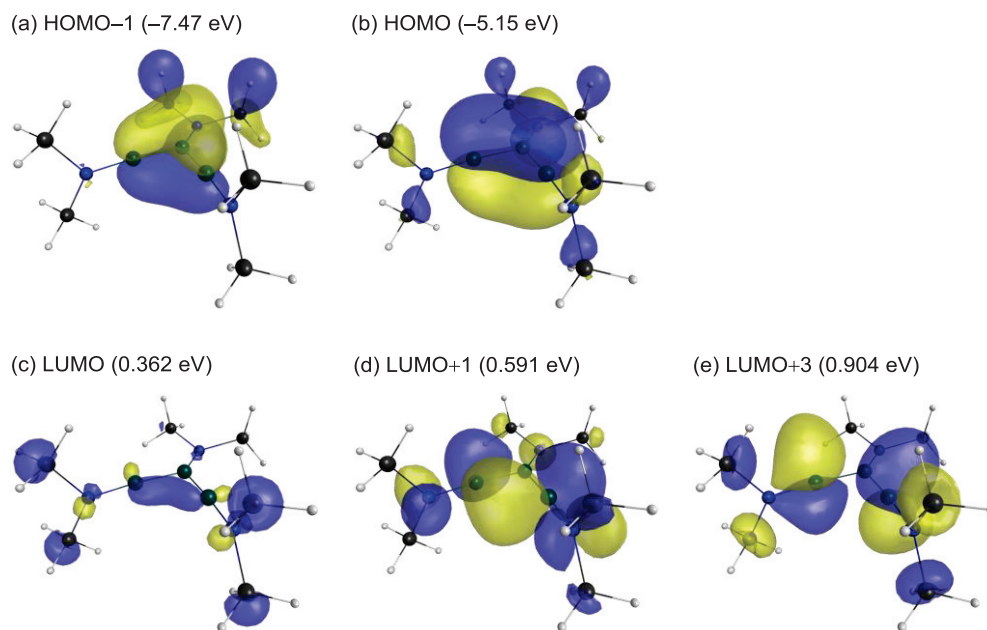


Figure S33. Selected frontier orbitals of **7** at the CAM-B3LYP/6-31+G(d) level of theory.

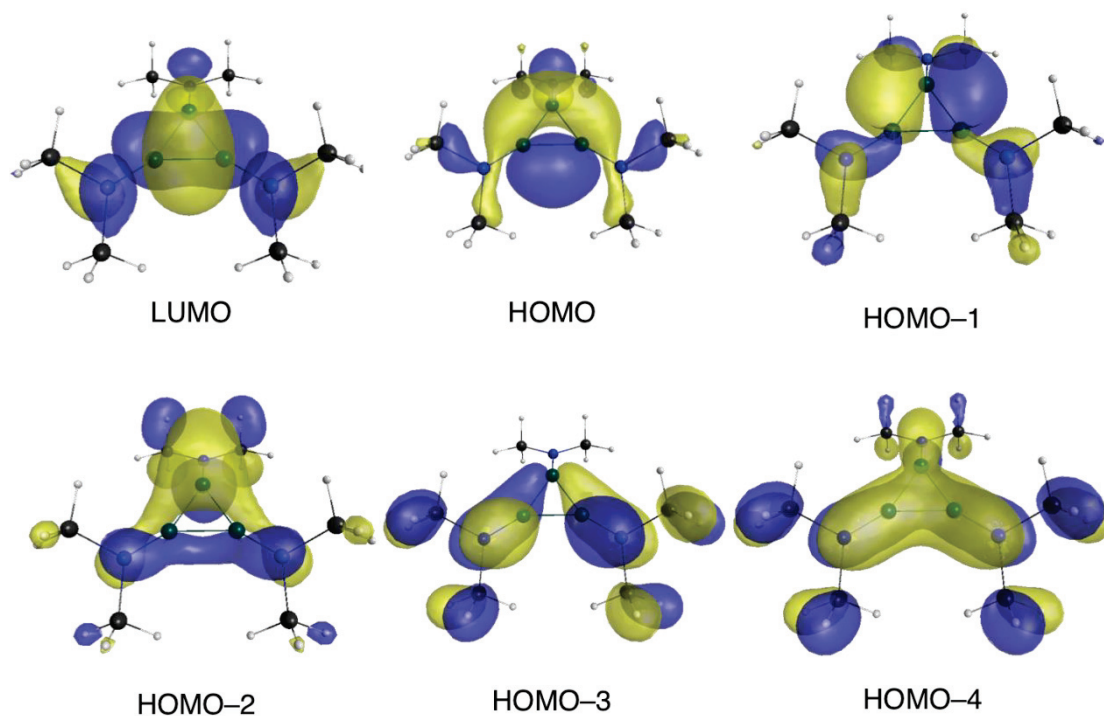


Figure S34. Selected frontier orbitals of **7^{opt}** at the CAM-B3LYP/6-31+G(d) level of theory.

GIAO Calculations

All calculations were performed in the gas phase using the *Gaussian 09* program package (Rev. D.01).⁶⁶ The ¹¹B chemical shifts calculated by Gauge-independent atomic orbital (GIAO) method at the B3LYP/6-311+G(2d,p) level of theory for **3**^{opt}, **7**, **7**^{opt}, **11**^{opt}, **12**^{opt}, **18**^{opt} and B₃H₃ (C_{2v}) were compared with the value of B₂H₆ in GaussView (ver. 5.0: B3LYP/6-311+G(2d,p)). The obtained chemical shifts were corrected based on the chemical shift of B₂H₆ ($\delta_B = 16.6$ ppm) using BF₃·OEt₂ as the reference compound (Table S8).⁶⁸

Table S8. Calculated ¹¹B chemical shifts of **3**, **3**^{opt}, **7**, **7**^{opt}, **11**^{opt}, **12**^{opt}, **18a**, **18**^{opt}, **19**, **19**^{opt} and B₃H₃ (C_{2v}) based on BF₃·OEt₂ as the standard.

	δ_B (ppm)	average (ppm)
3	51.7 ^a (77.6, -4.8) ^b	
3 ^{opt}	86.3, 86.1, -8.0	54.8
7	86.0, 83.9, -11.5	52.8
7 ^{opt}	79.5, 79.5, 38.8	65.9
11 ^a	43.3	
11 ^{opt}	42.3, 44.3, 42.1	
12 ^a	53.9, 49.6, 32.4	
12 ^{opt}	53.7, 51.5, 31.7	
18a ^a	79.2, -2.8	
18 ^{opt}	80.9, 80.0, -4.2	
19 ^a	76.2, -3.6	
19 ^{opt}	79.4, 74.83, 1.66	
B₃H₃ (C_{2v})	165.7, 165.7, -3.5	109.3

^a Experimental datum in C₆D₆ at room temperature. ^b Experimental data in toluene-*d*₈ at -80 °C.

TD-DFT Calculations

All calculations were performed in the gas phase using the *Gaussian 09* program package (Rev. B.01).⁶⁵ Time-dependent density functional theory (TD-DFT)⁶⁹ calculations of **3^{opt}** and **3** was achieved with the CAM-B3LYP⁷⁰ functional using 6-31+G(d) basis set. The results for TD-DFT calculations are summarized in Table S9 and Table S10.

Table S9. Calculated wavelengths for absorption spectrum of **3^{opt}**, their oscillator strengths, and the associated transitions with |CI coefficient| > 0.2.

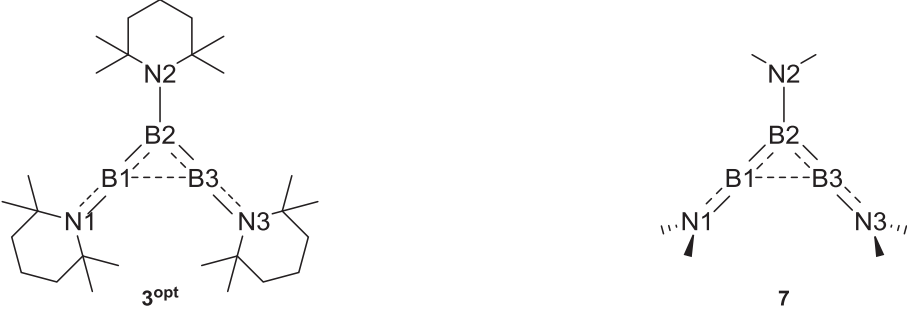
wavelengths (nm)	oscillator strengths	MO contributions	CI coefficients
296	0.0020	HOMO → LUMO	-0.26122
		HOMO → LUMO+2	0.37771
		HOMO → LUMO+3	0.21482
		HOMO → LUMO+4	0.40882
297	0.0011	HOMO → LUMO+2	-0.39255
		HOMO → LUMO+3	0.51114
		HOMO → LUMO+10	-0.22117
321	0.0013	HOMO → LUMO	0.62822
333	0.1568	HOMO → LUMO+9	0.63867
557	0.0010	HOMO → LUMO+2	0.36124
		HOMO → LUMO+3	0.32890
		HOMO → LUMO+4	-0.35137
		HOMO → LUMO+7	0.21513

Table S10. Calculated wavelengths for absorption spectrum of **7**, their oscillator strengths, and the associated transitions with |CI coefficient| > 0.2.

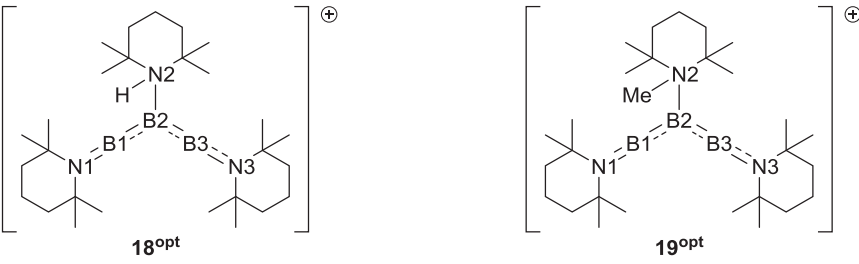
wavelengths (nm)	oscillator strengths	MO contributions	CI coefficients
298	0.0131	HOMO → LUMO+1	0.29584
		HOMO → LUMO+4	0.50044
		HOMO → LUMO+5	0.31189
308	0.0002	HOMO → LUMO+2	0.64143
		HOMO → LUMO+6	-0.22553
335	0.1544	HOMO → LUMO+3	0.63530
355	0.0667	HOMO → LUMO	0.61487
564	0.0035	HOMO → LUMO	-0.24185
		HOMO → LUMO+1	0.57976

NBO Analysis and NRT Analysis

All calculations were performed in the gas phase using the *Gaussian 09* program package (Rev. B.01).⁶⁵ Wiberg bond indices (WBIs) and natural charges of **3^{opt}**, **7**, **18^{opt}** and **19^{opt}** were obtained from natural bond orbital (NBO) analysis using the *NBO 3.1* program⁷¹ at the CAM-B3LYP/6-31+G(d) level of theory (Table S11, S12). Natural resonance theory (NRT) calculations of **7** and **7^{opt}** were performed at the same level of theory using the *NBO 5.9* program (Figure S35).⁷²

Table S11. Selected WBIs and natural charges of **3^{opt}** and **7**.


		WBIs		Natural charges				WBIs		Natural charges			
3^{opt}	B1–B2	1.36	B1	0.81	7	B1–B2	1.36	B1	0.623	B2–B3	1.36	B2	–0.335
	B2–B3	1.36	B2	–0.57		B1···B3	0.53	B3	0.622	N1–B1	1.10	NMe ₂ (1)	–0.286
	B1···B3	0.42	B3	0.81		N2–B2	0.89	NMe ₂ (2)	–0.336				
	N1–B1	0.98	N1	–0.85		N3–B3	1.09	NMe ₂ (3)	–0.288				
	N2–B2	0.84	N2	–0.73									
	N3–B3	0.98	N3	–0.85									

Table S12. Selected WBIs and natural charges of **18^{opt}** and **19^{opt}**.


		WBIs		Natural charges				WBIs		Natural charges			
18^{opt}	B1–B2	1.39	B1	0.98	19^{opt}	B1–B2	1.38	B1	1.01	B2–B3	1.38	B2	–0.88
	B2–B3	1.39	B2	–0.86		B1···B3	0.21	B3	1.02	N1–B1	1.00	N1	–0.88
	B1···B3	0.21	B3	1.01		N2–B2	0.66	N2	–0.50				
	N1–B1	1.05	N1	–0.85		N3–B3	0.98	N3	–0.89				
	N2–B2	0.68	N2	–0.63									
	N3–B3	1.00	N3	–0.88									

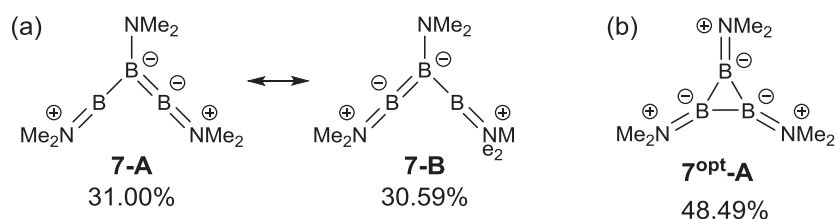


Figure S35. Selected main resonance structures of (a) **7** and (b) **7^{opt}** with their relative weights estimated by NRT calculations.

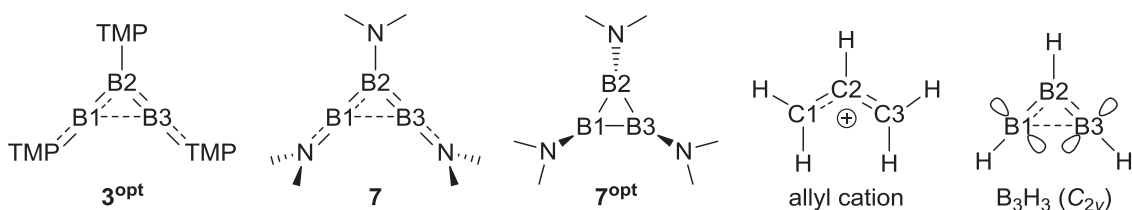
The 3c-2e π -bond was also confirmed by the natural resonance theory (NRT) calculation of **7** at the CAM-B3LYP/6-31+G(d) level of theory. Classical π -resonance between the central and terminal boron atoms were observed as similar weights, and N–B double bonds were only in terminal moieties.

NICS Calculations

All calculations were performed in the gas phase using the *Gaussian 09* program package (Rev. D.01).⁶⁶ Nucleus-independent chemical shift (NICS) calculations were carried out at the B3LYP/6-311+G(d,p) level of theory using the GIAO method. The magnetic shielding tensors computed in the center of the B₃ planes in **3^{opt}**, **7**, **7^{opt}**, **18^{opt}** and B₃H₃ (C_{2v}) or C₃ plane in allyl cation [NICS(0)], as well as 1 Å above those planes. The NICS values were calculated from the following functional (Table S13):

$$\text{NICS}(0 \text{ or } 1) = [\text{isotropic magnetic shielding tensor (ppm)}] \times (-1)$$

Table S13. NICS values and selected atomic distances of **3**, **3^{opt}**, **7**, **7^{opt}**, **18**, **18^{opt}** allyl cation and C_{2v}-symmetric B₃H₃.



	NICS values (ppm)		atomic distances (Å)					
	NICS (0)	NICS (1)	B1–B2	B2–B3	B1…B3			
3			B1–B2 ^a	1.561	B2–B3 ^a	1.558	B1…B3 ^a	2.177
3^{opt}	–14.0	–12.5	B1–B2	1.568	B2–B3	1.570	B1…B3	2.196
7	–14.4	–12.4	B1–B2	1.555	B2–B3	1.562	B1…B3	2.164
7^{opt}	8.9	–6.1	B1–B2	1.629	B2–B3	1.629	B1…B3	1.763

18a			B1–B2	1.561	B2–B3	1.558	B1⋯B3	2.409
18^{opt}	-16.2	-13.0	B1–B2	1.567	B2–B3	1.561	B1⋯B3	2.472
allyl cation	3.8	-12.4	C1–C2	1.385	C2–C3	1.385	C1⋯C3	2.384
B₃H₃ (C_{2v})^b	-16.2	-11.8	B1–B2	1.527	B2–B3	1.527	B1⋯B3	1.965

^a Average values estimated by a single-crystal X-ray diffraction. ^b C_{2v}-symmetric B₃H₃ is a local minimum. For a detailed discussion, see Ref. [27, 73].

Diradical Character

All calculations were performed in the gas phase using the *Gaussian 09* program package (Rev. B.01).⁶⁵ The diradical characters y^{40} of **3^{opt}** and **7** was estimated using spin projected (P)UHF method with 6-31+G(d) basis. The highest occupied natural orbital (HONO), lowest unoccupied natural orbital (LUNO) and spin density at the UHF/6-31+G(d) level of theory were shown in Figure S36.

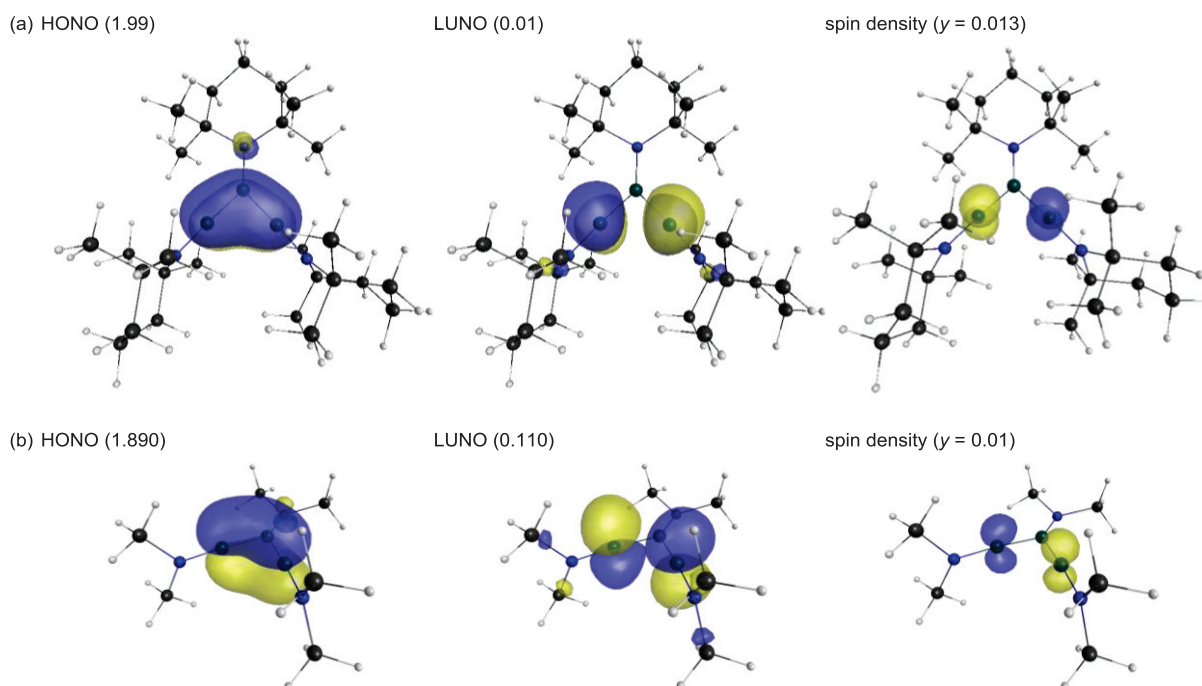
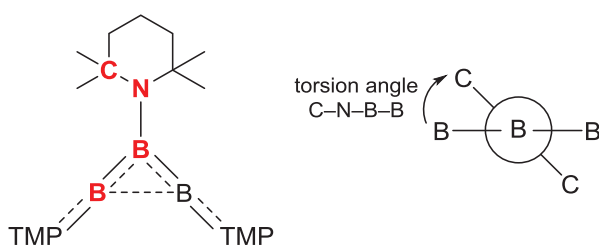


Figure S36. Selected natural orbitals and spin densities of (a) **3^{opt}** and (b) **7** at the UHF/6-31+G(d) level of theory. The natural orbitals and spin densities are drawn with a contour value of 0.05 and 0.01 atomic units respectively. The associated occupancies using the spin projected (P)UHF method with 6-31+G(d) are shown in parentheses.

Rotational Energies

All calculations were performed in the gas phase using the *Gaussian 09* program package (Rev. B.01).⁶⁵ The molecular structure of $\mathbf{3}^{\text{opt}}$ was used as initial structures of rotated structures with fixed torsion angles C–N–B–B of 111 ° and 201 ° ($\mathbf{3}^{\text{opt-90}}$ and $\mathbf{3}^{\text{opt-180}}$, respectively). From the optimized structure $\mathbf{3}^{\text{opt}}$, single point energy calculations were performed after rotating the central TMP-substituents 90 ° and 180 ° along the N2–B2 bond. All energies (a.u.) were estimated without zero-point energy corrections.

Table S14. Rotational energies of $\mathbf{3}^{\text{opt}}$ around the central N–B bond.



	torsion angles (°)	rotational angles (°)	energies (a.u.)	relative energies (kcal/mol)
$\mathbf{3}^{\text{opt}}$	21	0	-1300.22874745	0
$\mathbf{3}^{\text{opt-90}}$	111	90	-1300.21895043	6.15
$\mathbf{3}^{\text{opt-180}}$	201	180	-1300.22525106	2.19

References

- [1]. Neeve, E. C.; Geier, S. J.; Mkhaliid, I. A. I.; Westcott, S. A.; Marder, T. B. *Chem. Rev.* **2016**, *116*, 9091–9161.
- [2]. Stock, A.; Brandt, A.; Fischer, H. *Ber. Dtsch. Chem. Ges. B* **1925**, *58*, 643–657.
- [3]. For a recent review, see: Soleilhavoup, M.; Bertrand, G. *Angew. Chem. Int. Ed.* **2017**, *56*, 10282–10292; *Angew. Chem.* **2017**, *129*, 10416–10426.
- [4]. (a) Kinjo, R.; Donnadiou, B.; Celik, M. A.; Frenking, G.; Bertrand, G. *Science* **2011**, *333*, 610–613.
(b) Ruiz, D. A.; Melaimi, M.; Bertrand, G. *Chem. Commun.* **2014**, *50*, 7837–7839
(c) L. Kong, Y. Li, R. Ganguly, D. Vidovic, R. Kinjo, *Angew. Chem. Int. Ed.* **2014**, *53*, 9280–9283; *Angew. Chem.* **2014**, *126*, 9434–9437.
(d) Dahcheh, F.; Martin, D.; Stephan, D.W.; Bertrand, G. *Angew. Chem. Int. Ed.* **2014**, *53*, 13159–13163; *Angew. Chem.* **2014**, *126*, 13375–13379.
(e) Böchnke, J.; Braunschweig, H.; Dellermann, T.; Ewing, W. C.; Kramer, T.; Krummenacher, I.; Vargas, A. *Angew. Chem. Int. Ed.* **2015**, *54*, 4469–4473; *Angew. Chem.* **2015**, *127*, 4551–4555.
(f) Wang, H.; Zhang, J.; Lin, Z.; Xie, Z. *Chem. Commun.* **2015**, *51*, 16817–16820
(g) Braunschweig, H.; Dewhurst, R. D.; Hupp, F.; Nutz, M.; Radacki, K.; Tate, C. W.; Vargas, A.; Ye, Q. *Nature* **2015**, *522*, 327–330.
(h) Arrowsmith, M.; Auerhammer, D.; Bertermann, R.; Braunschweig, H.; Bringmann, G.; Celik, M. A.; Dewhurst, R. D.; Finze, M.; Grüne, M.; Hailmann, M.; Hertle, T.; Krummenacher, I. *Angew. Chem. Int. Ed.* **2016**, *55*, 14464–14468; *Angew. Chem.* **2016**, *128*, 14680–14684.
(i) Braunschweig, H.; Celik, M. A.; Dewhurst, R. D.; Ferkinghoff, K.; Hermann, A.; Jimenez-Halla, J. O. C.; Kramer, T.; Radacki, K.; Shang, R.; Siedler, E.; Weißenberger, F.; Werner, C. *Chem. Eur. J.* **2016**, *22*, 11736–11744.
(j) Kong, L.; Ganguly, R.; Li, Y.; Kinjo, R. *Chem. Eur. J.* **2016**, *22*, 1922–1925.
(k) Ledet, A. D.; Hudnall, T. W. *Dalton Trans.* **2016**, *45*, 9820–9826.
(l) Rosas-Sánchez, A.; Alvarado-Beltran, I.; Baceiredo, A.; Hashizume, D.; Saffon-Merceron, N.; Branchadell, V.; Kato, T. *Angew. Chem. Int. Ed.* **2017**, *56*, 4814–4818; *Angew. Chem.* **2017**, *129*, 4892–4896.
(m) Arrowsmith, M.; Auerhammer, D.; Bertermann, R.; Braunschweig, H.; Celik, M. A.; Erdmannsdörfer, J.; Krummenacher, I.; Kupfer, T. *Angew. Chem. Int. Ed.* **2017**, *56*, 11263–11267; *Angew. Chem.* **2017**, *129*, 11417–11421.
(n) Rosas-Sánchez, A.; Alvarado-Beltran, I.; Baceiredo, A.; Saffon-Merceron, N.; Massou, S.; Branchadell, V.; Kato, T. *Angew. Chem. Int. Ed.* **2017**, *56*, 10549–10554; *Angew. Chem.* **2017**, *129*, 10685–10690.

- (o)
- [5]. For a recent review, see: Arrowsmith, M.; Braunschweig, H.; Stennett, T. E. *Angew. Chem. Int. Ed.* **2017**, *56*, 96–115; *Angew. Chem.* **2017**, *129*, 100–120.
- [6]. (a) Wang, Y.; Quillian, B.; Wei, P.; Wannere, C. S.; Xie, Y.; King, R. B.; Schaefer, III, H. F.; Schleyer, P. von R.; Robinson, G. H. *J. Am. Chem. Soc.* **2007**, *129*, 12412–12413.
(b) Wang, Y.; Quillian, B.; Wei, P.; Xie, Y.; Wannere, C. S.; King, R. B.; Schaefer, III, H. F.; Schleyer, P. von R.; Robinson, G. H. *J. Am. Chem. Soc.* **2008**, *130*, 3298–3299.
(c) Bissinger, P.; Braunschweig, H.; Damme, A.; Kupfer, T.; Vargas, A. *Angew. Chem. Int. Ed.* **2012**, *51*, 9931–9934; *Angew. Chem.* **2012**, *124*, 10069–10073.
(d) Braunschweig, H.; Dewhurst, R. D.; Hammond, K.; Mies, J.; Radacki, K.; Vargas, A. *Science* **2012**, *336*, 1420–1422.
(e) Braunschweig, H.; Dewhurst, R. D.; Hörl, C.; Phukan, A. K.; Pinzner, F.; Ullrich, S. *Angew. Chem. Int. Ed.* **2014**, *53*, 3241–3244; *Angew. Chem.* **2014**, *126*, 3305–3308.
(f) Bissinger, P.; Braunschweig, H.; Damme, A.; Kupfer, T.; Krummenacher, I.; Vargas, A. *Angew. Chem. Int. Ed.* **2014**, *53*, 5689–5693; *Angew. Chem.* **2014**, *126*, 5797–5801.
(g) Bissinger, P.; Braunschweig, H.; Damme, A.; Hörl, C.; Krummenacher, I.; Kupfer, T. *Angew. Chem. Int. Ed.* **2015**, *54*, 359–362; *Angew. Chem.* **2015**, *127*, 366–369.
(h) Ref. [4e]
(i) Bissinger, P.; Braunschweig, H.; Celik, M. A.; Claes, C.; Dewhurst, R. D.; Endres, S.; Kelch, H.; Kramer, T.; Krummenacher, I.; Schneider, C. *Chem. Commun.* **2015**, *51*, 15917–15920.
(j) Arrowsmith, M.; Böhnke, J.; Braunschweig, H.; Celik, M. A.; Dellermann, T.; Hammond, K. *Chem. Eur. J.* **2016**, *22*, 17169–17172.
(k) Lu, W.; Li, Y.; Ganguly, R.; Kinjo, R. *J. Am. Chem. Soc.* **2017**, *139*, 5047–5050.
(l) Braunschweig, H.; Krummenacher, I.; Lichtenberg, C.; Mattock, J. D.; Schäfer, M.; Schmidt, U.; Schneider, C.; Steffenhagen, T.; Ullrich, S.; Vargas, A. *Angew. Chem. Int. Ed.* **2017**, *56*, 889–892; *Angew. Chem.* **2017**, *129*, 907–911.
(m) Wang, S. R.; Arrowsmith, M.; Böhnke, J.; Braunschweig, H.; Dellermann, T.; Dewhurst, R. D.; Kelch, H.; Krummenacher, I.; Mattock, J. D.; Müssig, J. H.; Thiess, T.; Vargas, A.; Zhang, J. *Angew. Chem. Int. Ed.* **2017**, *56*, 8009–8013; *Angew. Chem.* **2017**, *129*, 8122–8126.
(n) Lu, W.; Li, Y.; Ganguly, R.; Kinjo, R. *Angew. Chem. Int. Ed.* **2017**, *56*, 9829–9832; *Angew. Chem.* **2017**, *129*, 9961–9964.
- [7]. For borylenes with reactivities similar to those of amines and phosphines, see:
(a) Ref. [4a].
(b) Ref. [4c].
(c) Kong, L.; Ganguly, R.; Li, Y.; Kinjo, R. *Chem. Sci.* **2015**, *6*, 2893–2902.
(d) Braunschweig, H.; Dewhurst, R. D.; Pentecost, L.; Radacki, K.; Vargas, A.; Ye, Q. *Angew.*

- Chem. Int. Ed.* **2016**, *55*, 436–440; *Angew. Chem.* **2016**, *128*, 447–451.
- (e) Kong, L.; Lu, W.; Yongxin, L.; Ganguly, R.; Kinjo, R. *Inorg. Chem.* **2017**, *56*, 5586–5593.
- (f) Ref. [41].
- [8]. For one-electron-oxidation reactions of borylenes, see:
- (a) Ref. [4a].
- (b) Wang, H.; Zhang, J.; Lin, Z.; Xie, Z. *Organometallics* **2016**, *35*, 2579–2582.
- (c) Kong, L.; Lu, W.; Li, Y.; Ganguly, R.; Kinjo, R. *J. Am. Chem. Soc.* **2016**, *138*, 8623–8629.
- [9]. For side-on coordination of diborenes and a diboryne to coinage metals, see:
- (a) Braunschweig, H.; Damme, A.; Dewhurst, R. D.; Vargas, A. *Nat. Chem.* **2013**, *5*, 115–121.
- (b) Brand, J.; Braunschweig, H.; Sen, S. S. *Acc. Chem. Res.* **2014**, *47*, 180–191.
- (c) Bissinger, P.; Steffen, A.; Vargas, A.; Dewhurst, R. D.; Damme, A.; Braunschweig, H. *Angew. Chem. Int. Ed.* **2015**, *54*, 4362–4366; *Angew. Chem.* **2015**, *127*, 4436–4440.
- (d) Arnold, N.; Braunschweig, H.; Dewhurst, R. D.; Ewing, W. C. *J. Am. Chem. Soc.* **2016**, *138*, 76–79.
- (e) Braunschweig, H.; Dellermann, T.; Dewhurst, R. D.; Hupp, B.; Kramer, T.; Mattock, J. D.; Mies, J.; Phukan, A. K.; Steffen, A.; Vargas, A. *J. Am. Chem. Soc.* **2017**, *139*, 4887–4893.
- (d) Wang, S. R.; Arrowsmith, M.; Braunschweig, H.; Dewhurst, R. D.; Dömling, M.; Mattock, J. D.; Pranckevicius, C.; Vargas, A. *J. Am. Chem. Soc.* **2017**, *139*, 10661–10664.
- [10]. For one-electron-oxidation reactions of diborenes, see: (a) Ref. [6f]. (b) Ref. [6g].
- [11]. (a) Jouany, C.; Barthelat, J. C.; Daudey, J. P. *Chem. Phys. Lett.* **1987**, *136*, 52–56.
- (b) Timoshkin, A. Y.; Schaefer, III, H. F. *J. Phys. Chem. A* **2008**, *112*, 13180–13196.
- [12]. Gu, S.-Y.; Sheu, J.-H.; Su, M.-D. *Inorg. Chem.* **2007**, *46*, 2028–2034.
- [13]. McKee, M. L. *Inorg. Chem.* **1999**, *38*, 321–330.
- [14]. For attempts to isolate diaminodiborenes **IV**, see:
- (a) Meller, A.; Maringgele, W. in *Advances in Boron Chemistry* (Ed.: W. Siebert), The Royal Society of Chemistry, Cambridge, **1997**, *201*, pp. 224–231.
- (b) Maier, C.-J.; Pritzkow, H.; Siebert, W. *Angew. Chem. Int. Ed.* **1999**, *38*, 1666–1668; *Angew. Chem.* **1999**, *111*, 1772–1774.
- (c) Wang, Y.; Robinson, G. H. *Inorg. Chem.* **2011**, *50*, 12326–12337.
- [15]. For attempts to isolate triboriranes **V**, see:
- (a) Baudler, M.; Rockstein, K.; Oehlert, W. *Chem. Ber.* **1991**, *124*, 1149–1152.
- (b) Maier, A.; Hofmann, M.; Pritzkow, H.; Siebert, W. *Angew. Chem. Int. Ed.* **2002**, *41*, 1529–1532; *Angew. Chem.* **2002**, *114*, 1600–1602.
- (c) Mesbah, W.; Soleimani, M.; Kianfar, E.; Geiseler, G.; Massa, W.; Hofmann, M.; Berndt, A. *Eur. J. Inorg. Chem.* **2009**, 5577–5582.
- (d) Kupfer, T.; Braunschweig, H.; Radacki, K. *Angew. Chem. Int. Ed.* **2015**, *54*, 15084–15088;

- Angew. Chem.* **2015**, *127*, 15299–15303.
- [16]. Mass-spectrometric data corresponding to the formula $(R_2N-B)_3$ was observed from the mixture, see:
- (a) Ref. [13a].
- (b) Maringgele, W.; Heine, A.; Noltemeyer, M.; Meller, A. *J. Organomet. Chem.* **1994**, *468*, 25–35.
- (c) Ref. [12a].
- [17]. Nöth, H.; Pommerening, H. *Angew. Chem. Int. Ed.* **1980**, *19*, 482–483; *Angew. Chem.* **1980**, *92*, 481–482.
- [18]. Meller, Maringgele, and co-workers reported that the dehalogenation of $(TMP)BCl_2$ afforded a complex mixture which possibly contained $TMP-B(H)-B(H)-TMP$ as the main species (see Ref. [12a]). No spectroscopic data were provided.
- [19]. Siebert and co-workers reported the reduction of 1,2- Cl_2 -1,2-TMP₂-diborane(4) to afford **4** (see: Ref. [12b]).
- [20]. Nöth, H.; Weber, S. *Z. Naturforsch., B: Anorg. Chem., Org. Chem.* **1983**, *38B*, 1460–1465.
- [21]. (a) Braunschweig, H.; Herbst, T.; Rais, D.; Seeler, F. *Angew. Chem. Int. Ed.* **2005**, *44*, 7461–7463; *Angew. Chem.* **2005**, *117*, 7627–7629.
- (b) Bissinger, P.; Braunschweig, H.; Kraft, K.; Kupfer, T. *Angew. Chem. Int. Ed.* **2011**, *50*, 4704–4707; *Angew. Chem.* **2011**, *123*, 4801–4804.
- [22]. For evidence of the generation of aminoborylene ($R_2N-B:$) from the reduction of $(R_2N)BCl_2$, see:
- (a) Meller, A.; Bromm, D.; Maringgele, W.; Böehler, D.; Elter, G. *J. Organomet. Chem.* **1988**, *347*, 11–16.
- (b) Bromm, D.; Stalke, D.; Heine, A.; Meller, A.; Sheldrick, G. M. *J. Organomet. Chem.* **1990**, *386*, 1–7.
- (c) Maringgele, W.; Seebold, U.; Heine, A.; Stalke, D.; Noltemeyer, M.; Sheldrick, G. M.; Meller, A. *Organometallics* **1991**, *10*, 2097–2098.
- (d) Meller, A. *Pure Appl. Chem.* **1991**, *63*, 395–398.
- (e) Wrackmeyer, B. *Angew. Chem. Int. Ed.* **2016**, *55*, 1962–1964; *Angew. Chem.* **2016**, *128*, 1998–2000.
- [23]. (a) Fisch, H.; Pritzkow, H.; Siebert, W. *Angew. Chem. Int. Ed.* **1984**, *23*, 608–613; *Angew. Chem.* **1984**, *96*, 595.
- (b) Fisch, H.; Pritzkow, H.; Siebert, W. *Z. Naturforsch., B: Chem. Sci.* **1988**, *43*, 658–664.
- (c) Krämer, A.; Uhm, J. K.; Garner, S. E.; Pritzkow, H.; Siebert, W. *Z. Naturforsch., B: Chem. Sci.* **1990**, *45*, 1019–1021.
- (d) Nöth, H.; Wagner, M. *Chem. Ber.* **1991**, *124*, 1963–1972.

- (e) Knizek, J.; Krossing, I.; Nöth, H.; Ponikvar, W. *Eur. J. Inorg. Chem.* **1998**, 505–509.
- (f) Braunschweig, H.; Kupfer, T.; Mies, J.; Oechsner, A. *Eur. J. Inorg. Chem.* **2009**, 2844–2850.
- (g) Pospiech, S.; Brough, S.; Bolte, M.; Lerner, H.-W.; Bettinger, H. F.; Wagner, M. *Chem. Commun.* **2012**, 48, 5886–5888.
- (h) Pospiech, S.; Bolte, M.; Lerner, H.-W.; Wagner, M. *Organometallics* **2014**, 33, 6967–6974.
- [24]. Østby, K.-A.; Haaland, A.; Gundersen, G.; Nöth, H. *Organometallics* **2005**, 24, 5318–5328.
- [25]. Braunschweig and co-workers reported the isolation and full characterization of $[(\text{Cy}_2\text{N}-\text{B})_3]^{2-}$ (Cy = cyclohexyl), see: Ref. [15d].
- [26]. For the spectroscopic identification of π -aromatic cyclic $[\text{B}_3\text{L}_3]^+$ (L = N₂, CO), see: Jin, J.; Wang, G.; Zhou, M.; Andrada, D. M.; Hermann, M.; Frenking, G. *Angew. Chem. Int. Ed.* **2016**, 55, 2078–2082; *Angew. Chem.* **2016**, 128, 2118–2122.
- [27]. (a) Korkin, A. A.; Schleyer, P. von R.; McKee, M. L. *Inorg. Chem.* **1995**, 34, 961–977.
(b) Richard, R. M.; Ball, D. W. *J. Mol. Struct.: THEOCHEM* **2007**, 814, 91–98.
- [28]. Linti, G.; Loderer, D.; Nöth, H.; Polborn, K.; Rattay, W. *Chem. Ber.* **1994**, 127, 1909–1922.
- [29]. Paetzold, P.; G ret-Baumgarten, L.; Boese, R. *Angew. Chem. Int. Ed.* **1992**, 31, 1040–1072; *Angew. Chem.* **1992**, 104, 1073–1075.
- [30]. Dirschl, F.; Hanecker, E.; N th, H.; Rattay, W.; Wagner, W. *Z. Naturforsch., B: Anorg. Chem., Org. Chem.* **1986**, 41B, 32–37.
- [31]. (a) Braunschweig, H.; Ye, Q.; Vargas, A.; Dewhurst, R. D.; Radacki, K.; Damme, A. *Nat. Chem.* **2012**, 4, 563–567.
(b) Braunschweig, H.; Ye, Q.; Vargas, A.; Radacki, K.; Damme, A. *Angew. Chem. Int. Ed.* **2013**, 52, 10657–10660; *Angew. Chem.* **2013**, 125, 10851–10854.
- [32]. (a) Scheschkewitz, D.; Amii, H.; Gornitzka, H.; Schoeller, W. W.; Bourissou, D.; Bertrand, G. *Science* **2002**, 295, 1880–1881.
(b) Rodriguez, A.; Olsen, R. A.; Ghaderi, N.; Scheschkewitz, D.; Tham, F. S.; Mueller, L. J.; Bertrand, G. *Angew. Chem. Int. Ed.* **2004**, 43, 4880–4883; *Angew. Chem.* **2004**, 116, 4988–4991.
- [33]. Østby, K.-A.; Haaland, A.; Gundersen, G.; N th, H. *Organometallics* **2005**, 24, 5318–5328.
- [34]. (a) Glaser, B.; Hanecker, E.; N th, H.; Wagner, H. *Chem. Ber.* **1987**, 120, 659–667.
(b) Nakata, N.; Sekiguchi, A. *J. Am. Chem. Soc.* **2006**, 128, 422–423.
(c) Rivard, E.; Merrill, W. A.; Fettinger, J. C.; Wolf, R.; Spikes, G. H.; Power, P. P. *Inorg. Chem.* **2007**, 46, 2971–2978.
(d) Boese, R.; Paetzold, P.; Tapper, A. *Chem. Ber.* **1987**, 120, 1069–1071.
- [35]. Shoji, Y.; Tanaka, N.; Mikami, K.; Uchiyama, M.; Fukushima, T. *Nat. Chem.* **2014**, 6, 498–503.
- [36]. A reported borylene dicarbonyl complex also showed negative charge for the boron atom; see: Ref. [4g].

- [37]. Chen, Z.; Wannere, C. S.; Corminboeuf, C.; Puchta, R.; Schleyer, P. von R. *Chem. Rev.* **2005**, *105*, 3842–3888.
- [38]. Our calculated NICS(1) value for B₃H₃ (C_{2v}) is consistent with earlier work; see: Hofmann, M.; Berndt, A. *Heteroat. Chem.* **2006**, *17*, 224–237.
- [39]. For a recent review about boron-containing aromatic heterocycles, see: Su, B.; Kinjo, R. *Synthesis* **2017**, *49*, 2985–3034.
- [40]. Yamaguchi, K. in *Self-Consistent Field: Theory and Applications*, Studies in Physical and Theoretical Chemistry, Vol. 70 (Eds.: R. Carbo, M. Klobukowski), Elsevier, Amsterdam, **1990**, pp. 727.
- [41]. Similar aromatic adducts were synthesized through the reaction of 1,2-Cl₂-1,2-NMe₂-diborane(4) and dilithiated aromatics, see:
- (a) Pospiech, S.; Brough, S.; Bolte, M.; Lerner, H.-w.; Bettinger, H. F.; Wagner, M. *Chem. Commun.* **2012**, *48*, 5886–5888.
- (b) Pospiech, S.; Bolte, M.; Lerner, H.-w.; Wagner, M. *Organometallics* **2014**, *33*, 6967–6974.
- [42]. (a) Wright, R. J.; Philips, A. D.; Power, P. P. *J. Am. Chem. Soc.* **2003**, *125*, 10784–10785.
- (b) Agou, T.; Nagata, K.; Tokitoh, N. *Angew. Chem. Int. Ed.* **2013**, *52*, 10818–10821.
- [43]. Pilz, M.; Allwohn, J.; Willershausen, P.; Massa, W.; Berndt, A. *Angew. Int. Ed. Engl.* **1990**, *29*, 1030–1032; *Angew. Chem.* **1990**, *102*, 1085–1087.
- [44]. For the computational study about the cycloaddition reaction of Ph–E=E–Ph and toluene (E = B, Al, Ga, In and Tl), see: Gu, S.-Y.; Sheu, J.-H.; Su, M.-D. *Inorg. Chem.* **2007**, *46*, 2028–2034.
- [45]. A
- [46]. Asakawa, H.; Lee, K.-H.; Lin, Z.; Yamashita, M. *Nature Commun.* **2014**, *5*, 4245–4254.
- [47]. For the reaction of (pin)B–B(Mes) with xylyl isocyanide, in which a isocyanide C–N triple bond was not cleaved, see:
- (a) Katsuma, Y.; Asakawa, H.; Lee, K.-H.; Lin, Z.; Yamashita, M. *Organometallics* **2016**, *35*, 2563–2566.
- (b) Katsuma, Y.; Asakawa, H.; Yamashita, M. *Organometallics* **2016**, *35*, 2563–2566.
- [48]. Glaser, B.; Mayer, E. P.; Nöth, H.; Rattay, W.; Wietelmann, U. *Z. Naturforsch.* **1988**, *43B*, 449–456.
- [49]. (a) Glaser, B.; Nöth, H. *Angew. Chem. Int. Ed.* **1985**, *24*, 416–417 ; *Angew. Chem.* **1985**, *97*, 424–425.
- (b) Tapper, A.; Schmitz, T.; Paetzold, P. *Chem. Ber.* **1989**, *122*, 595–601.
- [50]. (a) Littger, R.; Nöth, H.; Thomann, M.; Wagner, M. *Angew. Chem. Int. Ed.* **1993**, *32*, 295–297; *Angew. Chem.* **1993**, *105*, 275–277.
- (b) Braunschweig, H.; Kupfer, T.; Mies, J.; Oechsner, A. *Eur. J. Inorg. Chem.* **2009**, 2844–2850.
- [51]. Laitar, D. S.; Tsui, E. Y.; Sadighi, J. P. *J. Am. Chem. Soc.* **2006**, *128*, 11036–11037.

- [52]. McIntosh, M. L.; Moore, C. M.; Clark, T. B. *Org. Lett.* **2010**, *12*, 1996–1999.
- [53]. Paetzold, P.; Kiesgen, J.; Luckert, S.; Spaniol, T.; Englet, U. *Z. Anorg. Allg. Chem.* **2002**, *628*, 1631–1635.
- [54]. Wu, D.; Wang, R.; Li, Y.; Ganguly, R.; Hirao, H.; Kinjo, R. *Chem.* **2017**, *3*, 134–151.
- [55]. Tsukahara, N.; Asakawa, H.; Lee, K.-H.; Lin, Z.; Yamashita, M. *J. Am. Chem. Soc.* **2017**, *139*, 2593–2596.
- [56]. Dettenrieder, N.; Aramaki, Y.; Wolf, B. M.; Maichle-Mössmer, C.; Zhao, X.; Yamashita, M.; Nozaki, K.; Anwander, R. *Angew. Chem. Int. Ed.* **2014**, *53*, 6259–6262; *Angew. Chem.* **2014**, *126*, 6373–6377.
- [57]. Braunschweig, H.; Hörl, C. *Chem. Commun.* **2014**, *50*, 10983–10985.
- [58]. For the synthesis and ^{11}B NMR signal of a $\text{DA}(\text{H})\cdot\text{BH}_3$ adduct, see: Jaska, C. A.; Temple, K.; Lough, A. J.; Manners, I. *J. Am. Chem. Soc.* **2003**, *125*, 9424–9434.
- [59]. (a) Braunschweig, H.; Dellermann, T.; Ewing, W. C.; Kramer, T.; Schneider, C.; Ulrich, S. *Angew. Chem. Int. Ed.* **2015**, *54*, 10271–10275; *Angew. Chem.* **2015**, *127*, 10409–10413.
(b) Braunschweig, H.; Constantinidis, P.; Dellermann, T.; Ewing, W. C.; Fischer, I.; Hess, M.; Knight, F. R.; Rempel, A.; Schneider, C.; Ulrich, S.; Vargas, A.; Woollins, J. D. *Angew. Chem. Int. Ed.* **2016**, *55*, 5606–5609; *Angew. Chem.* **2016**, *128*, 5697–5700.
- [60]. Connelly, N. G.; Geiger, W. E. *Chem. Rev.* **1996**, *96*, 877–910.
- [61]. For reviews about boron cations, see:
(a) Kölle, P.; Nöth, H. *Chem. Rev.* **1985**, *85*, 399–418.
(b) Piers, W. E.; Bourke, S. C.; Conroy, K. D. *Angew. Chem. Int. Ed.* **2005**, *44*, 5016–5036
Angew. Chem. **2005**, *117*, 5142–5163.
(c) Vries, T. S. D.; Prokofjevs, A.; Vedejs, E. *Chem. Rev.* **2012**, *112*, 4246–4282.
(d) Eisenberger, P.; Crudden, C. M. *Dalton Trans.* **2017**, *46*, 4874–4887.
- [62]. Sheldrick, G. M. A short history of *SHELX*. *Acta Cryst.* **2008**, *A64*, 112–122.
- [63]. Hübschle, C. B.; Sheldrick, G. M.; Dittrich, B. *ShelXle*: a Qt graphical user interface for *SHELXL*. *J. Appl. Cryst.* **2011**, *44*, 1281–1284.
- [64]. Persistence of Vision Raytracer (ver. 3.7.0); Persistence of Vision Pty. Ltd., 2016; Retrieved from <http://www.povray.org/download/>
- [65]. Gaussian 09, Revision B.01, Frisch, M. J.; Trucks, G. W.; Schlegel, H. B.; Scuseria, G. E.; Robb, M. A.; Cheeseman, J. R.; Scalmani, G.; Barone, V.; Mennucci, B.; Petersson, G. A.; Nakatsuji, H.; Caricato, M.; Li, X.; Hratchian, H. P.; Izmaylov, A. F.; Bloino, J.; Zheng, G.; Sonnenberg, J. L.; Hada, M.; Ehara, M.; Toyota, K.; Fukuda, R.; Hasegawa, J.; Ishida, M.; Nakajima, T.; Honda, Y.; Kitao, O.; Nakai, H.; Vreven, T.; Montgomery, Jr. J. A.; Peralta, J. E.; Ogliaro, F.; Bearpark, M.; Heyd, J. J.; Brothers, E.; Kudin, K. N.; Staroverov, V. N.; Keith,

- T.; Kobayashi, R.; Normand, J.; Raghavachari, K.; Rendell, A.; Burant, J. C.; Iyengar, S. S.; Tomasi, J.; Cossi, M.; Rega, N.; Millam, J. M.; Klene, M.; Knox, J. E.; Cross, J. B.; Bakken, V.; Adamo, C.; Jaramillo, J.; Gomperts, R.; Stratmann, R. E.; Yazyev, O.; Austin, A. J.; Cammi, R.; Pomelli, C.; Ochterski, J. W.; Martin, R. L.; Morokuma, K.; Zakrzewski, V. G.; Voth, G. A.; Salvador, P.; Dannenberg, J. J.; Dapprich, S.; Daniels, A. D.; Farkas, O.; Foresman, J. B.; Ortiz, J. V.; Cioslowski, J. and Fox, D. J. *Gaussian, Inc.*, Wallingford CT, 2010.
- [66]. Gaussian 09, Revision D.01, Frisch, M. J.; Trucks, G. W.; Schlegel, H. B.; Scuseria, G. E.; Robb, M. A.; Cheeseman, J. R.; Scalmani, G.; Barone, V.; Mennucci, B.; Petersson, G. A.; Nakatsuji, H.; Caricato, M.; Li, X.; Hratchian, H. P.; Izmaylov, A. F.; Bloino, J.; Zheng, G.; Sonnenberg, J. L.; Hada, M.; Ehara, M.; Toyota, K.; Fukuda, R.; Hasegawa, J.; Ishida, M.; Nakajima, T.; Honda, Y.; Kitao, O.; H. Nakai, O.; Vreven, T.; Montgomery, J. A., Jr.; Peralta, J. E.; Ogliaro, F.; Bearpark, M.; Heyd, J. J.; Brothers, E.; Kudin, K. N.; Staroverov, V. N.; Keith, T.; Kobayashi, R.; Normand, J.; Raghavachari, K.; Rendell, A.; Burant, J. C.; Iyengar, S. S.; Tomasi, J.; Cossi, M.; Rega, N.; Millam, J. M.; Klene, M.; Knox, J. E.; Cross, J. B.; Bakken, V.; Adamo, C.; Jaramillo, J.; Gomperts, R.; Stratmann, R. E.; Yazyev, O.; Austin, A. J.; Cammi, R.; Pomelli, C.; Ochterski, J. W.; Martin, R. L.; Morokuma, K.; Zakrzewski, V. G.; Voth, G. A.; Salvador, P.; Dannenberg, J. J.; Dapprich, S.; Daniels, A. D.; Farkas, O.; Foresman, J. B.; Ortiz, J. V.; Cioslowski, J.; Fox, D. J.; Gaussian, Inc.: Wallingford CT, 2013.
- [67]. (a) Becke, A. D. *Phys. Rev. A: Gen. Phys.* **1988**, *38*, 3098–3100.
(b) Lee, C.; Yang, W.; Parr, R. G. *Phys. Rev. B: Condens. Matter* **1988**, *37*, 785–789.
(c) Becke, A. D. *J. Chem. Phys.* **1993**, *98*, 1372–1377.
(d) Becke, A. D. *J. Chem. Phys.* **1993**, *98*, 5648–5652.
- [68]. Osak, T. P.; Landesman, H.; Williams, R. E.; Shapiro, I. *J. Phys. Chem.* **1959**, *63*, 1533–1535.
- [69]. (a) Bauernschmitt, R.; Ahlrichs, R. *Chem. Phys. Lett.* **1996**, *256*, 454–464.
(b) Casida, M. E.; Jamorski, C.; Casida, K. C.; Salahub, D. R. *J. Chem. Phys.* **1998**, *108*, 4439–4449.
- [70]. Yanai, T.; Tew, D.; Handy, N. *Chem. Phys. Lett.* **2004**, *393*, 51–57.
- [71]. (a) Reed, A. E.; Weinstock, R. B.; Weinhold, F. *J. Chem. Phys.* **1985**, *83*, 735–746.
(b) Reed, A. E.; Curtiss, L. A.; Weinhold, F. *Chem. Rev.* **1988**, *88*, 899–926.
- [72]. NBO 5.9., Glendening, E. D.; Badenhoop, J. K.; Reed, A. E.; Carpenter, J. E.; Bohmann, J. A.; Morales, C. M. and Weinhold, F. (Theoretical Chemistry Institute, University of Wisconsin, Madison, WI, 2009); <http://www.chem.wisc.edu/~nbo5>
- [73]. Hofmann, M.; Berndt, A. *Heteroat. Chem.* **2006**, *17*, 224–237.

公表論文

公表論文

- (1) Synthesis of a Sterically Demanding Dispiropiperidine and Its Application in Monoamidodialkyl Zincate Complexes

S. Morisako, R. Shang, Y. Yamamoto

Inorganic Chemistry, **2016**, *55*(20), 10767–10773.

- (2) Triaminotriborane(3): A Homocatenated Boron Chain Connected by B–B Multiple Bonds

S. Morisako, R. Shang, Y. Yamamoto, H. Matsui, M. Nakano

Angewandte Chemie International Edition, **2017**, *56*(48), 15234–15240;

Angewandte Chemie, **2017**, *129*(48), 15436–15442.

Acknowledgement

The studies described in this dissertation have been carried out under the direction of Prof. Yohsuke Yamamoto at the Department of Chemistry, Graduate School of Science, Hiroshima University.

The author sincerely wishes to express his appreciation to Prof. Yohsuke Yamamoto for his continuing guidance, valuable discussions and encouragement throughout the course of studies. Grateful acknowledgment is made to Assist. Prof. Dr. Rong Shang, Prof. Atsushi Kawachi (Hosei University), Dr. Satoshi Kojima and Assos. Prof. Masaaki Nakamoto (Hiroshima University) for their helpful discussions and suggestions.

The author wishes to thank Prof. Masayoshi Nakano (Osaka University), Assist. Prof. Ryohei Kishi (Osaka University), Mr. Hiroshi Matsui (Osaka University), Prof. Makoto Yamashita (Nagoya University), Dr. Shun-suke Asami (Chuo University), Ms. Nana Tsukahara (Chuo University), Mr. Atsumi Yagi (Nagoya University), Prof. Yoshiaki Nishibayashi (University of Tokyo), Prof. Tsutomu Mizuta (Hiroshima University), Prof. Takeharu Haino (Hiroshima University), and Prof. Manabu Abe (Hiroshima University), Prof. Takahiro Sasamori (Nagoya City University), Prof. Mao Minoura (Rikkyo University), Ms. Naomi Kawata (Hiroshima University) and glass-blowers (Hiroshima University) for their helpful discussions, kind assistance and collaborations.

The author would express his appreciation to Dr. Yusuke Inagaki, Dr. Shin-ichi Fuku-ene, Dr. Shun Sugawara, Dr. Yuan Shi, Dr. Yasuyuki Imada, Mr. Yuya Toya, Mr. Tatsuya Inoue, Mr. Tatsuya Hirofujii, Ms. Kaoko Sato, Ms. Aki Katori, Ms. Yuri Kuwana, Mr. Atsushi Nakamoto, Ms. Saki Kimura, Ms. Narumi Banden, Mr. Zhang Sihan, Ms. Yan Chenting, Mr. Kazuaki Okada, Mr. Masato Takeshita, Ms. Tomomi Kukita, Ms. Kanako Wada, Mr. Souta Saitou, Ms. Emiko Muneta, Mr. Masaru Sugiyama, Mr. Shuhei Maeda and all of the other members of Prof. Yamamoto's group for their helpful discussions and kind assistance.

The author wishes to thank Dr. Koh Sugamata, Dr. Koto Yuma, Dr. Maekawa Yuuki, Dr. Yamaguchi Kirara, Dr. Noritaka Takeuchi, Ms. Yuko Suzuki, Mr. Taichi Nakamura, Ms. Mariko Yukimoto, Mr. Tomoyuki Kosai, Mr. Takayuki Nakamuro, Mr. Tomohiro Sugahara, Ms. Shiori Fujimori, Mr. Takuya Kinoshita, Mr. Yuhei Katsuma and Mr. Jun Kobayashi for their fruitful discussion, kind encouragement, and continuous friendship.

Finally, the author is grateful to his parents Mr. Tsunenori Morisako and Ms. Chika Morisako and a his brother Mr. Keisuke Morisako for their constant assistance, affectionate encouragement, and providing the very comfortable environment to concentrate on research.

January, 2018

Shogo Morisako

Department of Chemistry, Graduate School of Science
Hiroshima University